RAPID ANALYSIS OF ENERGY CHARACTERISTICS OF BIOMASS USING NEAR INFRARED SPECTROSCOPY

JETSADA POSOM

A THESIS SUBMITTED IN PARTIAL FULFILLMENT

OF THE REQUIREMENTS FOR THE DEGREE OF

DOCTOR OF ENGINEERING IN AGRICULTURAL ENGINEERING

FACULTY OF ENGINEERING

KING MONGKUT'S INSTITUTE OF TECHNOLOGY LADKRABANG

2017

KMITL-2017-EN-D-108-036

หัวข้อวิทยานิพนธ์	การวิเคราะห์สมบัติเชิงพลังงานของชีวมวลแบบรวดเร็วโดยใช้เทคนิคเนียร์อินฟราเรดสเปกโทรสโกปี
นักศึกษา	นายเจษฎา โพธิ์สม
รหัสประจำตัว	57601073
ปริญญา	วิศวกรรมศาสตรดุษฎีบัณฑิต
สาขาวิชา	วิศวกรรมเกษตร
พ.ศ.	2560
อาจารย์ที่ปรึกษาวิทยานิพนธ์	รศ.ดร.ปานมนัส ศิริสมบูรณ์

บทคัดย่อ

งานวิจัยนี้จัดทำขึ้นเพื่อศึกษาความสามารถในการทำนายสมบัติเชิงพลังงานของชีวมวลโดยใช้เทคนิคเนียร์อินฟราเรดสเปกโทรสโกปี ซึ่งได้แบ่งออกเป็น 5 ส่วนย่อยดังนี้ ส่วนที่หนึ่งศึกษาการใช้เทคนิคที่ง่ายและรวดเร็วสำหรับวัดความชื้นและค่าความร้อนสูงของกระถินยักษ์อัดเม็ดผ่านการใช้เทคนิคเนียร์อินฟราเรดสเปกโทรสโกปี ส่วนที่สองศึกษาการประมาณค่าความร้อนสูงและค่าการวิเคราะห์โดยประมาณ (proximate analysis) ของไม้ไผ่บด ซึ่งได้แก่ ค่าสารระเหย (volatile matter) ค่าคาร์บอนคงที่ (fixed carbon) และเถ้า (ash) ส่วนที่สามทำนายสมบัติการสลายตัวเชิงความร้อน (pyrolysis) ของไม้ไผ่บดโดยใช้เทคนิคเนียร์อินฟราเรดสเปกโทรสโกปี ซึ่งได้แก่ อุณหภูมิเริ่มสลายตัว (T_{onset}) อุณหภูมิที่สลายตัวสูงสุดในช่วงที่สอง (T_{sh}) อุณหภูมิสลายตัวสูงสุดของชีวมวล (T_{peak}) อุณหภูมิที่ชีวมวลเริ่มไม่สลายตัว (T_{offset}) และอัตราการสลายตัวสูงสุด (DTG_{peak}) ซึ่งใช้เป็นวิธีที่รวดเร็ว สำหรับทดแทนวิธีเทอร์โมกราวิเมทรี (thermogravimetry) ส่วนที่สี่ทำนายค่าความร้อนต่ำและองค์ประกอบทางเคมี (elemental composition) ซึ่งได้แก่ คาร์บอน ไฮโดรเจน ไนโตรเจน ออกซิเจนและซัลเฟอร์ในไม้ไผ่บด และส่วนที่ห้าใช้เนียร์อินฟราเรดสเปโทรสโกปีในการทำนายค่าสมบัติการสลายตัวเชิงความร้อนและค่าสารระเหยในไม้ไผ่สับ

ข้อมูลเชิงแสงที่ใช้สำหรับสร้างโมเดลในการทำนายสมบัติเชิงพลังงาน ได้รับโดยผ่านการสแกนโดยใช้ฟูเรียร์ทรานฟอร์มเนียร์อินฟราเรด (FT-NIR) สเปกโทรมิเตอร์ ในช่วงจำนวนคลื่นระหว่าง 12500 - 3600 cm^{-1} ซึ่งใช้ log 1/R สำหรับเป็นค่าการดูดซับคลื่น และสร้างโมเดลโดยใช้วิธีตัวแปรเส้นทางกำลังสองน้อยที่สุดบางส่วนและทดสอบความสามารถของโมเดลโดยใช้ค่าทางสถิติ เช่น ค่าสัมประสิทธิ์การ

พิจารณา รากที่สองของความผิดพลาดเฉลี่ยยกกำลังสอง ค่าความผิดพลาดเฉลี่ย และค่าอัตราส่วนความเบี่ยงเบนเฉลี่ยของค่าอ้างอิงต่อค่าความผิดพลาด

ผลการทดลองพบว่าเนียร์อินฟราเรดสเปกโทรสโกปีสามารถทำนายความชื้น ค่าความร้อนสูงและค่าความร้อนต่ำได้ดี ถึงแม้ว่าพารามิเตอร์เหล่านี้ (ค่าความร้อนสูงและค่าความร้อนต่ำ) ไม่ได้เป็นตัวแปรทำนายโดยตรงที่สัมพันธ์การดูซับแสงแต่ก็สามารถทำนายได้เนื่องจากค่าการดูดกลืนแสงมีความสัมพันธ์กับองค์ประกอบในชีวมวล ที่สัมพันธ์กับค่าความร้อนของชีวมวลและพบว่าการสั่นของพันธะน้ำและลิกนินมีผลกับการทำนายค่าความร้อนสูง ส่วนค่าความร้อนต่ำก็มีความสัมพันธ์กับการสั่นพันธะของลิกนินเช่นกัน ส่วนการทำนายค่าสารระเหยและคาร์บอนต่ำได้ผลโดยรวมที่ดี และพบว่ามีความสัมพันธ์กับการสั่นของพันธะของสารประกอบลิกโนเซลลูโลสิก (เฮมิเซลลูโลส เซลลูโลสและลิกนิน) เนื่องจากสารประกอบเหล่านี้จะเกิดการสลายตัวเมื่อถูกความร้อน แต่ไม่สามารถทำนายปริมาณเถ้าได้ เนื่องจากส่วนประกอบของเถ้าไม่เกิดอันตระกริยากับแสง ดังนั้น ในการสร้างโมเดลทำนายค่าสารระเหยและคาร์บอนคงที่ ควรเลือกความยาวคลื่นที่สัมพันธ์กับการสั่นของสารประกอบลิกโนเซลลูโลสิก สำหรับภาพรวมโมเดลของสมบัติการสลายตัวเชิงความร้อน สมรรถนะของโมเดล T_{peak} และ T_{offset} ให้ผลการทนายที่ดี สามารถใช้ในการทำนายเชิงคุณภาพได้ สำหรับโมเดล T_{sh} ให้ผลการทำนายพอใช้สามารถใช้ในการประมาณได้ โมเดล T_{onset} และ DTG_{peak} ให้ประสิทธิภาพที่ต่ำ สำหรับการทำนายค่าองค์ประกอบทางเคมี โมเดลสำหรับการทำนาย N ให้ประสิทธิภาพดีที่สุดและโมเดลการทำนาย O ให้ประสิทธิภาพแย่ที่สุด ซึ่งจะเห็นได้จาก มีค่าความแตกต่างจากการทำซ้ำที่สูง โมเดลในการทำนายสมบัติเชิงพลังงานของชีวมวลสามารถเป็นประโยชน์ด้านการค้าชีวมวลในการใช้ตรวจสอบคุณภาพและประโยชน์กับอุตสาหกรรมพลังงานเพื่อใช้ควบคุมและออกแบบกระบวนการแปรรูปพลังงานให้มีประสิทธิภาพ

Thesis	Rapid analysis of energy characteristics of biomass using near infrared spectroscopy
Student	Mr. Jetsada Posom
Student ID.	57601073
Degree	Doctor of Engineering
Program	Agricultural Engineering
Year	2017
Thesis Advisor	Assoc. Prof. Dr. Panmanas Sirisomboon

ABSTRACT

The purpose of this thesis was to forecast the energy characteristics of biomass using near infrared spectroscopy. The overall work was divided into five parts. The first part of the study was to develop a simplified technique as a rapid and low-cost for predicting moisture content (MC) and higher heating value (HHV) of *Leucaena leucocephala* pellets. This is the first time to use NIR spectroscopy with biomass pellets. The second part was to optimize the model for evaluating the HHV and proximate value (volatile matter, VM; fixed carbon, FC; and ash, A) of milled bamboo. The third part was to predict the pyrolysis characteristics (T_{onset}, T_{sh}, T_{peak}, T_{offset}, DTG_{peak}: T_{peak} is temperature as a highest degradation and presents the maximum of production rate, T_{offset} is the temperature of the end decomposition rate, it can be used to know which temperature should be stopped to heat, DTG_{peak} is the maximum of decomposition rate which can be used to manage feedstock) of ground bamboo as an alternative thermogravimetry method. The fourth part investigated the lower heating value (LHV) and element composition of ground bamboo, which was the first study to generate the relationship between LHV and NIR absorption. Meanwhile, the bamboo chip was investigated in the fifth part for evaluation of pyrolysis characteristics and volatile matter.

The NIR spectrometer for scanning was Fourier transform NIR (FT-NIR) spectrometer using spectral region of 12500 to 3600 cm^{-1}. The absorption value was recorded into log 1/R and the models were optimized by partial least squares (PLS) regression. The performance of models was evaluated by statistical terms of coefficients of determination (R^2), root mean square error of prediction (RMSEP) or root

mean square error of cross validation (RMSECV), ratio of prediction to deviation (RPD) and bias. The effective models were selected with the lowest RMSEP.

The overview shows that NIR spectroscopy can be used to evaluate the MC, HHV and LHV well. Even though HHV and LHV were not direct property detected by NIR radiance, but it can be also predicted when the interaction between NIR radiance and organic compound was known. The vibration bands of MC and lignin greatly affected the prediction of HHV, and lignin band affected the prediction of LHV. NIR spectroscopy gave good performance for evaluating of VM and FC, meanwhile model for A was very poor Because ash is not NIR absorber. Because lignocellulosic (hemicellulose, cellulose and lignin) compound in biomass can be converted to volatile matter, then vibration band of those occurred in modelling of VM and FC model. The model of VM and FC should be generated by the absorbance of lignocellulosic. The overall pyrolysis characteristic predicted by NIR spectroscopy was good performance. The T_{peak} and T_{offset} models is usable for most applications and may be used as a nondestructive technique for quality assurance. The T_{sh} model was fair, and T_{onset} and DTG_{peak} models gave poor result. For overall elemental composition, N prediction provided the highest performance, which could be used for most application. The O model was poor. The reference methods for elemental composition were observed that there was high repeatability value, it led to low model performance.

For determination of energy characteristic of biomass, the results could be a guide for applying in trading, design and operation control of energy conversion.

Acknowledgements

This thesis would not have been successful if Assoc. Prof. Dr. Panmanas Sirisomboon, who is my thesis advisor, has not provided me with the opportunity to undertake a Doctor of Engineering program. My sincere thanks also goes to Assoc. Prof. Dr. Panmanas Sirisomboon, who gave access to the laboratory and research facilities. Without advisor, precious support it would not be possible to conduct this research. In particular, I thanks to financial support from the Royal Golden Jubilee PhD scholarship (PHD/0070/2557) of Thailand research fund (TRF), they finance to do the research in foreign country i.e. Germany and Japan.

I also thank to Near Infrared Spectroscopy Research Center for Agricultural Product and Food (www.nirsresearch.com) at King Mongkut's Institute of technology Ladkrabang, Bangkok, Thailand, for NIR instrument i.e. Fourier Transform Near Infrared (FT-NIR), NIR Gun, MicroNir-NIR, Thermogravimetry (TG) analyzer and Bomb calorimetry, and thanks to Chemical Engineering department for CHNS analyzer. During the did experiment in Germany for six month, I acknowledge Karlsruhe Institute of Technology, Institute of Catalysis Research and Technology (IKFT), Hermann-von-Helmholtz-Platz 1, 76344 Eggenstein-Leopoldshafen, Germany, for TGA instrument. I am very grateful to Dr. Axel Funke who was the co-advisor, and thanks to Mrs. Jessica Heinrich, Mrs. Jessica Maier and Mrs. Pia Griesheimer who were the scientist members in IKFT laboratory.

I am grateful to all of the lecturers at at King Mongkut's Institute of Technology Ladkrabang (KMITL) for their educating. During the course of this work in Japan, I was assisted by Mr. Ma for guidelines of using laboratory equipment. My special thanks go to Prof. Dr. Satoru Tsuchikawa and Dr. Tetsuya Inagaki not only for being an excellent supervisor but also for taking care of my living during the research visit at Nagoya University of Bioresource Engineering, Nagoya, Japan.

Last but not the least, I would like to thank my family: my parents and to my brothers and sister for supporting me spiritually throughout writing this thesis and my life in general.

Jetsada Posom

Symbols and abbreviations

Notation

A	Ash	$\dot{R}$	reflectance
B	regression coefficient	R^2	coefficient of determination
C	carbon	RMSECV	root mean square error of cross validation
E	residue matrix of spectral	RPD	ratio of prediction to deviation
F	residue matric of reference value	SD	standard deviation of the measured values
f	final	RMSEE	root mean square error of estimation
FT	Fourier transform	RH	relative humidity
H	hydrogen	wb	wet basis
i	initial	X_i	measured value of sample i
LV	factor of PLS models	$\overline{X}$	average of the measured values
m	mass, g	Bias	average error of prediction
MC	moisture content	HHV	higher heating value
R^2_{max}	maximum coefficient of determination	LHV	lower heating value
N	nitrogen	db	dry basis
NIR	near infrared	SEC	standard error of calibration
O	oxygen	SEP	standard error of prediction
TGA	thermogravimetric analysis	VM	volatile matter
DTG	derivative thermogravimetric analysis	FC	fixed carbon
S	sulphur		

Table of contents

Table of contents (continued)

Table of contents (continued)

List of tables

List of tables (continued)

List of tables (continued)

List of tables (continued)

List of figures

List of figures (continued)

List of figures (continued)

List of figures (continued)

Overview

Statement and significance of the problem

The demand for energy continuously increases with the growth of population. The world's population will increase approximately of 1.5 billion and will be reached 8.8 billion by 2035. For this reason, energy consumption has been raised by 34% from 2014 to 2035 [1]. Presently, fossil fuels are mainly dominant source of energy power in the world, and approximately of 80 % of the total energy have been supplied by those. Consequently, the fossil fuels will be diminished and alternative energy sources will obviously be required in near future.

In the present scenario of energy consumption of Thailand in 2016, showed that energy generation obtained from fossil fuels about 78.09%, new renewable energy about 13.38%, current renewable energy about 5.97% and imported hydro power about 2.11% [2]. It obviously showed that most of renewable energy used although Thailand largely came from agriculture wastes and forest residues. These feedstocks could be generated to usable energy. Thailand has agricultural plantation and agricultural crop residues enormously, around 80 million tons per year of agriculture was produced [3] e.g. rice husk (432 tons/year), rice straw (4.1 million tons/year), bagasse (21.2 million tons/year), cassava rhizomes (2.8 million tons/year), palm shell (619,959 tons/year) [2]. The seventh-fast-growing species including *Casuarina junghuhniana, Leucaena leucocephala, Acacia spp, Eucalyptus spp, Bamboo, Melaleuca cajuputi,* and *Pennisetum purpureum (Napier Grass)* have potential to grow and can be used as a suitable alternative for fossil fuels in upcoming days [4]. The plantation of the fast-growing trees helps to absorb and decrease in CO_2 in the atmosphere [5]. The fast-growing energy crops can alleviate the current energy crisis because it has less impact on environmental pollution. Owing to the climate change, biomass is extremely interested because its combustion does not contribute to net increase in CO_2. There is balancing between the CO_2 releasing during combustion process of biomass and the intake of CO_2 during the growth of the fast-growing plants [6,7,8]. This prominent point of biomass led to planning of an Alternative Energy Development Plan (AEDP2015) for 2015-2036 by the Ministry of Energy of Thailand. The

aim was to increase in the portion of renewable energy generation from the current level to 30% of total power requirement [1] and to increase the electricity generation from biomass from 2,452 MW in 2014 to 5,570 MW in 2036 [3].

In the future planning for 2036, the Ministry of Energy attempts to increase the use of alternative energy of 22,100 ktoe for biomass, 495 ktoe for waste, 1,283 ktoe for natural gas,. 1,200 ktoe for solar energy, and 10 ktoe for other resources [1]. Then, the alternative energy production from biomass is the highest. This policy will help to reduce in amount of import fuel such as fossil-oil and electricity. Although the government has promoted to use the biomass as an alternative source of energy, the outcome seemed not to be successful as expectation. This is due to low capacity of the thermal conversion process and their disposal problems. In order to efficiently use biomass, the knowledge of energy characteristic of biomass is essentially required, it will help to achieve high efficiency of thermal conversion process as combustion, gasification, and pyrolysis.

The energy characteristic of biomass includes heating value (higher and lower heating value), proximate data (moisture content, volatile matter, fixed carbon and ash), element composition (carbon, hydrogen, nitrogen, oxygen, and sulfur), and pyrolysis characteristic. The heating value, proximate data and element composition are used to design and to operate biomass combustion systems [9,10]. In commercial, the moisture content and the heating value are essentially aspects in the specification of biomass feedstock to set a price instead of weight [11]. In fast pyrolysis and gasification plants, pyrolysis characteristic, proximate data and element composition are important for estimating the total of liquid and gas fuels in pyrolysis and gasification [12], and this will help to design a reactor and to improve process development for pyrolysis of biomass [13].

Generally, the biomass used in thermal conversion systems was performed into four patterns such as whole wood, wood pellets, wood chips, and wood powder. The form of pellets, chips, and powder can reduce waste, transportation and storage cost. Pellets form help to increase the combustion time of char [14]. Wood pellets and chips are generally used in combustion and gasification process, respectively, wood powder and

whole wood are usually used in both fast pyrolysis and slow pyrolysis process, respectively. Developments with non-destructive methods of the thermal conversion systems in aspects of low-cost, accuracy, and fast are required for efficient biomass analysis [15]. Near infrared spectroscopy has been recommended as a low-cost, rapid, and non-destructive method to substitute the current method. The biomass consists of water, extractives, cell wall components (lignocellulosic: hemicellulose, cellulose and lignin) and ash. Their complex functions are composed of the chains of C-H, O-H, C=O, N-H, -COOH and their bonds correspond to NIR radiance with overtone and combination [16]. Therefore, it is highly possible to predict biomass's properties as an alternative instead of the bomb calorimeter for determining the higher heating value. NIR may forecast pyrolysis characteristic and proximate data as an alternative instead of the thermogravimetric analysis. For determination of element composition, pyrolysis characteristic, and bomb calorimetry are limited by cost and labor skills. For example, time-consuming of determination of its properties: thermogravimetric analysis (TGA) (16-24 hrs/samples), bomb calorimeter (50 min/sample) and dry oven (24 hrs at least) are very long process while NIR method significantly develops the time to 2-3 mins.

In Thailand, near infrared spectroscopy has a high potential for evaluating chemical and physical of agricultural products including gamma oryzanol of germinated brown rice [17], moisture content of tapioca starch [18], dry matter and soluble solid of durian [19], pectin constituents of Japanese pear [20], salt content in canned sardine in oil [21]. However, there was no a report of the use of NIR spectroscopy to evaluate biomass characteristic as an alternative energy. Recently, many research projects are undergoing to discover the possibilities of the near infrared spectroscopy to forecast the heating value of biomass [11,22,23,24,25,26], thermal properties and biomass composition of biomass [27,28,29,30]. Xue et al. [13] successfully used on-line measurement of proximate and lignocellulose components of corn stover using near infrared spectroscopy, provided coefficient of determination (R^2) of 0.75, 0.84, 0.68, 0.66, 0.77, 0.62, and 0.61 for moisture content, ash, volatile matter, fixed carbon, cellulose, semi-cellulose, and lignin, respectively. From the literature review, the main advantage of NIR was cost-effectiveness and a rapid method. NIR technology can be a non-destructive sensing technique in

biomass feedstock for thermal conversion systems. Therefore, we proposed a research of 'Determination of energy characteristic of biomass using near infrared spectroscopy including pyrolysis characteristic, proximate data, higher and lower heating value'. The main purpose was to solve the problem of slow and complicated measurement. This was the first study of the NIR spectroscopy modelling for evaluation of energy properties of *Leucaena leucocephala* pellet, milled bamboo and chopped bamboo.

Goal and Objectives

The overall objective of this thesis was to predict energy characteristic of biomass processes i.e. higher heating value, lower heating value, pyrolysis characteristic, proximate data, element composition of biomass, for converting biomasses to potential fuels. The research scheme includes wood pellets, wood chips and wood powder as raw materials. The specific objectives of this research were as follows.

- To investigate the rapid non-destructive evaluation of moisture content and higher heating value of *Leucaena leucocephala* pellets using near infrared spectroscopy
- To evaluate higher heating value, volatile matter, fixed carbon and ash content of bamboo powder using near infrared spectroscopy
- To evaluate pyrolysis characteristics of milled bamboo using near-infrared spectroscopy
- To evaluate lower heating value and elemental composition of milled bamboo using near infrared spectroscopy
- To study about feasibility of evaluation pyrolysis characteristic of bamboo chips using near infrared spectroscopy
- To investigate near infrared spectroscopy as an alternative method to thermogravimetric analysis for evaluation of volatile matter of bamboo wood chips

Hypothesis to be tested

The energy characteristic of biomass including higher heating value, lower heating value, pyrolysis characteristic, proximate data, element composition have the correlation with the NIR spectral characteristic.

Scope or limitation of the study

In this research, Taramba variety of *Leucaena leucocephala* and Phamon variety of bamboo, which both are well-known and popular in Thailand, were used and NIR range of 12,500-4,000 cm^{-1} (800-2,500 nm) was selected. The moisture content and higher heating value of the *Leucaena leucocephala* pellets was investigated. The higher and lower heating value; pyrolysis characteristic; proximate data; element composition of bamboo powders was studied. The pyrolysis characteristics and volatile matter of chips were investigated.

Process of study

1. The literatures about using near infrared spectroscopy for evaluating energy characteristics were reviewed.

2. The current method including bomb calorimeter, thermogravimetric analysis, CHNS analyzer for determination of energy characteristics of biomass were reviewed.

3. The samples of biomass were collected. *Leucaena leucocephala*, variety "Tarramba" samples were collected from Nakhonrachasima Province, Thailand.; bamboo, *Dendrocalamus sericeus* cl. "Phamon" samples were obtained from the forestry plantations in Uttaradit province.

4. Samples preparation were carried on, and divided into three parts: *Leucaena leucocephala* was performed in pellets form, while bamboo was formed in wood chips and powders.

5. To scan the sample: FT-NIR spectrometer was used for scanning in diffuse reflectance mode at a wavenumber of 12,500-4000 cm^{-1} (800-2500 nm).

6. The referenced value of samples were determined including higher heating value by bomb calorimeters; proximate data and pyrolysis characteristic by thermogravimetric; CHNS by CHNS analyzer; moisture content by dry oven; and lower heat value and oxygen content by calculation.

7. The model was optimized using with partial least squares (PLS) regression using the test set validation method. The samples were randomly sub-divided into 80% for the calibration sample set and 20% for the validation sample set. Spectrum preprocessing was performed by the constant offset elimination; straight line subtraction; vector normalization, min-max normalization; multiplicative scatter correction (MSC); first derivatives, second derivatives; first derivatives + straight line subtraction; first derivatives + vector normalization and first derivatives + MSC techniques.

8. The NIRS models (regression data) were developed using the NIR spectra and the energy characteristic obtained from reference data, by partial least square regression (PLS) for predicted energy characteristic. The models were optimized by partial least squares regression (PLSR) with 80% of samples for the calibration set and 20% for the validation set. Performance's models were indicated by statistics term, coefficient of determination (R^2), standard error of prediction (SEP), the ratio of standard error of prediction to standard deviation (RPD), and bias.

9. The results of thesis were summarized.

References

[1] The Power Department Plan (PDP). [Online]. Available:http://www.dede.go.th/ewt_w3c/ewt_dl_link.php?nid=43412. Accessed on 15 January, 2017.

[2] Department of Alternative Energy Development and Efficiency Minister of Energy. [Online]. Available: (http://www.dede.go.th/download/state_59/frontpage_jan_dec59.pdf). Accessed on 15 January, 2017.

[3] Bioenergy in thailand. Published by: Netherlands Embassy in Bangkok Follow us on Facebook (Netherlands Embassy in Bangkok) and LinkedIn (ASEAN Business Dialogue) Ministry of Foreign Affairs, September 2016.Pp 1-2. [Online]. Available: https://www.rvo.nl/sites/default/files/2017/03/FACTSHEET%20BIOENERGY%20IN%20THAILAND.pdf. Accessed on 6 April, 2017.

[4] Power pellet. Biomass. [Online]. Available: http://www.renewableenergy-asia.com/Portals/0/seminar/Presentation.pdf. Accessed on 7 April, 2017.

[5] Keeratiurai P., Phankasem P., Prempree T., Patamatamkul S. and N. Tanee. "Carbon Sequestration of Fast Growing Tree." **European Journal of Scientific Research, ISSN 1450-216X.** vol. 81(4), 2012. Pp. 459-464.

[6] Demirbas A. "Potential applications of renewable energy sources, biomass combustion problems in boiler power systems and combustion related environmental issues." **Prog. Energ. Combust,** vol. 31,2005. Pp. 171-192.

[7] Hein K.R.G., Bemtgen J.M. "EU clean coal technology, co combustion of coal and biomass." **Fuel Process. Technol.,** vol. 54, 1998. Pp. 159-169.

[8] Spliethoff H. and Hein K.R.G. "Effect of co-combustion of biomass on emissions in pulverized fuel furnaces." **Fuel Process. Technol.,** vol. 54, 1998. Pp. 189-205.

[9] Yin C-Y. "Prediction of heating values of biomass from proximate and ultimate analyses." **Fuel,** vol. 90, 2011. Pp. 1128-1132.

[10] Jenkins BM., Baxter LL., Miles Jr TR. and Miles TR. "Combustion properties of biomass." **Fuel Process Technol,** vol. 54, 1998. Pp. 17-46.

[11] Posom J., Shrestha A., Saechua W. and Sirisomboon P. "Rapid non-destructive evaluation of moisture content and higher heating value of *Leucaena leucocephala* pellets using near infrared." **Energy, vol.**107, 2016. Pp. 464-472.

[12] Posom J., Sirisomboon P., Funke A., Heinrich J., Maier J. and Griesheimer P. "Near infrared spectroscopy as an alternative method to thermogravimetric analysis for evaluation of volatile matter of bamboo wood chips." **The 9th TSAE International Conference.** 2016. Vol. EE-01. Pp. 1-7.

[13] Xue J., Yang Z., Han L., Liu Y., Liu Y. And Zhou C. "On-line measurement of proximate and lignocellulose components of corn stover using NIRS." **Applied Energy,** vol. 137, 2015. Pp. 18-25.

[14] Rhén C., Öhman M., Gref R. and Wästerlund I. "Effect of raw material composition in woody biomass pellets on combustion characteristics." **Biomass Bioenergy,** vol. 31, 2007. Pp. 66–72.

[15] Xu F., Yu J., Tesso T., Dowell F. and Wang D. "Qualitative and quantitative analysis of lignocellulosic biomass using infrared techniques: A mini-review." **Applied energy**, vol. 104, 2013. Pp. 801-809.

[16] Acquah GE., Via BV., Fasina O.O. and Eckhardt LG. "Non-destructive prediction of the properties of the forest biomass for chemical and bioenergy applications using near infrared spectroscopy." **J. Near Infrared Spectroscopy**, vol. 23, 2015. Pp. 93-102.

[17] Kaewsorn K. and Sirisomboon P. "Study on evaluation of gamma oryzanol of germinated brown rice by near infrared spectroscopy." **Journal of Innovative Optical Health Sciences**, vol. 7, No. 4, 2014. 1450002 (7 pages). DOI: 10.1142/S1793545814500023.

[18] Phetpan K. and Sirisomboon P. "Evaluation of the moisture content of tapioca starch using nearinfrared spectroscopy." **Journal of Innovative Optical Health Sciences.**, vol. 8, 2015. Pp. 1-12.

[19] Onsawai P. and Sirisomboon P. "Determination of dry matter and soluble solid of durian pulp using diffuse reflectance near infrared spectroscopy." **J. Near infrared spectroscopy**. Vol. 23, 2015. Pp.167-179.

[20] Sirisomboon P., Tanaka M., Fujita S. and Kojima T. "Evaluation of pectin constituents of Japanese pear by near infrared spectroscopy." **Journal of Food Engineering**, vol. 78 (2), 2007. Pp. 701-707.

[21] Srikornkarn S. and Sirisomboon P. "Feasibility of Evaluation of Salt Content in Canned Sardine in Oil by Near Infrared Spectroscopy." **Agriculture and Agricultural Science Procedia**, (2), 2014. Pp. 381-385.

[22] Preece S.L.M., Auvermann B.W., MacDonald J.C. and Morgan C.L.S. "Predicting the heating value of solid manure with visible and near-infrared spectroscopy." **Fuel**, Vol. 106, 2013. Pp. 712–717.

[23] Everard C.D., McDonnell K.P. and Fagan C.C. "Prediction of biomass gross calorific values using visible and near infrared spectroscopy." **Biomass and Bioenergy**, vol. 45, 2012. Pp. 203-211.

[24] Gillespie G.D., Everard C.D. and McDonnell K.P. "Prediction of biomass pellet quality indices using near infrared spectroscopy." **Energy**, vol. 80(1), 2015. Pp. 582-588.

[25] Zhang K., Zhou L., Brady M., Xu F., Yu J. and Wang D. "Fast analysis of high heating value and elemental compositions of sorghum biomass using near-infrared spectroscopy." **Energy,** vol. 118, 2017. Pp. 1353-1360.

[26] C. Huang, L. Han, Z. Yang, X. Liu. "Prediction of heating value of straw by proximate data, and near infrared spectroscopy." **Energy Conversion and Management.**, vol. 49, 2008. Pp. 3433–3438.

[27] Karlinasari L., Sabed M., Nyoman I. and Wistara J. "Near infrared (NIR) spectroscopy for estimating the chemical composition of (Acacia mangium willd.) wood." **J Indian Acad Wood sci.** vol. 11(2), 2014. Pp. 162-167.

[28] Murphy PT., Moore KJ., Raman DR., Anex RP. and Fales SL. "Rapid biomass quality determination of corn stover using Near-infrared reflectance spectroscopy." **Bioenergy Res.**, vol. 5, 2012. Pp. 79-85.

[29] Sanderson MA., Agblevor F., Collins M. and Johnson DK. "Composition analysis of biomass feedstocks by near infrared spectroscopy." **Biomass and Bioenergy**, 11 (5), 1996. Pp. 365-370.

[30] Acquah GE., Via BK., Fasina OO. and Eckhardt LG. "Non-destructive prediction of the properties of forest biomass for chemical and bioenergy application using near infrared spectroscopy." **J. Near infrared spectroscopy,** vol. 23, 2015. Pp. 93-2012.

Literature review

Characteristic of biomass

Biomass is fuels obtained from organic materials, which is oldest source of renewable energy. Biomass garneres much interest due to the increase in worldwide energy demand. At present, due to climate change, biomass is interesting topic than ever because of the increasing demand for energy [1]. Biomass is collected from plant material (include agricultural waste or fast growing plants) and animal waste. They can be used as alternative resource of energy through generating via thermal conversion process. Thermal conversion process is thermal systems converting biomass material to be energy production. Biomass can be converted to energy by direct combustion for providing heat to generate steam production used for the process of generating electric power, by gasification to provide a fuel gas which is clean gas, by fast pyrolysis to provide a liquid fuel [2], and slow pyrolysis giving bio-char. The advantage of fuel in liquid form is easy to store and transfer, while bio-char is convenient use in household. Figure 1 shows three forms of the marketing fuel products obtained from three main thermal processes including combustion, gasification and pyrolysis [3].

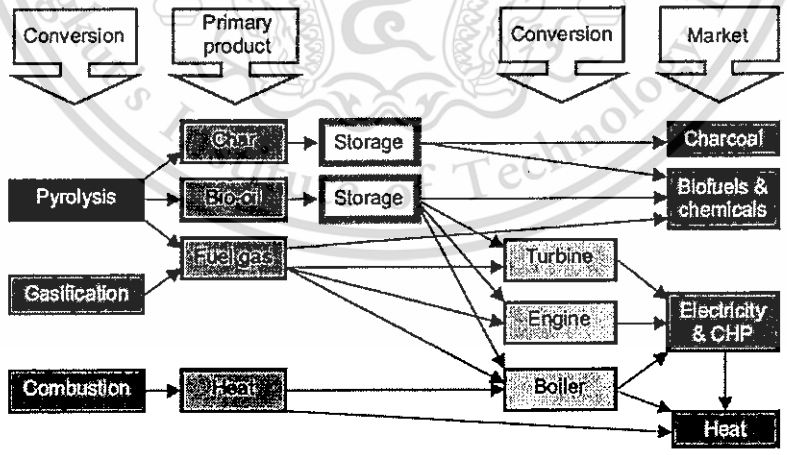

Figure 1 Products from thermal biomass conversion [3]

The pyrolysis process gives three products such as bio-char, bio-oil, and fuel gas. The main propose of gasification is to generate the clean fuel gas, and combustion provide the heat

for boiler. To convert the biomass to fuel energy, the energy characteristics is required. The characteristic of biomass incudes:

Heating value (HV)

The HV has been called either calorific value or heat of combustion. HV is the total energy of biomass releasing when it is burned.HV is divided into higher heating value (HHV) and lower heating value (LHV). The energy content or HV is one of the most necessary parameter for the use of biomass in thermal conversion systems, it is used for designing, calculating, planning and operating the thermal power plant [4][5][6][7]. The HV explains about how biomass is used to achieve process efficiency [8][9]. HHV is called gross heating value (GHV), while LHV is called net heating value (NHV). The HHV is "*the amount of heat released from combustion of a certain amount of fuel and assuming its combustion product water had returned to liquid state at the end of a measurement in which it took the latent heat of vaporization of product water into account*", meanwhile LHV is the amount of heat released under conditions that "the product water was still at vapor state and its latent heat of vaporization was not recovered" [10]. Then, LHV is the real energy without water. Generally, the HHV is determined by bomb calorimetry. HHV is normally obtained by complete combustion of fuel in bomb calorimeter, the ideal was that HHV equal to energy generating temperature increase (ΔT) of water in mass m. It is calculated by Eq. (1);

$$HHV = mc_p\Delta T \quad (1)$$

When HHV is higher heating value of biomass, m is mass of water (kg), c_p is specific heat of water (J/kg-K) and ΔT is change in temperature (K) of water. HHV is determined by the bomb calorimetric method according to DIN 51900 T3 (testing of solid and liquid fuels, determination of gross calorific value by the bomb calorimeter and calculation of net calorific value [11].

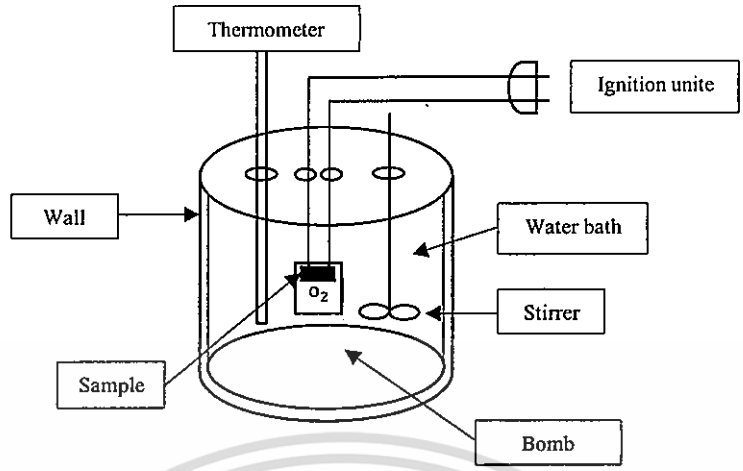

Figure 2 Construction of a bomb calorimeter [12]

Figure 2 shows construction of a bomb calorimeter: It consists of a bomb which is made by a strong cylindrical stainless steel. It is screwed to the body of the bomb to make a perfect gas tight seal. The bomb is placed by sample and filled by oxygen. For ignitions, there are two electrodes and then the electric current is released for burning the sample. Stirrer is placed in the water jacket to maintain uniform distribution of heat and thermometer is placed to measure increase in water temperature. For wall, it help to prevents heat loss due to radiation.

Bomb calorimetric can be divided into two large classes: isothermal and isoperibol calorimeters, and the adiabatic calorimeters. Wunderlich [13] explained that the isothermal calorimeter, measurements are made at constant temperature of calorimeter and surrounding. If only the surrounding is kept isothermal, the mode of operation is called isoperibol (equal surround). In the isoperibol calorimeter, the temperature changes with time are governed by the thermal resistance between calorimeter and surroundings. In adiabatic calorimeters, the exchange of the heat between calorimeter and surrounding is kept close to zero by making the temperature difference small and the thermal resistance large.

The LHV is generally determined by calculating using theoretical function of the HHV via subtraction from moisture content (MC) as follows [14]:

$$\mathrm{LHW_{wb}} = \mathrm{HHV_{wb}} - 2.443\mathrm{MC} \quad (2)$$

where LHV_{wb} is the lower heating value (MJ/wet kg), HHV_{wb} is the higher heating value (MJ/wet kg), the HHV measurements were expressed on a wet weight basis (MJ/wet kg). MC is moisture content. Therefore, the LHV call "real energy content" which operate under actual operating conditions. LHV is better than HHV [15] and is defined as efficiency of thermal process.

Proximate analysis

Proximate data includes moisture content (MC), volatile matter (VM), fixed carbon (FC), and ash content (A). MC is the amount of water content in biomass. It affects to HV of biomass, the HV decrease with increasing MC. MC gave a positive effect on HHV and, conversely, it gave a negative effect on the pyrolysis and combustion process. In pyrolysis, MC negatively effect on process and quality of bio-oil such as temperature drop during pyrolysis and more water contents in bio-oil. MC into feedstock will evaporate before the feedstock will be burnt, this mean that the net energy is released during evaporation although it is useful heat. HV of biomass can increase by drying. The HV depend on MC, the HV increased with decreasing of MC [16][14]. Generally, MC is determined by drying oven (ASTM E1756-08 standard test method for determination of total solids in biomass) [17]. It usually takes time at least 24 hr.

Volatile matter (VM) is the vapor gas that is released after MC released. Biomass contain generally VM around 70-80%. The amount of VM indicates how the biomass can be gasified easily which effects the design of boiler and gasifier [18]. Both A and FC remain constant after of the volatilization. The rate of volatilization can be used to evaluate liquid fuel and gas fuel rate in the fast pyrolysis and gasification process, respectively. In fast pyrolysis, heavy VM gas will be condensed to be liquid fuel and light gas will be released. Amount of VM can evaluate the ability of the feedstock used in pyrolysis and gasification that if any biomass contain of more VM, that biomass should be used. Due to diferent biomass contains different VM, the design reactor's capacity, process development of pyrolysis and combustion involve with VM [19]. The commercial market of biomass to be energy purpose involve amount of VM as reference for setting price instead of weight. Generally, VM can be determined by muffle furnace as standard method i.e. American Society for Testing and Materials (ASTM E872-82, 2006) for particular wood fuels [20].

For fixed carbon (FC), its composition consists the most of carbon content, high carbon content is higher heating value, and high FC content usually provide high capacity of combustion process. In fast pyrolysis, FC and A is solid residue after biomass volatilizes at high temperature, and the FC in fuel woods remains in the char form before combusted to ash [21]. For slow pyrolysis, coal char is the main product and the biomass is volatilizes at low temperature (approximately 400 C°). It is expected that this process want to obtain more coal char. The coal char consists of carbon, volatile and ash for 75%, 10%, and 5% [22], respectively. Then, FC of biomass can be used for setting price instead of weight. FC can be calculated as FC=100-(MC%+VM%+A%) as as-received base.

Ash is the solid residue after FC burned. Ash content (A) effects to HV of biomass, higher A give low HV. In addition, it was negative effect of storage and transportation because it has no energy content. Generally, A content can be determined using muffle furnace method following American Society for Testing and Materials (ASTM E1755-01 (2007), is standard test method for ash in biomass [23]. The major constituents of ash of biomass are the silica, aluminum, iron and calcium, small amount of magnesium, titanium, sodium, and potassium [21], then it make trouble for waste systems due to it become to fouling and slagging.

The proximate data and HHV of the raw material for biomass feedstock was demonstrated in Table 1. The HHV of biomass feedstock including *Leucaena leucocephala*, palm shell, wood and bamboo gave high HHV. They are suitable to use in power combustion process.

The MC content was the range of 5.43 to 60%, while VM was in range of 16-84%, they may use in pyrolysis and gasification. The biomass in which consists of much water content, invlove the drying cost and preparing time. The lignite bituminous coal contained low VM, however it had more FC, so it is suitable for combustion. Bamboo and sawdust contain more VM about 80%, so they can be good raw material in pyrolysis and gasification process. The A of bamboo, bagasse, parawood, palm trunk, palm leaf, tapioca rhizome, and *leucaena leucocephala* is lower than 2%. The highest A is found in the rice husk about 26% by weight. The big problem is the waste management , because it need big storage area. The biomass is suitable to be alternative energy must give the high

HHVand low ash content. The biomass is easy to ignite and burn due to general high VM and low ash [24]. Then, they should be invested for being source of energy.

Table 1 Specific properties of the raw material for biomass

Material	MC	VM	FC	A	HHV (MJ/Kg)
Bituminous coal (Armutck)[b][25]	-	32.81	62.83	4.36	-
Coconut husk[b][26]	5.43	61.15	29.70	3.72	17.35
Rice husk[b][26]	8.20	51.10	14.40	26.30	13.24
Sugarcane bagasse[b][27]	4.99	73.5	19.1	2.41	17.44
Cotton stalks[b][27]	9.14	64	22.2	4.66	15.92
Empty fruit bunch (EFB)[a][28]	8.2	74.2	12.8	4.8	18.4^{LHV}
Palm kernel shell (PKS)[ac][28]	5.4	71.1	18.8	4.7	16.3^{LHV}
Groundnut cake (MJ/Kg)[29]	5.6	83	6.6	4.8	15.00
Wood[22]	3.5	77.4	16.6	2.5	17.8
Bamboo[1]	6.14	83.95	16.05	1.95	17.87
Sawdust[1]	10.81	83.12	16.88	2.58	16.63
Rice Husk[30]	12.05	56.98	18.88	12.73	14.638
Rice Straw[30]	10.12	60.87	18.80	10.42	13.275
Bagasse[30]	50.76	41.99	5.86	1.75	9.664
Cane Trash[30]	9.34	67.78	16.90	6.23	16.342
Parawood[30]	45.32	45.67	7.71	1.70	10.112
Palm Fiber[30]	38.57	42.53	14.39	4.55	13.279
Palm Shell[30]	12.12	68.31	16.30	3.66	18.446
Empty Fruit Bunch[30]	58.67	30.52	8.90	2.09	9.265
Palm Trunk[30]	48.34	38.98	11.70	1.34	9.370
Palm Leaf[30]	78.34	16.42	4.60	0.72	3.889
Corncob[30]	40.11	45.55	13.68	0.95	11.198
Corn Stalk[30]	41.69	46.98	8.14	3.80	11.634
Tapioca Rhizome[30]	59.78	31.09	8.10	1.69	7.423
Eucalyptus Bark[30]	60.09	28.02	9.56	2.33	6.723
Bamboo Gimsung (*Bambusa Deecheyama*)[30]	14.30	63.10	18.90	3.70	15.700
Bamboo Tong (*Dendrocalamus asper*)[30]	5.80	71.70	19.80	2.70	17.585
Pseudosasa amabilis and *Pleioblastus chino* bamboo [31]	-	-	-	-	19.4–19.9
Leucaena leucocephala[32]					
Cunningham	-	-	-	1.69	19.91
Tarramba	-	-	-	2.01	19.87
Peru	-	-	-	1.69	19.91
Leucaena leucocephala pellets[33]	7.59	72.91	17.55	1.96	17.69-18.12*

[b]=(wt% on air dry basis), [a]=(wt% on pre-dry basis), [ac]=(wt% on as received), * Chotchutima et al. [34]

Due to the long time consumption and cost imply with proximate data by American Society for Testing and Materials method [21. The alternative method by thermogravimetry (TG) is used to determine proximate data, it is direct method. This technique, the small sample is used and heated. Figure 3 demonstrated the thermal behavior of biomass carried on with TGA by recording the weight loss as a function of time and temperature, the TG curve sorts out in terms of its MC, VM, FC and A. The accuracy of proximate data obtained by TGA and standard method and TGA investigated by García et al. [35]. The results showed that the error criteria results were satisfactory with the average experimental error under 6% for MC and VM, and close to 10% for FC.

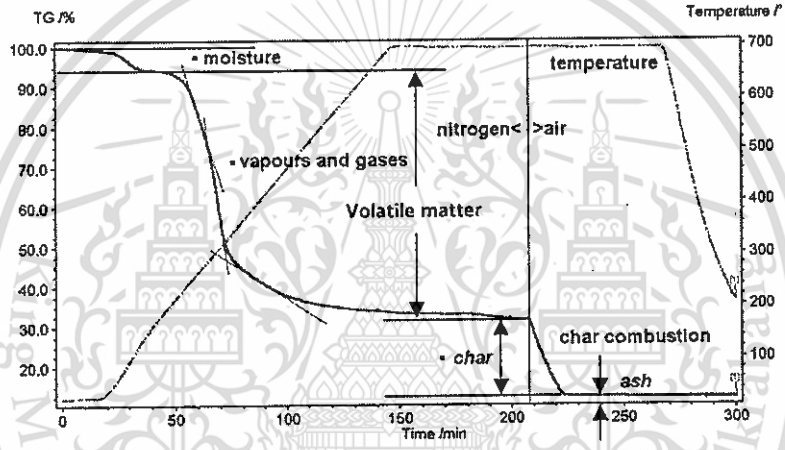

Figure 3 Thermal behavior of biomass carried on by TGA [36]

The sample (100% weight) were heated from 20 to 700 °C with 150 min by injecting N_2 into the system. The first shoulder is the mass loss which is MC (temperature at around 20-130 °C), and when keep the temperature at 700 °C for about 60 min to ensure compeleted pyrolysis. From process, the VM can be determined. Then, inject promptly the O_2 instead of N_2, the mass burned instantly, and keep 700 °C with O_2 for 1 hour to ensure compeleted combustion. The residue is the ash.

Elemental compositions

The commercial biomass concerning about the design of biomass conversion systems and critical atmosphere pollutants, it was indicated by analytical element coefficients for feedstock, and understanding for behavioral biomass degradation [7]. The elemental compositions of biomass including carbon (C), hydrogen (H), nitrogen (N),

oxygen (O), and sulfur (S) is expressed as C+H+O+N+S+A=100%. It has been essential for operating the overall thermal process and necessary to caculate heat content and heat balance of the process [37]. The detailed chemistry describing the behavioural reaction, use for estimating the flue gas flow rate or O_2/air requirement for complete combustion, meanwhile estimating the flue gas component in pyrolysis and gasification also required the percentage of chemistry component [5]. In combustion reaction, carbon content is used to estimate the O_2 flow rate to balance the ratio between C and O. The combustion of carbon presents $C+O_2=CO_2$-394 MJ/kmol, mean that 1 kmol of carbon was burnt in the air completely, it will produce 394 MJ heat [21]. If O or air is underload, the reaction will involve with incomplete combustion, the process will appear CO releasing to atmosphere. For firing fuel, S and N of feedstock become oxide emissions for the combustion such as SO_x, NO, and NO_x, they will release in atmosphere, and lead to acid rain precursors and greenhouse effect [21]. Moreover, high A in combustion also come from high S content, lead to fouling and slagging. Runge et al. [38] mentioned that C and H content depend upon the increasing of HV while high O content lead to decreasing HV. For pyrolysis, decomposition of the biomass can be described as [21]:

$$C_nH_mO_p \rightarrow \sum_{liquid} C_aH_bO_c + \sum_{gas} C_xH_yO_z + \sum_{solid} C \quad (3)$$

when n, m, p, a, b, c, x, y and z are the number of molecules. C is solid residue, contain the most carbon or bio-char. The biomass were volatilized and were condensed to be condensable gasses i.e. liquid oil and water. When elemental composition of biomass is known, therefore, non-condensable gases can also be estimated. The elemental composition is determined generally with CHNS analyzer. The sample is burnt into combustion chamber with a pure oxygn atmosphere, the gases (CO_2, N_2, SO_2, H_2O) obtained from combustion are separated by thermoconductometer detector and elemental composition are reported [37]. Table 2 illustrated the comparision of element composition for some biomass. The high C content were bituminous coal lignite, coconut husk, bamboo and wood, they were suitable for combustion due to providing high HV. While the low C content was in the group of cornstalk rice straw rice hull rice husk. Bamboo was low in the oxygen-to-carbon, low H/C and O/C was high HV. In currently commercial market, biomass feedstock is sold or bought by weight (price/kg) [39]. On

above mention, the different biomass properties lead to different energy charactieristic such as HV, elemental data and proximate data. To determine prices of biomass can set using elemental composition as the percent of C, H, O, N, S or H/C, O/C. For example, if feedstock contains higher C and H, it will set to be higher price. On the contrary, with feedstock is high N, O and S, they will sell for less price.

Table 2 Comparision of element composition for some biomass

Material	C	H	N	O	S	H/C	O/C
Coconut husk[b][26]	50.29	5.05	0.45	36.63	-	0.100	0.790
Rice husk[b][26]	35.60	4.50	0.19	33.40	-	0.130	0.790
Bituminous coal (Armutck)[b][25]	86.27	4.67	1.19	7.24	0.63	0.650	0.060
Sugarcane bagasse[b][27]	41.98	6.04	0.53	48.87	0.24	0.144	1.140
Cotton stalks[b][27]	41.44	5.84	1.43	46.44	0.17	0.141	1.080
Empty fruit bunch (EFB)[a][28]	48.20	6.49	0.47	31.74	0.10	-	-
Palm kernel shell (PKS)[ac][28]	48.06	6.38	1.27	34.10	0.09	-	-
Groundnut Cake[29]	46.37	7.02	6.89	39.44	0.287	1.820	7.852C/N
Bamboo[1]	50.52	6.04	0.58	42.80	0.09	1.425	0.636
Sawdust[1]	44.19	6.03	2.47	46.80	0.54	1.626	0.795
Rice straw[40]	44.20	6.20	0.80	48.80	-	-	-
Rice husk[40]	44.40	6.80	0.00	48.80	-	-	-
Cornstalk[ad][24]	37.95	6.47	0.77	40.76	0.59	-	-
Rice straw[ad][24]	36.55	5.49	0.78	40.01	0.56	-	-
Rice hull[ad][24]	36.31	4.05	0.51	22.90	0.12	-	-
Sawdust[ad][24]	45.55	5.42	0.60	33.31	0.17	-	-
Sorghum[37]	41.07	5.13	1.01	51.61	1.19	-	-
Wood[22]	48.80	5.20	1.40	44.60	-	-	-
Leucaena leucocephala[34]	44.13-4.35	7.05-7.38	0.55-0.92	47.48-47.87	0.07-0.08	-	-

[b]=(wt% on air dry basis), [a]=(wt% on pre-dry basis), [ac]=(wt% on as received), ad=as received.

Pyrolysis characteristic

Pyrolysis is a thermochemical degradation of biomass occurring in the complete absence of oxygen [41][21]. Pyrolysis is used for generating biomass into fuel energy and chemical products. Its products consist of bio-oil (liqud oil), solid biochar and gas [42]. Pyrolysis divided into fast and slow pyrolysis. Slow pyrolysis is carbonization, its result is

to maximize the charcoal or char. For fast pyrolysis, its goal is to maximize the production of liquid bio-oil [21]. The pyrolysis characteristics, i.e., T_{onset}, T_{sh}, T_{peak}, T_{offset}, and DTG_{peak}, are demonstrated in Figure 4. El-Sayed and Mostafa [27] mentioned about pyrolysis behavior that "*T_{onset} was the extrapolated onset temperature calculated from the partial peak that results from the decomposition of the hemicellulose component, T_{sh} was the temperature corresponding to the overall maximum of the hemicellulose decomposition rate, DTG_{peak} was the overall maximum of the cellulose decomposition rate (dm/dt at the highest peak, wt loss %/min), T_{peak} was the temperature corresponding to the overall maximum of the cellulose decomposition rate and T_{offset} was the extrapolated offset temperature of the DTG_{peak} curves determined using thermogravimetric analysis (TGA)*".

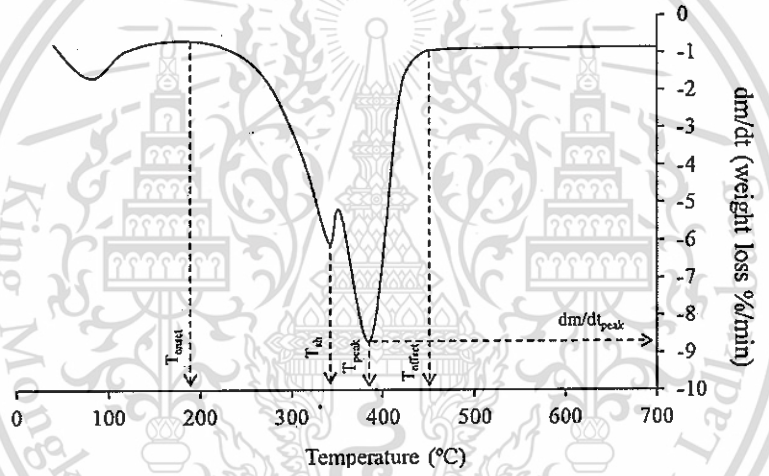

Figure 4 DTG profile for material's characteristic properties based on thermal degradation [43]

Pyrolysis characteristics are estimated by differential thermogravimetric (DTG). TG curve is determined by thermogravimetric analysis (TGA). This curve was totality of overall elemental component decomposing in the process. After that, TG curve is differentiated to obtain DTG curve, then pyrolysis properties peaks will appear as the Figure 4. These respects is used to operate the thermal conversion process during pyrolysis. T_{onset} is the starting decomposition of biomass, this respect is required to know when the biomass is decomposed and it helps to set the gas condensate collection time. T_{peak} is the maximum degradation. If biomass is decomposed at T_{peak}, the process will produce the maximum gas production rate equaling to DTG_{peak}. The temperature equaled to T_{offset}, has no

degradation of biomass. If process is heated over than T_{offset}, it involes about the cost of capital energy. In addition, many researchers have mentioned about pyrolysis behavior as follows: Wannapeera et al. [44] and Lv et al., [45] mentioned that proportions of element compositions effect the pyrolysis behaviour. For example, high lignin is slow degradation, high hemicellulose and cellulose provided fast degradation [44], [45], [46] [47]. High cellulose provides high yields of bio-oil; high hemicellulose content provided high gas yields; and high lignin content provided high charcoal residue [48]. Yang et al. [49] reported that hemicellulose was degrated at 220–315 °C, cellulose was decomposed at 315–400 °C, and lignin was slowly degrated in a wide range between 160 to 900 °C. Then, the pyrolysis behavior of biomass depends on the elemental component of biomass. Table 3 demonstraed the pyrolysis characteristics of biomass. It can be seen that each biomass has different degradation. Then, to understand the degradation behavior is important to achieve efficiency of thermal conversion.

Table 3 The pyrolysis characteristics of coal and some biomass

Material	T_{onset} (C°)	T_{sh} (C°)	T_{max} (C°)	DTG_{max} (% min^{-1})	T_{offset} (C°)
Bituminous coal (Armutck)[25]	350	-	460	-1.710	600
Bituminous coal (Amasra)[25]	350	-	450	-1.373	680
Sugarcane bagasse[27]	140	219.73	325.36	-0.192	520
Cotton stalks[27]	150	286.647	438.24	-0.114	525
Empty fruit bunch (EFB)[a][28]	258	-	436	-	-
Palm kernel shell (PKS)[ac][28]	260	-	330	-	-
Pinewood sawdust (PW)[50]	172.40	-	340.37	-	567.24
Fern (*Dicranopteris linearis*) stem (FS)[50]	141.47	-	321.79	-	588.00
Wheat stalk (WS)[50]	154.82	-	326.60	-	581.16
Sugarcane bagasse (SB)[50]	157.40	-	350.79	-	573.17
Jute (*Corchorus capsularis*) stick (JS)[50]	157.22	-	340.38	-	554.85
Lemno[51]	144	245	307	-	570
Spirodela[51]	150	-	322	-	560
D. tertiolecta A[51]	98	265	332	-	690
D. tertiolecta B[51]	125	-	288	-	600
E. prolifra[51]	162	261	319	-	596
Bamboo fibres[52]	-	285.14	336.73	-1.0362	-
Giant[53]	198	-	336	-0.748	-

Above demonstrated the important of biomass characteristics involving the high efficiency of thermal conversion process. Certainly, the rapid; accurate, low cost operation; environmental friendly and safety is needed to compensate the current method. Then, near infrared (NIR) protocol is required due to more advantages sush as it takes only 2-3 minutes per sample, the maximum accuracy of its protocol can be equivalent to reference method, no chemical is used when the NIR models are used. It is safely technique for employee and the operating cost per sample is inexpensive. NIR provided at low cost (from 200 to 1 USD) and reduced the time (from 100 to 1 min) for predicting HHV and element composition [37]. The several reseachers have been investigated on NIR spectroscopy as an alternative technique for predicting of biomass properties such as corn stover and switchgrass [54], sweet sorghum [55], switchgrass [56], and *Jatropha curcas* L. kernels [57]. The other studies showed in Table 4, the predicted moisture content of

biomass using NIR spectroscopy. Table 5 showed the predicting of ash content and Table 6 illustrated the HHV. For VM and FC of corn stover was investigated by Xue et al. [19], they showed that NIR spectroscpy is possible to predict volatile matter with R^2 of 0.68 and 0.66, RMSEP of 9.92 and 7.83 g kg^{-1}, respectively. The overall results showed that predicted moisture contents have provided a good result, and the performance depend on the particle size. If its particle size is too small, they will give mostly good result than bigger size. The famous scanning mode is used of diffuse reflectance mode and the absorbance is in the unit of log [1/R] because biomass had high solid density, transmittance mode is not suitable because transmittance provided as a weak signal. The developing method is optimized with using partial least square regression. The moisture content is prominent parameter to be well predicted by NIR spectroscopy. A few research reported on proximate data and there has been no pyrolysis characteristic and element composition predicted via NIR spectroscopy method.

Table 4 Predicted moisture content of biomass using NIR spectroscopy

Material	Absorbance	NIR region	Particle size	SD/range	R^2	SEP/RMSEP /RMSECV
Biomass[1][58]	log (1/R)	1140-2500 nm^{PLS}	1 mm	2.25%^{sd}	0.95	0.51
coal[59]	log (1/R)	1680, 1942, 2100, 2180, 2300 nm^{MLR}	Under 2mm, 2-5 mm, over 5 mm	7.83-18.99 %^{rs}	-	1.74%
wheat straw[60]	log (1/R)	400-2500 nm^{PLS}	1 mm screen	3.08-11.42%^{rs}	0.91	0.691%^{cv}
Miscanthus xgiganteus and short rotation coppice willow[61]	log 1/R	750-1100 nm	<3 mm	-	0.99	0.90%^{cv}
Jatropha curcas[62]	log (1/R)	4000-12500 cm^{-1}	Whole kernel	25.4% wb^{sd}	0.96	4.0% wb
Wood pellets[2][63]	Reflectance	400 nm - 2500 nm	-	0.63-14.16% wb^{rs}	0.95	0.670 % wb
wood, *Miscanthus* and herbaceous energy grasses pellet[64]	Reflectance	900-1700 nm^{PLS}	Dia. 6 mm	9.11%^{rs}	0.85	0.73^{cv}
corn stover[19]	Diffuse reflection	12,000 and 4000 cm−1^{PLS}	shorter than 50 mm	25.97–70.02 g/kg ^{rs}	0.75	3.76 g/kg

[1]switchgrass (*Panicum virgatum* L., 56 samples), sugarcane bagsse (*Saccharm* spp., 4 samples), corn stover (*Zea mays* L., 13 samples), lespedeza [*Lespedeza cuneate* (Dum.-Cours.) G.Don, 18] and various

wood species [*Eucalyptus* spp., 3 samples; hybrid poplar (*Populus* spp., 18 samples); American sycamore (*Platanus occidentalis*, 3 samples); black locust (*Robinia pseudoacacia*, 6 samples)]

Table 5 Predicted ash content of biomass using NIR spectroscopy

Biomass	Absorbance	NIR region	Particle size	SD/range	R^2	SEP/RMSEP /RMSECV
Biomass[1][58]	log (1/R)	1140-2500 nm^{PLS}	1 mm	2.25% ^{sd}	0.95	0.51
coal[59]	log (1/R)	1680, 1942, 2100, 2180, 2300 nm ^{MLR}	Under 2mm, 2-5 mm, over 5 mm	7.83-18.99 %^{rg}	-	1.74%
Wheat straw[60]	log (1/R)	400-2500 nm^{PLS}	1 mm screen	3.08-11.42%^{rg}	0.91	0.691%^{cv}
Miscanthus xgiganteus and short rotation coppice willow[61]	log 1/R	750-1100 nm	<3 mm	-	0.58	0.42%^{cv}
Biomass pellet[64]	Reflectance	900-1700 nm^{PLS}	Dia. 6 mm	6.22%^{rg}	0.82	0.62^{cv}
Corn stover[19]	Diffuse reflection	12,000 and 4000 cm^{-1} ^{PLS}	shorter than 50 mm	42.99–125.27 g/kg ^{rg}	0.84	7.55 g/kg

[1]switchgrass (*Panicum virgatum* L., 56 samples), sugarcane bagsse (*Saccharm* spp., 4 samples), corn stover (*Zea mays* L., 13 samples), lespedeza [*Lespedeza cuneate* (Dum.-Cours.) G.Don, 18] and various wood species [*Eucalyptus* spp., 3 samples; hybrid poplar (*Populus* spp., 18 samples); American sycamore (*Platanus occidentalis*, 3 samples); black locust (*Robinia pseudoacacia*, 6 samples)]

Table 6 Predicted higher heating value of biomass using NIR spectroscopy

Biomass	Absorbance	NIR region	Particle size	SD/ range	R^2	SEP/RMSEP/RMSECV
Straw[6]	Log (1/R)	400 – 2498 nm	4–5 cm long	815.09 Jg^{-1} ^{sd}	0.95	173.64 Jg^{-1} ^{cv}
coal[59]	Log (1/R)	1680, 1942, 2100, 2180, 2300 nm ^{MLR}	Under 2mm, 2-5 mm, over 5 mm	702.91 Jg^{-1} ^{sd}	-	532.04 Jg^{-1}
Miscanthus xgiganteus and short rotation coppice willow[61]	Log 1/R	750-1100 nm	<3 mm	-	0.99	130 Jg^{-1} ^{cv}
biomass pellet[64]	Reflectance	900-1700 nm	Dia. 6 mm	326 Jg^{-1} ^{rg}	0.94	240 Jg^{-1} ^{cv}
Jatropha curcas[62]	Log (1/R)	4000-12500 cm^{-1}	Whole kernel	950 Jg^{-1} ^{sd}	0.86	360 Jg^{-1}
Sorghum[37]	Reflectance	6000–7000 cm^{-1}	Ground 0.5 mm	270 Jg^{-1} ^{sd}	0.96	61 Jg^{-1}

^{cv} *cross validation*, ^{sd}*standard deviation*, ^{rg}*range*, ^{MLR}*multiple linear regression*, ^{PLS}*partial least square regression*

Near infrared (NIR) spectroscopy

This chapter demonstrate a literature review of NIR technology including its history, principle, background, theory, optimizing method, models and performance analysis.

History and Background

In the 1800, Willaim Herschel who was the musician and astronomer, did experiments by the sunlight that was divided into various particular color, and he want to know that how was the different heat capacity between any particular light color. During his experiment, he discovered that beyond red color which was in the end of spectra provided the highest heat [65]. He did not believe that it was light because the position at beyond red color was pellucid. Then, he also called 'heat radian'. Until in 1835, Ampere illustrated that it was only different wavelength in light and he also called "infrared radiation" [66]. In the 1960, there were many papers reported about NIR analysis and demonstrated the evaluation of water in various liquids, led the NIR spectroscopy interested to be new method [67]. At the same time, Karl H Norris started and succeeded to use spectroscopic method such as visible and NIR including transmittance and reflectance, for determination of bio-agriculture sample such as leave and grains. This century regarded as the first use for analytical methods. After that, in 1970 there many researchers further studied and published the use of NIR spectroscopy with food and agricultural product. This was the big use for NIR spectroscopy, which led to develop the NIR instruments [68].

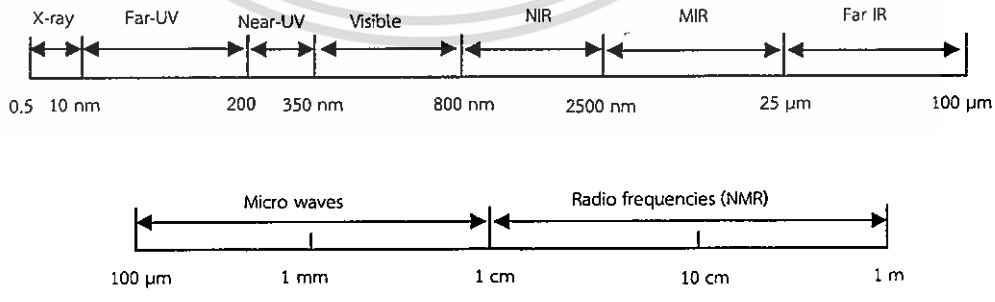

Figure 5 Electromagnetic spectral regions [68]

Figure 5 demonstrated the electromagnetic spectral regions. The NIR region covers in the range of approximately 800-2500 nm, and MIR is between 2500-25000 nm. The NIR region is related to overtones and combinations of fundamental vibrations of C–H, N–H, O–H and S–H functional groups [69]. In the obvious developments, NIR was not famous due to its overlapping peaks and difficult to analyze. However, in present this problem can be solved using the chemometrics evaluation methods. "Chemometrics" is multivariate calibration. There are more advantages in of chemometrics in analytical chemistry, compared to the previous univariate calibration [70]. The classical calibration method used only one spectral data point, but chemometric used whole spectra. This advantage was that all information in analyte were considered. At present, NIR and chemometric can improve the efficiency of both qualitative and quantitative analysis. NIR spectroscopy is method that use the near infrared region of electromagnetic field to find the answer in matter [71]. But the weakness is that, if concentration of the analyte is less than about 0.1% of the total composition into sample, the results are not acceptable [72], due to other peaks hide the peak of analytes. NIR spectroscopy have been famous technique, it is the one of sensor to determine the quality parameter of food and agricultural products e.g. moisture content of tapioca starch [73], dry matter of durian [74], salt content in canned sardine [75].

The fundamental of NIR spectroscopy is the creation of the models using measured data obtained from reference method and NIR spectra. After that, the model was validated by unknown spectra and its corresponding. The goal of NIR spectroscopy, is to know the calibration function, when $Y_{pre}=X_{un}*b$, where Y_{pre} is the predicted value, X_{un} is spectra of unknown, and b is regression coefficient. The b-coefficient value is constant value and very important, or we can call "models". The aim of multivariate analysis (MVA) method, such as multiple linear regression (MLR), principal component regression (PCR), and partial least regression (PLS), want to determine the final b-coefficient, when it multiply with spectra of unknown, we can predict the predicted value as a nearby measured value. The both predicted value and measured value were compared, and mathematical performance were invested, i.e. coefficient of determination (R^2), root mean square error of calibration (RMSEC), root mean square error of validation (RMSEP), standard error of calibration (SEC), standard error of validation (SEP), residue prediction deviation (RPD), and Bias. Their

mathematical term was used to consider its models whether they should be use for predicting or not. The procedure for NIR spectroscopy illustrated in Figure 6.

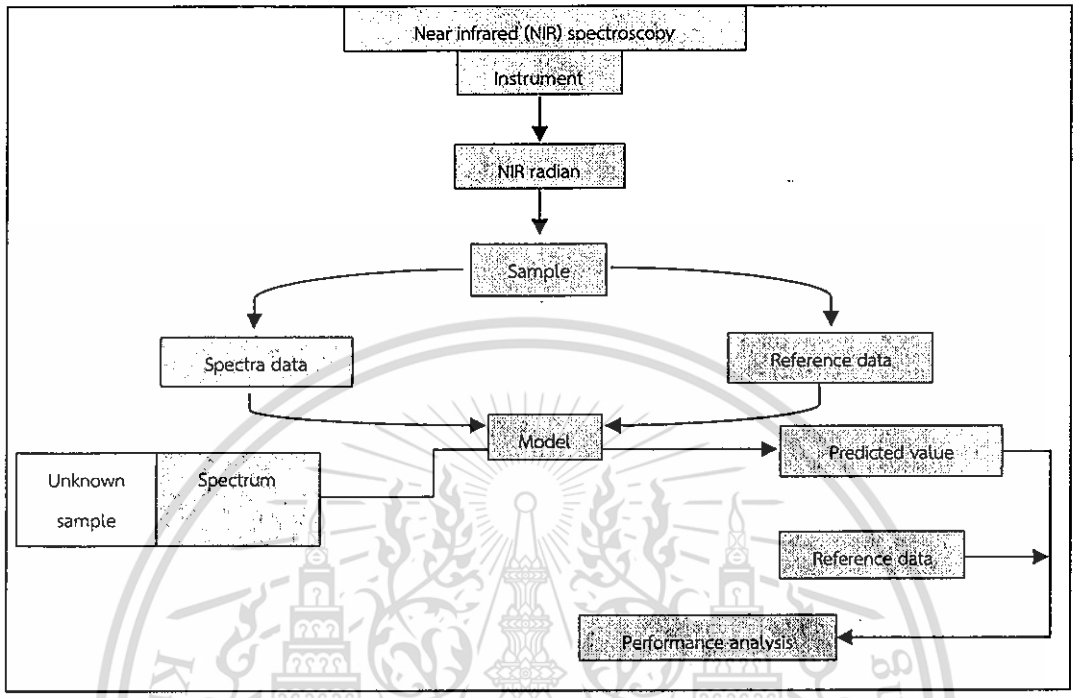

Figure 6 The procedure for near infrared spectroscopy

Why is NIR used in the future?

NIR spectroscopy is a fast, low-cost, easy-to-use, non-destructive, reliable and versatile analytical method [65]. Only 2-3 min are needed for measurement without sample preparation. Mcclure [76] stated that it provided four advantages over other kinds of spectroscopy;

1) It is fast method with very little sample preparation. In addition, a spectrum can be obtained only by 30 seconds.
2) It is nondestructive method. The same sample can be retained for other analytical procedures or returned to the population.
3) It is multi analytical. More than one constituent can be determined from a single scan or spectrum.
4) It is not depended on highly skilled personnel to operate the instrument.

Theory and Principle

Basic laws and NIR interaction with matter

The scientists have tried to describe how the interaction between lights and objects are. The understanding of its behavior is going to help for improving the measuring technique. When the light beam emits on the sample's surface, one part of beam was absorbed via object, or one part transferred though out the sample, or one part of light cannot emit through surface and then 100% reflected back, or one part of beam go inside, it scattered and reflected back to the surface [77].

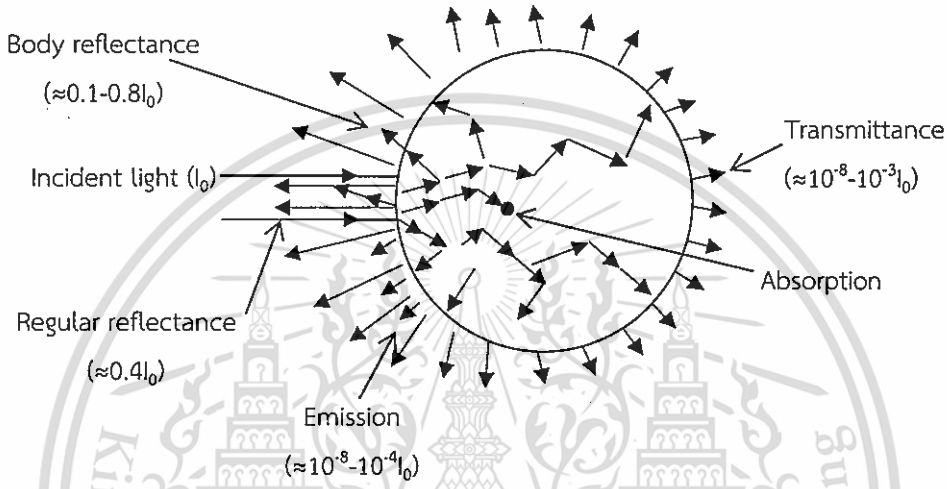

Figure 7 Simplified schematic drawing showing the interaction between light and sample [77]

In order to understand the interaction between light and sample (see Figure 7), Birth [78] explained that the incident light (I_0) falls down on sample. There were four parts of interaction i.e. regular reflectance, emission, body reflectance, absorption and transmittance. He measured the intensity after interaction and found that the beams intensity of regular reflectance, emission, body reflectance, and transmittance were about 0.4I_0, 10^{-8}-$10^{-4}$$I_0$, 0.1-0.8$I_0$, and 10^{-8}-$10^{-3}$$I_0$, respectively. The intensity remaining of beam scattered deeply into sample, it was absorption. The regular reflectance was the no light emitted through the surface and then it will be reflected back of 100 percent. The maximum intensity after interaction was the body reflection and the minimum was the transmittance. Then, the information into samples was intensely taken out of object by body reflectance, while radiation intensity via transmittance was weakest. The transmittance mode required high-intensity of light source [77]. Therefore, the suitable light source and detector is very important for measuring method. Transmission spectroscopy is the oldest. It is the

basic infrared method which is based on absorption radiation at specific wavelength as it passes through the sample [79]. Considering in Figure 8, the monochromatic radiation (I_0) is shined into the sample, I_A was the absorbance, I_T was the transmittance and I_R was the reflectance. The sum of all radiant power must be equal to (I_0), equation is defined as [67]

$$I_0 = I_T + I_R + I_A \tag{4}$$

The ideals of transmittance mode, I_R presents to zero. There are no lights reflect back to surface of sample. Therefore, when detector detected the signal of transmission mode. Transmittance (T), is defined as [80];

$$T = \frac{I_t}{I_0} \tag{5}$$

When, I_0 is the incident intensity, and I_t is the transmittance intensity. However, absorbed energy cannot be directly measured, but can be collected by measuring all the non-absorbed energy (transmittance, T). The mechanism of absorbance techniques use Beer-Lambert law, it supposes that I_R equal to zero [67]. Absorbance (A) defined as $A=\log_{10}(1/T)$. Then, we can know A if we know I_t or I_R.

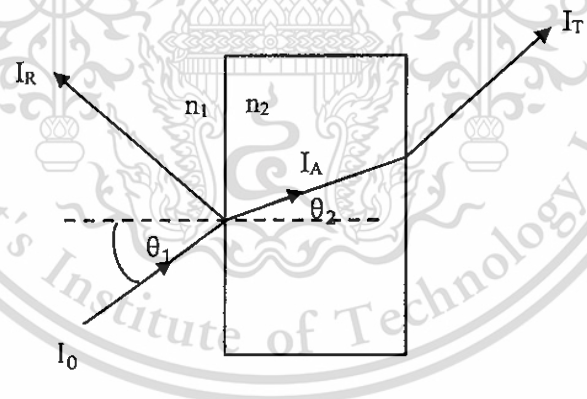

Figure 8 Interaction of radiation with matter [67]

Due to body reflectance is high intensity, reflectance is usually easier to use for analyzing the quality of agricultural products and is widely used. Either the high light intensity of light or the high sensitive of detector do not need. Its intensity is higher than signal of noise. Body reflectance can call 'diffuse reflectance'. The reflectance method is used when it is difficult to analyze by normal transmission. Specially, diffuse reflectance was considered where light penetrates one or more particle and

reflected in all directions [67]. Kubelka and Munk optimized a theory explaining the diffuse reflectance mechanism for powder sample [79]. The equation that developed by Kubelka and Munk was defined as [81]

$$F(R_\infty) = \frac{(1-R_\infty)^2}{2R_\infty} = \frac{k}{S} \quad (6)$$

Where $F(R_\infty)$ is the Kubelka and Munk (K-M) function or value. R_∞ is the absolute reflected light of an infinitely thick sample, s is the scattering coefficient and k is the molar absorption coefficient. R is defined by $R_\infty = I_R/I_0$, I_R is intensity of reflect light and I_0 is intensity of incident light. For diffuse reflectance, the function was assumed for infinitely thick sample. The thickness of samples have to be thick enough for ensuring that its diffuse reflectance intensity will not change when increase the thickness. In addition, the scattering coefficient (s) is pretended that it is constant at any wavelength of all spectrum, and scattering coefficient depend on particle size or path length [82].

When $R_\infty < 0.01$, the alternative function that is $\log 1/R_\infty = kc$ (c is the concentration and k is the absorption coefficient) is usually used in NIR diffuse reflectance spectroscopy, because small R_∞ value is generally found in the NIR region [83]. The manly ideal was the portion between the reflectance of standard and diffuse reflectance of sample, i.e. log ($\dot{R}/R$), when $\dot{R}$ is the reflectance of standard (equal to 1: it was assumed that reflection was 100 percent), R is diffuse reflectance of sample [67]. Then the information in the object can be fully taken out to be the diffuse NIR spectra [84] for modelling.

Modeling and performance analysis

Modeling

This subtopic lists basically the modeling method, which is divided into five step. The fundamental methodology of NIR spectroscopy was illustrated in Figure 9.

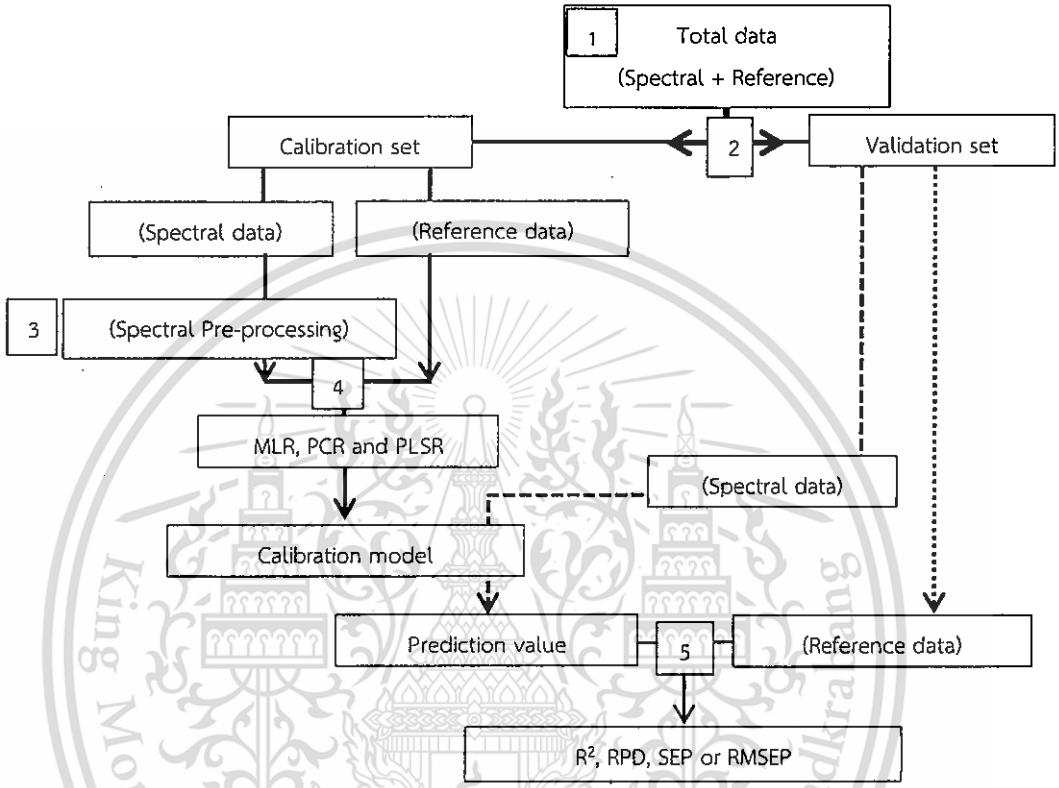

Figure 9 1) Sample scanning and reference lab 2) Data separation data for calibration set and validation set 3) Spectra preprocessing 4) Modeling 5) Validation and model performance analysis. SLR is simple linear regression, MLR is multiple linear regression, PCR is principal component regression, and PLSR is partial least square regression.

1. Sample scanning and reference lab

The first step of NIR spectroscopy is the sample scanning. The correctly scanning method produce the good spectrum and accurately predicted result. The type of samples presentation to NIR radian are mainly divided in to (a) transmittance, (b) reflectance, (c) specular reflectance, (d) diffuse or body reflectance and (e) interaction modes, is shown in Figure 10.

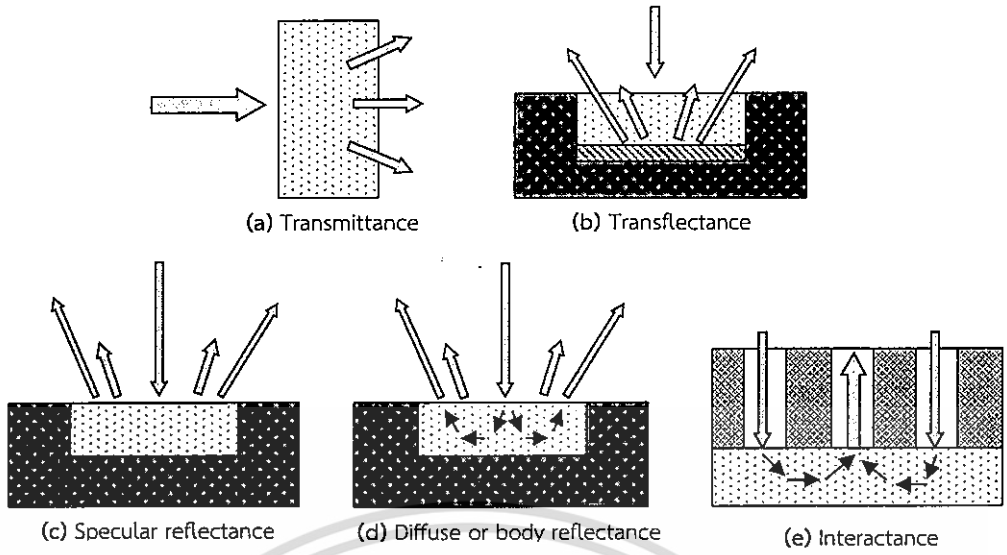

Figure 10 Five methods for obtaining NIR spectra [85]

The different types of interaction of radiation with matter was between transmittance and reflectance. Transmission is the oldest technique and basic of infrared spectroscopy. Reflection technique is a wide use at present including diffuses reflectance or body reflectance and interactance. Transflectance is the combination of transmission and reflection. In the case of interaction method, an interaction probe with a concentric outer ring of illuminate and an inner portion of receptor is used as the one side of the probe is in contact with the surface of the sample [85]. When samples are scanned by NIR spectrometer to obtain the NIR spectra, the transmitted spectra are obtained by $T = \frac{I_t}{I}$, when, I is the incident intensity, and I_t is the transmittance intensity. Meanwhile, absorbance is recorded by A=log (1/T) for transmittance mode, and either A=log(1/R) or $F(R) = \frac{(1-R)^2}{2R}$ is recorded for diffuse reflectance mode, when R is diffuse reflectance of sample.

After that the reference data of samples are immediately determined by the standard method. For example, the MC is determined by dry oven, HHV is usually determined by bomb calorimeter. Afterward references data have to check for outlier. If outliers are found, they are removed from data set. The outlier of references data is determined using $\frac{(X_i-\bar{X})}{SD} \geq \pm 3$ [86], where X_i is the measured value of sample i. $\bar{X}$ and SD were the average and standard deviation of the measured values, respectively. If the result is satisfied, the sample (i) will be removed from data set. This step, the precision of reference method and NIR

spectrometer are concerned using repeatability and reproducibility, respectively. For reference method, the repeatability is the standard deviation of the different duplicate and reproducibility is the standard deviation of the different duplicate obtained from blind samples. Then, the maximum coefficient of determination (R^2_{max}) is calculated by $R^2_{max} = \frac{SD_y^2 - Rep^2}{SD_y^2}$ [87], where SD_y is the standard deviation of measured value. R^2_{max} is used to estimate the possibility of the modeling. If there are no errors in the spectra in modeling, the coefficient of determine (R^2) is close to R^2_{max}. The R^2_{max} can be approximately notified that should be continually developed the models or not. For repeatability of NIR instrument, either one or more than one sample is re-scanned for n time, the absorbance value at obvious peak of NIR spectra are selected and collected. Then, the repeatability is the standard deviation of n absorbance value. For reproducibility, is the standard deviation of the absorbance value when that sample is re-loaded and re-scanned for n time (personal communication with Phil Williams).

2. Separations of sample set to calibration and validation sets

The samples set are divided into calibration and validation set by the ratio of, for example, 50:50, 60:40, 70:30, 80:20. If the samples number are less than 50, the model should be validated by cross validation [70]. The measured data to be calibration set have to cover the widest range of reference data.

3. Spectrum Manipulation

When the calibration set is selected, then its spectra will be pretreated. The spectral preprocessing methods help to reduce the contribution of noise or error in experiment which cannot be eliminated by the regression technique [88]. The irrelevant information was the effect of different temperature, particle size, relative humidity, human error, sample holding, and multiplicative effect of scattering. The spectra preprocessing method is described as follow.

Baseline offset

NIR spectra shift because of physical effect such as the different particle size and non-uniform and inhomogeneous. Baseline offset technique is used to correct the baseline shifted spectra. It is conducted by adjusting the data to the minimum

point. The original spectra are subtracted by minimum absorption. The formula for the baseline offset correction can be written as [89].

$$X_{SLS,i} = X_{org} - X_{min} \quad (7)$$

$X_{SLS,i}$ is the new absorbance at sample i, X_{org} is the original absorption, X_{min} is the minimum of absorption.

Multiplicative signal correction or multiplicative scatter correction (MSC)

It is used to reduce the multiplicative effect of scatter arising because of differences in particle size between samples [90]. Its original name is "multiplicative scatter correction" because it is used to reduce for types of multiplicative problem more than arising from scatter only [91]. Firstly, slope (a) and intercept (b) are calculated from regression between each individual spectrum and a reference spectrum (usually, it is used the average spectrum).

$$X = aX_{ref} + b \quad (8)$$

Coefficient a and b are used to correct each spectrum by using the expression below [90]:

$$X_{corr} = \frac{X-b}{a} \quad (9)$$

Where X_{corr} is corrected sample spectrum, X_{ref} is reference spectrum (average spectrum), X is original sample spectrum and a is slope and b is intercept.

Standard normal variate (SNV)

SNV is similar as the multiplicative scatter correction (MSC), which is used to reduce the multiplicative effect of scattering [90]. The mean and standard deviation of each spectrum is calculated, and then it is defined as:

$$X_{SNV,i} = \frac{X_i - X_{avg}}{SD} \quad (10)$$

Where X_i is absorbance for the spectrum at wavelength i, $X_{SNV,i}$ is the new absorbance as standard normal variate of each spectrum at wavelength i. X_{avg} and SD is average and standard deviation of spectrum.

Smoothing

All the spectral points are smoothen using n-point (g is gab width) average moving to reduce the effect of noise in the spectra [92]:

$$A_{new} = (A_{n-2g} + A_{n-g} + A_n + A_{n+g} + A_{n+2g})/n \quad (11)$$

Where A_{new} is the new absorbance value at the wavelength at n nm, A_n is the original absorbance in the wavelength at n nm, n is the smoothing point, and g is gap.

Centering

Mean centering is used the data set to reposition the centroid of the data to origin of the coordinate [93]. It is calculated by subtracting the average response from each individual response as follow [90]:

$$X_{mc} = X - X_{av} \quad (12)$$

X_{mc}, X and X_{av} are mean centering absorbance value of each spectrum, absorbance value of each spectrum and mean of spectra data, respectively. After this step, all means are zero and variances are spread around zero and mean centering is often powerful in resolution enhancement [93].

Normalization

There are four forms of normalization, vector normalization, mean normalization, maximum normalization and range normalization. Normalization is used to get all data in approximately to same scaling [94]. Vector and mean normalization are the popular normalization procedures [93], the normalization is written as [94]:

$$X_{vector,nor} = \frac{X_i}{\sqrt{\sum X_{i,k}^2}} \quad (13)$$

$X_{vector,nor}$ is normalization absorbance value of each variable, X_i is absorbance value of each variable, k is number of variable.

$$X_{mean,nor} = \frac{X_i}{X_{mean}} \quad (14)$$

$X_{mean,nor}$ is mean normalization absorbance value of each variable, X_i is absorbance value of each variable, X_{mean} is mean of spectra data.

$$X_{max,nor} = \frac{X_i}{X_{max}} \quad (15)$$

$X_{max,nor}$ is maximum normalization absorbance value of each variable, X_i is absorbance value of each variable, X_{max} is mean of spectra data.

$$X_{range,nor} = \frac{X_i}{X_{i,max} - X_{i,min}} \quad (16)$$

$X_{range,nor}$ is range normalization absorbance value of each variable, X_i is absorbance value of each variable, X_{min} is minimum of spectra data.

Derivatives

This method has been used in NIR spectroscopy. The first derivative is use to reduce difference in baseline shift, while second derivative use to reduce difference

in slope and separate overlapped peak, however higher order derivative is not recommended because they increase noise in the signal and reduces its magnitude [90].

Hruschka [95] and Ozaki et al. [93] described that a derivative spectrum is an expression of derivative value, $d^nA/d^n\lambda$ (n=1,2,...), of a spectrum $A(\lambda)$ as a function of λ. The first derivative is written as $dA/d\lambda$, second derivative is written as $d^2A/d^2\lambda$ and third derivative is written as $d^3A/d^3\lambda$. Transformations to first, second and third derivative are then

$$dA_n = A_{n+g} - A_{n-g} \quad (17)$$

$$\begin{aligned} d^2A_n &= d\left(A_{n+g} - A_{n-g}\right) \\ &= A_{n+2g} - 2 * A_n + A_{n-2g} \end{aligned} \quad (18)$$

$$\begin{aligned} d^3A_n &= d\left(A_{n+2g} - 2 * A_n + A_{n-2g}\right) \\ &= A_{n+3g} - 3 * A_{n+g} + 3 * A_{n-g} - A_{n-3g} \end{aligned} \quad (19)$$

Where dA_n, d^2A_n and d^3A_n is first, second and third derivative at point n, g is an integer called the gap or derivative size and A_n is the log(1/R) value at point n.

4 The calibration Model

There are several methods to optimize the calibration model. This step discusses three method including multiple linear regression (MLR) , principal component analysis (PCR) and partial least square regression (PLS).

Multiple linear regressions (MLR)

Mark [9 6] described that: when several independent variables (x) were used to predict a dependent variable (y), it is called a multiple regression. It is advance regression than simple regression. The idea of MLR is $y=y_{pre}+e$, when y, y_{pre}, and e is the matrix of analyte concentration, predicted analyte concentration and residue matrix, respectively. The solution forms $y_{pre}= xb$, when b is regression coefficient matrix. Then b can estimate from $b=x^+y$, where x+ is the pseudo-invers of x, x+ is calculated by $(x^Tx)^{-1}x^T$, and x is independent variable (absorbance value). The prediction of dependent variable (y_i) was calculated by $y_{pre}= x(x^Tx)^{-1}x^Ty$, and $y= x(x^Tx)^{-1}x^Ty+ e$. If the matrix of x contain of noise, the term of $(x^Tx)^{-1}$ will provide double noise. We can see that MLR is unstable when the independent variable contains noise.

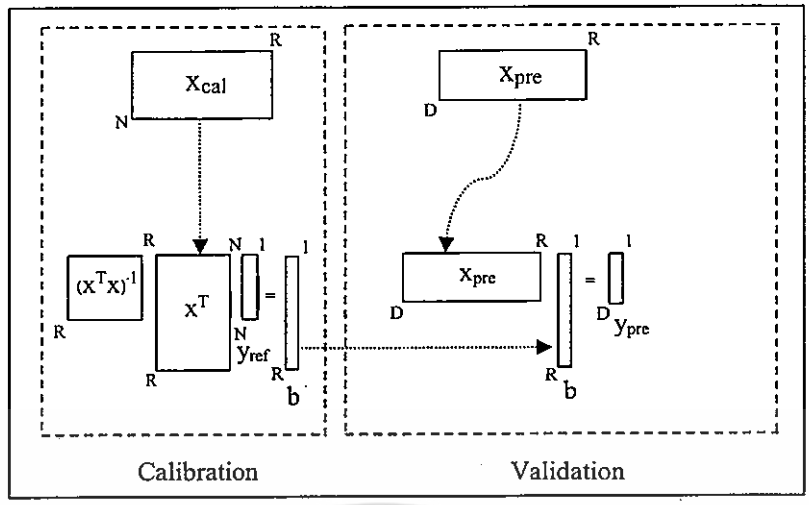

Figure 11 Schema for the calibration of a multiple linear regression model and the prediction of new sample. Step: (1) Calculation of regression vector. (2) Prediction of the property of the new sample. N and D is number of sample for calibration and validation set, R is wavelength.

Figure 11 is the overall of MLR concept. Firstly, the data set is separated to calibration set and validation set. After that, regression coefficient matrix (b) will be calculated by calibration set as

$$b = (x_{cal}^{T}x_{cal})^{-1}x_{cal}^{T}y_{cal} \quad (20)$$

Secondly, regression coefficient matrix will be used to calculate the predicted value (y_{pre}) as

$$y_{pre} = x_{pre}b \quad (21)$$

Principal component regression (PCR)

1) Rotational axis and principal component analysis (PCA)

Rotational axis base on principle component analysis, it was explained by Krzanowski [97], Figure 12 demonstrated the effect of rotating axes around the coordinates of the midpoint (point O). The point M has coordinates (x_1,x_2), refer to the original axes lines OX_1, OX_2, respectively. When the axes OX_1, OX_2 are anticlockwise rotated through an angle of θ to be the new axes i.e. OT_1, OT_2, the new coordinates of M become to (t_1,t_2) when refer to new axes OT_1, OT_2, respectively.

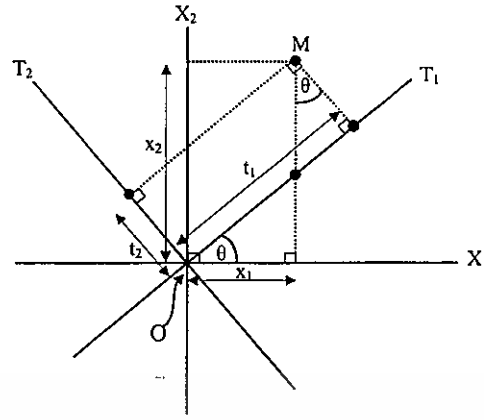

Figure 12 Effect of a rotation of axis on the coordinates of a point [97]

Thus, if we know the coordinate (x_1, x_2) at point M which referred to a pair of orthogonal axis, and we can deduce its new coordinates (t_1, t_2) when the axis is anticlockwise rotated through an angle θ. The coordinates (t_1, t_2) of new axis relate the original axis (x_1, x_2) as follows:

$$t_1 = x_1\cos\theta + x_2\sin\theta \tag{22}$$

$$t_2 = -x_1\sin\theta + x_2\cos\theta \tag{23}$$

$T=[t_1,t_2,..,t_a]$, $X=[x_1,x_2,...x_a]$, $P=[p_{11},p_{12},..,p_{1a}]$, then $T=XP$, when a is number of axis,

and x_1 and x_2 can convert to the coordinate (t_1, t_2) as:

$$x_1 = t_1\cos\theta - t_2\sin\theta \tag{24}$$

$$x_2 = t_1\sin\theta + t_2\cos\theta \tag{25}$$

$$X=TP^T \tag{26}$$

The relationship between P and P^T are presented as

$$PP^T = P^TP = I \tag{27}$$

where I is a identify matrix, T is a score matrix (new coordinate), P is a loading weight matrix, and P matrix is orthogonal with P^T.

PCA is widely used in data-processing. It is a famous and dimension-reduction technique, with numerous applications in engineering, biology, and social science [98]. Næs[2] et al. [99] noticed that "it is a method of data reduction or data

compression". The PCA can be conducted using rotational axis. PCA is similar to singular value decomposition (SVD), the SVD forms $X=USV^T$, when T=US and P=V, while PCA forms $X=TP^T+E$. The matrix X (n×a) is the independent variable (absorbance value), it was decomposed as $X=\sum_1^R T_R P_R^T$: n is number of sample, and a is number of wavelength. The matrix of X can write as $X=\sum_1^k T_k P_k^T+E$, when k<R, k is the number of reduced factors, E is residue between $\sum_1^R T_R P_R^T$ and $T_k P_k^T$, then $\lim_{k\to R} T_k P_k^T \approx \sum_1^R T_R P_R^T$. Then the number of factor of X matrix will be reduced from a to k.

2) Perform multiple regressions (MLR)

PCR is based on the basic concept continuing from principal component analysis (PCA) [99]. The PCR is combination between PCA and MLR. The data set contain of dependent variable (Y or analyte concentration) and independent variable (X or absorbance value). In Figure 13, the matrix of X is converted to new coordinate using PCA technique and called "score matrix (T)". The information in $X(x_1, x_2)$ of two dimensions is compressed down in t line (Figure 13). It is the reduced process from many variables to a few components. The components t is used as independent variable, it is regressed with y as dependent variable [99]. After that the score matrix is related linearly with dependent variable for obtaining regression coefficient matrix by MLR.

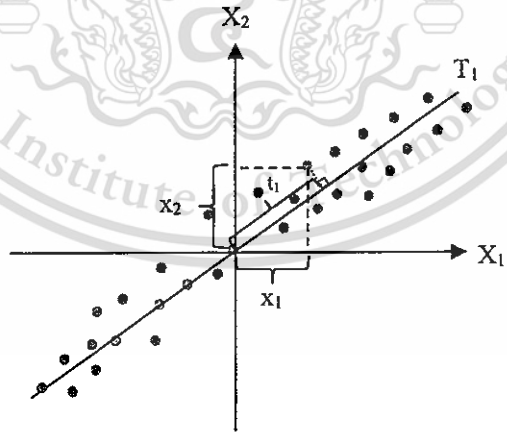

Figure 13 The projection from two dimensions to one [97]

The data set of X is the matrix of spectral in dimension of N×R, N is the sample number, and R is number of wavelength. The matrix X is constructed as [90]

$$X = T_R P_R^T = T_k P_k^T + E \quad (28)$$

, when k<R, E is the residue matrix of variance between variance $T_R P_R^T$ and $T_k P_k^T$. T_a is new dimension called score matrix (N×k), P is called loading (k×R) and E is called residue matrix of model (N×R). X can be presented by its score matrix as

$$T_k = XP_k \tag{29}$$

Matrix of referenced value (Y) can be calculated by regressing Y against T:

$$Y = T_k b + F \tag{30}$$

Where Y is dependent data (N×1), b is regression coefficient matrix (N×1) that is obtained from least square regression by multiple linear regressions, F (N×1) is residue, is defined a:

$$b = (T_k{}^T T_k)^{-1}(T_k{}^T Y) \tag{31}$$

The step of principal component analysis is shown in Figure 14 and obtained as:

1) Decomposition of independent variable calibration data matrix in score and loading matrix. 2) Calculation of regression vector (using MLR) of calibration set. 3) Projection of prediction spectral into calibration space. 4) Prediction of the property of the new sample. Where T* is score matrix of prediction set, X_{pre} and X_{cal} are absorption spectra of prediction set and calibration set, Y_{pre} is predicted value of prediction set and Y_{ref} is reference value of calibration set.

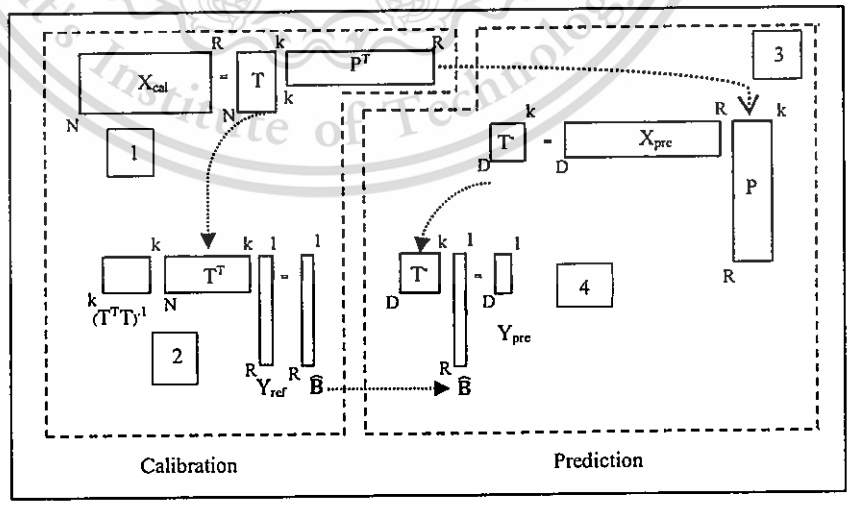

Figure 14 Schema for the calibration of a PCR model and the prediction of new sample [90]

Partial least squares regression

PLS regression is a technique that combines the properties of principal component analysis (PCA) and multiple linear regressions (MLR), it is a method for relating two data matrices X and Y by a linear multivariate model (Wold et al., 2001). PLS is constructed of the relationship of two matrices X and Y by score vectors and is based on the basic latent component decomposition [100] and both matrices can be decomposed as:

$$X = \sum_{a=1}^{a} t_R p_R^T = TP^T + E \quad (32)$$

$$y = \sum_{a=1}^{a} t_R q_R^t = TQ^T + F \quad (33)$$

P and Q is called X-loading and Y-loading, is used to describe that how the variables in T related to matrixes X and Y [99], respectively. E and F is residue matrix of X and Y, respectively. T is called score matrix or latent component. For PLS and PCR, a matrix of score T can be defined by X matric and weight matrix (W) as covariance of y and T must be the maximum. Then, the weight matrix (W) can write as:

$$w=\frac{X^T y}{\|X^T y\|} \quad (34)$$

and score T can be calculated as:

$$T = Xw \quad (35)$$

From equation 2.56, data set is any dimension, Q^T will be defined as:

$$Q^T = (T^T T)^{-1}(T^T Y) \quad (36)$$

The regression coefficient matrix (B) can be estimated as a function of loadings of X, Y and P and Q, respectively, in addition to W(X) [90]:

$$B=W(P^TW)^{-1}Q^T \quad (37)$$

Then predicted valued matrix is calculated as:

$$\hat{Y} = X_{pre}B = X_{pre}W(P^TW)^{-1}Q^T=X_{pre}W(P^TW)^{-1}(T^TT)^{-1}(T^TY) \quad (38)$$

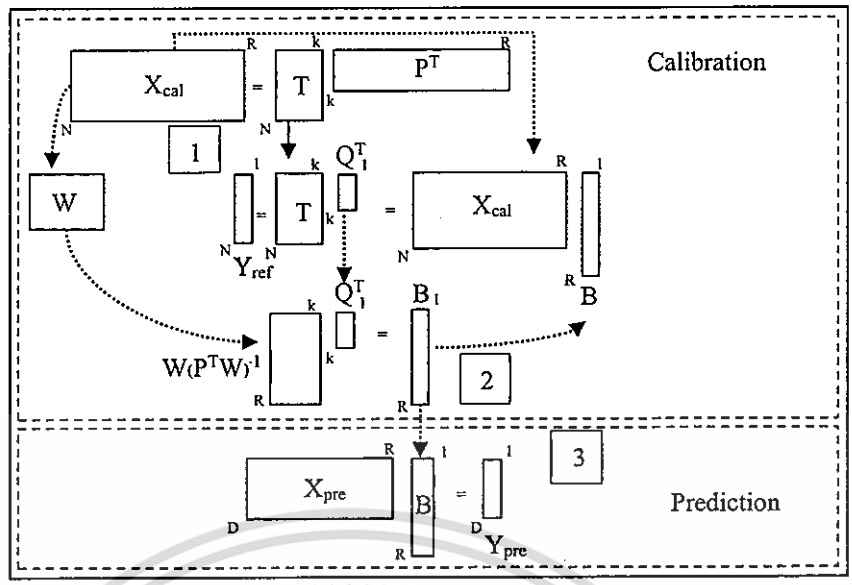

Figure 15 Schema for the calibration of a PLSR model and the prediction of new sample [90]

In Figure 15 shows the procedure for the calibration of a PLSR model. The first step is decomposition of X and calculation of weight matrix, second step is calculation of regression matrix of calibration set. The third step is prediction of prediction set.

Performance analysis

When calibration equation is calculated, it is needed to determine the performance of prediction model. There are two types of validation including internal validation or cross validation and external validation or test set validation. The step by step of a cross validation is shown with Figure 16 [70] and it is described as:

1. A sample is removed from a data set.

2. Calibration model is computed from the remaining samples.

3. Removed sample is analyzed by calculate the error of analysis for this sample: $y_{cv,i} - \hat{y}_{cv,i}$

4. Removed sample is returned to the data set and then a new sample is removed and calculate new model and predict new sample: $y_{2-cv,i} - \hat{y}_{2-cv,i}$

5: Repeat step 4 until all samples of the calibration data set were removed. Then the root mean square error of cross validation is calculated.

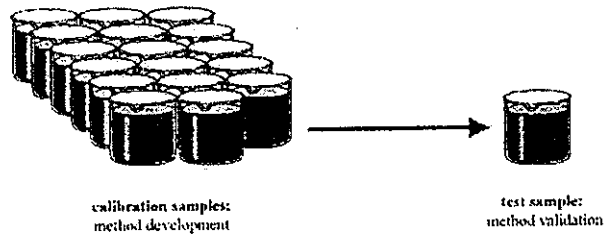

Figure 16 Schematic of cross validation [70]

Root mean square of cross validation (RMSECV) is one of parameter that implies a performance of modeling and is defined as:

$$\mathrm{RMSECV} = \sqrt{\frac{\sum_{i=1}^{N}(\hat{y}_{cv,i} - y_{cv,i})^2}{N_t}} \quad (39)$$

When $\hat{y}_{cv,i}$ is prediction value of cross validation test and $y_{cv,i}$ is measurement value of cross validation test set and N_t is number of total sample.

For external validation set, the total data set is divided to calibration set and validation set. It will be built when the data set is more than 50 samples. The calibration model will be created by calibration set and then it will be validated by validation set. It is essential to know the performance of model. The performance of the model was indicated by the coefficient of determination (R^2), root mean square error of calibration (RMSEC), root mean square error of prediction (RMSEP), ratio of prediction to deviation (standard error of validation to the standard deviation, RPD) and bias.

Coefficient of determination (R^2). It is the proportion of explained variance to total variance. Williams [84] described that "it is the showing of percentage of variance in X data that can be explained by the variance in the Y data". For unexplained variance is attributable to other factor. It cannot be controlled such as sample preparation, reference testing etc. Figure 17 shows the scatter plots of the comparison of measured by the reference laboratory technique and predicted by near-infrared (NIR) spectroscopy.

Considerably, $P(\hat{y}_i, y_i)$ is the scatter plots between of y_i (measured value) and $\hat{y}_i$ (predicted value). The residue (e) is the difference between the measured and predicted as can be defined as:

$$e = y_i - \hat{y}_i \tag{40}$$

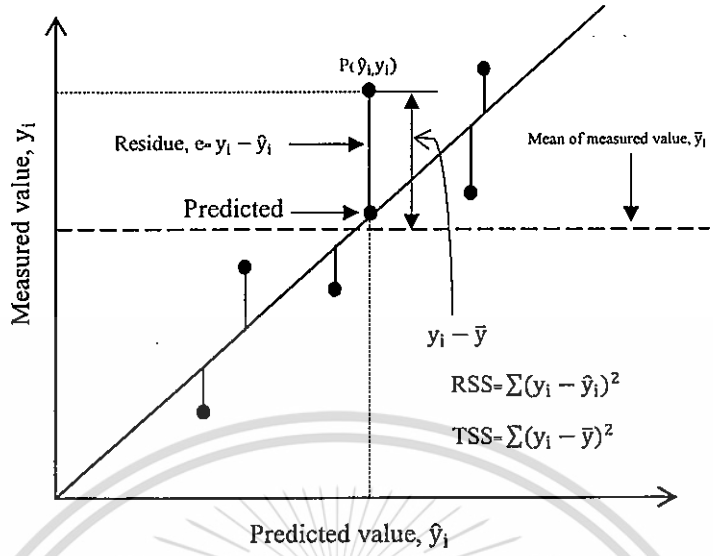

Figure 17 Comparison of measured by the reference laboratory technique and predicted by near-infrared (NIR) spectroscopy [67]

e^2 is called the sum squared of residuals (SSR) or sum of squared errors of prediction (SSE), it can be written as:

$$SSR = e^2 = \sum(y_i - \hat{y}_i)^2 \tag{41}$$

While sum squares of the difference of the measured value and its mean is called total sum square (TSS). It can be written as:

$$TSS = \sum(y_i - \bar{y})^2 \tag{42}$$

SSR is called "unexplained variance", TSS is called "total variance" and $TSS - SSR$ is called "explained variance".

The coefficient of determine (R^2) can be calculated as:

$$R^2 = 1 - \frac{SSR}{TSS} = 1 - \frac{(y_i - \hat{y}_i)^2}{(y_i - \bar{y})^2} = \frac{(y_i - \bar{y})^2 - (y_i - \hat{y}_i)^2}{(y_i - \bar{y})^2} \tag{43}$$

y_i is measured value, $\bar{y}$ is mean of measured value, $\hat{y}_i$ is predicted value. For example, if R^2 equals to 90, this means that 90% variance of reference data can be explained by NIR spectra data, and 10% was the unexplained variance. Zornoza et al. [101] suggested about R^2 that "*the model provides excellent prediction if $R^2 > 0.90$ and good prediction if $0.81 < R^2 < 0.90$ and it permits only approximate prediction if $0.66 < R^2 < 0.80$ and were poorly predicted if $R^2 < 0.66$ and RPD < 2*".

Williams [84] guided about the use of R^2 as follow Table 7.

Table 7 Guidelines for the Interpretation of R^2 [84]

R^2	Interpretation
Up to 0.25	Not usable in NIR spectroscopy calibration
0.26-0.49	Poor correlation, reason should be researched
0.50-0.64	OK for rough screening
0.66-0.81	OK for screening and some other " approximate" calibrations
0.83-0.90	Usable with caution for most applications, including research
0.92-0.96	Usable in most applications, including quality assurance
0.98+	Excellent, usable in any application

For validation based on the validation set, the performance was explained by root mean square of prediction (RMSEP), it is defined as

$$\mathrm{RMSEP} = \sqrt{\frac{\sum_{i=1}^{N_p}(\hat{y}_{ip}-y_{ip})^2}{N_p}} \tag{44}$$

when $\hat{y}_{ip}$ is prediction value of prediction set and y_{ip} is measurement value of prediction set and N_p is number of sample in prediction set. RMSEP is the average uncertainty that can be expected for forecasting of future sample [88]. It is a qualitative measure for the accuracy of the analysis.

Bias is one of the most important parameter to imply the model performance. It is the mean difference between predicted data and measured data. It measures the overall accuracy of the calibration model [84] and can be calculated as:

$$\mathrm{Bias}_p = \frac{\sum_{i=1}^{N_p}\hat{y}_{ip}-y_{ip}}{N_p} \tag{45}$$

SEC is the standard deviation of error of calibration. It shows the standard deviation of the different between measured value and predicted value of calibration set. It can be calculated as:

$$\mathrm{SEC} = \sqrt{\frac{\sum_{i=1}^{N_c}(\hat{y}_{ic}-y_{ic}-\mathrm{Bias}_c)^2}{N_c-1}} \tag{46}$$

For validation set is written as:

$$SEP = \sqrt{\frac{\sum_{i=1}^{N_p}(\hat{y}_i - y_i - Bias)^2}{N_p - 1}} \quad (47)$$

RPD is the Ratio of SEP to the SD (standard deviation of measured value of validation set). It is a qualitative measure for the assessment of the validation results. It is calculated by

$$RPD = \frac{SD}{SEP} \quad (48)$$

where SD is the standard deviation of the measured valued of the validation set, and SEP is the standard deviation of error of the validation set. If RPD is low, its means are narrow reference data or high SEP, then model is not necessary [84]. The guideline for RPD have recommended by researcher such as:

Williams [84] recommended for RPD that "*if the model provided RPD between 0.0 and 2.3, its use is not recommended, RPD between 2.4 and 3.0 could be used for very rough screening, RPD between 3.1 and 4.9 could be used for screening, RPD between 5.0 and 6.4 could be used for quality control, RPD between 6.5 and 8.0 could be used for process control; and RPD>8.1 could be used for any application*".

Zornoza et al. [101] suggested about R^2 and RPD that "*the model provides excellent prediction if RPD>3 and good prediction if 2.5 < RPD < 3, and it permits only approximate prediction if 2.0 < RPD < 2.5 and were poorly predicted if RPD < 2*".

Nicolaï et al. [88] guided that "*RPD between 1.5 and 2 means that the model can discriminate low from high values of the response variable; a value between 2 and 2.5 indicates that coarse quantitative predictions are possible, and a value between 2.5 and 3 or above corresponds to good and excellent prediction accuracy*".

The RPD^2 is:

$$RPD^2 = \frac{SD^2}{SEP^2} \quad (49)$$

Substitute SEP in Eq. 47

$$RPD^2 = \frac{\Sigma(y_i - \bar{y}_i)^2/N_p - 1}{\sum_{i=1}^{N_p}(\hat{y}_i - y_i - Bias)^2/N_p - 1} \quad (50)$$

And then, if bias very less≈ 0. Equation 50 become as:

$$R^2 = 1 - \frac{1}{RPD^2} \quad (51)$$

This is shown that $R^2 \propto RPD^2$. $RMSEP^2$ can be defined by

$$RMSEP^2 \approx Bias^2 + SEP^2 \quad (52)$$

and become as:

$$\frac{\sum_{i=1}^{Np}(\hat{y}_i - y_i)^2}{N_p} \approx \left[\sum_{i=1}^{Np} \frac{\hat{y}_i - y_i}{N_p}\right]^2 + \frac{\sum_{i=1}^{Np}(\hat{y}_i - y_i - \sum_{i=1}^{Np} \frac{\hat{y}_i - y_i}{N_p})^2}{N_p - 1} \quad (53)$$

$$\frac{\sum_{i=1}^{Np}(\hat{y}_i - y_i)^2}{N_p} \approx + \frac{\sum_{i=1}^{Np}(\hat{y}_i - y_i)^2}{N_p - 1} \quad (54)$$

Correlation coefficient (R) shows the performance of model. It is the correlation coefficient between the predicted and measured, defined as:

$$R = \left[\frac{(SD)^2 - (RMSEP)^2 x \frac{N}{N-1}}{(SD)^2}\right]^{1/2} \quad (55)$$

where SD is the standard deviation of measured value (y_i). S_{ref} is standard error of the laboratory of reference method and is defined as:

$$S_{ref} = \sqrt{\frac{\sum_{i=1}^{N}\sum_{j=1}^{M}(y_{ij} - \bar{y}_i)^2/(M-1)}{N}} \quad (56)$$

Where M is a replicates for sample i and N is a total sample. The standard error of the laboratory reference method is an estimate of the precision of the reference method [102]. If two is a replicate for sample and N is a total sample, S_{ref} can be written as:

$$S_{ref} = \sqrt{\frac{\sum_{i=1}^{N}(y_1 - y_2)^2}{N}} \quad (57)$$

Where y_1 and y_2 are the replicate 1 and 2 respectively.

References

[1] Oyedun A.O., Gebreegziabher T., Hui C.W. "Mechanism and modelling of bamboo pyrolysis." Fuel Processing Technology, vol. 106, 2013. Pp. 595–604.

[2] Bridgwater A.V. "Fast pyrolysis of biomass: A handbook. An introduction to fast pyrolysis of biomass for fuels and chemical." Printed in the UK. Second reprint, 2008.

[3] Bridgwater A.V. "Review of fast pyrolysis of biomass and product upgrading." Biomass and bioenergy, vol. 38, 2012, Pp.68-94.

[4] Hla SS, Roberts D. "Characterisation of chemical composition and energy content of green waste and municipal solid waste from Greater Brisbane, Australia." Waste Manage, vol. 41, 2015. Pp. 12–19.

[5] Nhuchhen D.R. "Prediction of carbon, hydrogen, and oxygen compositions of raw and torrefied biomass using proximate analysis." Fuel, vol. 180, 2016. Pp. 348–356.

[6] Huang C., Han L., Yang Z. and Liu X. "Prediction of heating value of straw by proximate data, and near infrared spectroscopy." Energy Conversion and Management, vol. 49(12), 2008. Pp. 3433–3438.

[7] Jenkins B.M, Baxter L.L, Miles Jr, T. R, Miles T.R. "Combustion properties of biomass." Fuel Process. Technol, vol. 54, 1998, Pp. 17–46.

[8] Werther J., Saenger M., Hartge EU., Ogada T., Siagi Z. "Combustion of agricultural residues." Prog. Energy Combust. Sci, vol. 26(1), 2000. Pp. 1–27.

[9] Sheng C, Azevedo J.L.T. "Estimating the higher heating value of biomass fuels from basic analysis data." Biomass Bioenergy, vol. 28, 2005. Pp. 499–507.

[10] Shi H, Mahinpey N, Aqsha A, Silbermann R. "Characterization, thermochemical conversion studies, and heating value modeling of municipal solid waste." Waste Manage, vol. 48, 2016. Pp. 34–47.

[11] Friedl A., Padouvas E., Rotter H., Varmuza K. "Prediction of heating values of biomass fuel from elemental composition." Analytica Chimica Acta, vol. 544, 2005. Pp.191–198.

[12] Bomb calorimetry (2015). Available from: http://www.chem.hope.edu/~polik/Chem345-2000/bombcalorimetry.htm, available on: 10/July/2015.

[13] Wunderlich B. "Calorimetry." Thermal analysis. Academic press, INC. London, England, 1990.

[14] Komilis D., Kissas K. and Symeonidis A. "Effect of organic matter and moisture on the calorific value of solid wastes: An update of the Tanner diagram." **Waste Management**, vol. 34, 2014. Pp. 249–255.

[15] Cooper C.D, Kim B, MacDonald J. "Estimating the Lower Heating Values of Hazardous and Solid Wastes." **J Air Waste Manage**, vol. 49. Assoc, 1999.

[16] Mahapatra K., Harris DL., Durham DL., Lucas S., Terrill TH., Kouakou B., Kannan G. "Effects of moisture change on the physical and thermal properties of *sericea lespedeza* pellets." **Int Agr Eng**, vol.19(3), 2010. Pp. 23-29.

[17] ASTM E1756-08 Standard test method for determination of total solids in biomass. ASTM International, USA, 2008.

[18] Jameel H., Keshwani D.R., Carter S.F. and Treasure T.H. "Thermochemical conversion of biomass to power and fuel. Biomass to renewable energy process." **CRC Press**, Chapter 10, Editor, Jay Cheng, USA, 2010.

[19] Xue J, Yang Z, Han L, Liu Y, Liu Y, Zhou C. "On-line measurement of proximates and lignocellulose components of corn stover using NIRS." Applied Energy, vol. 137, 2015. Pp. 18–25.

[20] ASTM E872-82: Standard test method for volatile matter in the analysis of particulate wood fuels: ASTM International, USA, 2006.

[21] Basu P. Biomass characteristics. "Biomass gasification and pyrolysis: practical design and theory." Academic press is an imprint of Elsevier, USA, 2010.

[22] Tippayawong N, Saengow N, Chaiya E, Srisang N. "Production charcoal from woods and bamboo in a small natural draft carbonizer." **International Journal of Energy and Environment**, Vol 1(5), 2010. Pp 911-918.

[23] ASTM E1755-01: Test method for ash in biomass: ASTM International, USA, 2007.

[24] Wang Q, Zhao W, Liu H, Jia C, Xu H. "Reactivity and kinetic analysis of biomass during combustion." **Energy Procedia**, vol. 17, 2012. Pp. 869-875.

[25] Elbeyli Y., PişkİN S. "Pyrolysis Kinetics of Turkish Bituminous Coals by Thermal Analysis." **Turkish J. Eng. Env. Sci.**, vol. 28, 2004. Pp. 233-239.

[26] Said MM., John GR., Mhilu CF., Manyele SV. "Analysis of pyrolysis kinetic and energy content of agricultural and forest waste." **Open Journal Renewable Energy and Sustainable Development**, Vol. 1, 2014. Pp. 36-44.

[27] El-Sayed S.A., Mostafa M.E. "Pyrolysis characteristic and kinetic parameters determination of biomass fuel powders by differential thermal gravimetric analysis (TGA/DTG)." **Energ Convers Manage**, vol. 85, 2014. Pp. 165-172.

[28] Ninduangdee P., Kuprianov V.I., E.Y. Cha, R. Kaewrath, P. Youngyuen, W. Atthawethworawuth. "Thermogravimetric Studies of Oil Palm Empty Fruit Bunch and Palm Kernel Shell: TG/DTG Analysis and Modeling." **International Conference on Alternative Energy in Developing Countries and Emerging Economies. Energy Procedia**, vol.79, 2015, Pp. 453 – 458.

[29] Kumar S., Agrawalla A., Singh R.K. "Thermogravimetric Analysis of Groundnut Cake." **International Journal of Chemical Engineering and Application**, Vol.2(4), 2011.

[30] Sritong C., Kunavongkrit A. and Piumsombun C. "Bamboo: An Innovative Alternative Raw Material for Biomass Power Plants." **International Journal of Innovation, Management and Technology**, vol.3(6), 2012. Pp. 759-762.

[31] Cheng L., Adhikari S., Wang Z. and Y Ding. "Characterization of bamboo species at different ages and bio-oil production." **Journal of Analytical and Applied Pyrolysis**, vol.116, 2015. Pp. 215–222.

[32] Sripongpakapun K, Tudsri S, Sripichitt P, Kaewtrakulpong K. "Comparation of wood productivity and calorific value of five varieties/lines of Leucaena leucocephala after three years of establishment for sustainable renewable energy." **J. Agr Sci**, vol. 41, 2010. Pp. 149-152.

[33] Shrestha A., Saechua W., P. Sirisomboon. "Some physical and combustion characteristic of leucaena leucocephala pellet." **TSAE 8th International conference. ET-08**, Pp. 128-132.

[34] Chotchutima S., Tudsri S., Kangvansaichol K., Sripichitt P. "Effects of sulfur and phosphorus application on the growth, biomass yield and fuel properties of leucaena (*Leucaena leucocephala* (Lam.) de Wit.) as bioenergy crop on sandy infertile soil." **Agriculture and Natural Resources**, Vol. 50(1), 2016. Pp. 54–59.

[35] García R., Pizarro C., Lavín A.G., Bueno J.L. "Biomass proximate analysis using thermogravimetry." **Bioresource Technology**, vol. 139, 2013. Pp. 1–4.

[36] Stahl R., Henrich E., Gehrmann H.J., Vodegel S., Koch M. "Definition of a standard biomass." SES6-CT-2003-502705. [Online]. Available : https://www.google.co.th/url?sa=t&rct=j&q=&esrc=s&source=web&cd=1&cad=rja

&uact=8&ved=0ahUKEwiJmpOCxIzTAhVHLY8KHROfBfgQFggYMAA&url=http%3A%2F%2Fwww.renew-fuel.com%2Fdownload.php%3Fdl%3Ddel_sp2_wp1_2-1-1_05-01-10-fzk.pdf%26kat%3D14&usg=AFQjCNHZxpkD6MoWpUoe1pig9x6uCuHx-A&sig2=G5nqfCvsav9YZ0z8scGYlg.

[37] Zhang K., Zhou L., Brady M., Xu F., Yu J. and Wang D. "Fast analysis of high heating value and elemental compositions of sorghum biomass using near-infrared spectroscopy." **Energy**. vol.118, 2017, Pp. 1353–1360.

[38] Runge TM., Zhang C, Mueller J, Wipperfurth P. "Economic and Environmental Impact of Biomass Types for Bioenergy Power Plants." Environmental and economic research and development program. 2013. URL: https://www.focusonenergy.com/sites/default/files/research/1010RungeFinalReportx.pdf.

[39] Posom J., Shrestha A., Saechua W., Sirisomboon P. "Rapid non-destructive evaluation of moisture content and higher heating value of Leucaena leucocephala pellets using near infrared spectroscopy." **Energy**, vol. 107, 2016. Pp. 464–472.

[40] Sonobe T., Worasuwannarak N. "Kinetic analysises of biomass pyrolysis using the distributed activation energy model." **Fuel**, vol. 87, 2008. Pp. 414-421.

[41] Chadwick D.T., McDonnell K.P., Brennan L.P., Fagan C.C., Everard C.D. "Evaluation of infrared techniques for the assessment of biomass and biofuel quality parameters and conversion technology processes: A review." **Renew Sust Energ Rev**, vol. 30, 2014. Pp. 672–681.

[42] Kan T., Strezov V., Evans T.J. "Lignocellulosic biomass pyrolysis: A review of product properties and effects of pyrolysis parameters." **Renew Sust Energ Rev**, vol. 57, 2016. Pp. 1126–1140.

[43] Posom J., Saechua W. and Sirisomboon P. "Evaluation of pyrolysis characteristics of milled bamboo using near-infrared spectroscopy." **Renewable Energy**, vol.103, 2017. Pp. 653-665.

[44] Wannapeera J., Worasuwannarak N., Pipatmanomai S. "Product yields and characteristics of rice husk, rice straw and corncob during fast pyrolysis in a drop-tube/fixed-bed reactor." **Songklanakarin J Sci Technol**, vol. 30(3), 2008. Pp. 393-404.

[45] Lv D., Xu M., Liu X., Zhan Z., Li Z., Yao H. "Effect of cellulose, lignin, alkali and alkaline earth metallic species on biomass pyrolysis and gasification" **Fuel Process Technol**, vol. 91, 2010. Pp. 903–909.

[46] Burhenne L., Messmer J., Aicher T., Laborie M-P. "The effect of the biomass components lignin, cellulose and hemicellulose on TGA and fixed bed pyrolysis." **Journal of Analytical and Applied Pyrolysis**, vol. 101, 2013. Pp. 177–184.

[47] Dorez L. , Ferry R. , Sonnier A., Taguet J.-M., Lopez-Cuesta G. "Effect of cellulose, hemicellulose and lignin contents on pyrolysis andcombustion of natural fibers." **Journal of Analytical and Applied Pyrolysis**, vol. 107, 2014. Pp. 323–331.

[48] Stefanidis S.D., Kalogiannis K.G., Iliopoulou E.F., Michailof C.M., Pilavachi P.A., Lappas A.A. "A study of lignocellulosic biomass pyrolysis via the pyrolysis of cellulose, hemicellulose and lignin." **J Anal Appl Pyrol**, vol. 105, 2014. Pp. 143–150.

[49] Yang H., Yan R., Chen H., Lee D.H., Zheng C. "Characteristics of hemicellulose, cellulose and lignin pyrolysis." **Fuel**, vol. 86, 2007. Pp. 1781–1788.

[50] Chen Z., Hu M., Zhu X., Guo D., Liu S., Hu Z., Xiao B., Wang J., Laghari M. "Characteristics and kinetic study on pyrolysis of five lignocellulosic biomass via thermogravimetric analysis. " **Bioresource Technology**, Vol. 192, 2015. Pp. 441–450.

[51] Wu K., Liu J., Wu Y., Chen Y., Li Q., Xiao X., Yang M. "Pyrolysis characteristics and kinetics of aquatic biomass using thermogravimetric analyzer." **Bioresource Technology**, Vol. 163, 2014. Pp. 18–25.

[52] Chaishome J., Rakmae S., 7th Internation Conference on Agrcultural Engineering (TSAE) 2014 2nd April-4th, Krungsri river Hotel Pranakhornsriayothanya.

[53] Wongsiriamnuay T., Tippayawong N. "Non-isothermal pyrolysis characteristics of giant sensitive plants using thermogravimetric analysis." **Bioresource Tehnology**, vol. 101, 2010. Pp. 5638-5644.

[54] Liu L., Ye X.P., Womac AR., Sokhansanj S. "Variability of biomass chemical composition and rapid analysis using FT-NIR techniques." **Carbohyd Polym**, vol. 81, 2010. Pp. 820–829.

[55] Guimarães C.C., Simeone M.L., Parrella R.A.C., Sena M.M. "Use of NIRS to predict composition and bioethanol yield from cell wall structure components of sweet sorghum biomass." **Microchem J**, vol. 117, 2014. Pp. 194-201.

[56] Park J.I., Liu L., Ye X.P., Jeong M.K., Jeong Y-S. "Improved prediction of biomass composition for switchgrass using reproducing kernel methods with wavelet compressed FT-NIR spectra." **Expert Syst Appl**, vol. 39, 2012. Pp. 1555–1564.

[57] Posom J., Sirisomboon P. "Evaluation of the thermal properties of Jatropha curcas L. kernels using near-infrared spectroscopy." **Biosystem Eng**, vol. 125, 2014. Pp. 45-53.

[58] Sanderson MA., Agblevor F., Collins M. and Johnson DK. "Compositional analysis of biomass feedstocks by near infrared spectroscopy." **Biomass and Bioenergy,** vol. 11 (5), 1996. Pp. 365-370.

[59] Kim DW., Lee JM., Kim JS. "Application of near infrared spectroscopy for on-line measurement of coal properties." **Korean J. Chem. Eng**, Vol.26(2), 2009. Pp. 489-495.

[60] Bruun S., Jensen JW., Magid J., Lindedam J. and Engelsen SB. "Prediction of the degradability and ash content of wheat straw from different cultivars using near infrared spectroscopy." **Industrial Crops and Products**, vol. 31(2), 2010. Pp. 321–326.

[61] Fagan C.C., Everard C.D., McDonnell K. "Prediction of moisture, calorific value, ash and carbon content of two dedicated bioenergy crops using near-infrared spectroscopy." **Bioresour Technol**, vol. 102, 2011. Pp. 5200–5206.

[62] Posom J., Sirisomboon P. "Evaluation of the moisture content of *Jatropha curcas* kernels and the heating value of the oil-extracted residue using near-infrared spectroscopy." **Biosystems Engineering**, Vol.130, 2015. Pp. 52–59.

[63] Sundaram J., Mani S., Kandala CV.K., Holser RA. "Application of NIR Reflectance Spectroscopy on Rapid Determination of Moisture Content of Wood Pellets." **American Journal of Analytical Chemistry**, vol. 6, 2015. Pp. 923-932.

[64] Gillespie GD., Everard CD., and McDonnell KP. "Prediction of biomass pellet quality indices using near infrared spectroscopy." **Energy**, vol. 80, 2015. Pp. 582–588.

[65] Næs T., Isaksson T., Fearn T., Davies T. "Multivriate calibration and Classification." NIR Publication, Charlton Mill, Charlton, Chichester, West Sussex PO18 0HY, UK. (P. 323, 2004.

[66] Davies A.M.C. "An introduction to near infrared (nir) spectroscopy." https://www.impublications.com/content/introduction-near-infrared-nir-spectroscopy; online in 4/3/2017.

[67] Osborne BG, Fearn T. "Near infrared spectroscopy in food analysis." Theory of near infrared spectroscopy, USA: Longman Scientific & Technical: New York; 1986. P. 36-40, 133.

[68] Dufour É. "Principle of Infrared spectroscopy." Infrared spectroscopy for food quality analysis and control, p. 5. Printed and bound in the United states of America, Edited by Da-Wen Sun. Typeset by Charon Tec LTD, 2009.

[69] Bokobza L. **J. Near Infrared Spectrosc**, vol. 6, 1998. Pp. 3–17.

[70] Conzen J-P. "Multivariate Calibration: A practical guide for developing methods in the quantitative analytical chemistry." 2006.

[71] Wikipedia (2015). Near-infrared spectroscopy. Web site: https://en.wikipedia.org/wiki/Near-infrared spectroscopy. Online: 10 July 2015.

[72] Burns D.A., Ciurczak E.W. "Handbook of Near-Infrared Analysis." Edited by Donald A. Burns and Emil W. Ciurczak, Vol. 13, Marcel Dekker, INC, America, 1992.

[73] Phetpan K., Sirisomboon P. "Evaluation of the moisture content of tapioca starch using nearinfrared spectroscopy." **Journal of Innovative Optical Health Sciences**, vol. 8, 2015. Pp. 1-12.

[74] Onsawai P., Sirisomboon P. "Determination of dry matter and soluble solids of durian pulp using diffuse reflectance near infrared spectroscopy." **Journal of Near Infrared Spectroscopy**, vol. 23, 2015. Pp. 167–179.

[75] Srikornkarn S., Sirisomboon P. "Feasibility of Evaluation of Salt Content in Canned Sardine in Oil by Near Infrared Spectroscopy." **Agriculture and Agricultural Science Procedia**, vol. 2, 2014. Pp. 381–385.

[76] Mcclure W.F. "Spectroscopic Techniques for Food Analysis. Near-Infrared Spectroscopy." Edited by Reginald H. Wilson. P. 13. Printed in the history-10, Printed in the United states of America, New York, 1994.

[77] Chen P. "Use of optical properties of food materials in quality evaluation and material sorting." **J. of food process engineering**, vol. 2, 1978. Pp. 307-322.

[78] Birth G.S. "How light interacts with foods." ASAE Publication 1-76, Quality Detection in Food, 1976. Pp. 6-11. St. Joseph, Michigan.

[79] Stuart B. "Modern Infrared Spectroscopy." Editor. David J. Ando. John Wiley & Sons, New york, USA, 1996.

[80] S. GUNASEKARAN, M. R. PAULSEN, SHOVE G.C. "Optical Methods for Nondestructive Quality Evaluation of Agricultural and Biological Materials". **J. agric. Engng Res.**, vol. 32, 1985. Pp. 209-241

[81] Law D.P., R. Tkachuk. "Determination of moisture content in wheat by near infrared diffuse reflectance spectrophotometry American of celeal chemists," Inc.,3340 Pilot Knob Road, St. Paul, Minnesota 55121. 874-881, 1975.

[82] Gunde M.K, Logar J.K, Orel Z.C, Orel B. "Application of the Kubelka-Munk Theory to Thickness-Dependent Diffuse Reflectance of Black Paints in the Mid-IR." **Appl. Spectrosc**, vol. 49(5), 1995. Pp. 623-629.

[83] Khoshhesab Z.M. "Reflectance IR Spectroscopy, Infrared Spectroscopy - Materials Science." Engineering and Technology, Prof. Theophanides Theophile (Ed.), ISBN: 978-953-51-0537-4, 2012. InTech, Available from: http://www.intechopen.com/books/infrared-spectroscopy-materials-science-engineering-andtechnology/fundamental-of-reflectance-ir-spectroscopy.

[84] Williams P. "Near-infrared technology-Getting the best out of light." Nanaimo, British Columbia, and Winnipeg, Manitoba, Canada; 2007: PDK Grain.

[85] Tsuchikawa S. "Sampling technique. Near Infrared spectroscopy in food science and technology." Edited by Yukihio Ozaki, W. Fred McClure, and Alfred A. Christy. USA. P. 138, 2007.

[86] Sirisomboon P., Tanaka M., Kojima T., Williams P. "Nondestructive estimation of maturity and textural properties on tomato 'Momotaro' by near infrared spectroscopy." **Journal of Food Engineering**, vol. 112, 2012. Pp. 218–226.

[87] Dardenne P. "Some considerations about NIR spectroscopy: Closing speech at NIR-2009." **NIR news**, vol. 21, 2010. Pp. 8–14.

[88] Nicolaï B.M., Beullens K., Bobelyn E., Peirs A., Saeys W., Theron K.I., Lammertyn J. "Nondestructive measurement of fruit and vegetable quality by means of NIR spectroscopy: A review." **Postharvest Biology and Technology**, vol. 46(2), 2007. Pp. 99–118.

[89] CAMO. "The Unscrambler Appendices: Method References." [Online]. Available: http://www.camo.com/TheUnscrambler/Appendices. Accessed on February 23, 2015.

[90] Romia M.B., Bernàrdez M.A. "Infrared spectroscopy for Food quality analysis and control." Pp. 74-75, 2009.

[91] Rinnan A., Nφrgaard L., Berg F.V.D., Thygesen J., Bro R., Engelsen S.B. "Data pre-processing. Infrared spectroscopy for Food quality analysis and control." Pp. 31, 2009.

[92] Lamp D.T., Hurburgh Jr CR. "Moisture Determination in Single Soybean Seeds by Near Infrared Transmittance." **Agricultural and Biosystems Engineering**, vol. 34(5), 1991. Pp. 2123-2129.

[93] Ozaki Y., Morita S., Du Y. "Near-infrared spectroscopy in food science and technology." Printed in the United States of America, 2007.

[94] Cho J.H. "Vibration spectroscopic techniques and application: Chemometrics tools for multivariate analysis". Symposium for online near infrared spectroscopy for industrial process control. Bangkok, Thailand, 2013. Pp. 1-29.

[95] Hruschka W.R. "Data analysis: Wavelength selection method. Editor: Phill William and Narl Norris." Near-infrared technology in agricultural and food industries. American association of cereal checmists, Inc. St Paul, Minesota, USA, 1990.

[96] Mark H. "Data Analysis: Multilinear Regression and Principal Component Analysis". **Handbook of Near-Infrared Analysis.** Third edition. Edited by Donald A. Burns and Emil W. Ciurczak. CRC press Taylor & Francis Droup. London, 2007.

[97] Krzanowski W.J. "Motivation and fundamental concepts." Principles of multivaraite analysis. The university Press (Belfast) Ltd, Northern Ireland, 1988.

[98] Zou H., Hastie T., Tibshirani R. "Sparse Principal Component Analysis." American Statistical Association, Institute of Mathematical Statistics, and Interface Foundation of North America, **Journal of Computational and Graphical Statistics**, vol. 15(2), 2006. Pp. 265–286.

[99] Næs[2] T., Isaksson T., Fearn T., Davies T. "Data compression by PCR and PLS. Multivriate calibration and Classification." **NIR Publication**, Charlton Mill, Charlton, Chichester, West Sussex PO18 0HY, UK. (P. 28), 2004.

[100] Boulesteix A-L., Strimmer K. "Patial least square: A versatile tool for the Analysis of High-dimension genomic data." **Seminar for applied stochastics**, Germany, 2007.

[101] Zornoza R., Guerrero C., Mataix-Solera J., Scow K.M., Arcenegui V., Mataix-Beneyto J. "Near infrared spectroscopy for determination of various physical, chemical and biochemical properties in Mediterranean soils." **Soil Biol Biochem**, vol. 40(7), 2008. Pp. 1923–1930

[102] Isaksson T., Segtnan V. H. "Meat and Fish products. Near Infrared spectroscopy in food science and technology. Edited by Yukihio Ozaki, W. Fred McClure, and Alfred A. Christy. USA. P. 248, 2007.

Introduction

The information of biomass properties are particularly required in order to optimize the thermal conversion process as the resource of energy generated by biomass feedstock. Biomass is generally characterized by its energy properties including heating value (HHV, LHV); proximate data (MC, VM, FC, and A), pyrolysis characteristics (T_{onset}, T_{sh}, T_{peak}, T_{offset}, and DTG_{peak}); and elemental compositions (C, H, N, O, and S) compared to fossil fuels [1]. Generally, the MC is water content in biomass and it is a negative parameter for thermal conversion. The moisture content (MC) in biomass contributes to temperature drop during burning in combustion process because one part of energy was used to heat the water. In pyrolysis, high MC leads to high MC in bio-oil in which made the poor-quality bio-oil. Demirbaş [2] stated that the HHV of fuel was decreased with increasing in MC. Therefore, the MC could be used to predict the HHV due to high correlation with the MC. Thus, determination of HHV by using dry oven based on MC is obviously cheaper than bomb calorimetry technique.

The HHV is not only affected by MC, but it is also influenced by major component in biomass. The determinations of major component in biomass were divided into three terms such as lignocellulosic, proximate data, ultimate data. Lignocellulosic terms are the cell wall of biomass including hemicellulose, cellulose, and lignin; they are polysaccharides which contain the molecule of hydrocarbon [3]. Proximate data term is the weight percentages of MC, VM, FC, and Ash of biomass. The ultimate data term is weight percentages of chemical element contents (C, H, O, N, and S) [4]. For lignocellulosic term, hemicellulose, cellulose and lignin were approximately made up by 20-30%, 40-44%, and 18-25% [5]. A higher lignin content (corresponding to lower cellulose) results in slower decomposition, while higher hemicellulose and cellulose contents lead to faster decomposition [6-9]. Stefanidis et al. [10] reported that pyrolysis of cellulose gave high yields of bio-oil; high content of hemicellulose gave higher gas yields and moderate yields of bio-oil; and high content of lignin gave the highest solid residue yield. Hemicellulose

and cellulose were quickly decomposed at 220-315 °C and 315-400 °C, respectively, while lignin was decomposed in a wide temperature range from 160 to 900 °C [11]. Hemicellulose decomposition had a shoulder peak at 290 °C, cellulose decomposition occurred at the highest peak at 347 °C, while lignin was decomposed in a wide temperature range without an observable peak [12]. This meant that T_{onset} was the started decomposition of lignin and hemicellulose, while T_{sh} was the maximum degradation of hemicellulose. T_{peak} was the degradation of cellulose and lignin and DTG_{peak} was the decomposition rate among lignin and cellulose. To consider the proximate data, the real energy of biomass obtained only from the combustion of VM and FC. Ash was the residue solid. It consisted of silica, aluminum, iron and calcium, small amount of magnesium, titanium, sodium, and potassium which could not be burnt. VM was fuel gas releasing after the water released completely which consisted of hydrogen and carbon. The FC was the products of the carbonization of biomass matter (bio-char). It was seen that VM was fuel gas obtained from decomposition of hemicellulose, cellulose, and lignin. Moreover, HHV could be predicted using proximate data. Yin [4] gave the equation for predicting HHV based on proximate analysis as follows: HHV (MJ/kg) =0.1905VM+0.2521×FC. While the correlation based on ash content for predicting HHV was presented by Sheng and Azevedo [13], the equation was HHV=19.914-0.2324×Ash. For ultimate data, the C content was about 30-60%, H was around 5-6% and O was approximately of 30-45% meanwhile N and S were less than 1% [14]. Its C, H and O content highly affected to higher heating value. In pyrolysis process, C and H became to VM, and bio-oil and C became to fixed carbon. The HHV could be predicted by the ultimate data. Yin [4] generated the equation for predicting HHV of biomass based on ultimate analysis as follows: HHV (MJ/kg)=0.2949C+0.8250×H. Meanwhile, S and N content were necessary in term of environmental protection [15], they led to releasing of SO_2, NO and NO_2 and became to acid rain. During combustion, C_2O was emitted from combustion between C and O whereas H and O became to H_2O. The knowledge of C and H in biomass could be used to predict

the amount of air used in combustion process. If the air is inadequate, the C and O will become to CO.

In addition, the HHV could be converted to LHV by LHV=HHV (100-M)/100-rM [16], where M is the moisture content (wt%), and r is the latent heat of vaporization of water at normal pressure. The HHV was determined by ultimate or proximate data, it is easy to predict LHV when MC was known. As mentioned above, it clearly showed the relationship among biomass constituents.

References

[1] Werther J, Saenger M, Hartge E, Ogada T., Siagi Z. "Combustion of agricultural residues." **Prog. Energy Combust. Sci.** Vol. 26, 2000. Pp. 1–27.

[2] Demirbaş A. "Effects of Moisture and Hydrogen Content on the Heating Value of Fuels." **Article in Energy Sources Part A**, vol. 7, 2007. Pp. 649-655.

[3] Xu F, Shi YC, Wang D. "Enhanced production of glucose and xylose with partial dissolution of corn stover in ionic liquid. 1-Ethyl-3-methylimidazolium acetate." **Bioresour Technol**, vol. 114, 2012. PP. 720-4.

[4] Yin C-Y. "Prediction of higher heating value of biomass from proximate and ultimate analyses." **Fuel**, vol. 90. 2011. Pp. 1128-1132.

[5] Basu P. "Biomass characteristics. Biomass gasification and pyrolysis: practical design and theory," **Academic press is an imprint of Elsevier**, USA. 2010.

[6] Wannapeera J., Worasuwannarak N., Pipatmanomai S. "Product yields and characteristics of rice husk, rice straw and corncob during fast pyrolysis in a drop-tube/fixed-bed reactor." **Songklanakarin J. Sci. Technol.** Vol. 30 (3), 2008. Pp. 393-404.

[7] Lv D., Xu M., Liu X., Zhan Z., Li Z., Yao H. "Effect of cellulose, lignin, alkali and alkaline earth metallic species on biomass pyrolysis and gasification." **Fuel Process Technol**, vol. 91, 2010. Pp. 903-909.

[8] Burhenne L., Messmer J., Aicher T., Laborie M.-P. "The effect of the biomass components lignin, cellulose and hemicellulose on TGA and fixed bed pyrolysis." **J. Anal. Appl. Pyrol**, vol. 101, 2013. Pp. 177-184.

[9] Dorez G., Ferry L., Sonnier R., Taguet A., Lopez-Cuesta J.-M. "Effect of cellulose, hemicellulose and lignin contents on pyrolysis and combustion of natural fibres." **J. Anal. Appl. Pyrol,** vol. 107, 2014. Pp. 323-331.

[10] Stefanidis S.D., Kalogiannis K.G., Iliopoulou E.F., Michailof C.M., Pilavachi P.A., Lappas A.A. "A study of lignocellulosic biomass pyrolysis via the pyrolysis of cellulose, hemicellulose and lignin." **J. Anal. Appl. Pyrol**, vol. 105, 2014. Pp. 143-150.

[11] Yang H., Yan R., Chen H., Lee D.H., Zheng C. "Characteristics of hemicellulose, cellulose and lignin pyrolysis." **Fuel**, vol. 86, 2007. Pp. 1781-1788.

[12] Guan Y., Ma Y., Zhang K., Chen H., Xu G., Liu W., Yang Y. "Co-pyrolysis behaviours of energy grass and lignite." **Energ Convers. Manage**, vol. 93, 2015. Pp. 132-140.

[13] Sheng C, Azevedo JLT. "Estimating the higher heating value of biomass fuels from basic analysis data." **Biomass Bioenergy**, vol. 28, 2005, Pp. 499-507.

[14] Vargas-Moreno J.M., Callejón-Ferre A.J., Pèrez-Alonso J., Velázquez-Martí B. "A review of the mathematical models for predicting the heating value of biomass materials." **Renewable and Sustainable Reviews**, vol. 16, 2012. Pp. 3065-3083.

[15] Telmo C, Lousada J, Moreira N. "Proximate analysis backwards stepwise regression between gross calorific value, ultimate and chemical analysis of wood." **Bioresour Technol**, vol. 101, 2010. Pp. 3808-15.

[16] Xuebin L, Fei W, Yong C, Qunxing H, Jianhua Y. "A simple method for predicting the lower heating value of municipal in China based on wet physical composition." **Waste Manag**, vol. 36, 2015. Pp. 24–32.

Chapter 1

Rapid non-destructive evaluation of moisture content and higher heating value of *leucaena leucocephala* pellets using near infrared spectroscopy

1.1 Abstract

The MC (moisture content) and HHV (higher heating value) of *Leucaena leucocephala* pellets using NIR (near infrared) spectroscopy was investigated in this study. The MC of the pellets was adjusted by subjecting the samples to different relative humidity environments. The samples were scanned in diffuse reflection mode at wavenumbers of 12,500-4000 cm^{-1}. Partial least squares regression models correlating the MC and HHV with the NIR spectra were developed and validated by full cross validation. The models for MC and HHV provided coefficients of determination (R^2) of 0.995 and 0.964, a root mean square error of cross validation (RMSECV) of 0.187%wb and 79.2 J g^{-1}, bias of -0.0008%wb and 1.29 J g^{-1} and a RPD (ratio of prediction to deviation) of 13.9 and 5.30, respectively. The models had excellent accuracy. This rapid quality evaluation method may be used for trading of biomass pellets. An equation related MC and HHV was also developed.

*This chapter constituted the journal article: Posom J, Shrestha A, Saechua W, Sirisomboon P. "Rapid non-destructive evaluation of moisture content and higher heating value of *Leucaena leucocephala* pellets using near infrared spectroscopy." **Energy**, vol. 107, 2016. Pp. 464-472.

1.2 Introduction

The fast-growing plant is garnered much interest to be biomass due to its characteristics is rapid growth, easy care, and durable drought [1]. *Leucaena leucocephala* is one kind of seven fast-growing trees promoted by government sector [2]. *Leucaena* can plant in all part of Thailand. It is one of alternatives to fossil fuels. Thailand has the large area of growing *Leucaena leucocephala* in Lopburi and Nakhonratchasima Province where are in the central and northeastern area of the country, respectively. *Leucaena leucocephala* is considering for biomass production due to its reported yield of wood around 30–40 m^3/ha/year [3]. Mainoo and Ulzen-Apiah [4] stated that *Leucaena leucocephala* had the highest heating value and it is a better choice when the users are interested in burning quality. *Leucaena* is the nitrogen-fix tree, then help to reduce the fertilizer prices and improve soil nutrient respect [1].

The wood pellets are a good choice for heating. The densification into pellets could reduce material waste and improve the ease of transporting and storage [5]. Pellets is convenient and easy to use which can be store at less space [6], have a high HHV and increasing pellets density would increase char combustion time [7]. Owing to low density of biomass involved handling, transportation and storage costs, therefore biomass should be kept in pellets forms [8].

The global wood pellet production has continuely increased since in 2000 (2 Mt) to present (more than 28 Mt) [9]. In 2015, global wood pellet demand equal to around 28 Mt, European Union member countries (EU28) imports 13.4Mt, Japan imports 232kt, South Korea imports 1.5Mt [10]. From total asian imports Q1-Q3 at 2015, Korea imported approximately 19 thousand tonnes from Thailand [11]. Moreover, Thailand want to increase the use of biomass for generating heat combustion from 5,144 ktoe in 2015 to 22,100 ktoe in 2036 [12]. Then wood pellet quality was also concerned for commercial products and generating heat.

Since *Leucaena leucocephala* woody gave a HHV, approximately 17.69-18.12 MJ/kg [13] for pellets forms. The HHV and MC of pellets are very necessary, it is the main respect to set price of pellets. If pellets had high HHV or low water content, the price is high. The measurement of HHV and MC by NIR is required for factory because of rapid

measurement, convenient and low cost per sample. In addition, the rapid measurement of MC also helps to improve the pelletizing process in real time. NIR is promising and more useful for intact biomass because many different species of feedstock are investing in further, the bonds of O-H and C-H in organic are expected depending on anharmonicity as well as modeling.

1.3 Objective

The aim of this work was to investigate the effect of moisture content on the higher heating value of *Leucaena leucocephala* pellets and evaluate the properties using near infrared spectroscopy calibration models developed by PLS (partial least squares) regression.

1.4 Materials and methods

1.4.1 Sample

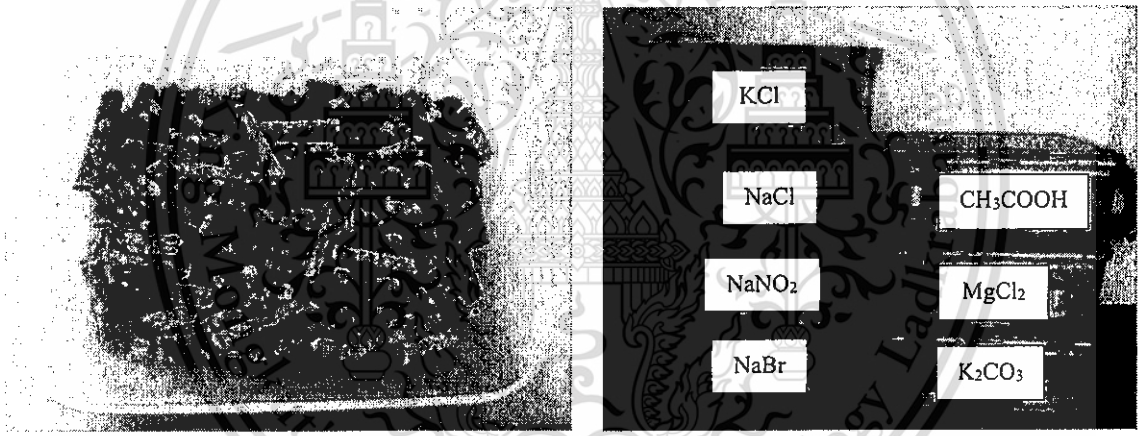

Figure 1.1 a) *Leucaena leucocephala* pellets, b) the subjected pellet samples into 7 plastic boxes (RH, relative humidity)

Leucaena leucocephala variety "Tarramba" samples were collected from Nakhonratchasima Province, Thailand. It was consecutively chopped, dried, and ground. The ground wood was formed to 8-mm diameter pellets by a pelletization process (see in Figure 1.1a). The pellet samples were subjected to a 7 RH (relative humidity) environment including 22.6, 32.7, 43.8, 57.5, 63.5, 75.3 and 84.3% RH by putting the samples into 7 plastic boxes that each contained a saturated aqueous solution of

CH_3COOH, $MgCl_2$, K_2CO_3, NaBr, $NaNO_2$, NaCl and KCl, respectively, for 2 months (see in Figure 1.1b). Furthermore, 6 samples (1 L per sample) were placed in one box.

1.4.2 Near infrared scanning of the Leucaena leucocephala pellets

A FT (Fourier transform)-NIR spectrometer (Bruker Ltd., Germany) (see in Figure 1.2) was used for scanning. Each sample at the same volume of 200 ml in a quartz-sampling cup (87.0-mm diameter and 87.5mm height) was scanned through the quartz window in a rotary diffuse reflectance mode at a wavenumber of 12,500-4000 cm^{-1} (800-2500 nm) with a resolution of 16 cm^{-1}. The scanning was completed 64 times per one average spectrum. Before each sample scanning, the gold used as a reference material was scanned for background. All scanning was conducted at room temperature (25.0 ± 1.00 °C).

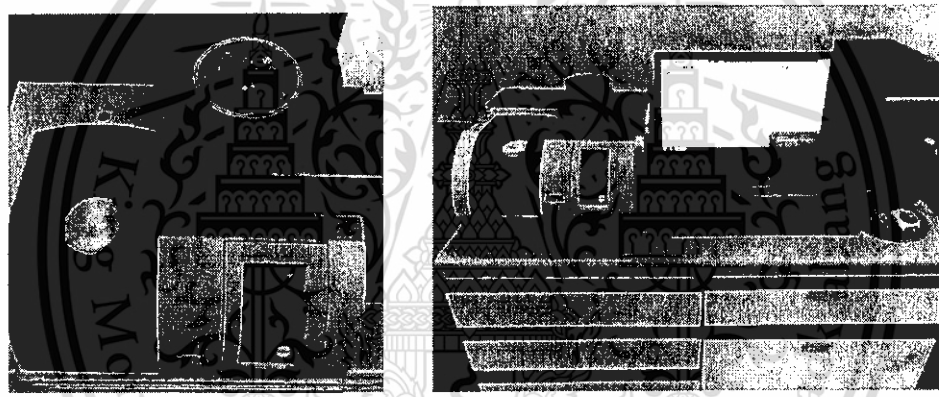

Figure 1.2 Scanning pellets by FT-NIR spectrometer

1.4.3 Determination of the Leucaena leucocephala pellets moisture content

After scanning, 3 g of the scanned sample was broken and put in aluminum cans (5-cm diameter and 4 cm height) for measuring the moisture content with a hot air oven (Memmert, model ULM 500, Germany) at 105 °C for 24 h, The samples were re-heated at 6 h interval until the sample weights remained constant. Weighing was completed using a digital balance (Adventure AR2140, OHAUS, resolution of 0.0001 g). The moisture content (% wet basis) was calculated using Equation (1.1):

$$\mathbf{MC\ (\%wb)} = \left[\frac{m_i - m_f}{m_i}\right] \times 100 \qquad (1.1)$$

where MC is moisture content in % wb, m is mass in g, and the subscripts i and f are initial and final, respectively. There were 3 replicates per sample.

1.4.4 Determination of the Leucaena leucocephala pellet higher heating value

The scanned pellets were weighed (0.50-1.00 g) (Adventure AR2140, OHAUS) and measured for their higher heating values using a bomb calorimeter (C200, IKA, Germany) in isoperibol mode. Before the measurements were taken, the sample vessel was calibrated using pelletized benzoic acid (IKA C 723, IKA, Germany). There were 2 replicates per sample.

The calculation method of higher heating value by calorimeter system C 200 (Figure 1.3).

a b

Figure 1.3 a) Decomposition vessel (C5010, IKA, Germany), b) Bomb calorimeter (C200, IKA, Germany)

Determine of heat capacity (C-value) of systems

The calorimeter system is calibrated before accurate measurements are possible. So, heat capacity will be determined in this step. The heat quantity required to raise the temperature of the calorimeter system by a Kelvin is used to determine the heat capacity of the so-called "$C-value$" of the system. $C-value$ (J/K) can be calculated from Eq. (1.2) (Operating instructions, ITS (Thailand) co., Ltd):

$$C-value = \frac{(H_S * m_S + QExt1 + QExt2)}{\Delta T} \quad (1.2)$$

Where H_s is standard heating value of benzoic acid (gross calorific value: 26460 J/g), m_s is weight of standard sample (Benzoic acid, about 1.0 g), QExt1 is correction value for the heat energy generated by the cotton thread as ignition aid (50 J) and QExt2 is correction value for the heat energy from other burning aids (If sample holder is quartz or glass, QExt2 equal zero) and ΔT is calculated temperature increase of water in inner vessel of measuring cell (K). This value is used for determining the following calorific value of material. It is the $C - value$ of system (J/K) (water and decomposition vessel).

Calculated calorific value

Combustion is carried out in a calorimeter under specific conditions. The decomposition vessel is filled with fuel sample and oxygen the fuel sample is ignited and the temperature increase in the calorimeter system measured. The specific calorific value of the sample is calculated as follows (Operating instructions, ITS (Thailand) co., Ltd):

$$H_o = \frac{C-value*\Delta T-QExt1-QExt2}{m} \quad (1.3)$$

where H_0 is heating value (J/g), C-value is heat capacity of calorimeter system that is obtained from step 1 (J/K), and m is weight of fuel sample (g). QExt2 will equal zero if quartz or glass is used for sample holder and QExt2 do not equal zero if is made from plastic.

1.4.5 Repeatability and maximum coefficient of determination

The precision of the moisture content and higher heating values of the reference data were determined using the repeatability (Rep) value. It was calculated from the standard deviation of the differences values between duplication; then, the repeatability was also used to calculate the maximum coefficient of determination (R^2_{max}) that was calculated by the following formula [14]:

$$R^2_{Max} = \frac{SD_y^2-Rep^2}{SD_y^2} \quad (1.4)$$

where SD_y is the standard deviation of the calibration set data. Thus, if no error occurs in the spectra or the model, the coefficient of determination (R^2) should be equal to R^2_{max}. SD_y and Rep can indicate whether a range is too narrow and/or a reference method is not sufficiently precise [14].

1.4.6 Determination of outliers of the reference data

The outlier of the reference data was determined using Equation (1.5).

$$\frac{(x_i-\bar{x})}{SD} \geq \pm 3.00 \quad (1.5)$$

where X_i is the measured value of sample i. $\bar{X}$ and SD are the average and standard deviation of the measured values of all samples, respectively. If the equation is satisfied, the sample was considered an outlier.

1.4.7 Spectrum pre-processing and NIR spectroscopy modelling

The NIR spectroscopy models for predicting the moisture content and higher heating values of the *Leucaena leucocephala* pellets were established using PLS (partial least squares) regression. The software for multivariate analysis (OPUS, v. 7.0.129, Germany) was used in both spectrum pre-processing and model development. The NIR spectra used for model development were no preprocessing spectra or pre-processing spectra using any of the following methods: constant offset elimination, straight line subtraction, vector normalization, min-max normalization, MSC (multiplicative scatter correction), first derivatives, second derivatives, first derivatives + straight line subtraction, first derivatives + vector normalization and first derivatives + MSC.

After model development, the spectral outlier samples were identified using the Mahalanobis distance limit by the software. The limit was determined on the basis of distribution of all calibration spectra. Assuming a normal distribution, a one-sided limit is defined that covers a probability of 99.999%.

The optimum model was selected from the combination of the number of latent variables, the wavenumber ranges and the preprocessing methods which provided the minimum RMSECV (root mean square error of cross validation). The models were validated by full cross validation. The determination coefficients of calibration and validation (R^2), ratio of prediction to deviation (standard deviation to the standard error of validation, RPD) and bias were calculated. The regression coefficient and X-loading of each PLS latent variable was determined and plotted. In addition, the other models were developed from the wavenumber ranges that were not selected by the software. The results were validated by full cross validation, and the same performance parameters were calculated.

1.4.8. Diffuse reflectance measurement assumption and partial least squares modelling

The method of NIR spectroscopy is the determination of a linear relationship between the spectral data (absorbance) and the sample constituent concentration. For reflectance measurement, Kubelka-Munk equation [$f(R) = (1-R)^2/2R = (k/s)$], where R is the diffuse reflectance of an infinitely thick sample, k is the molar absorption coefficient and s is the scattering coefficient could be applied [15]. The equation of a linear relationship between the spectral intensity and the concentration could be created. This equation was assumed for infinitely thick sample, where the sample had to be thick enough to ensure that its diffuse reflectance would not change with increasing thickness and the scattering coefficient was assumed to be constant at any wavelength of the spectrum which depended on particle size [15]. These restrictions reduced the number of spectra presentable in Kubelka-Munk units, but did not restrict "non-ideal" samples from quantitative diffuse reflection analysis [16]. Typically, quantitative diffuse reflection measurements are presented in log (1/R) units. The ideal relationship of the spectral collected from diffuse reflection measurement was log (Ṙ/R), when Ṙ is the reflectance of standard i.e. reference material, R is diffuse reflectance radiation of sample [17]. The assumption was the reflectance of standard was 100 percent (Ṙ equal to 1) and the sample was infinitely thick, and light could not emit through the sample. Furthermore, the diffuse reflectance could carry information on composition .and functionality from within the sample to the detector a NIR instrument [18] for model development.

1.5 Results and discussions

1.5.1 Reference data of the moisture content and higher heating value of Leucaena leucocephala pellets

Figure 1.4a illustrated the vibrational band of *Leucaena leucocephala* pellets. Spectra of heartwood, sapwood, cellulose and lignin were shown in Figure 1.4b, there is considerable overlap; however, they found the obvious differences between cellulose and lignin for some regions of the NIR spectra [19]. The average NIR spectra of *L. leucocephala* pellets was quite similar to heartwood and sapwood and some regions have a bit different shape as lignin's and cellulose's spectra. The repeatability and maximum coefficient of determination (R^2_{max}) of moisture content and higher heating value were 0.293%wb, 141 J g^{-1} and 0.988 and 0.890, respectively. Table 1 shows the standard

deviation and average moisture content and higher heating values of *Leucaena leucocephala* pellets in different relative humidity environments and in a range from 7.31 to 14.9%wb and 16,891 to 17,662 J g^{-1}, respectively.

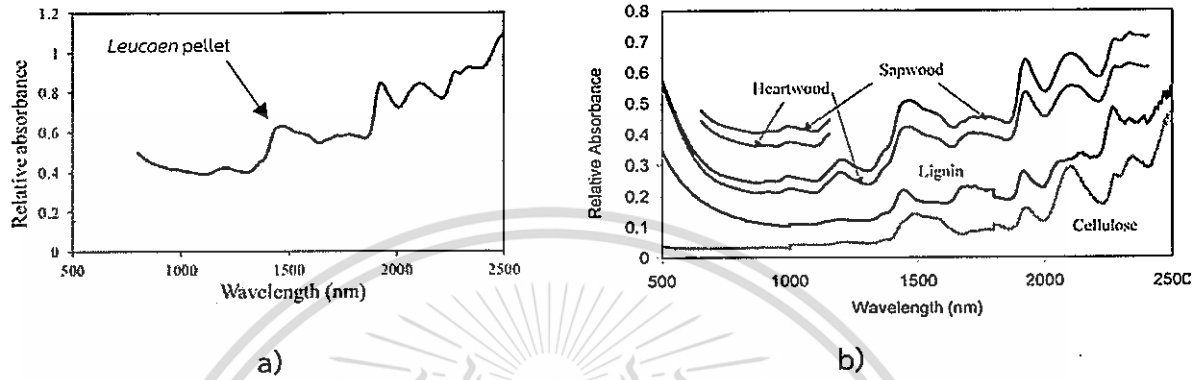

Figure 1.4 a) average NIR spectral of *Leucaena leucocephala* pellets and (b) NIR spectra of heartwood, sapwood, cellulose and lignin [19]

Figure 1.5 shows the relationship between moisture content and higher heating value of *Leucaena leucocephala* pellets where the heating value increased with decreasing moisture content. The relationship can be written using linear regression equations as HHV = -159MC + 18,780, when HHV is the higher heating value (J g^{-1}) and MC is the moisture content (%wb) with a coefficient of determination (R^2) of 0.962. In the higher moisture content samples, there was less dry matter in the biomass, i.e., lower heating value results. Thus, the HHV of dry *L. leucocephala* pellets is approximately 18,780 J g^{-1}. This value is not too low for biofuel. For example, biofuel can be used in the case of as-received biomass such as wheat straw [20], wood sawdust [20], sunflower seed husk [20], straw [21], rice husk [22], *Eucalyptus globulus* [23], millet [24], hemp [24] in which HHV were 17,344 J g^{-1}, 18,207 J g^{-1}, 17,998 J g^{-1}, 17,640 J g^{-1}, 15,944 J g^{-1}, 17,600 J g^{-1}, 18,165 J g^{-1} and 18,036 J g^{-1}, respectively.

The relationship between moisture content and higher heating value was similar to that reported on S. *lespedeza* pellets [25], solid wastes (i.e., newsprint, biodried municipal solid wastes, municipal solid waste derived composts, wastewater sludge, and sea weed derived compost) [26], coal and biomass [27]. The results confirmed that the higher heating value was dependent on the moisture content.

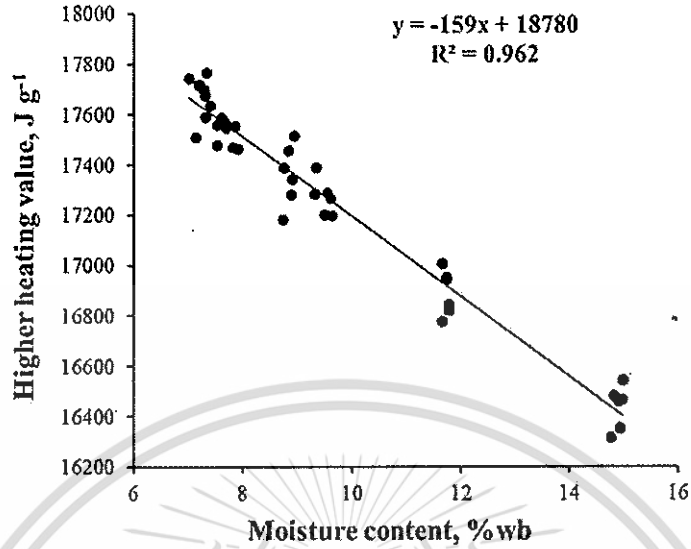

Figure 1.5 Relationship between the higher heating value of *Leucaena leucocephala* pellets and moisture content

Table 1.1 Equilibrium moisture content at different relative humidities and the corresponding higher heating value of *Leucaena leucocephala* pellets

Saturated aqueous solution	%Relative humidity	MC (%wb)		HHV (J g^{-1})	
		Average	Standard deviation	Average	Standard deviation
CH_3COOH	22.6	7.31	0.345	17662	89.0
$MgCl_2$	32.7	7.35	0.224	17613	32.6
K_2CO_3	43.8	7.75	0.207	17559	19.5
NaBr	57.5	8.83	0.132	17422	87.4
$NaNO_2$	63.5	9.47	0.157	17260	41.4
NaCl	75.3	11.7	0.088	16891	88.8
KCl	84.3	14.9	0.139	16440	39.2

1.5.2 Near infrared spectroscopy models for moisture content and higher heating value of Leucaena leucocephala pellets

Table 1.2 shows the statistical data regarding the moisture content and higher heating value of *Leucaena leucocephala* pellet samples including minimum, maximum, mean and standard deviation that were used for model development. Table 1.3 shows

the result of the wavenumber range, spectrum pre-processing method, number of PLS latent variables, coefficient of determination (R^2) of both calibration and validation, RMSEE (root mean square error of estimation), RMSECV (root mean square error of cross validation), RPD (ratio of prediction to deviation) and bias of the optimum PLS models.

Table 1.2 Statistical moisture content and higher heating value data of *Leucaena leucocephala* pellet samples used in model development

Parameter	N	Max	Min	Mean	SD
Moisture content (%wb)	42	14.9	7.01	9.62	2.63
Heating value (J g^{-1})	42	17765	16460	17253	425

N is number of samples. Min is minimum. Max is the maximum. SD is standard deviation

Table 1.3 Results of the partial least squares regression models for determining the moisture content and higher heating value of *Leucaena leucocephala* pellets

Parameter	Wavenumber range (cm^{-1})	Pre-processing	Calibration			Validation			
			Factors	R^2	RMSEE	R^2	RMSECV	RPD	Bias
MC (%wb)	7506-5446.3 4428-4242.9	Min-max normalization	4	0.996	0.168	0.995	0.187	13.9	-8.0×10^{-4}
	5446.6-4420.3	Min-max normalization	4	0.996	0.181	0.995	0.193	13.4	0.00181
HHV (J g^{-1})	9403.8-7498.3 6102 – 5446.3	Min-max normalization	4	0.972	74.5	0.964	79.2	5.3	1.29
	5446.3-4242.9	First derivative+MSC	1	0.959	87.0	0.955	89.2	4.71	-0.102

R^2 is coefficient of determination. RMSEE is the root mean square error of estimation. RMSECV is the root mean square error of cross validation. RPD is ratio of standard deviation, and Bias is average error of prediction. MSC is the multiplicative scatter correction.

The wavenumber ranges were effective for the determination of the properties and were 7506-5446.3 and 4428-4242.9 cm^{-1} for moisture content and 9403.8-7498.3 and 6102-5446.3 cm^{-1} for higher heating value. The spectra pre-processing by min-max

normalization was the best pre-treatment method that provided the best model performance for both moisture content and higher heating value. Therefore, by this mathematic manipulation, the spectra were shifted linearly so that the minimum absorption equaled zero, which helped to reduce the influences from different material densities or particle sizes [28]. The number of PLS latent variables used for the model development was 4 for both moisture content and higher heating value. The calibration models of moisture content and higher heating value showed 0.996 and 0.972 of R^2, 0.168%wb and 74.5 J g^{-1} of RMSEE, respectively, while the validation models of moisture content and higher heating value provided 0.995 and 0.964 of R^2, 0.187%wb and 72.9 J g^{-1} of RMSECV, 13.9 and 5.30 of RPD and -0.0008%wb and 1.29 J g^{-1} of bias, respectively. The R^2_{max} of the moisture content model was 0.988, while R^2 values were 0.996 and 0.995 for the calibration and validation model. For this case, approximately 1.24% error was found from the reference test, and no error was found from the NIR spectra. For the higher heating value model, R^2_{max} was 0.890, while R^2 were 0.972 and 0.964 for the calibration and validation model. The information on the NIR spectrum demonstrated a dependent variance of 96.4% and a 3.56% error from an unexplained source. However, the moisture content and higher heating value models provided less R^2_{max} than R^2. This indicated that optimum PLS models and pre-processing method could eradicate the error from the reference laboratory and spectra. Williams [18] suggested that the models with $R^2 > 0.980$ and RPD > 8.10 were excellent and could be used in any application including quality assurance. Furthermore, models with R^2 = 0.920-0.960 and RPD of 5.00-6.40 were good and could be used for most applications, including quality assurance. So, the moisture content and higher heating value models developed here could be used in any applications including quality assurance. For higher heating value, the model provided a low bias of approximately 1.10×10^{-3}% of the mean value (0.020 J $g^{-1}$of 17,253 J g^{-1}); therefore, the model was excellent for the approximation of heating value. Posom and Sirisomboon [29] also reported that the model for heating value of *J. curcas* kernel oil extracted residue showed R^2 of 0.860, RMSEP of 360 J g^{-1}, bias of -17.0 J g^{-1} and RPD of 2.60. It showed a low bias of approximately 0.100% of the mean value; therefore, the model was acceptable for the approximation of the heating value.

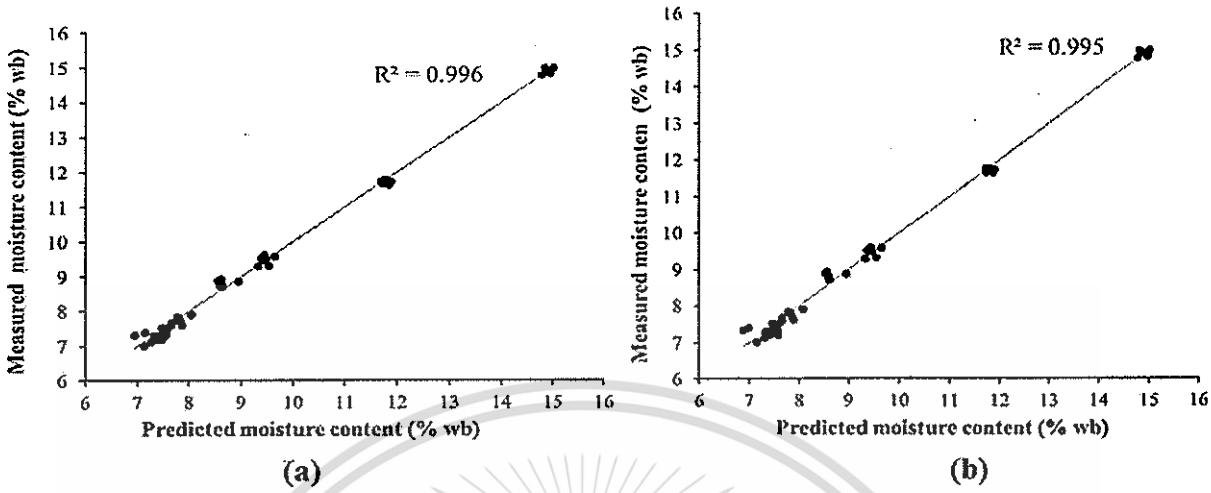

Figure 1.6 Comparison of the moisture content of *Leucaena leucocephala* pellets predicted by near infrared spectroscopy and measured by the reference laboratory of (a) the calibration model and (b) the validation model

Figure 1.6a and 1.6b show the scatter plots of the moisture content models comparing the moisture content predicted by NIR spectroscopy and measured with the reference laboratory technique of calibration and validation modelling, respectively.

Figure 1.7a NIR spectra pretreated by min-max normalization, Figure 1.7b shows the regression coefficient plot of the moisture content model, and Figure 1.7c shows the corresponded X-loading plot of 4 PLS LV (latent variables), respectively.

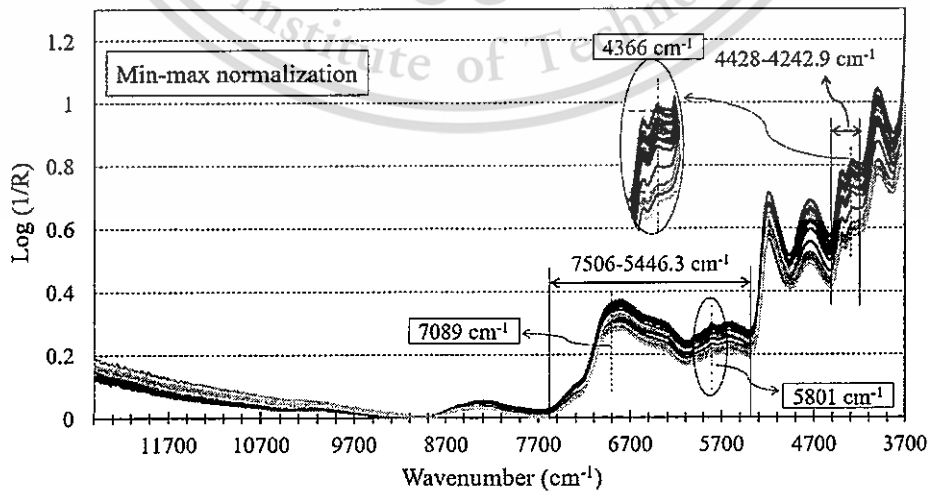

a)

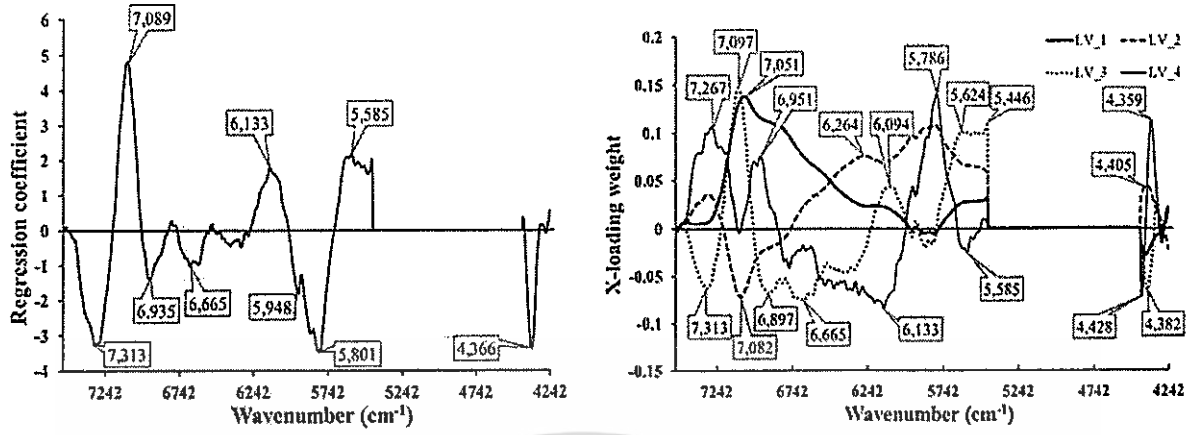

b) c)

Figure 1.7 (a) NIR spectra pretreated by min-max normalization, (b) PLS model regression coefficient plot for the moisture content of *Leucaena leucocephala* pellets. (c) X-loading weight plot of the PLS model for the moisture content of *Leucaena leucocephala* pellets. LV_1, LV_2, LV_3 and LV_4 are PLS latent variables 1, 2, 3 and 4, respectively.

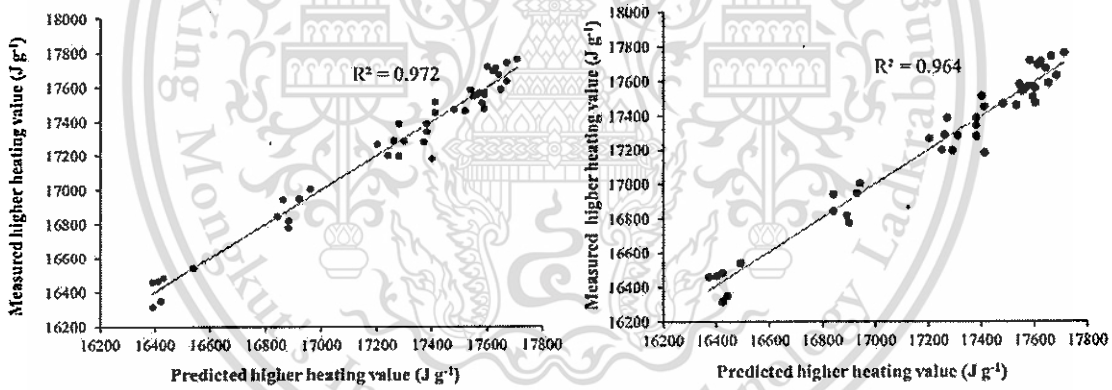

a) b)

Figure 1.8 Comparison of higher heating values of *Leucaena leucocephala* pellets predicted by near infrared spectroscopy and measured by reference laboratory of (a) the calibration model and (b) the validation model

If the regression coefficient and X-loading weight at any wavenumber is high, the vibration of the particular bond occurring at that frequency will have a significant influence on the model prediction. The absorption bands at a high regression coefficient and X-loading weight plot for predicting the moisture content are shown in Table 1.4, in which

the intensity of the peaks is presented in descending order. The highest peak was approximately 7089 cm^{-1} (1410 nm) in the regression coefficient plot. The highest peaks of the X-loading weight plots of PLS latent variables 1, 2 and 3 was at approximately 7097 cm^{-1} (1409 nm), which was the vibration of ROH (O-H stretch first overtone) [17]. The high peaks at approximately 5801 cm^{-1} (1724 nm), 7313 cm^{-1} (1367 nm) and 4366 cm^{-1} (2290 nm) in the regression coefficient plot and X-loading weight plot were due to the vibration of CH_2 (C-H stretch first overtone), the CH_3 (2xC-H stretch + C-H deformation) and the amino acids (N-H stretching + C=O stretching) [17], respectively. Onsawai and Sirisomboon [30] found that the bond vibration of O-H stretching in a cellulose structure highly influenced the prediction of the dry matter of durian pulp. Phetpan and Sirisomboon [31] also found that O-H bands of starch and O-H bands of water influenced the prediction of the moisture content of tapioca starch. Posom and Sirisomboon [29] reported that the vibration band of CH_3 (C-H stretch, second overtone), CH (C-H stretch, second overtone), starch (O-H stretch + C-C stretch) and cellulose highly affect the prediction of moisture content in *J. curcas* kernels. Fagan et al. [32] also reported the effect of O-H stretching on prediction of moisture content of SRCW (Short Rotational Coppice Willow) and *Miscanthus* samples.

Figure 1.8a and Figure 1.8b show the scatter plots of the higher heating value models developed from calibration and validation, respectively. Figure 1.9a NIR spectra pretreated by min-max normalization (b) show the regression coefficient plot and (c) X-loading weight plot of the higher heating value model of *Leucaena leucocephala* pellets. The absorption bands at the peaks of the regression coefficient plot and those of the X-loading weight plot correspond to the bond vibration as concluded in Table 1.5.

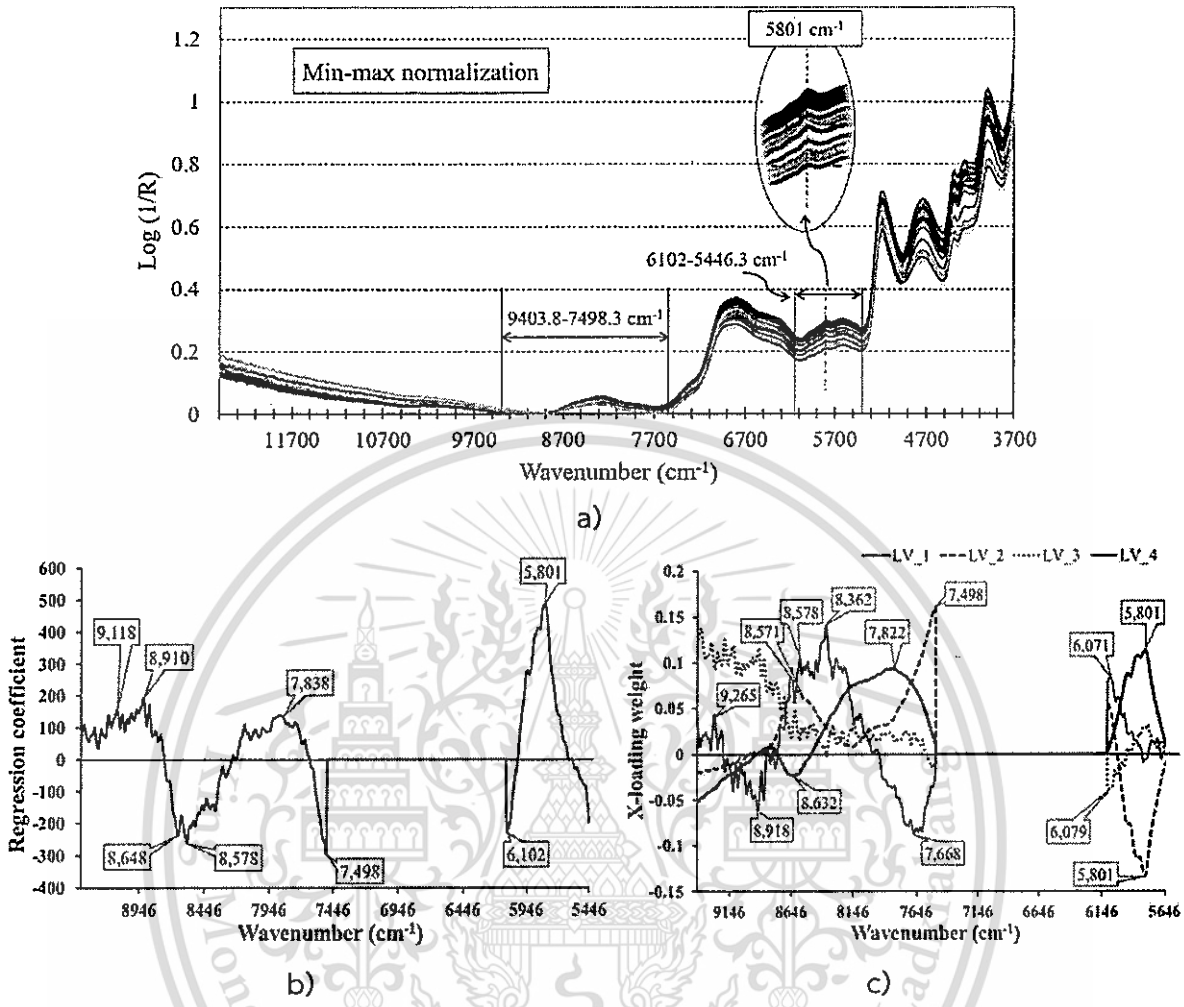

Figure 1.9 (a) NIR spectra pretreated by min-max normalization, (b) Regression coefficient plot of the PLS model for higher heating value of *Leucaena leucocephala* pellets. (c) X-loading weight plot of the PLS model for higher heating value of *Leucaena leucocephala* pellets. LV_1, LV_2, LV_3 and LV_4 are PLS latent variable 1, 2, 3 and 4, respectively.

The obvious peaks at approximately 5801 cm^1 (1724 nm) in the regression coefficient and X-loading weight plots was at CH_2 (C-H stretch first overtone), indicating the highest influence on the prediction of higher heating value of *Leucaena leucocephala* pellets. This peak appeared on the NIR spectral curve pretreated by min-max normalization (Figure 1.9a). The wavenumbers in range of 6102-5446.3 cm^{-1} was used for modelling, there were wave band of 1682 nm [33], 1730 nm [34], 1750 nm [34], and 1780

nm [35] corresponded with the vibration band of lignin, hemicellulose, hemicellulose, and cellulose, respectively. From the results, author recommended that the wave band in range of 6102-5446.3 cm^{-1} should be used to develop as an NIR instrument for predicting higher heating value of biomass. In the regression coefficient and X-loading weight plots, there were high peaks at approximately 7498 cm^{-1} (1334 nm) and 7822 cm^{-1} (1278 nm) due to CH (C-H stretching second overtone). A peak also occurred at 6102 cm^{-1} (1639 nm) due to R-CH-CH (C-H stretching first overtone). Therefore, the vibration of C-H stretching highly affected the prediction of the higher heating value of *Leucaena leucocephala* pellets. C-H bonds are in the structure of lignin, cellulose and hemicellulose. Table 1.5 shows the first three highest peaks in the regression coefficient and X-loading plot as the vibration bands of CH_2, CH_3 and HC=CH. These bonds are in the structure of lignin polymers. In fact, lignin in its pure form has a higher HHV than cellulose or hemicellulose [36, 37, 38, 39, 40], so its contribution to the overall biomass HHV should be significant. The higher heating values of *Leucaena leucocephala* pellets samples were the heat obtained from combustion of organic matter, i.e., cellulose, hemicellulose, lignin and starch. This result was similar to Posom and Sirisomboon [29] that the vibration bands of fibre and cellulose have important effects on the prediction of the higher heating value of *J. curcas* kernels. Gillespie et al. [41] reported that the absorption band at 915 nm was related to the 3rd overtone stretching of the C-H bonds of CH_2, at 1314 nm to 1377 nm and at 1643 nm.

Furthermore, the stretching and deformation of the C-H bonds also influenced the absorption band and the region at 1454 nm, which is related to the 1st overtone of stretching of the O-H bonds of H_2O. The bands were important for higher heating value of wood, *Miscanthus* and herbaceous energy grasses. Fagan et al. [32] also reported that the vibration of the C-H stretching (second overtone) of aromatic and the CH_3 structure effected the prediction of the higher heating value of biomass (*Miscanthus x giganteus*). Huang et al. [42] found that absorption bands at 1194 nm related with C-H stretch second overtone at 1724 nm, 1766 nm related with the C-H first overtone, 1930 nm related with O-H stretch/H-O-H deformation combination, 2100 nm related with the O-H bend/C-O stretch combination, 2280 nm related with C-H stretch/CH_2 deformation, 2236 related with C-H stretch/C-H deformation. Each of these results effected the heating value prediction

for straw samples. However, a different trend was found by Everard et al. [43], where the O-H stretching first overtone, O-H stretching, and N-H stretching first overtone, i.e., 1430 nm, were related for the higher heating value of bioenergy crops (i.e., *Miscanthus* and two varieties of SRCW). The higher heating value model of *Leucaena leucocephala* pellets was developed from the waveband of 9403.8-7498.3 cm^{-1} (1063-1333 nm) and 6102-5446.3 cm^{-1} (1638-1836 nm). These waveband ranges were strongly associated with C-H vibration in the structure of CH, CH_2, CH_3 in lignocellulosic, which effected the heat of combustion. The range of 7498 to 6102 cm^{-1} (1333-1638 nm) was not used to create the model. The N-H first overtone band was in this range and was the structure of CONH, CONHR, $CONH_2$, $ArNH_2$, NH, protein, RNH_2 [17]. This indicated that the N-H bond in the chemical structure did not relate to the heat combustion of *Leucaena leucocephala* pellets.

However, the wavenumber ranges that were not selected for modelling above were used for new modelling. In the case of moisture content, the 5446.6-4420.3 cm^{-1} that contained a water band at 5154.6 cm^{-1} was used. The validation model with PLS LV (latent variables) equal to 4 provided the R^2 of 0.995, RMSECV of 0.193% wb, RPD of 13.4 and bias of 0.00181% wb (Table 1.3). The result was excellent and close to the results of the previous model. Therefore, the vibration band of water can also be used to optimize NIR instrument for evaluating moisture content of biomass. Therefore, the combination vibration of O-H stretching and O-H deformation [17] effected the moisture content prediction. This was also confirmed by the highest X-loading of the PLS LV1 and the high regression coefficient at the wavenumber.

In case of higher heating value, three bands were used (12500-9403.8, 7498.3-6102, 5446.3-4242.9 cm^{-1}); these bands were not used for previous model development. However, the band between 5446.3 and 4242.9 cm^{-1} showed good performance of the developed model while the other bands did not. However, this wave band was the region of water, the result provided good performance because higher heating value related to moisture content. The performance was similar to that of the previous model. The model with PLS latent variables equal to 1 showed R^2 of 0.955, RMSECV of 89.2 J g^{-1}, RPD of 4.71 and bias of -0.102 J g^1 (Table 1.3). Remarkably, bias decreased from 1.29 to 0.102 J g^{-1}, and the PLS latent variables reduced from 4 to 1. The model characteristic was better than

the previous model where the information in the NIR spectrum extracted by only one PLS latent variable was enough to explain the dependent variable. With only 1 latent variable, it was ensured that this model could eliminate the noise or bias that came from scanning, sample preparation, instrument error and other sources. In addition, the highest X-loading of LV_1 was at 4921.7 cm^{-1}, which corresponded to the vibration of the C=O stretch second overtone of amide [17] and the high peak at 5322.9 cm^{-1} that corresponded to the same vibration.

1.6 Conclusion

NIR spectroscopy could be an alternative method for oven drying and bomb calorimetry for the evaluation of MC (moisture content) and the HHV (higher heating value) of *Leucaena leucocephala* pellets, respectively. The MC model was excellent for use in any application, and the HHV model could be used for quality assurance. These will be benefit the biomass pellet industry for the rapid quantification of properties as price set parameters and monitoring conversion processes of the pellets with less cost. A good relationship between HHV and MC was HHV=-159MC+18,780. Thus, the HHV of the pellets can be evaluated using the MC obtained from the oven analysis.

This chapter shows that the MC affects the HHV significantly and NIR spectroscopy has high ability for predicting both MC and HHV. The MC can be used to predict HHV. The next chapter investigates about the use of NIR spectroscopy for the determination of HHV, VM, FC and A of ground bamboo when MC is constant.

Table 1.4 The absorption bands with high regression coefficients and the X-loading weight of the model for the moisture content of *Leucaena leucocephala* pellets

Regression coefficient				
Wavenumber (cm^{-1})	Wavelength (nm)	Wavelength (nm) referred from reference [17]	Bond vibration	Structure
7089	1410	1410	O-H stretching first overtone	Lignin
5801	1724	1725	C-H stretching first overtone	CH_2
4366	2290	2294	N-H stretching + C=O stretching	Amino acid
7313	1367	1368	-	Sucrose
5948	1681	1685	C-H stretching first overtone	Aromatic
5585	1790	1780	C-H stretching first overtone	Cellulose
6133	1630	1620	C-H stretching first overtone	$=CH_2$
6935	1442	1440	O-H stretching first overtone	Sucrose, starch
6665	1500	1500	N-H stretching first overtone	NH

X-loading weight					
Wavenumber (cm^{-1})	Wavelength (nm)	Wavelength(nm) referred from reference [17]	PLS latent variable	Bond vibration	Structure
7097	1409	1410	LV_3	O-H stretching first overtone	ROH
7051	1418	1420	LV_1	O-H stretching first overtone	ArOH
5786	1728	1725	LV_4,2	C-H stretching first overtone	CH_2
7267	1376	1371	LV_4	-	α-D-glucose
4359	2294	2294	LV_4	N-H stretching + C=O stretching	Amino acid
5446	1836	1820	LV_3	O-H stretching +2xC-O stretching	Cellulose
5624	1778	1780	LV_3	C-H stretching first overtone	Cellulose
6133	1630	1620	LV_4	C-H stretching first overtone	$=CH_2$
4428	2258	2252	LV_4	O-H stretching + O-H deformation	Starch
4382	2282	2280	LV_3	C-H stretching + C-H deformation	CH_3
6665	1500	1500	LV_3	N-H stretching first overtone	NH
7082	1412	1410	LV_2	O-H stretching first overtone	ROH
6897	1449	1450	LV_3	O-H stretching first overtone	Starch, H_2O
7313	1367	1368	LV_3	-	Sucrose
4450	2247	2252	LV_2	O-H stretching + O-H deformation	Starch
5585	1790	1789	LV_4	-	α-D-glucose

Remark: The intensity of the peaks was running in descending order.

Table 1.5 The absorption bands with high regression coefficient and X-loading weight of the model for higher heating values of *Leucaena leucocephala* pellets

Regression coefficient

Wavenumber (cm^{-1})	Wavelength (nm)	Wavelength (nm) referred from reference [17]	Bond vibration	Structure
5801	1724	1725	C-H stretching first overtone	CH_2
7498	1334	1360	2×C-H stretching + 2×C-H deformation	CH_3
8578	1166	1170	C-H stretching second overtone	HC=CH
8648	1156	1152	C-H stretching second overtone	CH_3
6102	1639	1645	C-H stretching first overtone	R-CH-CH
8910	1122	1143	C-H stretching second overtone	Aromatic
9118	1097	1097	2×C-H stretching + 2×C-C stretching	Cyclopropane
7838	1276	1278	-	Cellulose and Hemicellulose

X-loading weight

Wavenumber (cm^{-1})	Wavelength (nm)	Wavelength (nm) referred from reference [17]	PLS latent variable (LV)	Bond vibration	Structure
7498	1334	1360	LV_2	2×C-H stretching + 2×C-H deformation	CH_3
8362	1196	1195	LV_4	C-H stretching second overtone	CH_3
5801	1724	1725	LV_2,1	C-H stretching first overtone	CH_2
8578	1166	1170	LV_4	C-H stretching second overtone	HC=CH
7668	1304	1278	LV_4	-	Cellulose and Hemicellulose
7822	1278	1278	LV_1	-	
6071	1647	1645	LV_4	C-H stretching first overtone	R-CH-O-CH
8571	1167	1170	LV_2	C-H stretching second overtone	HC=CH
8918	1121	1143	LV_4	C-H stretching second overtone	Aromatic
9265	1079	1080	LV_4	2×C-H stretching + 2×C-C stretching	Benzene
8632	1158	1152	LV_1	C-H stretching second overtone	CH_3
6079	1645	1645	LV_3	C-H stretching first overtone	R-CH-O-CH

Remark: The intensity of the peaks was running in descending order.

1.7 References

[1] Sripongpakapun K, Tudsri S, Sripichitt P, Kaewtrakulpong K. "Comparation of wood productivity and calorific value of five varieties/lines of *Leucaena leucocephala* after three years of establishment for sustainable renewable energy." **J. Agr Sci**, vol. 41, 2010. Pp. 149-152.

[2] Power Pellet: [Online]. Available : http://www.renewableenergy-asia.com/Portals/0/seminar/Presentation/01.1-A2.pdf.

[3] *Leucaena leucocephala.* From Wikipedia, the free encyclopedia. This page was last modified on 23 December 2016, at 07:58. [Online]. Available : https://en.wikipedia.org/wiki/Leucaena_leucocephala

[4] Mainoo AY, Ulzen-Appiah F. "Growth, wood yield and energy characteristics of *Leucaena leucocephala*, *Gliricidia sepium* and *Senna siamea* at age four years." **Ghana J. Forestry**, vol.3, 1996.

[5] Adapa PK, Singh AK, Schoenau GJ, Tabil LG. "Pelleting characteristics of fractionated alfalfa grinds: hardness models." **Power Handling and Processing**, vol. 18, 2006. Pp. 1-6.

[6] Birchenough D., Cook A., Keeney W., Magnus K. "Guidebook. Wood pellets heating." Massachusetts Division of Energy Resources, 2007.

[7] Rhén C, Öhman M, Gref R, Wästerlund I. "Effect of raw material composition in woody biomass pellets on combustion characteristics." **Biomass Bioenergy**, vol. 31, 2007. Pp. 66–72.

[8] Kaliyan N, Morey RV. "Natural binders and solid bridge type binding mechanisms in briquettes and pellets made from corn stover and switchgrass." **Bioresour Technol,** vol. 1010, 2010. Pp. 1082–1090.

[9] Bingham J. "The global outlook for wood pellet markets". [Online]. Available: https://www.pellet.org/wpac-agm/images/2016/JohnBingham-The-global-outlook-for-wood-pellet-markets.pdf

[10] L. Blair. Global wood pellet market update. 7th International Bioenergy Conference & Exhibition Prince George, June 2016. [Online]. Available : http://www.bioenergyconference.org/wp-content/uploads/2016/06/Blair-Louisa.pdf

[11] Fiona (McDermott) Matthews. Global wood pellet market outlook. Halifax, November. 2015. WPAC Annual Conference. [Online]. Available : https://www.pellet.org/images/2015/FionaMcDermottHawkinsWright.pdf

[12] Alternative Energy Development Plan (AEDP2015). [Online]. Available : http://www.dede.go.th/download/files/AEDP2015_Final_version.pdf

[13] Shrestha A., saechua W., sirisomboon P. Some physical and combustion characteristic of leucaena leucocephala pellet. **The 8th TSAE International Conference ET-08,** 2015. [Online]. Available : http://www.tsae.asia/2015conf/proceeding/et08.pdf.

[14] Dardenne P. "Some considerations about NIR spectroscopy: Closing speech at NIR-2009." **NIR news,** 2010. Pp. 21:8–14.

[15] Gunde M.K, Logar J.K, Orel Z.C, and Orel B. "Application of the Kubelka-Munk Theory to Thickness-Dependent Diffuse Reflectance of Black Paints in the Mid-IR. Appl." **Spectrosc,** vol. 49(5), 1995. Pp. 623-629.

[16] Voort P.V.D, Vansant E.F. Spectroscopy of Transition Metal Ions on Surfaces, Infrared spectroscopy, Leuven University press: Belgium; 2000. Pp. 169.

[17] Osborne BG, Fearn T. Near infrared spectroscopy in food analysis. Theory of near infrared spectroscopy, USA: Longman Scientific & Technical: New York; 1986. Pp. 36-40, 133.

[18] Williams P. "Near-infrared technology-Getting the best out of light." Nanaimo, British Columbia, and Winnipeg, Manitoba, Canada; 2007: PDK Grain.

[19] Kelley S.S, Rials T.G, Snell R, Groom L.H, Sluiter A. "Use of near infrared spectroscopy to measure the chemical and mechanical properties of solid wood." **Wood Sci Technol,** vol. 38, 2004. Pp. 257–276.

[20] Garcia R, Pizarro C, Lavín AG, Bueno JL. "Spanish biofuels heating value estimation. Part I: ultimate analysis data." **Fuel,** vol. 117, 2014. Pp.1130–1138.

[21] Kakitis A, Ancans D, Nulle I. "Evaluation of combustion properties of biomass mixtures." **Engineering for Rural Development,** vol. 29, 2014. Pp. 423-427.

[22] Shen J, Zhu S, Liu X, Zhang H, Tan J. "Measurement of heating value of rice husk by using oxygen bomb calorimeter with benzoic acid as combustion adjuvant." **Energy Procedia,** vol. 17, 2012. Pp. 208 – 213.

[23] Telmo C, Lousada J, Moreira N. "Proximate analysis, backwards stepwise regression between gross calorific value, ultimate and chemical analysis of wood." **Bioresour Technol**, vol. 101, 2010. Pp. 3808–3815.

[24] Friedl EP, Rotter H, Varmuza K. "Prediction of heating values of biomass fuel from elemental composition." **Anal Chim Acta**, 2005. Pp. 191–198.

[25] Mahapatra K, Harris DL, Durham DL, Lucas S, Terrill TH, Kouakou B, Kannan G. "Effects of moisture change on the physical and thermal properties of *sericea lespedeza* pellets." **Int Agr Eng**, vol. 19(3), 2010. Pp. 23-29.

[26] Komilis D, Kissas K, Symeonidis A. "Effect of organic matter and moisture on the calorific value of solid wastes: An update of the Tanner diagram." **Waste Management**, vol. 34, 2014. Pp. 249–255.

[27] Demirbas A. "Effects of moisture and hydrogen content on the heating value of fuels." **Energ Source**, vol. 29(7), 2007. Pp. 649-655.

[28] Conzen JP. Selection criteria for a PLS calibration; Method optimization. "Multivariate calibration". Bruker Optik GmbH; 2006, 2rd edition.

[29] Posom J, Sirisomboon P. "Evaluation of the moisture content of *Jatropha curcas* kernels and the heating value of the oil extracted residue using near-infrared spectroscopy." **Biosystem Eng**, vol. 130, 2015. Pp. 52-59.

[30] Onsawai P, Sirisomboon P. "Determination of dry matter and soluble solids of durian pulp using diffuse reflectance near infrared spectroscopy." **J. Near Infrared Spec**, vol. 23, 2015. Pp. 167–179.

[31] Phetpan K, Sirisomboon P. "Evaluation of the moisture content of tapioca starch using near infrared spectroscopy." **J. Innov Opt Health Sci**, vol. 8, 2015. Pp. 1-12.

[32] Fagan CC, Everard CD, McDonnell K. "Prediction of moisture, calorific value, ash and carbon content of two dedicated bioenergy crops using near-infrared spectroscopy." **Bioresour Technol**, vol. 102, 2011. Pp. 5200–5206.

[33] Kubo S, Kadla JF. "Hydrogen bonding in lignin: a Fourier transform infrared model compound study." **Biomacromolecules**, vol. 6, 2005. Pp. 2815-21.

[34] Sills DL, Gossett JM. "Using FTIR to predict saccharification from enzymatic hydrolysis of alkali pretreated biomasses." **Biotechnol Bioeng**, vol. 109, 2012. Pp. 353-62.

[35] Workman JJ, Weyer L. "Practical guide to interpretive near infrared spectroscopy." CRC Press, New York.

[36] Álvarez A, Pizarro, García R, Bueno JL. "Spanish biofuels heating value estimation based on structural analysis." **Ind Crop Prod**, vol. 77, 2015. Pp. 983–991.

[37] Tanger P, Field JL, Jahn CE, DeFoort MW, Leach JE. "Biomass for thermochemical conversion: targets and challenges." **Front Plant Sci**, vol.4, 2013. Pp. 218.

[38] Demirbas A. "Relationships between heating value and lignin, moisture, ash and extractive contents of biomass fuels." **Energ Explor Exploit**, vol. 20, 2002. Pp. 105-111.

[39] Demirbaş A. "Relationships between lignin contents and heating values of biomass." **Energy Convers**, vol. 42, 2001. Pp. 183–188.

[40] Helsel ZR, Wedin WF. "Direct combustion energy from crops and crop residues produced in Iowa." **Energ Agr**, vol. 1, 1981–1982. Pp. 317-329.

[41] Gillespie GD, Everard CD, McDonnell KP. "Prediction of biomass pellet quality indices using near infrared spectroscopy." **Energy**, vol. 80, 2015. Pp. 582-588.

[42] Huang C, Han L, Yang Z, Liu X. "Prediction of heating value of straw by proximate data, and near infrared spectroscopy." **Energ Convers Manage**, vol. 49, 2008. Pp. 3433–3438.

[43] Everard CD, McDonnell KP, Fagan CC. "Prediction of biomass gross calorific values using visible and near infrared spectroscopy." **Biomass Bioenergy**, vol.45, 2012. Pp. 203-211.

Chapter 2

Evaluation of the higher heating value, volatile matter, fixed carbon and ash content of ground bamboo using near infrared spectroscopy

2.1 Abstract

This research aimed to determine the higher heating value (HHV), volatile matter (VM), fixed carbon (FC) and ash content (A) of ground bamboo using Fourier transform near-infrared spectroscopy as an alternative to bomb calorimetry and thermogravimetry. Bamboo culms used in this study have circumferences ranging from 16-40 cm. Model development was performed using partial least squares (PLS) regression. The HHV, VM, FC and A were predicted with coefficient of determination (r^2) of 0.92, 0.82, 0.85 and 0.51; root mean square error of prediction (RMSEP) of 122 Jg^{-1}, 1.15%, 1.00% and 0.768%; ratio of the standard deviation to standard error of validation (RPD) of 3.66, 2.55, 2.62 and 1.44; bias of 14.4 Jg^{-1}, -0.427%, 0.0256% and -0.108%, respectively. This report shows that NIR spectroscopy is quite successful in predicting the HHV, and is usable with screening for the determination of FC and VM. For A, the method is not recommended. The models should be able to predict the properties of bamboo for achieving highly efficient of biomass conversion process.

* This chapter is under review for the journal article (J Near Infrared Spectroscopy): Posom J. and Sirisomboon P. "Evaluation of the higher heating value, volatile matter, fixed carbon and ash content of ground bamboo using near infrared spectroscopy."

2.2 Introduction

Bamboo is a type of biomass which has many advantages including a fast-growth rate, high strength, and a high yielding natural source [1-2]. Bamboos are large woody grasses that consists of 1250 species within 75 genera. It produces rapid growth and attains stand maturity within five years [3]. Some species can grow up to a foot a day under the right condition [4]. In the south of Asia, bamboo is used for the construction of walls, floor, roof, apparatus, and handicrafts. In addition, bamboo also has great potential as a renewable energy source [5-6]. Scurlock et al. [3] reported that bamboo is an ideal bioenergy source due to its low ash content (A) (1% or less) and higher heating value (HHV) that ranges from 19090-19570 Jg^{-1}. Darabant et al. [7] reported that bamboo *B. beecheyana* and *D. membranaceus* species were attractive options for use as bioenergy feedstocks due to their high volatile mater (VM), low A and high HHV of 74.08 and 74.17%; 1.92 and 1.97%; and 19347 and 19513 Jg^{-1}, respectively. Furthermore, Cheng et al.[6] reported that the HHV of these two bamboo species were in the range of 19.4–19.9 $MJkg^{-1}$. It is also reported that age differences in bamboo biomass can have a significant effect on yield and properties of the fast pyrolysis products [6]. It is possible that the chemical composition of biomass also changes with age and other external factors such as location, harvest age, soil fertility and so on. Additionally, different locations can lead to different biomass yield, as reported by Darabant et al. [7], who demonstrated that the bamboo biomass characteristics can show vast differences under differing plantation management conditions. It was observed that the cellulose content decreased, lignin content increased and ash content increased when the age of bamboo increased from one year to three years [6]. These factors also affected the thermal processing characteristics.

Understanding the characteristics of biomass helps in the design of optimum thermal conversion systems [8]. The HHV and proximate analysis data are important in thermal processing [9,10]. The HHV is one of the thermal characteristics that expresses how much energy can be obtained from biomass material [11]. When biomass is used in thermal conversion processes and in power plants, knowledge of its HHV is required. It is an important parameter for power plants planning to use biomass fuel [12, 13, 14]. Furthermore, the VM and fixed carbon (FC) provides information to understand the combustion behavior which significantly influences plant design [9]. In fast pyrolysis processing, the VM of a substance is the extent to which it vaporizes. It is used to

evaluate the performance of the biomass pyrolysis and gasifier based on the rate of gas production [15]. In addition, it also helps in the evaluation of bio-oil condensation. In slow pyrolysis, the information provided by the FC helps operators to evaluate the weight of bio-char or solid products. Finally, A represents the solid residue after the fuel is burned. It is the negative of the heat consumption and the information described by A is important for the design of the storage bins in thermal conversion processing [16]. It is known that a high A value also has implications for transportation systems [9].

The cost of biomass per kilogram should be set in a fair way by considering parameters such as the HHV and proximate analysis data. Normally, the HHV can be determined by calorimetry. The proximate analysis data can be determined using thermogravimetric (TG) analysis by the direct measure of weight changes of a sample's TG chart [9]. Both parameters require the services of a high skilled technician. These highly skilled workers are then required to spend between 3-24 hrs for TG analysis and 50 min for assessment in a bomb calorimeter, per sample. Hence, a new method that can be used to rapidly determine these properties to allow the setting of a reliable price for biomass fuel is essential as the role of this material increases.

In addition, determining the characteristics of biomass (thermal properties and proximate analysis data) by rapid non-destructive methods is important in determining the theoretical yield associated with biochemical conversion [20]. It can be used to monitor biological or thermochemical conversion processes of bamboo such as for quality evaluation and to design thermal chemical conversion methods such as gasification and pyrolysis processes of bio-energy.

There have been a number of application of NIR spectroscopy to study biomass including the moisture content and HHV of *Jatropha curcas* L.[17], thermal properties of *Jatropha curcas* L.[18], hemicellulose, cellulose and lignin in sorghum[19], HHV of biomass from dedicated Irish bioenergy crops, (i.e. *Miscanthus* and two varieties of short rotational coppice willow (SRCW)) [20], moisture, calorific value, ash and carbon content of harvested *Miscanthus* and SRCW [21], and moisture content, total carbon content, A and HHV of a multi-variety biomass pellet sample set [22]. Near infrared (NIR) spectroscopy is a non-destructive analytical technique with many advantages over calorimetry including the fact that it is non-destructive (the sample can be

returned to population), it is rapid (usually time consumption was 2-3 minute), environmentally friendly (no or few chemical required) and has a low labor cost.

2.3 Objective

This study is therefore focused on the application of NIR spectroscopy beyond just biomass and moisture content, to the determination of HHV, VM, FC and A of ground bamboo.

2.4 Materials and methods

2.4.1 Sample preparation

Bamboo at different ages of the Phamon variety was obtained from Uttaradit province in Thailand. The samples were split into 12 different groups based on their culm circumference (approximately 16-18, 18-20, 20-22, 22-24, 24-26, 26-28, 28-30, 30-32, 32-34, 34-36, 36-38 and 38-40 cm). The circumference was measured from 10 cm above the ground where planted. The bamboo trunk was then cut at 10 cm above the ground to avoid retaining any soil or root that can attach to the trunk for 1 m long. The bamboo samples of different culm circumferences were collected because it was assumed that the different culm sizes would provide different thermal and energy properties. In this experiment, the standard deviation of the culm sizes was 6.85 cm. A total of 80 samples were obtained. The whole trunk, approximately five kg, of each bamboo sample were chopped by a chopping machine (P5508, Patipong, Thailand) and dried under the sun until the moisture reached around 5% wb. The samples were then ground and passed through a sieve with a mesh diameter of 3 mm (60201, QC, UK) and kept in the aluminum bag until experiments were performed. The 5% moisture content value of the dried bamboo wood chips was determined by randomly selected 10 samples for determination of moisture content using a hot air oven method at the temperature of 105°C until constant weight was achieved.

2.4.2 Near infrared spectral scanning

Experiment were performed at the laboratory of Near Infrared Spectroscopy Research Center for Agricultural Products and Food (www.nirsresearch.com), part of the Curriculum of Agricultural Engineering, Department of Mechanical Engineering, Faculty of Engineering, King Mongkut's Institute of Technology Ladkrabang. The scanning of samples were done using an FT-NIR Spectrometer (MPA, Bruker, Germany) in diffuse reflectance mode between a wavenumber range of 12500-3600 cm^{-1}, with resolution of 8 cm^{-1}. A quartz bottom sample cup of 43 mm in diameter and 50 mm in height,

was used, which contained the ground samples of at the height, which there was no light leaked. This was determined by observing that there was no leaked light from the surface of the ground bamboo. Before each sample was scanned, a gold plate was scanned as a reference. A resolution of 8 cm^{-1} was used and each reported result was taken as the average of 64 repeat spectra.

2.4.3 Biomass characterization

The higher heating value (HHV) of biomass was measured with a bomb calorimeter (C200, IKA, Germany) and evaluated using the *isoperibol* method. In this method, the temperature changes over time are governed by the thermal resistance between *isoperibol* calorimeter and the surroundings [23]. Before the measurement were taken, the bomb calorimeter was calibrated using two 0.5 g Benzoic acid pellets (C723, IKA, Germany). Then, between 0.5-1 g of biomass sample was weighed out using an electronic balance (ARC 140 Adventure, OHAUSS, 0.0001 g resolution), pelletized and then evaluated in the bomb calorimeter.

Biomass characteristics including VM, A, and FC were determined using thermogravimetric analysis. Monitoring the mass loss and mass loss rate was performed using a thermogravimetric analyser (TG 209 F3 Tarsus, Netzsch, Germany, with a 0.1 µg resolution; 6.8 mm diameter aluminum oxide (AL_2O_3) crucible). Bamboo samples of 6.0±0.5 mg were used. The thermal program started by maintaining the temperature at 30°C in 20 ml/min N_2 flushed environment for 1 hour to ensure a zero O_2 environment. Then the temperature was increased to 700°C with a heat rate of 10°C/min for pyrolysis. The temperature was maintained at 700°C for 1 hour to ensure complete pyrolysis, and then 20 ml/min O_2 was added for 1 hour to achieve combustion. The mass loss at different times and temperatures were recorded. The thermogravimetric (TG) profile and differential thermogravimetric (DTG) profiles were obtained using Proteus 6.0.0. (NETZSCH Software, Germany). TG and DTG curve was typical of degradation processes such as moisture release, devolatilization and char degradation which can be used for the approximation of the composition of biomass. The biomass characteristics were determined by the direct measure of weight changes on each sample's TG chart. The VM and A were determined from sample's DTG chart. The A is the mass residue after burned. After that, FC can be calculated as follows [24]:

$$FC\% = 100 - (MC\% + VM\% + Ash\%) \quad (2.1)$$

where MC% VM%, FC% and Ash% were the moisture content, volatile matter, fixed carbon and ash content of ground bamboo, respectively. Therefore, VM%, FC% and Ash% were presented on as-receive basis.

When the HHV and proximate analysis data were determined, outliers in the reference data were identified using the following equation [25,26]:

$$\frac{(X_i - \bar{X})}{SD} \geq \pm 3 \quad (2.2)$$

Where X_i is the measured value of sample i. $\bar{X}$ and SD are the average and standard deviation of the measured values of all samples, respectively. If the equation was satisfied, the sample was outlier and it was then removed from reference data set.

2.4.4 Repeatability, reproducibility and maximum coefficient of determination (R^2_{max})

Before model development, the spectral data and the measured reference data were checked for both repeatability and reproducibility. The reproducibility of spectral data is the standard deviation of absorbance values, when the sample was re-loaded and re-scanned 10 separate times (Phil Williams, personal communication). The 10th loading was left in the cell and re-scanned 9 more times, to achieve 10 scans with this sample in the same position within the cell. The standard deviation of these 10 absorbance values was the repeatability of the instrument. The samples number 16, 28 and 44 were selected to determine the repeatability and reproducibility. The absorbance value at wavenumber of 4011 cm^{-1} (2493 nm), 4397 cm^{-1} (2274 nm) and 5176 cm^{-1} (1932 nm) were used for the calculation because they are obvious peaks. The absorption at any wavenumber could be selected for determination of the repeatability and reproducibility of the NIR scanning method. The wavenumber at 4397 cm^{-1} (2274 nm), 4011 cm^{-1} (2493 nm) and 5176 cm^{-1} (1932 nm) corresponds to the absorption band of cellulose, starch [27] and polysaccharides [28], respectively. In addition, the peak showed the greatest change when the scanning conditions and sample conditions were varied. When the absorption of spectra obtained from the samples number 16, 28 and 44 for repeatability and reproducibility tests were collected, the average and standard deviation of the difference between measured value and predicted value were also calculated. The predicted value obtained from repeatability and reproducibility tests were determined using PLS regression of calibration set. A comparison of predicted results on the repeat scans were helpful in

showing the contribution of sample reloading error and instrument error (scanned without reloading) to show the magnitude of instrument error and sample presentation error.

The repeatability of the measured reference value corresponds to the standard deviation of the differences between the duplicates. On the other hand, the reproducibility of the measured reference value was the standard deviation of the differences between the duplicates, which were obtained from blind samples. Then the repeatability of measured reference value (Rep) was used to determine the maximum coefficient of determination (R^2_{max}), which was calculated using following formula [29]:

$$R^2_{max} = \frac{SD_y^2 - Rep^2}{SD_y^2} \quad (2.3)$$

where SD_y is the standard deviation of data of measured value in calibration set. R^2_{max} is possible only when there are no errors in the spectra or the model.

2.4.5 Spectrum pre-processing and NIR spectroscopy modeling

The NIR spectroscopy models were established using partial least squares regression (PLS). The software program (OPUS, v. 7.0.129, Germany) was used for the multivariate analysis including spectrum preprocessing and model development. The spectra were used with and without pre-processing using the following methods: constant offset elimination, straight line subtraction, vector normalization, min-max normalization, multiplicative scatter correction (MSC), first derivatives, second derivatives, first derivatives + straight line subtraction, first derivatives+ vector normalization and first derivatives + MSC were used for model development. Spectral preprocessing helps to reduce the contribution of noise or error in experiment which are the effect of several factor including differences in temperature, particle size, relative humidity, human errors, sample handling, multiplicative effect of scattering and so on. The samples were then split 80/20% into the calibration and validation sample sets, respectively, at random using the software package. The maximum value and minimum value of the reference data were set to be in the calibration set. The optimal model was selected according to the model that had the lowest root mean square error of prediction. Outliers were calculated based on the Mahalanobis distance limit.

The regression coefficient and X-loading weight of each PLS factor were determined by the software program and plotted. The coefficients of determination (R^2), root mean

square error of prediction, (RMSEP), ratio of prediction to deviation (the standard deviation to standard error of prediction, RPD) and bias were used to assess the performance of the PLS model. According to Williams [30], a model with an R^2 between 0.66-0.81 can be used for screening and some other "approximate" applications. Therefore an R^2 below 0.66 means a model cannot be used for quantitative analysis. However, if the standard deviation of dependent variable of calibration set is more than repeatability of dependent variable for 10 times, the R^2 maximum will be more than 0.9.

2.5 Results and discussions

2.5.1 Repeatability, reproducibility and R^2_{max}

Repeatability, reproducibility and R^2_{max} of HHV, and proximate data i.e. VM, FC, A on as-receive of ground bamboo are shown in Table 2.1. The values of R^2_{max} of HHV (0.95), VM (0.96) and FC (0.86) were high indicating that the NIR model was reasonable for development use. Though the value for A was rather low (0.56) this indicates that it is not reasonable to develop an NIR-based model. R^2_{max} is possible only when there is no error in the spectra *[29]*.

Table 2.1 Repeatability, reproducibility and R^2_{max} of HHV, VM, FC and A

Parameter	Repeatability		Reproducibility		R^2_{max}
	Mean of the difference of duplicate	Standard deviation of the difference of duplicate	Mean of the difference of blind duplicate	Standard deviation of the difference of blind duplicate	
HHV	88.38 J/g	68.34 J/g	109.8 J/g	64.46 J/g	0.955
VM	1.010%	0.593%	1.095%	0.916%	0.960
FC	0.885%	1.087%	0.809%	0.845%	0.862
A	1.046%	0.829%	0.516%	0.552%	0.561

Table 2.2 shows the repeatability and reproducibility of absorption at 5176 cm^{-1} (1932 nm), 4397 cm^{-1} (2274 nm), and 4011 cm^{-1} (2493 nm) of ground bamboo. The mean of absorption in repeatability side was almost the same with that of reproducibility side, but the standard deviation or the reproducibility was

approximately more than the repeatability for six times. The average and standard deviation of the difference between measured value and predicted value calculated by the spectra from repeatability and reproducibility tests for HHV, VM, FC and A of sample number 16, 28 and 44 are shown in Table 2.3. The error in NIR protocol could be described as follows, for example, for HHV model, the overall R^2_{max} and R^2 were 0.95 and 0.92, respectively. This means that 5% (100-95%) of the total variation was unexplained variance due to reference method. Thus, it is that 3% (8-5%) was the unexplained variance due to either NIR spectra error, sample error or something else. The standard deviation between the difference of the measured and predicted value from repeatability and reproducibility test to its measured value was 0.121% (21.7×100/17981.5) (Table 2.3) and 0.302% (54.4×100/17981.5) (Table 2.3), respectively. When R^2 was 0.92, the unexplained variances were 5%, 0.121%, and 0.302% due to reference method, NIR spectrometer and sample presentation, respectively, and the residual of 2.57% was the unexplained variance due to other things.

Table 2.2 Repeatability and reproducibility of absorption at 5176 cm^{-1} (1932 nm), 4397 cm^{-1} (2274 nm), and 4011 cm^{-1} (2493 nm) of ground bamboo of sample number 16, 28 and 44

Sample number	Absorption value	Repeatability		Reproducibility	
		Mean of absorption	Repeatability	Mean of absorption	Reproducibility
16	At 5176 cm^{-1} (1932 nm)	0.389	0.00376	0.381	0.0141
	At 4397 cm^{-1} (2274 nm)	0.437	0.00321	0.425	0.0163
	At 4011 cm^{-1} (2493 nm)	0.578	0.00273	0.565	0.0181
Average		0.468	0.00323	0.457	0.0161
28	At 5176 cm^{-1} (1932 nm)	0.408	0.00466	0.401	0.0181
	At 4397 cm^{-1} (2274 nm)	0.461	0.00342	0.453	0.0191
	At 4011 cm^{-1} (2493 nm)	0.603	0.00301	0.598	0.0218
Average		0.490	0.00369	0.484	0.0196
44	At 5176 cm^{-1} (1932 nm)	0.407	0.00388	0.412	0.0196
	At 4397 cm^{-1} (2274 nm)	0.468	0.00427	0.469	0.0199
	At 4011 cm^{-1} (2493 nm)	0.614	0.00244	0.611	0.0228
Average		0.496	0.00353	0.497	0.0207

Table 2.3 The average (AVE) and standard deviation (SD) of the difference between measured value and predicted value obtained using the spectra from repeatability and reproducibility tests for HHV, VM, FC and A of the sample number 16, 28 and 44

Parameters	Sample 16				Sample 28				Sample 44				Average			
	Repeatability		Reproducibility		Repeatability		Reproducibility		Repeatability		Reproducibility		Repeatability		Reproducibility	
	AVE	SD	AVE	SD	AVE	SD	AVE	SD	AVE	SD	AVE	SD	AVE	SD	AVE	SD
HHV (Jg^{-1})	64.7	25.06	147.6	71.83	78.8	8.24	75.5	51.3	49.7	31.7	41.7	40.2	64.4	21.7	88.3	54.4
VM (%)	1.46	0.53	0.99	0.49	1.05	0.11	0.55	0.5	0.52	0.49	1.01	0.54	1.01	0.38	0.85	0.51
FC (%)	1.26	0.47	2.26	1.97	1.52	0.32	0.95	0.88	2.51	0.77	1.52	1.01	1.76	0.52	1.58	1.29
A (%)	0.56	0.38	0.28	0.21	0.62	0.33	0.47	0.22	0.7	0.57	0.68	0.61	0.63	0.43	0.48	0.35

2.5.2 Sample spectra

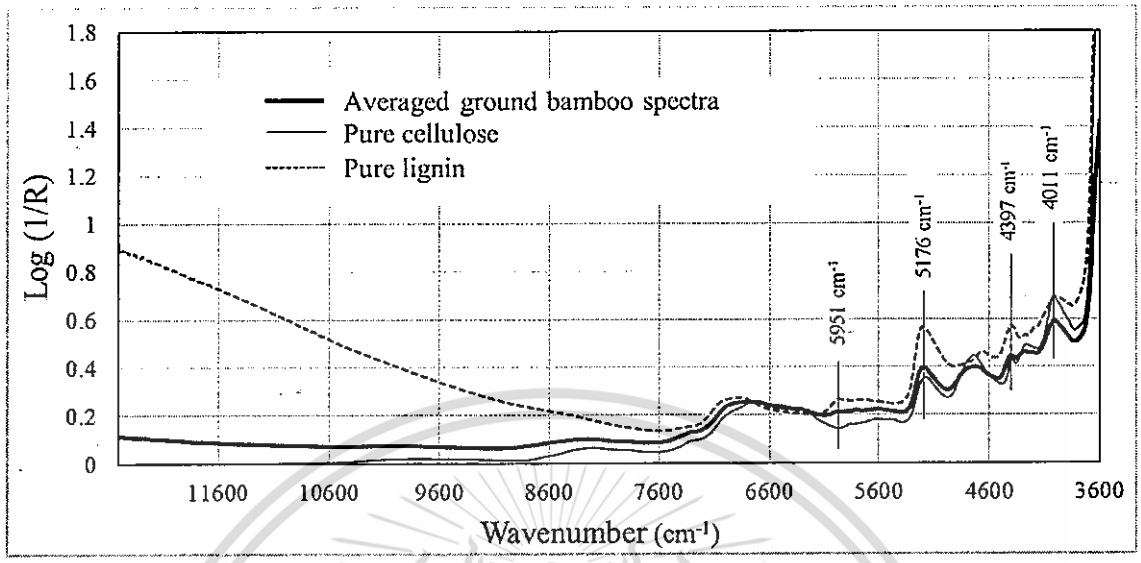

Figure 2.1 Averaged NIR spectra of ground bamboo, pure cellulose and lignin

The averaged NIR spectrum of ground bamboo, pure cellulose and lignin displayed the same obvious peaks at 5176, 4397 and 4011 cm^{-1} (1932, 2274 and 2493 nm) (Figure 2.1). The wavebands of 1930 nm correspond to O-H stretching + H-O-H bending combination of polysaccharides [28], 2276 nm is O-H stretching + C-C stretching of starch [28], 2500 nm is C-H stretching and C-C stretching of starch [28]. Polysaccharides are the major component of starch and cellulose structure, and consist of many individual monosaccharides. Cellulose is a linear polysaccharide polymer. It is the primary component of biological cell walls. Starch also is a major source of energy for plant cells. Furthermore, the CH_2 group appears on lignocellulosic such as hemicelluloses, cellulose and lignin. The peak at 5951 cm^{-1} (1680 nm) demonstrated the different absorption among three materials, lignin is highest, ground bamboo is in the middle, and cellulose is lowest. The wave band at 1685 nm is the C-H stretching of lignin [28].

2.5.3 Model and validation

The statistical data used for model development are shown in Table 2.4.

Table 2.4 Statistical data of higher heating value and proximate data i.e. volatile matter, fixed carbon and ash content on as-receive of ground bamboo used in model development

Parameters	Calibration set					Validation set				
	N	Max	Min	Mean	SD	N	Max	Min	Mean	SD
HHV (Jg^{-1})	64	18357.0	16534.5	17842.9	323.3	16	18319.5	16898.5	17701.9	456.5
VM (%)	64	65.015	52.83	58.2529	2.365	15	63.03	53.56	58.348	2.826
FC (%)	64	36.28	25.76	32.074	2.229	16	35.47	26.19	31.760	2.708
A (%)	64	6.65	1.72	3.868	0.957	16	6.13	1.84	3.726	1.130

N, Max, Min Mean and SD are number of samples, maximum, minimum, average and standard deviation, respectively.

Higher heating value

The most effective model for the prediction of HHV was developed using the wavenumber range of 6102-4597.7 cm^{-1} (1639-2175 nm), spectrum pre-processing consisting of min-max normalization and PLS factor number of 7. It was selected based on the fact it displayed the lowest RMSEP. Scatter plots of measured value by reference laboratory technique (Y axis) and the predicted value obtained by NIR spectroscopy (X axis) for the validation set are shown in Figure 2.2a. The R^2 and RMSEE of calibration were 0.87 and 124 Jg^{-1}, respectively. The r^2, RMSEP, RPD and bias of validation were 0.92, 122 Jg^{-1}, 3.66 and 14.4 Jg^{-1}, respectively. Williams [30] has indicated that the model provided R^2 between 0.92 and 0.96 could be used for most applications, including quality assurance and RPD in the range of 3.1-4.9 could be used for screening. The bias (14.4 Jg^{-1}) was very small compared to the mean of reference value (17701.9 Jg^{-1}).

Figure 2.3a illustrates the spectra of validation set pretreated by min-max normalization, regression coefficient and X-loading weight plot. The regression coefficient plot and X-loading weight plots for the first three PLS factors used in model development are used to interpret the effect of absorbance at the peak wavenumber (X variable) on the prediction of the constituent or properties (Y variable) on the molecular level. A high value at any wavenumber indicates that the vibration of the particular bonds at the wavenumber strongly influences the model prediction.

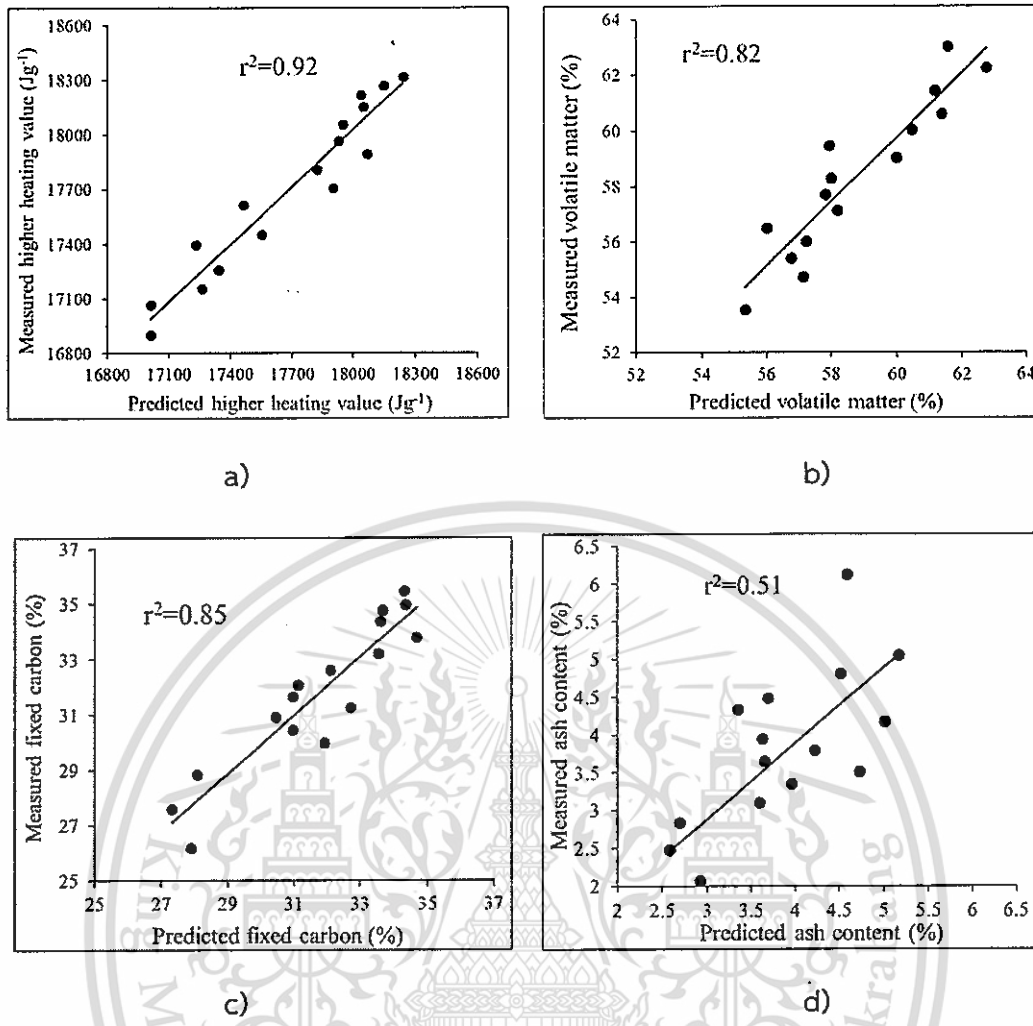

Figure 2.2 Measured vs predicted a) higher heating value, b) volatile matter, c) fixed carbon and d) ash content of validation set

The absorbance region corresponding to 5180 cm^{-1}(1930 nm), 4686 cm^{-1}(2134 nm) and 5994 cm^{-1} (1668 nm) at peak 1, 2 and 3, respectively, were important in the prediction of HHV. The wavebands of 1930 nm correspond to O-H stretching + H-O-H bending combination of polysaccharides [28]. The peak at 2134 corresponded to lignin [31] and 1685 nm corresponded to lignin [28].

The HHV of biomass depended on its chemical composition i.e. lignocellulosic. Even though the HHV was not direct property determining by NIR spectroscopy, but it could be predicted when the interaction between its property and NIR radiation were known [32]. These results were compared to Guimarães et al.[19], that the peaks at about 5940 cm^{-1} (1684 nm) (first overtone of aromatic C-H stretching), 5230 cm^{-1} (first overtone of aromatic O-H stretching), 4415 cm^{-1} (2265 nm) (combination band of O-H

and C-O stretching) were dependent on lignin. These corresponded to hydrocarbons which are the primary energy source of bamboo.

The lignin content is strongly related to the HHV of biomass [33,34]. Posom and Sirisomboon [17] reported that vibration bands of fiber and cellulose had an important effect on the prediction of HHV of *Jatropha curcas* L. Thus, the determination of HHV was affected by the vibration of the C-H bonds associated with lignocellulosic compound.

Volatile matter

The most useful model was developed using a wavenumber range of 7502.2-4597.7 cm^{-1} (1333-2175 nm), with spectrum pre-processing considering of the first derivative + straight line subtraction and PLS factor number of 9. Figure 2.2b shows the scatter plots of measured value by reference laboratory technique (Y axis) and the predicted value obtained by NIR spectroscopy (X axis) for the validation set. The R^2 and RMSEE of calibration set were 0.87 and 0.905%. The r^2, RMSEP, RPD and bias on the validation set were 0.82, 1.15%, 2.55 and -0.427%. The r^2 of 0.82 indicated that the model was acceptable for screening and RPD of 2.55 indicated that the model was acceptable for rough screening [30]. The bias was low compared to the mean measured value (-0.427% of 58.223%).

The spectra of validation set pretreated by first derivative + straight line subtraction, regression coefficient and X-loading weight plot are demonstrated in Figure 2.3b. The obvious peak 1, 2, 3, 4, 5 and 6 were approximately at 5276 cm^{-1} (1895 nm), 7116 cm^{-1} (1405 nm), 5785 cm^{-1} (1728 nm) and 4651 cm^{-1} (2146 nm), 4883 cm^{-1} (2047 nm) and 5091 cm^{-1} (1964 nm), respectively. The wave band at 1896 nm relate to O-H stretching + C-O stretching of C=O and CO_2H [36]. The vibration band of 1728 nm correspond to hemicellulose [27]. The peak at 2146 nm is vibration band of HC=CH [27]. Lignocellulosic compound can be converted into gas product [36]. Both Lv et al.[37] and Burhenne et al.[38] stated that the gas yield of biomass pyrolysis increased with increase of cellulose content, but bio-char yield decreased. Wannapeera et al.[39] reported that biomass (rice husk, rice straw and corncob) contains the highest cellulose content, and gave the highest total gas yield. Xue et al.[40] reported three peak including O-H first overtone (7092 cm^{-1}), C-H stretching first overtone (5797 cm^{-1}), and O-H bend/C-O stretching combination corresponded to prediction of VM into corn stover.

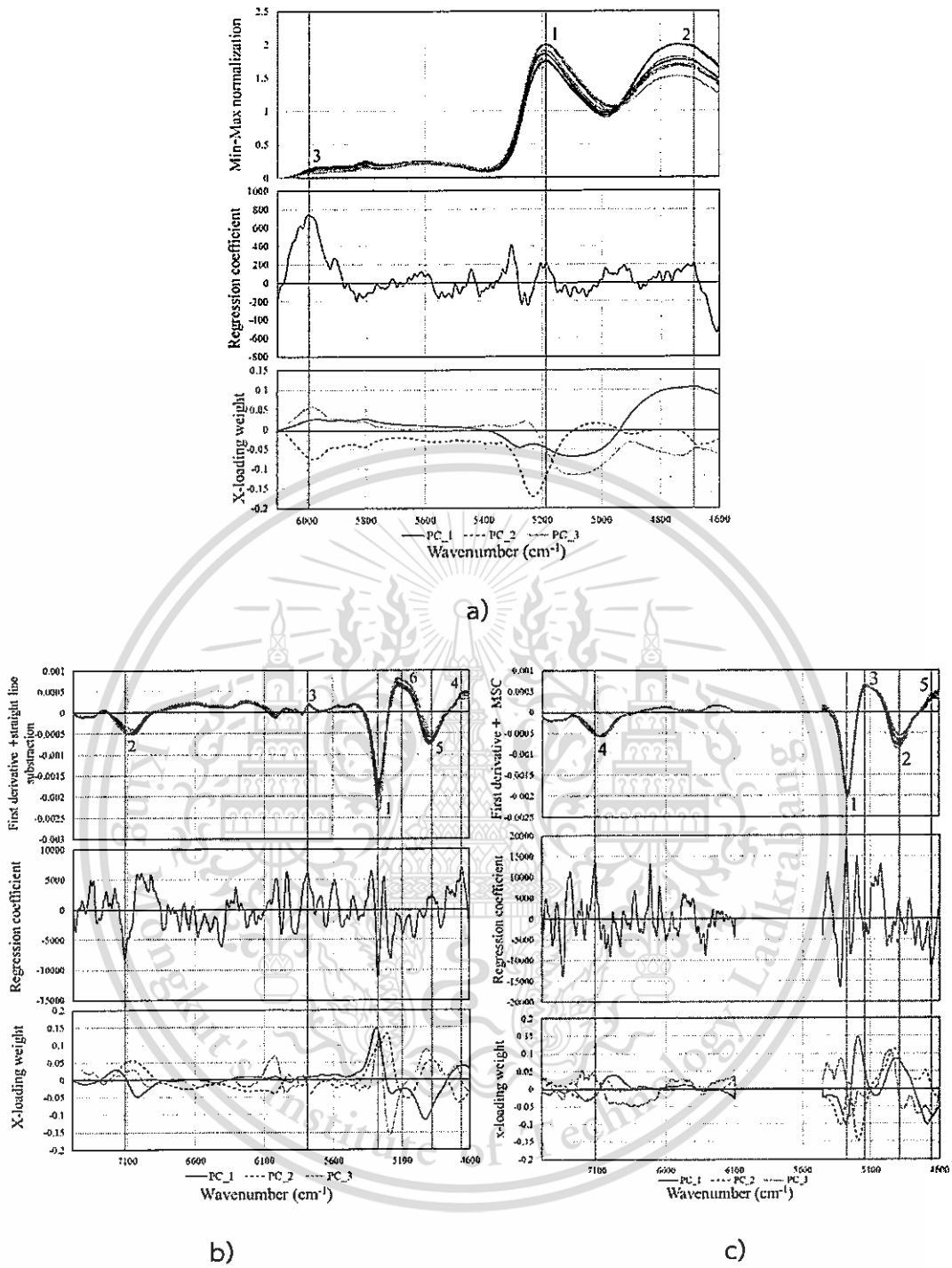

Figure 2.3 Pretreated spectra, regression coefficient plot, X-loading plots of a) higher heating value, b) volatile matter and c) fixed carbon. PC_1, PC_2 and PC_3 are PLS factor 1, 2 and 3, respectively

Fixed carbon

The most effective model for the prediction of the fixed carbon was developed using a wavenumber range of 7502.2-6098.2 cm^{-1} (1333-1639.8 nm) and 5450.2-4597.7

cm^{-1} (1835-2175 nm), with spectrum pre-processing consisting of the first derivative + MSC, with a PLS factor number of 10. Scatter plots of measured value by reference laboratory technique (Y axis) and the predicted value obtained by NIR spectroscopy (X axis) for the validation set are shown in Figure 2.2c. The R^2 and RMSEE of calibration set were 0.89 and 0.778%. The r^2, RMSEP, RPD and bias of the validation model were 0.85, 1.00%, 2.62 and 0.0256 %. A model that provided an R^2 between 0.83 and 0.90 could be used with caution for most applications, including research and RPD in the range of 2.4-3.0 could be used for rough screening [30].

The spectra of validation set pretreated by first derivative + MSC, regression coefficient and X-loading weight plot are demonstrated in Figure 2.3c. The important peaks were at 5276 cm^{-1} (1895 nm) (peak 1), 4898 cm^{-1} (2041 nm) (peak 2), 5141 cm^{-1} (1945 nm) (peak 3), 7112 cm^{-1} (1406 nm) (peak 4), and 4659 cm^{-1} (2146 nm) (peak 5). The wave band at 1896 nm relate to O-H stretching + C-O stretching of C=O, CO_2H [36]. The peak at 2140 nm correspond to =C-H stretching + C=C stretching of HC=CH [27].

Xue et al.[40] reported the many peaks were useful for predicting fixed carbon of corn stover such as C-H stretch/C=O stretch combination (4545 cm^{-1}), C=O stretch second overtone (4926 cm^{-1}), C-H stretch first overtone (5935 cm^{-1}), and C=O stretch third overtone (6897 cm^{-1}). The main peaks observed were due to alcohol OH and CH, both of which are in lignocellulosic structure, as either lignin or cellulose. Notably, OH was one functional group of lignin chemical structure. Burhenne et al.[38] reported that biomass containing a high lignin content can produce high bio-char. In addition, peaks associated with polysaccharides were found. According to Floch et al.[41], fibrous polysaccharides were either starch or cellulose, both a good source of energy. It can therefore be concluded that the model for fixed carbon depended strongly on the lignin and cellulose content.

Ash content

Scatter plot of the measured ash content value obtained by the reference laboratory technique (Y axis) and the predicted value by NIR spectroscopy (X axis) of validation set is shown in Figure 2.2d. The most effective model for the prediction of ash content were developed using a wavenumber range between 9828-8933.2 cm^{-1} (1018-1119 nm) and 8046-5376.9 cm^{-1} (1243-1860 nm), spectrum preprocessing of first derivative and straight line substation and PLS factor number of 8. The R^2 and RMSEE

of calibration set were 0.67 and 0.587%. The r^2, RMSEP, RPD and bias of validation model were 0.51, 0.768%, 1.44 and -0.108%. This low r^2 means that only 51% of the variance in absorbance values can be accounted for by variance in ash content. The models by Acquah et al.[32] to predict the ash content of loblolly pine wood provided fair result. They reported the R^2 of 0.68, SEC of 0.61% and RPD of 1.08.
Consequently, model analysis was not necessary [30]. In this case the unexplained variance was due to the sample, and this was because the ash was not the NIR absorber and the range of reference values was very narrow, so the prediction model was less effective.

2.6 Conclusion

In this study we observed that the HHV and A values do not vary with the culm circumference. HHV, VM, FC, and A showed a high standard deviation, meant that the culm size does not influence the reference value. The PLS model development for the evaluation of the HHV, VM and FC of ground bamboo were feasible for screening only. However, it was not possible to develop a useful predictive method for A, largely because the ash was not NIR absorber and the range of ash data was also narrow. The peaks associated with O-H stretching + H-O-H bending combination and lignin greatly affected the prediction of HHV. The prediction of VM and FC, was primarily influenced by the O-H stretching + C-O stretching of C=O, CO_2H. Moreover, the results showed that the reference method had the highest influence on error of prediction. Collectively the results indicate that NIR spectroscopy could be used as a nondestructive technique for most applications, including quality assurance, for the prediction of HHV. Also there was a model that could be used for prediction of VM and FC with screening. However, because of a limited data set (80 samples), the further evaluation on more samples sampling in different area are recommended for more robust models. These properties can be used to design thermal chemical conversion methods such as combustion, gasification and pyrolysis processes associated with biomass, as well as to monitor biological or thermochemical conversion processes. The properties can be used to set a fair market price for such biomass materials.

This chapter demonstrates that NIR spectroscopy can predict HHV and proximate data when MC is controlled at about 5 wt% because the proximate data was different. Even though bamboo was of the same species, chemical component was different because of different diameter size. When NIR spectroscopy can predict

proximate data, then it may predict pyrolysis characteristic. Therefore, next chapter aims to use NIR spectroscopy to evaluate pyrolysis characteristic of milled bamboo.

2.7 References

[1] Villar-Cociña E., Morales E.V., Santos S.F., Savastano Jr H., Frías M. "Pozzolanic behavior of bamboo leaf ash: Characterization and determination of the kinetic parameters." **Cem. Concr. Compos.**, vol. 33, 2011. Pp. 68–73.

[2] Jiang Z., Liu Z., Fei B., Cai Z., Yu Y., Liu X. "The pyrolysis characteristics of moso bamboo." **J. Anal Appl Pyrol**, vol. 94, 2012. Pp. 48–52.

[3] Scurlock J.M.O., Dayton D.C., Hames B. "Bamboo: an overlooked biomass resource?." **Biomass Bioenergy**, vol. 19, 2000. Pp. 229-244.

[4] Oyedun A.O., Gebreegziabher T., Hui C.W. "Mechanism and modelling of bamboo pyrolysis." **Fuel Process. Technol**, vol. 106, 2013. Pp. 595–604.

[5] Peng P., She D. "Isolation, structural characterization, and potential applications of hemicelluloses from bamboo: A review." **Carbohydr. Polym**, vol. 112, 2014. Pp. 701–720.

[6] Cheng L., Adhikari S., Wang Z., Ding Y. "Characterization of bamboo species at different ages and bio-oil production." **J. Anal. Appl. Pyrol**, vol. 116, 2015. Pp. 215–222.

[7] Darabant A., Haruthaithanasana M., Atklaa W., Phudphonga T., Thanavata E. "Bamboo biomass yield and feedstock characteristics of energy plantations in Thailand." **Energy Procedia**, vol. 59, 2014. Pp. 134 – 141.

[8] Chiang K-Y., Chien K-L., Lu C-H. "Characterization and comparison of biomass produced from various sources: suggestions for selection of pretreatment technologies in biomass-to-energy." **Appl. Energy**, vol. 100, 2012. Pp. 164–171.

[9] García R., Pizarro C., Lavín A.G., Bueno J.L. "Biomass proximate analysis using thermogravimetry", **Bioresour. Technol**, vol. 139, 2013. Pp. 1–4.

[10] García R., Pizarro C., Lavín A.G., Bueno L.J. "Characterization of Spanish biomass wastes for energy use." **Bioresour. Technol.**, vol. 103, 2012. Pp. 249–258.

[11] Huang C., Han L., Yang Z., Liu X. "Prediction of heating value of straw by proximate data, and near infrared spectroscopy", **Energ Convers Manage**, vol. 49, 2008. Pp. 3433–3438.

[12] Nhuchhen D.R., Salam P.A. "Estimation of higher heating value of biomass from proximate analysis: A new approach." **Fuel**, vol. 99, 2012. Pp. 55–63.

[13] Sheng C., Azevedo J.L.T. "Estimating the higher heating value of biomass fuels from basic analysis data." **Biomass Bioenergy**, vol. 28, 2005. Pp. 499–507.

[14] E.P. Friedl, H. Rotter and K. Varmuza, "Prediction of heating values of biomass fuel from elemental composition", **Analytica Chimica Acta** 544, 191–198(2005).

[15] Sheth P.N., Babu B.V. "Production of hydrogen energy through biomass (waste wood) gasification." **Int. J. Hydrogen Energy**, vol. 35, 2010. Pp. 10803 -10810.

[16] Lanzerstorfer C. "Chemical composition and physical properties of filter fly ashes from eight grate-fired biomass combustion plants." **J. Environ. Sci.**, vol. 1, 2015. Pp. 191–197.

[17] Posom J., Sirisomboon P. "Evaluation of the moisture content of *Jatropha curcas* kernels and the heating value of the oil extracted residue using near-infrared spectroscopy." **Biosystem eng**, vol. 130, 2015. Pp. 52-59.

[18] Posom J., Sirisomboon P. "Evaluation of the thermal properties of Jatropha curcas L. kernels using near-infrared spectroscopy." **Biosystem eng**, vol. 125, 2014. Pp. 45-53.

[19] Guimarães C.C., Simeone M.L., Parrella R.A.C., Sena M.M. "Use of NIRS to predict composition and bioethanol yield from cell wall structure components of sweet sorghum biomass." **Microchem. J.**, vol. 117, 2014. Pp. 194-201.

[20] Everard C.D., McDonnell K.P., Fagan C.C. "Prediction of biomass gross calorific values using visible and near infrared spectroscopy." **Biomass bioenerg**, vol. 45, 2012. Pp. 203-211.

[21] C.C. Fagan, C.D. Everard, K.McDonnell, "Prediction of moisture, calorific value, ash and carbon content of two dedicated bioenergy crops using near-infrared spectroscopy." **Bioresour. Technol**, vol. 102, 2011. Pp. 5200–5206.

[22] G.D. Gillespie, C.D. Everard, K.P. McDonnell, "Prediction of biomass pellet quality indices using near infrared spectroscopy." **Energy**, vol. 80, 2015. Pp. 582-588.

[23] B. Wunderlich, *Calorimetry*. Thermal analysis. Academic press, INC. London, England (1990).

[24] S.S. Hla, D. Roberts, "Characterisation of chemical composition and energy content of green waste and municipal solid waste from Greater Brisbane, Australia." **Waste Management**, vol. 41, 2015. Pp. 12–19.

[25] J. Posom, A. Shrestha, W. Saechua, P. Sirisomboon, "Rapid non-destructive evaluation of moisture content and higher heating value of *Leucaena leucocephala* pellets using near infrared spectroscopy." **Energy**, vol. 107, 2016. Pp. 464-472.

[26] P. Sirisomboon, M. Tanaka, T. Kojima, P. Williams, "Nondestructive estimation of maturity and textural properties on tomato 'Momotaro' by near infrared spectroscopy." **J. food engineering**, vol. 112, 2012. Pp. 218-226.

[27] B.G. Osborne, T. Fearn, *Near Infrared Spectroscopy in Food Analysis*. Longman Science & Technical, London, 1986.

[28] J. Workman Jr., L. Weyer, *Practical Guide to Interpretive Near-Infrared Spectroscopy*. Taylor & Francis, Boca Raton, FL, pp. 240–262 (2007).

[29] P. Dardenne, "Some considerations about NIR spectroscopy: Closing speech at NIR-2009." **NIR news**, vol. 21(1), 2010. Pp. 8-14.

[30] P. Williams, Near-Infrared Technology—Getting the Best Out of Light Edition 5.0. A Short Course in the Practical Implementation of Near-Infrared Spectroscopy for the User. PDK Grain, Nanaimo, Canada (2007).

[31] JS. Shenk, JJ. Workman, MO. Westerhaus, "Application of NIR spectroscopy to agricultural products. In: Burns DA, Ciurzack EW (eds) Handbook of near infrared analysis. Marcel Dekker, New York, pp 383-431(2001).

[32] G.E. Acquah, B.K. Via, O.O. Fasina, L.G. Eckhardt, "Non-destructive prediction of the properties of forest biomass for chemical and bioenergy applications using near infrared spectroscopy." **J. Near Infrared Spectrosc**, vol. 23, 2015. Pp. 93-102.

[33] A. Álvarez, C. Pizarro, R. García, JL. Bueno, "Spanish biofuels heating value estimation based on structural analysis." **Ind Crop Prod**, vol. 77, 2015. Pp. 983–991.

[34] G. Dorez, L. Ferry, R. Sonnier, A. Taguet, J.-M. Lopez-Cuesta, "Effect of cellulose, hemicellulose and lignin contents on pyrolysis and combustion of natural fibers." **J. Anal. Appl. Pyrol**, vol. 107, 2014. Pp. 323–331.

[35] H. Baillères, F. Davriux, F. Ham-Pichavant, "Near infrared analysis as a tool for rapid screening of some major wood characteristics in a eucalyptus breeding program." **Annal Forest Sci**, vol. 59, 2002. Pp. 479-90.

[36] Y-F. Huang, P-T. Chiueh, S-L. Lo, "A review on microwave pyrolysis of lignocellulosic biomass." **Sustain. Environ. Res**, vol. 26(3), 2016. Pp. 103-109.

[37] D. Lv, M. Xu, X. Liu, Z. Zhan, Z. Li and H. Yao, "Effect of cellulose, lignin, alkali and alkaline earth metallic species on biomass pyrolysis and gasification." **Fuel Process. Technol**, vol. 91, 2010. Pp. 903–909.

[38] L. Burhenne, J. Messmer, T. Aicher, M-P. Laborie, "The effect of the biomass components lignin, cellulose and hemicellulose on TGA and fixed bed pyrolysis." **J. Anal. Appl. Pyrol**, vol. 101, 2013. Pp. 177–184.

[39] J. Wannapeera, N. Worasuwannarak, S. Pipatmanomai, "Product yields and characteristics of rice husk, rice straw and corncob during fast pyrolysis in a drop-tube/fixed-bed reactor." **Songklanakarin J. Sci. Technol**, vol. 30(3), 2008. Pp. 393-404.

[40] J. Xue, Z. Yang, L. Han, Y. Liu, Y. Liu, C. Zhou, "On-line measurement of proximates and lignocellulose components of corn stover using NIRS." **Applied Energy**, vol. 137, 2015. Pp. 18-25.

[41] A.L. Floch, M. Jourdes, P-L. Teissedre, "Polysaccharides and lignin from oak wood used in cooperage: Composition, interest, assays: A review." **Carbohydr. Res**, vol. 417, 2015. Pp. 94-102.

Chapter 3

Evaluation of pyrolysis characteristics of milled bamboo using near-infrared spectroscopy

3.1 Abstract

This paper reports the development of a rapid and low-cost method based on near-infrared spectroscopy as an alternative for thermogravimetric determination of the pyrolysis characteristics, including T_{onset}, T_{sh}, T_{peak}, T_{offset} and DTG_{peak}, of milled bamboo. T_{onset} is the extrapolated onset temperature that is calculated from the partial peak resulting from the decomposition of the hemicellulose component, T_{sh} is the temperature corresponding to the overall maximum of the hemicellulose decomposition rate, DTG_{peak} is the overall maximum of the cellulose decomposition rate, T_{peak} is the temperature corresponding to the overall maximum of the cellulose decomposition rate and T_{offset} is the extrapolated offset temperature of the DTG_{peak} curves determined using thermogravimetric analysis (TGA). The models may be used to control the pyrolysis processes of bamboo to achieve the most economical and environmental conditions. 80 samples of bamboo with various circumferences of culms in the ranges of approximately 16–18, 18–20, 20–22, 22–24, 24–26, 26–28, 28–30, 30–32, 32–34, 34–36, 36–38 and 38–40 cm were randomly collected for optimization of the models. The models were optimized by partial least squares regression (PLSR) with 80% of samples for the calibration set and 20% for the validation set. For T_{onset}, T_{sh}, T_{peak}, T_{offset} and DTG_{peak}, the models showed coefficients of determination (R^2) of 0.566, 0.845, 0.917, 0.973, and 0.671; root mean square errors of prediction (RMSEP) of 9.7 °C, 4.36 °C, 3.77 °C, 2.66 °C, and 0.428 wt loss %/min; ratios of prediction to deviation (RPD) of 1.52, 2.58, 3.48, 3.55, and 1.75; and biases of −0.344 °C, −0.765 °C, 0.349 °C, −5.41 °C, and 0.045 wt loss %/min, respectively. In addition, the results showed that pyrolysis characteristics did not depend on the circumference. The vibrational bands of water and CH_3, O-H stretch, first overtones of Ar–OH, CH_2 and HC=CH in the cellulose and lignin structures, O-H hydrogen bonds of polyvinyl alcohol and C-H stretch corresponding to the first overtone of CH_2 had the highest

influence on the values of T_{onset}, T_{sh}, T_{peak}, and T_{offset}, respectively. The vibrational band of the C-O-C asymmetrical stretches of cellulose and hemicellulose, and the combination of O-H stretch and HOH bend of polysaccharides influenced the DTG_{peak} value. These results are beneficial for studying the thermal behavior of milled bamboo as a potential resource for producing biofuels, especially in the pyrolysis process.

*This chapter constituted the journal article: Posom J, Saechua W, Sirisomboon P. "Evaluation of pyrolysis characteristics of milled bamboo using near-infrared spectroscopy." **Renewable energy**, vol. 103, 2016, Pp. 653-665.

3.2 Introduction

Bamboo can be one of economic crops. It is one of seven fast-growing trees promoted by government sector used to be alternative energy resource [1]. It is the most important non-wood species which is abundantly grows in most of the tropical and subtropical zone [2]. It encompasses 1250 species within 75 genera, ranging from 10 cm to 40 m in height which is relatively fast-growing, attaining stand maturity within five years and it is the vernacular or common term for members of a particular taxonomic group of large woody grasses (subfamily *Bambusoideae*, family *Andropogoneae/Poaceae*) [3]. Bamboo plant is a complex system and is parts of grass family [4]. It is a tall glass, fast-growing and typically woody.

Bamboo is a native plant of Thailand which has been used for several activities. Thailand is the tropical zone which is the center of diversity of bamboos [5]. Some species can grow up to a foot a day [6]. In Thailand, there are 13 generals, and 60 species [7] where culm or stem are used for several products such as food (from shoots), food containers, fishhook, agricultural equipment, chopsticks, furniture, flooring, raft, paper, boats, charcoal, musical instruments, bridges, scaffolding and housing. It is usually comfortable but temporary structural material. In addition, it is used for renewable energy such as biodiesel and biogas, and charcoal production [8]. Bamboos like wood, consists of the extractives, cell wall components and ash. Especially cell wall components, is consisted of cellulose, hemicellulose and lignin which are important composition for using as an alternative for energy production via thermochemical conversion processes [9], the characteristics of the bamboo biomass was shown in Table 3.1.

Table 3.1 Characteristics of the bamboo biomass [10]

Property	Value
High heating value (MJ/kg)	17.235 ± 0.143
Proximate analysis (% wet basis)	
Moisture	9.37 ± 0.80
Fixed carbon	17.75 ± 0.40
Volatile	70.31 ± 0.44
Ash	2.57 ± 0.41
Elementol Analysis (%dry basis)	
C	39 ± 3
H	6.1± 0.2
N	0.6 ± 0.3 0.018± 0.006
S	
O	54±3
Structural Composition (% dry basis)	
Cellulose	47.5 ±0.4
Hemicellulose	15.35 ±0.42
Lignin	26.25±0.07
Extractives	4.90 ±0.14
Silica	0.7±0.0

In proximate analysis, bamboo consists the more VM and C but had small A content. For elemental analysis, C content was highest and S content was smallest. Table 3.2 illustrated fuel properties of different bamboo species [11], the A and HHV of bamboo were different when different bamboo species.

Table 3.2 Fuel properties and potential of different bamboo species [11]

Species	Ash content	Energy content
	(in %)	(MJ/kg $_{db}$)
B. pallida	1.91	18.63
B. tulda	1.92	18.61
D. asper	4.23	17.92
D. membranaceus	4.99	18.81
G. apus	2.00	18.14

Why has bamboo gained interest?: Bamboo is a renewable energy crop that has been planted in many parts of the world. It is used for furniture, apparatus and fuel. According to literature [12] and [13], bamboo has a short growth cycle and provides high yields of natural resources. Several studies have reported the advantages of bamboo, such as its fast growth [6] and [14], high energy and low ash [5], easy propagation and high productivity [15]. Bamboo is a large, woody grass [5]. It has been previously noted that bamboo could be the biomass material and bio-energy resource of the future [14] and [16].

Bamboo, like wood, consists of hemicellulose, cellulose and lignin. Some studies have reported the content of hemicellulose, cellulose and lignin in bamboo (Table 3.3). Biomass are formed by the atoms C, O and H [17]. Near-infrared (NIR) radiation interacts with structure of O-H, N-H, C-H, C-O, C-O-C, HC=CH, C=C and so on [18] and [19]. Hence, biomass is a good absorber of NIR radiation. NIR spectroscopy is an appropriate and rapid method for evaluating the components and physical properties of agricultural products. Rapid methods are needed to characterize biomass for energy because of the increasing use of biomass in energy systems and the expanding varieties of biomasses available [20]. The different characteristics of biomass are important for controlling thermal processes. These should be monitored to achieve the most economical and environmental conditions. NIR spectroscopy has many advantages, such as being rapid, nondestructive, environmentally friendly due to no or low chemicals, and requiring minimal quantities of samples. Therefore, several recent studies have focused on applying NIR spectroscopy as an alternative method for the assessment of biomass characteristics, such as prediction of composition and bioethanol yield from the cell wall structural components of sweet sorghum biomass [21], evaluation of the thermal properties of *Jatropha curcas* L. kernels [22], prediction of the heating value and moisture content of *Jatropha curcas* L. kernels [23], prediction of moisture, calorific value, ash and carbon content of two dedicated bioenergy crops [24], prediction of biomass composition of switchgrass [25], determination of biochemical methane potential of plant biomass [26] and determination of the chemical compositional variability of corn stover and switchgrass [27]. These studies have shown the feasibility of NIR techniques for assessment of the thermal properties and

chemical composition of biomass. At present, there has been no report on the application of NIR spectroscopy to study pyrolysis characteristics.

3.3 Objective

Thus, this work is focused on the evaluation of pyrolysis characteristics of milled bamboo, including T_{onset}, T_{sh}, T_{peak}, T_{offset} and DTG_{peak} using Fourier Transform-NIR (FT-NIR) spectroscopy as an alternative to thermogravimetric analysis. The reference parameters were obtained from a thermogravimetric apparatus under non-isothermal conditions in a nitrogen atmosphere.

Table 3.3 Hemicellulose, cellulose and lignin content in bamboo

Material	Hemicellulose	Cellulose	Lignin	Reference
Bamboo	15-20%	35-45%	15-25%	[28]
Bamboo	24.2	43.1	27	[5]
Bamboo Shoots (*Bambusa blumeana*)	27.30 ± 2.8	27.90 ± 1.2	7.92 ± 0.0	[29]
2-Year-old (*Bambusa blumeana*)	27.51 ± 1.7	37.70 ± 1.5	25.73 ± 0.0	
5-Year-old (*Bambusa blumeana*)	22.94 ± 2.1	41.91 ± 1.0	27.11 ± 0.3	
3-year-old moso bamboo culms (*Phyllostachys pubescens*)	22.86±2.19	41.72±2.37	20.91±0.24	[30]

3.4 Materials and methods

3.4.1 Sample

The samples of bamboo, *Dendrocalamus sericeus* cl. Phamon, in this study were obtained from the Uttaradit province, Thailand, and had different circumferences of culms. A total of 80 samples in 12 ranges of culm circumference (16–18, 18–20, 20–22, 22–24, 24–26, 26–28, 28–30, 30–32, 32–34, 34–36, 36–38 and 38–40 cm) were randomly cut 10 cm above the ground. Each sample was chopped by a chopping machine (P5508, Patipong, Thailand). After this, the samples were dried under the sun until the moisture reached approximately 5%wb. The milled were passed through a sieve of diameter 3 mm (60201, QC, UK) and kept in an aluminum bag till the experiment.

3.4.2 Near infrared spectroscopy

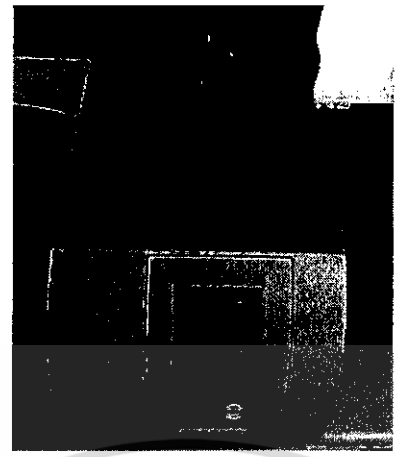

Figure 3.1 Scanning milled bamboo by FT-NIR

Figure 3.1 showed the scanning milled bamboo by FT-NIR. The milled sample was filled in a sample cup of 43 mm diameter and 50 mm height, the bottom of which was made of quartz. The sample was scanned using a FT-NIR spectrometer (MPA, Bruker, Germany) with the diffuse reflection mode, and the spectrum was recorded in the range of 12,500–3800 cm^{-1}, as an average of 64 scans with a resolution of 8 cm^{-1} at air-conditioning room temperature, i.e., 25 ± 2 °C. The sample at the bottom of the cup, irradiated by NIR radiation, was collected to determine the reference values because it contained more NIR spectral information than the remaining part of the cup.

3.4.3 Reference methods

Figure 3.2 Thermogravimetric analyser (TG 209 F3 Tarsus, Netzsch, Germany, 0.1 µg resolution; 6.8 mm diameter aluminium oxide (Al_2O_3) crucible)

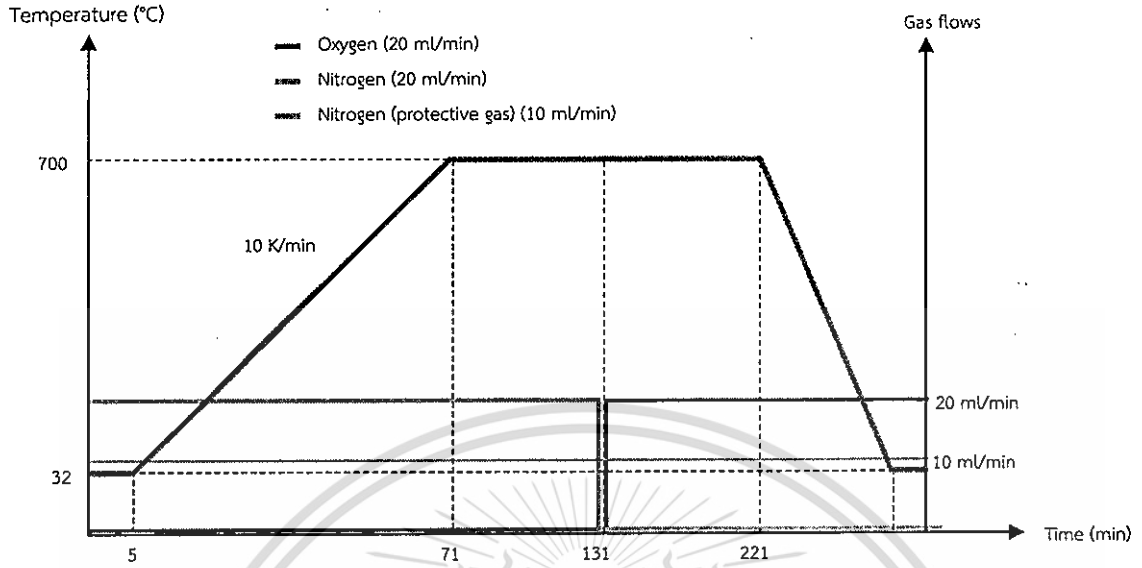

Figure 3.3 The temperature program for pyrolysis

The reference value of pyrolysis characteristics, including T_{onset}, T_{sh}, T_{peak}, T_{offset} and DTG_{peak} (dm/dt at the highest peak), of a milled sample were determined using a thermogravimetric analyser (TG 209 F3 Tarsus, Netzsch, Germany, 0.1 µg resolution; 6.8 mm diameter aluminum oxide (Al_2O_3) crucible). The milled sample of 6 ± 0.5 mg was put into aluminum oxide (Al_2O_3) crucible (see in Figure 3.2). The samples were heated from 32 °C to 700 °C with a flow rate of 20 ml/min of N_2, zero-O_2 environment and heating rate of 10 °C/min for pyrolysis. The temperature was maintained at 700 °C for 1 h to ensure completion of the pyrolysis process. The temperature program was demonstrated in Figure 3.3. After the pyrolysis characteristics were measured, the outliers were then calculated using equation (3.1).

$$\frac{(X_i - \overline{X})}{SD} \geq \pm 3 \qquad (3.1)$$

where X_i is the measured value of sample i. $\overline{X}$ and SD are the average and standard deviation of the measured values of all samples, respectively. If the equation was satisfied, the sample was outlier and it was then removed from reference data set.

3.4.4 Repeatability, reproducibility and maximum R^2

The precision of pyrolysis characteristics measured and spectral data scanned were determined using the parameters of repeatability and reproducibility. Maximum R^2 (R^2_{max})

is the maximum coefficient of determination, when there are no errors in the spectra. For the pyrolysis characteristic reference data; repeatability was the standard deviation of the difference between duplicates; while reproducibility was the standard deviation of the difference between duplicates from blind samples. In addition, the precision of the NIR instrument was also determined using repeatability and reproducibility. The absorbance value at the wavenumber of 5176 cm^{-1} (1932 nm) was used for the determination. Any wavenumber could be used to determine the repeatability and reproducibility of NIR scans. Therefore, we used the wavenumber 5176 cm^{-1} (1932 nm). This was the absorption band of water in the milled bamboo spectrum. The NIR absorption band of water was the highest peak that was obviously visible in the spectrum. The peak was easily changed when the scanning conditions were varied. The repeatability of the NIR instrument was the standard deviation of the absorbance values when the sample was re-scanned 10 times in the same position, and the reproducibility of spectral data was the standard deviation of the absorbance values when the sample was re-loaded and re-scanned 10 times (personal communication with Phil Williams). According to Dardenne [31], R^2_{max} can be calculated using equation (3.2):

$$R^2_{max} = \frac{SD_y^2 - Rep^2}{SD_y^2} \quad (3.2)$$

where SD_y is the standard deviation of the measured values in the calibration set. Rep is the repeatability of the pyrolysis characteristic reference data. R^2_{max} is possible only when there are no errors in the spectra or the model, and it depends on the range and precision of the reference data.

3.4.5 Spectrum pre-processing and NIR spectroscopy modelling

The model was optimized using the OPUS software, Version 7.0.129, Bruker Optik GmbH, Germany, with partial least squares (PLS) regression using the test set validation method. The samples were randomly sub-divided into 80% for the calibration sample set and 20% for the validation sample set. The wavenumber range of 12500–3800 cm^{-1} was equally divided into five sub-ranges. Spectrum preprocessing was performed by the constant offset elimination; straight line subtraction; vector normalization, min-max normalization; multiplicative scatter correction (MSC); first derivatives, second derivatives;

first derivatives + straight line subtraction; first derivatives + vector normalization and first derivatives + MSC techniques. The models were developed using a combination of sub-ranges of wavenumbers and spectrum pre-processing techniques, and the corresponding root mean square error of prediction (RMSEP) was determined. The model with the optimal sub-range of wavenumbers and spectrum pre-processing technique was selected by the lowest root RMSEP. Spectral pre-processing techniques are required for model development to remove any irrelevant information that cannot be properly handled by regression techniques [32]. The outliers were determined by the Mahalanobis distance limit. The regression coefficient and X-loading weight of each PLS latent variable was also determined by the software program and plotted.

3.5 Results and discussions

3.5.1 Pyrolysis characteristics of milled bamboo

The T_{onset}, T_{sh}, T_{peak}, T_{offset}, and DTG_{peak} of milled bamboo are illustrated Table 3.4. Based on ANOVA, there were 2 different levels for T_{onset} and DTG_{peak}, and 3 different levels for T_{sh}, T_{peak}, and T_{offset}. As seen in Table 3.4, the standard deviations were high, indicating the difference in pyrolysis characteristics, even for equal circumferences of culms. Thus, the pyrolysis characteristics did not depend on circumference. However, the age may have a significant influence on the properties of the fast-pyrolysis products [33]. Moreover, the different pyrolysis characteristics were affected by the lignin, cellulose and hemicellulose contents [34,35,36,37,38].

Table 3.4 T_{onset}, T_{sh}, T_{peak}, T_{offset} and DTG_{peak} of milled bamboo obtained from bamboo trunks with different circumferences of the culms

Range (mm)	N	T_{onset} (°C)	T_{sh} (°C)	T_{peak} (°C)	T_{offset} (°C)	DTG_{peak} (weight loss % /min)
16<L≤18	8	141.725±12.454ab	295.375±10.796abc	332.818±14.814abc	385.562±10.959abc	-8.835±0.739ab
18<L≤20	6	136.233±14.417b	303.250±17.394a	343.541±15.531a	390.833±11.910a	-9.486±1.046b
20<L≤22	6	133.550±8.519b	294.000±15.241abc	335.916±15.635abc	385.166±12.363abc	-8.733±0.678a
22<L≤24	7	141.657±9.866ab	289.857±12.821abc	326.471±12.958bc	380.928±8.757abc	-8.498±0.579a
24<L≤26	6	137.916±9.370ab	285.083±1.357c	322.000±2.393c	377.333±5.988c	-8.638±0.351a
26<L≤28	6	144.600±8.728ab	289.5±9.746abc	322.950±8.474c	376.583±5.219c	-8.623±0.574a
28<L≤30	8	139.162±13.116ab	288.875±8.096bc	323.812±8.110bc	378.812±8.668bc	-8.451±0.521a
30<L≤32	8	146.250±14.576ab	293.750±6.181abc	332.587±9.794abc	383.625±6.968abc	-8.402±0.261a
32<L≤34	7	138.442±11.296ab	290.428±10.357abc	327.685±12.020bc	379.500±7.643bc	-8.387±0.520a
34<L≤36	7	153.842±19.677a	294.214±10.676abc	332.028±11.605abc	383.928±8.115abc	-8.261±0.653a
36<L≤38	5	146.160±8.838ab	301.800±4.868ab	342.700±7.316a	389.900±6.328ab	-8.834±0.406ab
38<L≤40	6	141.883±8.628ab	298.583±9.951abc	338.183±8.857ab	387.500±7.661abc	-8.471±0.589a

Different letters in the same column indicates the different means that are significantly at p>0.05 by the Duncan multiple range test. N is number of samples. L is circumference of the bamboo culms.

3.5.2 NIR spectral characteristics of milled bamboo

The vibrational bands of milled bamboo can be observed in Figure 3.4, which shows the NIR spectra of 80 samples. The main spectral regions were at 6823 cm^{-1} (1466 nm), 5192 cm^{-1} (1926 nm), 4752 cm^{-1} (2104 nm) and 3992 cm^{-1} (2505 nm). The waveband at 1471 nm is the first overtone of N-H stretching of CONHR [18], 1930 nm is the combination band of O-H stretching + H-O-H bending polysaccharides [19], 2103 nm is the band for glucose, and 2500 nm is the band corresponding to C-H stretching + C-C stretching of starch [18]. Similar results were also reported by Yang et al. [39] for mature bamboo (two years old) and juvenile bamboo (one month old), with many absorption bands in the wavelength region of 1100–2500 nm, including peaks at approximately 1473, 1925, 2095, 2267 and 2328 nm.

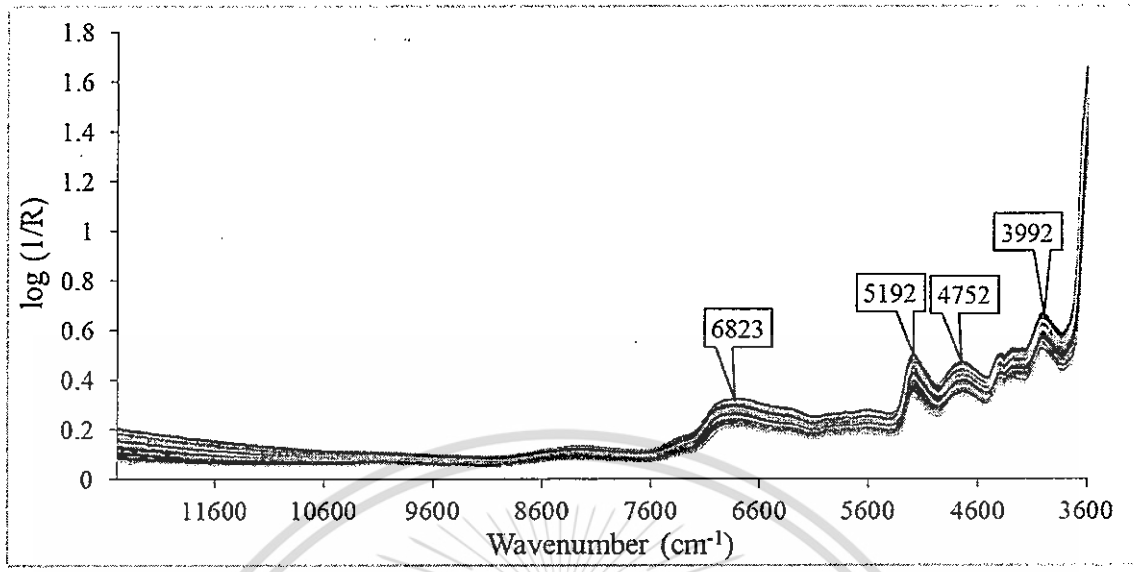

Figure 3.4 NIR spectra of 80 samples of milled bamboo

The NIR spectra obtained by scanning the milled bamboo raw material changed when the scanning environment, i.e., ambient temperature and water dissolved in the ambient air penetrating into the spectrometer, was changed [40]. In our scanning protocol, this environment was kept constant by means of an air conditioning temperature controller and a spectrometer humidity controller using a molecular sieve. However, parameters such as heating rate, inert gas flow rate and pyrolysis temperature, which were the reference test conditions, might have an effect on the pyrolysis characteristics. Further, the change of pyrolysis characteristics might affect the prediction models. Some researchers concluded that the maximum weight loss rate (DTG_{peak}) decreased with increasing heating rate because their curves shifted obviously towards the high temperature range as the heating rate rose [41,42,43]. By observing the DTG curves of these reports, it might be concluded that T_{onset}, T_{sh}, T_{peak} and T_{offset} increased with increasing heating rate. Modifications of reference test conditions, such as heating rate, pyrolysis temperature and inert gas flow rate, would affect the product and residue yield. Oyedun et al. [6] reported that residue yields increased with increasing heating rate, but were very similar. Higher heating rates lead to higher liquid yields, while lower heating rates lead to higher biochar yields [44]. The pyrolysis temperature influences the bio-product yield. Thus, Irfan et al. [45] reported that for pyrolysis of *Achnatherum splendens* L. under three different pyrolysis temperatures (300, 500, and 700 °C), the biochar yield

decreased and syngas yield increased when pyrolysis temperature was increased, and the maximum bio-oil yield was obtained at 500 °C. In addition, the pyrolysis temperature also has an effect on the product properties. Lower pyrolysis temperatures and heating rates promote higher mass and energy yields of biochar, while higher pyrolysis temperatures and heating rates lead to higher mass and energy yields of the non-condensable gas [46]. Kim et al. [47] reported that increasing the N_2 gas flow rate from 20 to 40 L/min did not change the yield of the pyrolysis products. However, it did change the bio-oil properties, e.g., by decreasing the water content and increasing the amount of organic compounds. In our experiment, both scanning and thermogravimetric protocols were fixed. When the models are proven to be suitable for use, the developed protocol must be applied to update the model.

Table 3.5 Repeatability, reproducibility and R^2_{max} of reference laboratory for T_{onset}, T_{sh}, T_{peak}, T_{offset} and DTG_{peak} and of absorption at 5176 cm^{-1} (1932 nm) of milled bamboo

Parameter	Repeatability	Reproducibility	R^2_{max}
T_{onset}	8.8	7.0	0.465
T_{sh}	3.9	5.2	0.877
T_{peak}	1.81	2.39	0.979
T_{offset}	1.58	1.89	0.970
DTG_{peak}	0.199	0.333	0.903
Absorption value at 5176 cm^{-1} (1932 nm) of sample number 28	0.00467	0.01816	-

3.5.3 Overall precision of reference test

The repeatability, reproducibility and R^2_{max} of T_{onset}, T_{sh}, T_{peak}, T_{offset}, DTG_{peak} and the absorption at 5176 cm^{-1} (1932 nm) of milled bamboo are demonstrated in Table 3.5. They had the same precision as the reference laboratory and NIR spectrometer. While R^2_{max} is possible only when there are no errors in the spectra [31], it can be used to indicate whether the NIR model should be developed or not. R^2_{max} of T_{onset} was the lowest, and it was not reasonable to develop a NIR model for this parameter. However, those of T_{sh},

T_{peak}, T_{offset}, and DTG_{peak} were high, due to which it was reasonable that NIR models should be developed for these.

3.5.4 Performance of PLS models

Statistical data for T_{onset}, T_{sh}, T_{peak}, T_{offset}, and DTG_{peak} of milled bamboo in the total samples, calibration set and validation set are shown in Table 3.6. The data were used for model development and validation. The results of the optimal PLS models for the studied properties are shown in Table 3.7, where the wavenumber range, spectrum pre-processing method, number of PLS latent variables, coefficients of determination (R^2) of both calibration and validation, root mean square error of estimate (RMSEE), root mean square error of prediction (RMSEP), ratio of prediction to deviation (RPD) and bias are shown. The R^2_{max} in Table 3.5 was determined when there was no error in the scanning and the only error was from the reference laboratory source. It was the maximum possible value of R^2. In Table 3.7, the R^2 was the normal R^2, where the sources of error came from NIR scanning, reference laboratory as well as other unknown sources. Figure 3.5 displays the scatter plots of measured versus predicted values of the prediction sample set. The best models for prediction were developed using the wavenumber range of 6102–5446.3 cm^{-1} for T_{onset}; 8046–7155 and 6267.9–4485.9 cm^{-1} for T_{sh}; 5874.5–4246.7 cm^{-1} for T_{peak}; and 9403.8–7498.3 and 6102–4597.7 cm^{-1} for T_{offset}; and 9403.8–7498.3 and 5450.2–4246.7 cm^{-1} for DTG_{peak}. The second-derivative spectrum pre-processing method was used for model development of T_{onset} and T_{sh}, and first derivative + vector normalization was used for T_{peak}, T_{offset}, and DTG_{peak}. The PLS latent variable numbers were 7, 7, 9, 9 and 9 for T_{onset}, T_{sh}, T_{peak}, T_{offset} and DTG_{peak}, respectively.

Table 3.6 Statistical data of T_{onset}, T_{sh}, T_{peak}, T_{offset} and DTG_{peak} of milled bamboo used in model development

Parameters	Data set	N[a]	Max	Min	Mean	Range	SD[b]
T_{onset} (°C)	Total sample	80	182.6	115.7	141.882	66.9	12.574
	Calibration set	64	182.6	115.7	141.540	66.9	11.941
	Prediction set	16	172.5	117.3	143.250	55.2	15.213
T_{sh} (°C)	Total sample	79	319	277	293.063	42	10.471
	Calibration set	63	319	277	292.777	42	10.336
	Prediction set	16	316	278	293.437	38	11.458
T_{peak} (°C)	Total sample	80	357	313.2	331.007	43.8	12.283
	Calibration set	64	357	313.2	330.407	43.8	12.003
	Prediction set	16	353.8	313.2	333.368	40.6	13.476
T_{offset} (°C)	Total sample	78	403.5	367	382.565	36.5	8.646
	Calibration set	62	403.5	367	382.270	36.5	8.457
	Prediction set	16	398	368	383.687	30	9.539
DTG_{peak} (weight loss % /min)	Total sample	80	-7.25	-11.27	-8.618	4.02	0.638
	Calibration set	64	-7.25	-11.27	-8.641	4.02	0.605
	Prediction set	16	-7.43	-10.25	-8.525	2.82	0.771

[a] Number of samples, [b] Standard deviation.

Table 3.7 Result of partial least squares regression models for determination of T_{onset}, T_{sh}, T_{peak}, T_{offset} and DTG_{peak} of milled bamboo

Parameters	Wavenumber range (cm^{-1})	Pre-processing	Calibration			Validation			
			PLS latent variables	R^2	RMSEE	R^2	RMSEP	RPD	Bias
T_{onset}	6102-5446.3	Second derivative	7	0.545	8.55	0.566	9.70	1.52	-0.344
T_{sh}	8046-7155 6267.9-4485.9	Second derivative	7	0.865	4.02	0.845	4.36	2.58	-0.765
T_{peak}	5874.5-4246.7	First derivative + vector normalization	9	0.921	3.66	0.917	3.77	3.48	0.349
T_{offset}	9403.8-7498.3 6102-4597.7	First derivative + vector normalization	9	0.939	2.27	0.917	2.66	3.55	-0.541
DTG_{peak}	9403.8-7498.3 5450.2-4246.7	First derivative + vector normalization	9	0.692	0.363	0.671	0.428	1.75	0.0452

R^2 is coefficient of determination. RMSEE is root mean square error of estimation. RMSEP is root mean square error of prediction. RPD is ratio of standard deviation and Bias is average error of prediction.

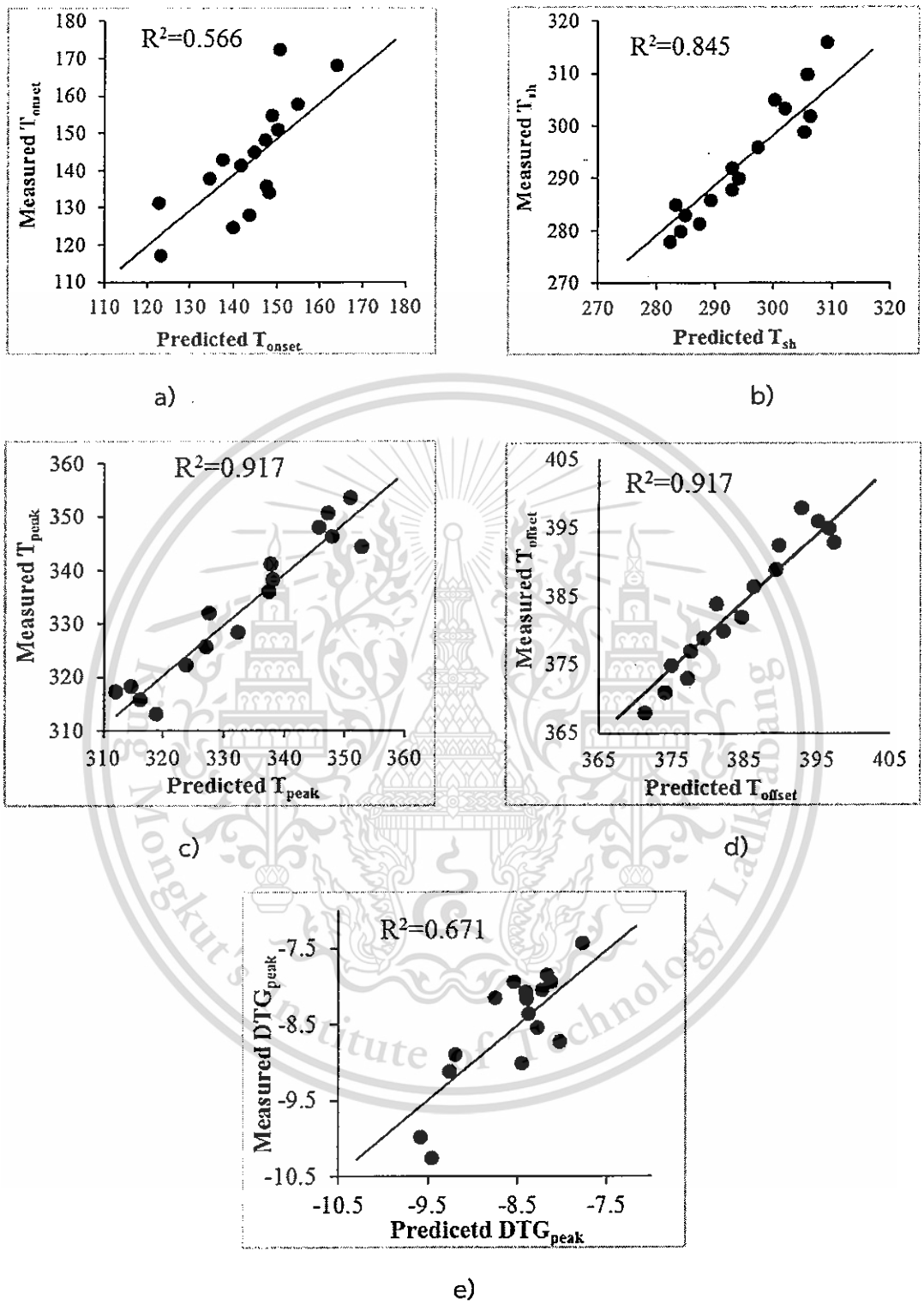

Figure 3.5 Scatter plots of measured vs predicted a) T_{onset}, b) T_{sh}, c) T_{peak}, d) T_{offset} and e) DTG_{peak} of validation set

The R^2 were 0.566, 0.847, 0.917, 0.894, 0.671; RMSEP were 9.7 °C, 4.87 °C, 3.77 °C, 3.32 °C, 0.428 wt loss %/min; RPD were 1.52, 2.59, 3.48, 3.08, 1.75; and biases were −0.344 °C, −0.78 °C, 0.349 °C, 0.352 °C, 0.0452 wt loss %/min for T_{onset}, T_{sh}, T_{peak}, T_{offset} and DTG_{peak}, respectively. Our results show that the models for T_{onset} and DTG_{peak} yielded low R^2 of 0.566 and 0.671, respectively. Those models were not applicable due to the following reasons: R^2 of 0.566 indicates that 56.6% of the total variation can be explained by NIR spectra, while 43.4% (100–56.6) of the total variation is unexplained variance that cannot be explained by NIR spectra. R^2 of 0.671 indicates that 67.1 can be explained by NIR spectra while the remaining 32.9% cannot be explained by NIR spectra. If R^2 is too low, the model results in a high error (unexplained variance). Many researchers have suggested guidelines for R^2 and RPD. For example, the model that gives R^2 between 0.50 and 0.64 could be used for rough screening, 0.66–0.81 for screening and some other "approximate" calibrations, 0.83–0.90 could be used with caution for most applications and 0.92–0.96 could be usable for most applications [48]; the model shows excellent predictions if $R^2 > 0.90$ and RPD > 3, good predictions if $0.81 < R^2 < 0.90$ and $2.5 < RPD < 3$, only approximate predictions if $0.66 < R^2 < 0.80$ and $2.0 < RPD < 2.5$ and poor predictions if $R^2 < 0.66$ and RPD < 2 [49]; RPD between 1.5 and 2 means that the model can discriminate between low and high values of the response variable; a value between 2 and 2.5 indicates that coarse quantitative predictions are possible; and a value between 2.5 and 3 or above corresponds to good and excellent prediction accuracies, respectively [32]. Therefore, the T_{onset} prediction model is not recommended due to low R^2 and RPD. T_{onset} showed 43.4% variance, which cannot be explained by absorption data. Although the measured data were in a wide range, it had high values of repeatability and reproducibility. The T_{sh} model showed low bias (approximately −0.765 °C), low RMSEP, and high R^2 and RPD. The ratio between RMSEP and the mean of the reference value (4.36 °C/293.437 °C) was approximately 1.48%. Therefore, the T_{sh} model showed good predictions and could be used with caution for most applications. For T_{peak}, the model showed high R^2 and RPD, low RMSEP and bias. The ratio between RMSEP and the mean of the reference value (3.77 °C/333.368 °C) was approximately 1.13%. This model is excellent and could be used for most applications. For T_{offset}, the model displayed

excellent predictive accuracy with high R^2 and RPD and low RMSEP and bias, and may be used with caution for most applications. The ratio between RMSEP and the mean of the reference value (2.66 °C/383.687 °C) was approximately 0.693%. On the other hand, for DTG_{peak}, the ratio between RMSEP and the mean of the reference value (0.428 wt loss %/min/−8.525 wt loss %/min) was approximately 5.020%. It only permitted approximate predictions and could be used for screening. Moreover, all parameters showed low bias. This means that a better model could be provided with a wider range of reference data.

3.5.5 Regression coefficient and X-loading

The regression coefficient plots of the models developed for T_{onset}, T_{sh}, T_{peak}, T_{offset} and DTG_{peak} are shown in Figure 3.6, while the X-loading plots of the first three factors are shown in Figure 3.7. The high values of the regression coefficient and X-loading weight at any wavenumber meant that the vibration of a particular bond at that wavenumber was the main factor influencing the model prediction.

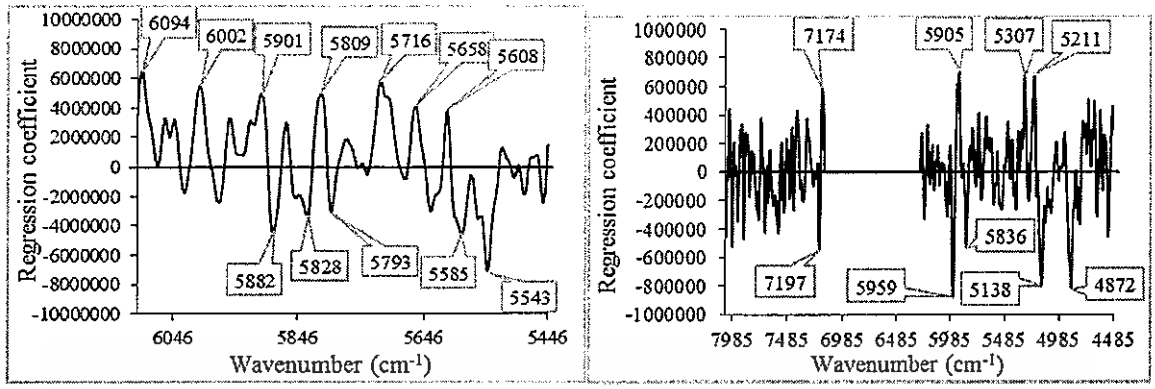

a) b)

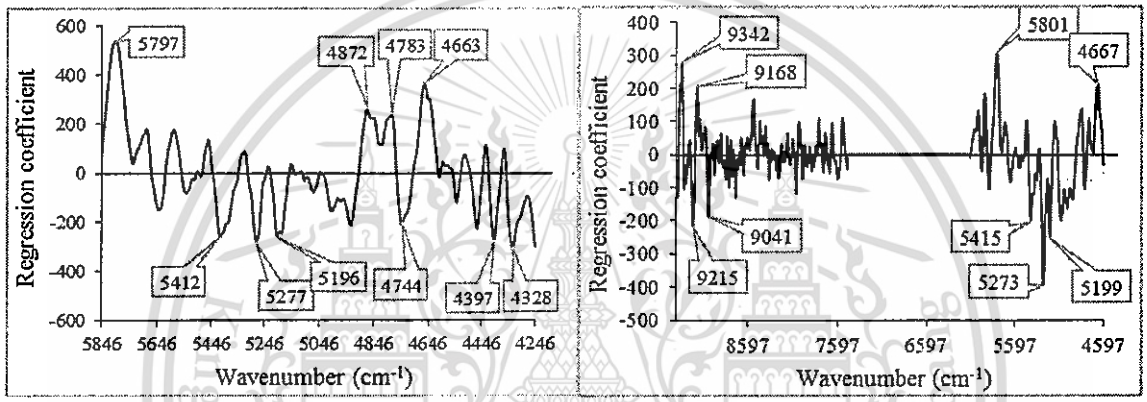

c) d)

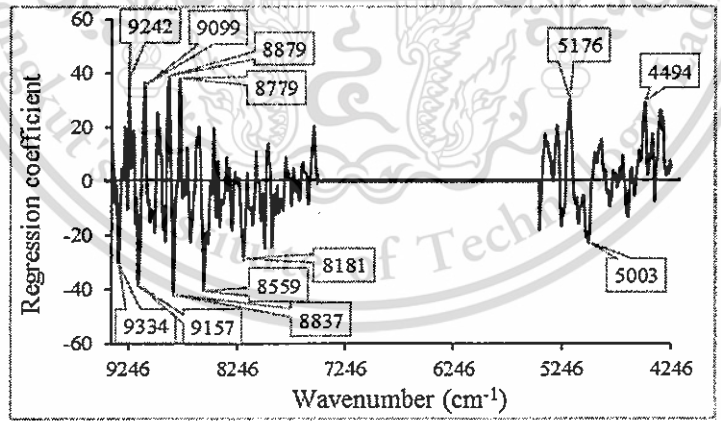

e)

Figure 3.6 Regression coefficient plots of the models for a) T_{onset}, b) T_{sh}, c) T_{peak}, d) T_{offset} and e) DTG_{peak}

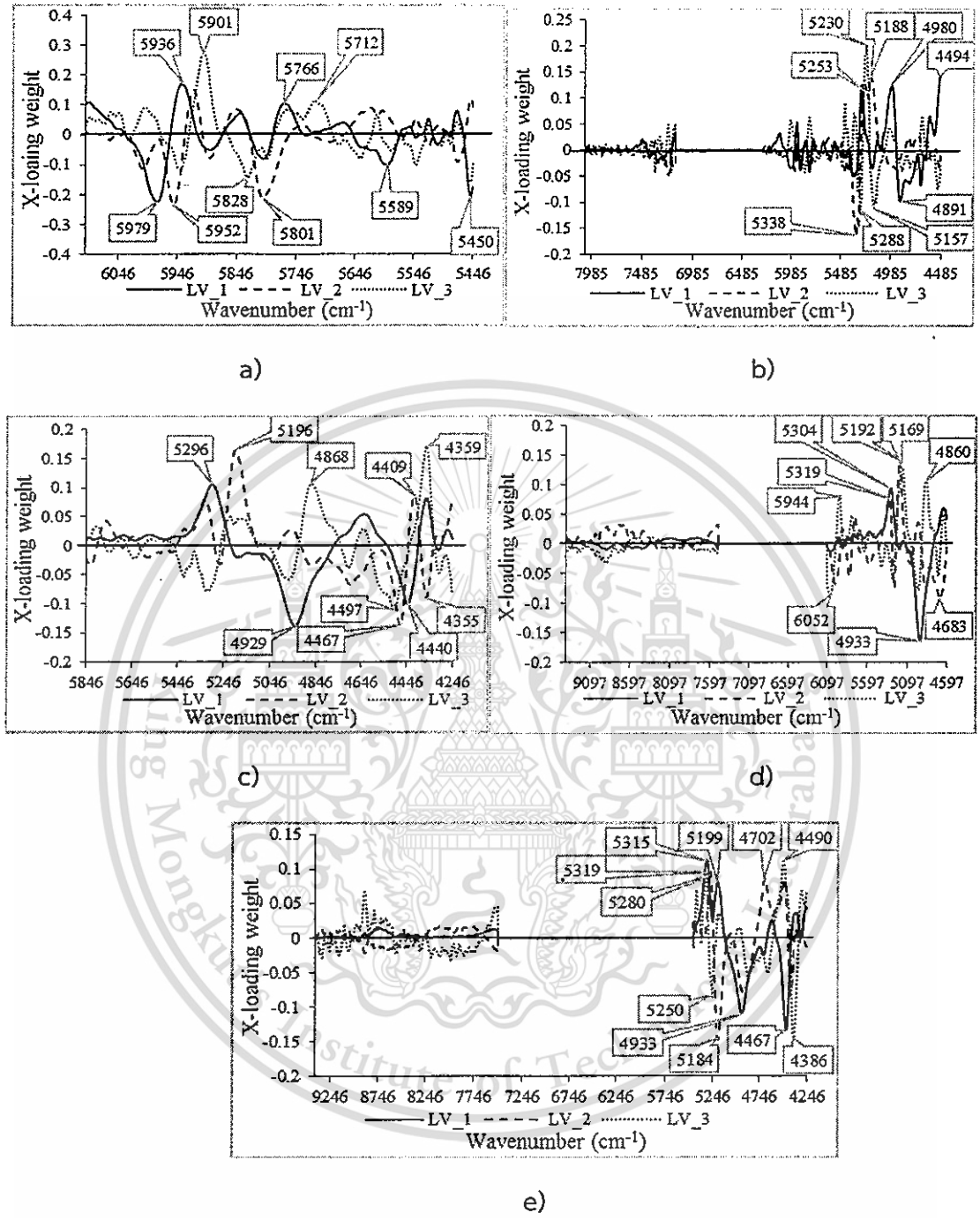

Figure 3.7 X-loading weight plots of the models for a) T_{onset}, b) T_{sh}, c) T_{peak}, d) T_{offset} and e) DTG_{peak}. LV_1, LV_2 and LV_3 are PLS latent variable 1, 2 and 3, respectively

T_{onset}

The regression coefficient plot of T_{onset} is displayed in Figure 3.6a. The most important peaks are at approximately 5543 cm^{-1} (1804 nm) (O-H combination of water) [19], 6094 cm^{-1} (1641 nm) (first overtone of C-H stretching of R-C_2H_2O) [18] and 5716 cm^{-1} (1750 nm) (related to the structure of α-D glucose) [18]. While the corresponding X-loading weight plot is also shown in Figure 3.7a, the most important peaks are at approximately 5901 cm^{-1} (1695 nm) (related to first overtone of C-H stretching of CH_3), 5952 cm^{-1} (1680 nm) (related to aromatic C-H of hydrocarbon or aromatic) and 5979 cm^{-1} (1673 nm) (related to C-H aromatic C-H (aryl)). The corresponding absorption bands with high regression coefficients and X-loading weights are displayed in Table 3.8. The results indicate that the O-H vibrations of water and C-H vibrations of CH_3 had the highest influence because there was no volatilization of water during the initial decomposition of hemicellulose [50]. The CH_3 is found in the hemicellulose structure. Guimarães et al. [21] also reported that the most important peaks affecting the hemicellulose evaluation model were the first overtone of O-H stretching, the first overtone of C-H stretching and the combination of the C-H stretching.

T_{sh}

For T_{sh}, the regression coefficient and X-loading weight plots of the first three factors are shown in Figures. 3.6b and 3.7b, respectively. The most important peaks of the regression coefficient plots are at approximately 5959 cm^{-1} (1678 nm) (C-H methyl, carbonyl adjacent to (.C=OCH_3) of ketones) [19], 5138 cm−1 (1946 nm) (C=O esters and acids (C=OOR) of acids and esters) [19] and 4872 cm−1 (2052 nm) (NH combination from polyamide II of polyamide II) [19]. For the X-loading weight plots, the most important peaks are at approximately 5338 cm^{-1} (1873 nm), 4494 cm^{-1} (2225 nm) (related to CHO) [19] and 5230 cm^{-1} (1912 nm) (related to O-H stretch first overtone of Ar–OH) [51]. The corresponding absorption bands with high regression coefficients and X-loading weights are displayed in Table 3.9. Guimarães et al. [21] also reported that the first overtone of the O-H stretch and first overtone of the C-H stretch affected the hemicellulose predictions.

T_{peak}

For T_{peak}, the regression coefficient plots are shown in Figure 3.6c. The most important peaks are at approximately 5797 cm^{-1} (1725 nm) (related to the first overtone of C-H stretching of CH_2) [18], 4663 cm^{-1} (2144 nm) (=C-H stretching + C=C stretching of HC=CH) [18] and 4328 cm^{-1} (2310 nm) (C-H stretching + C-H deformation of CH_2) [18]. The X-loading plots of the first three factors are shown in Figure 3.7c. The high peaks are at approximately 4359 cm^{-1} (2294 nm) (related to the C-H aromatic C-H (aryl) of C-H aryl) [19], 5196 cm^{-1} (1925 nm) (related to the assigned O-H) [19] and 4929 cm^{-1} (2029 nm) (related to the second overtone of the C=O stretch of $CONH_2$) [18]. The corresponding absorption bands with high regression coefficients and X-loadings are displayed in Table 3.10. T_{peak} is the temperature corresponding to the overall maximum of the cellulose decomposition rate [50]. The peaks of CH_2 and HC=CH, found in the cellulose and lignin structures, had the highest influence. The results are similar to those reported by Guimarães et al. [21], where the vibration band of the first overtone of C-H stretching was the most important for cellulose prediction. The T_{peak} of the milled bamboo samples had a range of 313.2–357 °C (Table 4), in agreement with the result of Jiang et al. [14], where the critical temperature of maximum weight loss was 347 °C with 10 °C/min for moso bamboo in the pyrolysis process. Cellulose was quickly decomposed at 315–400 °C [52] and highly decomposed at 347 °C [53]. Lignin was degraded in a wide temperature range of 200–600 °C [54]. Accordingly, it may be concluded that not only cellulose but lignin was also degraded at T_{peak}.

T_{offset}

For T_{offset}, the regression coefficient and X-loading weight plots of the first three factors are displayed in Figures 3.6d and 3.7d, respectively. The important peaks of the regression coefficient are at approximately 5273 cm^{-1} (1896 nm) (related to the O-H hydrogen bonding between water and exposed polyvinyl alcohol OH of water and polyvinyl alcohol) [19], 5801 cm^{-1} (1724 nm) (first overtone of C-H stretching of CH_2) [18], and 9342 cm^{-1} (1070 nm) (O-H combination band, alcohol or water of alcohols as R-C-O-H) [19]. The X-loading weight plots showed important peaks at 4933 cm^{-1} (2027 nm)

(related to C=O stretching + second overtone of $CONH_2$) [18], 5192 cm^{-1} (1926 nm) (combination of O-H stretching and HOH deformation from water molecules in the 3-aminopropyltriethoxysilane-ethanol-water system) [19]. The corresponding absorption bands with high regression coefficients and X-loading weight plots are shown in Table 3.11. T_{offset} is the extrapolated offset temperature. It is the temperature at the end of the DTG curves at which there is little or no volatilization of the biomass. The O-H bond of polyvinyl alcohol, found in the lignin structure, had a significant influence. The CH_2 bond, present in both lignin and cellulose structures, also had a high influence.

DTG_{peak}

For DTG_{peak}, the regression coefficient and X-loading weight plots of the first three factors are displayed in Figures 3.6e and 3.7e, respectively. The important peaks are at approximately 8837 cm^{-1} (1132 nm), 8559 cm^{-1} (1168 nm) (C-O-C asymmetrical stretch of cellulose and hemicellulose) [55], and 9157 cm^{-1} (1092 nm) (2 x C-H stretches + 2 x C-C stretches of cyclopropane) [19]. The important peaks in the X-loading weight plots are at 5184 cm^{-1} (1929 nm) (combination of O-H stretch and HOH bend of polysaccharides) [19] and 4386 cm^{-1} (2280 nm) (C-H stretch + C-H stretch deformation of CH_3) [18]. The corresponding absorption bands with high regression coefficients and X-loading weights are shown in Table 3.12. The results show that polysaccharides strongly influence DTG_{peak} prediction. Polysaccharides, such as hemicellulose, holocellulose and cellulose, have a similar molecular structure of -OH groups [56]. The DTG_{peak}, which was the overall maximum of the cellulose decomposition rate [50], increased with increasing cellulose content [34,35,36,37].

3.6 Conclusion

This study focused on NIR spectroscopic methods as an alternative for thermogravimetric analysis (TGA) to determine T_{onset}, T_{sh}, T_{peak}, T_{offset} and DTG_{peak} of milled bamboo. The results show that the pyrolysis characteristics did not depend on the culm circumference, and the lignocellulosic content in the bamboo influenced the predictions of the models. The models developed for T_{sh} and T_{offset} may be used as a nondestructive technique with caution for most applications, and the model developed for T_{peak} is usable

for most applications. On the other hand, the model for DTG_{peak} may be used for screening. However, the predictive model for T_{onset} is not usable due to high RMSEP and low R^2. However, all models showed low bias. This indicates that the developed protocol could be used to control the pyrolysis processes of bamboo to achieve the most economical and environmental conditions. In the authors' opinion, T_{onset} and T_{offset} can be used to set the starting temperature and the final target temperature of the pyrolysis, both of which are very important parameters. Oyedun et al. [6] explained that the final target temperature could greatly influence the amount of energy used during pyrolysis, and its value could significantly affect the energy cost and completion time. If the value is too low, the biomass will contain some volatile gas and the process will take a long time to complete, thus leading to a low amount of bio-oil. On the other hand, if the value is too high, the amount of energy used by the heater is too high, which affects the energy cost. T_{onset} is the temperature at which biomass starts to decompose, and it can be used to set the gas collection time. If the gas is collected before the biomass starts to decompose, there will be a high amount of moisture in the gas, which results in low-quality bio-oil. T_{peak} is the temperature at the highest degradation rate and DTG_{peak} is the maximum rate of decomposition. Their values can significantly affect the processing time. It was assumed that if the biomass pyrolysis was carried out at the temperature T_{peak}, it will give the highest decomposition rate of DTG_{peak}, thus resulting in the highest processing rate. The NIR spectroscopic model for these pyrolysis characteristics could be applied to control the process online in real time. The information found in this research can be used to manage the bamboo biomass feedstock, pyrolysis process, and storage. In addition, the authors recommend the development of a universal model using different types of biomass, where the reference value will be in a wide range. Such a model may be useful for many types of biomass materials.

This chapter illustrates that NIR spectroscopy has the possibility to determine the pyrolysis characteristic. The next chapter will describe about the use of NIR spectroscopy for evaluating LHV and elemental composition. The conclusion was made from the chapter 3 that NIR spectroscopy has the ability for predicting proximate data and HHV. Generally, HHV can be converted to LHV, and HHV is the energy from the combustion of C, H, and

O. Then NIR spectroscopy may also have high possibility for predicting the LHV and elemental components.

Table 3.8 The absorption bands with high regression coefficient and X-loading weight of the model for T_{onset} of milled bamboo

Regression coefficient				
Wavenumber (cm^{-1})	Wavelength (nm)	Wavelength (nm) referred from reference	Bond vibration	Structure
5543	1804	1790[19]	O–H combination	Water
6094	1641	1645[18]	C–H stretching first overtone	R-CH-CH (O)
5716	1750	1750[18]	-	α-D-glucose
6002	1666	1664[19]	C–H methyl, OH associated as $ROHCH_3$	Alcohols, diols
5585	1790	1790[19]	O–H combination	Water
5882	1700	1700[19]	C–H methyl, CH_3Cl	Halogenated (CH_3Cl)
5901	1695	1695[19]	C–H methyl, CH_3Br	Halogenated (CH_3Br)
5809	1721	1725[18]	C–H stretching first overtone	CH_2
5658	1767	1765[18]	C–H stretching first overtone	CH_2
5608	1783	1780[18]	C–H stretching first overtone	Cellulose
5828	1715	1711[19]	C–H methyl, CH_3Br	Halogenated (CH_3I)
5793	1726	1728[18]	-	Hemicellulose
X-loading weight				
Wavenumber (cm^{-1})	Wavelength (nm)	Wavelength (nm) referred from reference	PLS latent variable	Bond vibration	Structure
5901	1695	1695[18]	3	C–H stretching first overtone	CH_3
5952	1680	1680[19]	2	Aromatic C–H	Hydrocarbon, aromatic
5979	1673	1671[19]	1	C–H aromatic C–H (aryl)	C–H aryl
5936	1685	1685[19]	1	C–H aromatic C–H	Hydrocarbon, aromatic
5450	1835	1834[18]	1	-	α–D–glucose
5801	1724	1725[18]	2	C-H stretching first overtone	CH_2
5712	1751	1750[18]	3	-	α–D–glucose
5766	1734	1733[19]	1	C–H methyl C–H, ether associated as (R–O–CH_3)	Ether
5828	1716	1711[19]	3	C-H methyl, CH_3Br	Halogenated (CH_3I)
5589	1789	1789[18]	1	-	α–D–glucose

The intensity of the peaks was running in descending order.

Table 3.9 The absorption bands with high regression coefficient and X-loading weight of the model for T_{sh} of milled bamboo

Regression coefficient				
Wavenumber (cm^{-1})	Wavelength (nm)	Wavelength (nm) referred from reference	Bond vibration	Structure
5959	1678	1678[19]	C–H methyl, carbonyl adjacent as (.C=OCH_3)	Ketones
5138	1946	1950[19]	C=O esters and acids (.C=OOR)	Acids and esters
4872	2052	2053[19]	N–H combination from polyamide II	Polyamide II
5905	1693	1694[19]	C–H methyl C–H, (.CH_3)	Hydrocarbons, aliphatic
5307	1884	1892[19]	O–H hydrogen bonding between water and exposed polyvinyl alcohol OH	Water and polyvinyl
5211	1919	1920[18]	C=O stretching second overtone	CONH
7174	1394	1395[18]	2xC–H stretching + C–H deformation	CH_2
7197	1389	1390[19]	Si–OH	Silica; optical fibers
5836	1714	1711[19]	C–H methyl C–H, iodine (CH_3I)	Halogenated (CH_3I)
X-loading weight				
Wavenumber (cm^{-1})	Wavelength (nm)	Wavelength(nm) referred from reference	PLS latent variable	Bond vibration	Structure
5338	1873	-	2	-	-
4494	2225	2230[19]	1	CHO	-
5230	1912	1910 [51]	3	O-H stretch first overtone	Ar-OH
5188	1928	1928[19]	2	O–H stretching and HOH deformation combination	3-aminopropyltriethoxysilane-ethanol-water system
4980	2008	2008[18]	1	-	Sucrose
5253	1904	1900[18]	1	O–H stretching second overtone	Starch
5288	1891	1892[19]	3	O–H hydrogen bonding between water and exposed polyvinyl alcohol OH	Water and polyvinyl alcohol OH
5157	1939	1940[18]	3	O–H stretching + O–H deformation	Water
4891	2045	2050[18]	1	N-H asym. Stretching+ amide III	$CONH_2$

The intensity of the peaks was running in descending order.

Table 3.10 The absorption bands with high regression coefficient and X-loading weight of the model for T_{peak} of milled bamboo

Regression coefficient				
Wavenumber (cm^{-1})	Wavelength (nm)	Wavelength (nm) referred from reference	Bond vibration	Structure
5797	1725	1725[18]	C–H stretching first overtone	CH_2
4663	2144	2140[18]	=C–H stretching + C=C stretching	HC=CH
4328	2310	2310[18]	C–H stretching + C–H deformation	CH_2
5412	1847	-	-	-
4397	2274	2276[18]	O–H stretching + C–C stretching	Starch
5277	1895	1900[18]	O–H stretching + 2×C–O stretching	Starch
5196	1925	1923[19]	O–H assigned to molecular water (O-H stretching and HOH deformation)	O–H molecular water
4744	2108	2110[18]	-	Hemicellulose
4872	2053	2053[19]	N–H combination from polyamide 11	Polyamide 11
4783	2090	2090[19]	O–H combination	Polymeric OH
X-loading weight				
Wavenumber (cm^{-1})	Wavelength (nm)	Wavelength(nm) referred from reference	PLS latent variable	Bond vibration	Structure
4359	2294	2294[19]	3	C–H aromatic C–H (aryl)	C–H aryl
5196	1925	1923[19]	2	O–H assigned to molecular water	O–H molecular water
4929	2029	2030[18]	1	C=O stretching second overtone	$CONH_2$
4467	2239	-	2	-	-
4868	2054	2053[19]	3	N–H combination from polyamide II	Polyamide II
5296	1888	1900[18]	1	O–H stretching + 2x C–O stretching	Starch
4497	2224	2220[19]	3	NH combination band from urea ($N–H_2–C=O–NH_2$)	NH from urea
4440	2252	2252[18]	1	O–H stretching + O–H deformation	Starch
4409	2268	2270[19]	2	O–H stretching and C–O stretching combination	Cellulose
4355	2296	2294[18]	2	N–H stretching + C=O stretching	Amino acid

The intensity of the peaks was running in descending order.

Table 3.11 The absorption bands with high regression coefficient and X-loading weight of the model for T_{offset} of milled bamboo

Regression coefficient				
Wavenumber (cm^{-1})	Wavelength (nm)	Wavelength (nm) referred from reference	Bond vibration	Structure
5273	1896	1892[19]	O–H hydrogen bonding between water and exposed polyvinyl alcohol OH	Water and polyvinyl alcohol
5801	1724	1725[18]	C–H stretching first overtone	CH_2
9342	1070	1065[19]	O–H combination band, alcohol or water	Alcohols as R–C–O–H
5199	1923	1920[18]	C=O stretching second overtone	CONH
9215	1085	1080[18]	2×C–H stretching + 2×C–C stretching	Benzene
5415	1847	-	-	-
9168	1091	1097[18]	2×C–H stretching + 2×C–C stretching	Cyclopropane
4667	2143	2140[18]	=C–H stretching + C=C stretching	HC=CH
9041	1106	-	-	-
X-loading weight				
Wavenumber (cm^{-1})	Wavelength (nm)	Wavelength(nm) referred from reference	PLS latent variable	Bond vibration	Structure
4933	2027	2030[18]	1	C=O stretching + second overtone	$CONH_2$
5192	1926	1928[19]	2	O–H stretching and HOH deformation combination from water molecules in the 3-aminopropyltriethoxysilane-ethanol-water system	3-aminopropyltriethoxysilane-ethanol-water system
5169	1935	1933[19]	3	Si–O–H stretching + Si–O–Si combination from silicone	Silicone
4860	2058	2060[19]	3	N–H combination band from secondary amide in proteins	N–H from protein
4683	2135	2132[18]	2	N–H stretching + C=O stretching	Amino acid
5304	1885	1892[19]	1	O–H hydrogen bonding between water and exposed polyvinyl alcohol OH	Water and polyvinyl alcohol OH
6052	1652	1654[19]	3	C–H methyl C–H, nitro (CH_3NO_2)	Nitro (CH3) as (CH_3NO_2)
5319	1880	-	2	-	-
5944	1682	1685[18]	3	C–H stretching first overtone	Aromatic

The intensity of the peaks was running in descending order.

Table 3.12 The absorption bands with high regression coefficient and X-loading weight of the model for DTG_{peak} of milled bamboo

Regression coefficient				
Wavenumber (cm^{-1})	Wavelength (nm)	Wavelength (nm) referred from reference	Bond vibration	Structure
8837	1132	-	-	-
8559	1168	1160[55]	C–O–C asymmetrical stretching	Cellulose, hemicellulose
9157	1092	1097[18]	2×C–H stretching + 2× C–C stretching	Cyclopropane
8879	1126	-	-	-
8779	1139	1142[19]	C–H (3*v*), aromatic C–H	Hydrocarbon, aromatic
9242	1082	1080[18]	2×C–H stretching + 2× C–C stretching	Benzene
9099	1099	1097[18]	2×C–H stretching + 2× C–C stretching	Cyclopropane
5176	1932	1930[19]	O–H stretching and HOH bending combination	Polysaccharides
9334	1071	1065[19]	O–H combination band, alcohols or water	Alcohols
4494	2225	2230[19]	CHO	-
8181	1222	1225[18]	C–H stretching second overtone	CH
5003	1999	2000[18]	2× O–H stretching and C–O deformation	Starch
X-loading weight				
Wavenumber (cm^{-1})	Wavelength (nm)	Wavelength (nm) referred from reference	PLS latent variable	Bond vibration	Structure
5184	1929	1930[19]	2	O–H stretching and HOH bending combination	Polysaccharides
4386	2280	2280[18]	3	C–H stretching + C–H stretching deformation	CH_3
4467	2239	-	1	-	-
5315	1882	1900[18]	1	O–H stretching + 2×C–O stretching	Starch
4933	2027	2030[18]	1, 2	C=O stretching overtone	$CONH_2$
4490	2227	2230[19]	3, 2	CHO	-
5319	1880	1900[18]	3	O–H stretching + 2×C–O stretching	Starch
5280	1894	1892[19]	2	O–H hydrogen bonding between water and alcohol OH	Water and alcohol OH
5250	1905	1908[18]	3	O–H stretching + O–H deformation	POH
4702	2127	2027[19]	2	N–H/C=O combination from polyamide II	Polyamide II
5199	1923	1923[19]	1	O–H assigned to molecular water	O–H molecular water

The intensity of the peaks was running in descending order.

3.7 References

[1] Power Pellet: [Online]. Available : http://www.renewableenergy-asia.com/Portals/0/seminar/Presentation/01.1-A2.pdf.

[2] Chaowana P. "Bamboo: An Alternative Raw Material for Wood and Wood-Based Composites." **Journal of Materials Science Research**, vol. 2(2), 2013.

[3] Scurlock J.M.O., Dayton D.C., Hames B. "Bamboo: an overlooked biomass resource?", **Biomass Bioenerg**, vol. 19, 2000. Pp. 229-244.

[4] Falayi F.R., Soyoye B.O., Tehinse T.O. "The Influence of Age and Location on Selected Physical and Mechanical Properties of Bamboo (Phyllostachys Pubesces). **International Journal of Research in Agriculture and Forestry**, vol. 1(1), 2014. Pp. 44-54.

[5] Dransfield S., Widjaja E.A. Plant Resources of South-East Asia No.7: Bamboo, Backhuys Publishers, Netherlands, 1995. Pp. 189.

[6] Oyedun A.O., Gebreegziabher T., Hui C.W. "Mechanism and modelling of bamboo pyrolysis" **Fuel Process Technol**, vol. 106, 2013. Pp. 595-604.

[7] Permkam S. "Bamboo-shoot fruit flies (Diptera : Tephritidae) of southern Thailand." **Songklanakarin Journal of Science Technol**, Vol. 27(2), 2005. Pp. 223-237.

[8] Phuangchik T. "Is Bamboo Amazing Plant?." **Journal of Science and Technology (Thammasat University)**, vol. 2, 2013. Pp. 179-185.

[9] Carvalho W.S., Oliveira T.J., Cardoso C.R., Ataide C.H. "Thermogravimetric analysis and analyticalpyrolysis of a variety of lignocellulosic sorghum." **Chemical engineering research and design**, vol. 95, 2015. Pp. 337–345.

[10] Hernandez-Mena L.E., Pécora A.A.B., Beraldo A.L. "Slow Pyrolysis of Bamboo Biomass: Analysis of Biochar Properties." **Chemical engineering transactions**, vol. 37, 2014.

[11] Dannenmann B.M.E., Choocharoen C., Spreer W., Nagle M., Leis H., Neef A., Mueller J. "The Potential of Bamboo as a Source of Renewable Energy in Northern Laos. " **Tropentag 2007 University of Kassel-Witzenhausen and University of Göttingen**, October 9-11, 2007. Conference on International Agricultural Research for Development.

[12] Darabant A., Haruthaithanasana M., Atklaa W., Phudphonga T., Thanavata E. "Bamboo biomass yield and feedstock characteristics of energy plantations in Thailand." **Energy Procedia**, vol. 59, 2014. Pp. 134–141.

[13] Villar-Cociña E.V., Morales S.F., Santos H.S., Jr b., Frías M. "Pozzolanic behavior of bamboo leaf ash: Characterization and determination of the kinetic parameters." **Cem Concr Compos**, vol. 33, 2011. Pp. 68–73.

[14] Jiang Z., Liu Z., Fei B., Cai Z., Yu Y., Liu X. "The pyrolysis characteristics of moso bamboo." **J. Anal Appl Pyrol**, vol. 94, 2012. Pp. 48–52.

[15] Montaño C.M.D., Pels J.R., Fryda L.E., Zwart R.W.R. "Evaluation of torrefied bamboo for sustainable bioenergy production", in: J. Gielis (Ed.) 9th World Bamboo Congress, World Bamboo Organization, Antwerpen, 2012. Pp. 809-818.

[16] Liu Z., Jiang Z., Cai Z., Fei B., Yu Y., Liu X. "The Manufacturing Process of Bamboo Pellets." **Proceedings of the 55th International Convention of Society of Wood Science and Technology**. August 27-31, 2012 - Beijing, CHINA.

[17] Lestander T.A., Johnsson B., Grothage M. "NIR technique create added value for the pellet and biofuel industry". **Bioresource Technol**, vol. 100, 2009. Pp. 1589-1594.

[18] Osborne B.G., Fearn T. Near Infrared Spectroscopy in Food Analysis, Longman Science and Technical, London, 1986.

[19] Workman J., Weyer J.R.L. Practical Guide to Interpretive Near-Infrared Spectroscopy, Taylor and Francis, Boca Raton, FL, 2007. Pp. 240–262.

[20] Chadwick D.T., McDonnell K.P., Brennan L.P., Fagan C.C., Everard C.D. "Evaluation of infrared techniques for the assessment of biomass and biofuel quality parameters and conversion technology processes: A review." **Renew Sust Energ Rev**, vol. 30, 2014. Pp. 672–681.

[21] Guimarães C.C., Simeone M.L., Parrella R.A.C., Sena M.M. "Use of NIRS to predict composition and bioethanol yield from cell wall structure components of sweet sorghum biomass." **Microchem J**, vol. 117, 2014. Pp. 194-201.

[22] Posom J., Sirisomboon P. "Evaluation of the thermal properties of Jatropha curcas L. kernels using near-infrared spectroscopy." **Biosystem Eng**, vol. 125, 2014. Pp. 45-53.

[23] Posom J., Sirisomboon P. "Evaluation of the moisture content of Jatropha curcas kernels and the heating value of the oil extracted residue using near-infrared spectroscopy". **Biosystem Eng**, vol. 130, 2015. Pp. 52-59.

[24] Fagan C.C., Everard C.D., McDonnell K. "Prediction of moisture, calorific value, ash and carbon content of two dedicated bioenergy crops using near-infrared spectroscopy". **Bioresour Technol**, vol. 102, 2011. Pp. 5200–5206.

[25] Park J.I., Liu L., Ye X.P., Jeong M.K., Jeong Y-S. "Improved prediction of biomass composition for switchgrass using reproducing kernel methods with wavelet compressed FT-NIR spectra". **Expert Syst Appl**, vol. 39, 2012. Pp. 1555–1564.

[26] Triolo J.M., Ward AJ., Pedersen L., Løkke M.M., Qu H., Sommer S.G. "Near infrared reflectance spectroscopy (NIRS) for rapid determination of biochemical methane potential of plant biomass". **Appl Energ**, vol. 116, 2014. Pp. 52–57.

[27] Liu L., Ye X.P., Womac AR., Sokhansanj, S. "Variability of biomass chemical composition and rapid analysis using FT-NIR techniques". **Carbohyd Polym**, vol. 81, 2010. Pp. 820–829.

[28] Xiao G., Ni M-J., Huang H., Chi Y., Xiao R., Zhong Z-P., Cen K-F. "Fluidized-bed pyrolysis of waste bamboo". **J Zhejiang Univ Sci A**, vol. 8(9), 2007. Pp. 1495-1499.

[29] Jiang Z., Fei B., Li Z. "Pretreatment of bamboo by ultra-high pressure explosion with a highpressure homogenizer for enzymatic hydrolysis and ethanol fermentation". **Bioresource Technology**, vol. 214, 2016. Pp. 876–880.

[30] Xie J., Hse C-Y., Hoop C.F.D., Hu T., Qi J., Shupe T.F. "Isolation and characterization of cellulose nanofibers from bamboo using microwave liquefaction combined with chemical treatment and ultrasonication". **Carbohydr. Polym**, vol. 151, 2016. Pp. 725–734.

[31] Dardenne P. "Some considerations about NIR spectroscopy". **Closing speech at NIR-2009, NIR news**, vol. 21(1), 2010. Pp. 8–14.

[32] Nicolaï B.M, Beullens K., Bobelyn E., Peirs A., Saeys W., Theron K.I., Lammertyn J. "Nondestructive measurement of fruit and vegetable quality by means of NIR spectroscopy: A review". **Postharvest Biol Technol**, vol. 46, 2007. Pp. 99–118.

[33] Cheng L., Adhikari S., Wang Z., Ding Y. "Characterization of bamboo species at different ages and bio-oil production". **J Anal Appl Pyrol**, vol. 116, 2015. Pp. 215–222.

[34] Wannapeera J., Worasuwannarak N., Pipatmanomai S. "Product yields and characteristics of rice husk, rice straw and corncob during fast pyrolysis in a drop-tube/fixed-bed reactor." **Songklanakarin J Sci Technol**, vol. 30(3), 2008. Pp. 393-404.

[35] Lv D., Xu M., Liu X., Zhan Z., Li Z., Yao H. "Effect of cellulose, lignin, alkali and alkaline earth metallic species on biomass pyrolysis and gasification". **Fuel Process Technol**, vol. 91, 2010. Pp. 903–909.

[36] Burhenne L., Messmer J., Aicher T., Laborie M-P. "The effect of the biomass components lignin, cellulose and hemicellulose on TGA and fixed bed pyrolysis". **J Anal Appl Pyrol**, vol. 101, 2013. Pp. 177–184.

[37] Dorez G., Ferry L., Sonnier R., Taguet A., Lopez-Cuesta J.-M. "Effect of cellulose, hemicellulose and lignin contents on pyrolysis and combustion of natural fibers". **J Anal Appl Pyrol**, vol. 107, 2014. Pp. 323–331.

[38] Stefanidis S.D., Kalogiannis K.G., Iliopoulou E.F., Michailof C.M., Pilavachi P.A., Lappas A.A. "A study of lignocellulosic biomass pyrolysis via the pyrolysis of cellulose, hemicellulose and lignin". **J Anal Appl Pyrol**, vol. 105, 2014. Pp. 143–150.

[39] Yang Z., Li K., Zhang M., Xin D., Zhang J. "Rapid determination of chemical composition and classification of bamboo fractions using visible–near infrared spectroscopy coupled with multivariate data analysis." **Biotechnol Biofuels**, 2016. Pp. 1-18.

[40] Conzen JP. Selection criteria for a PLS calibration; Method optimization. "Multivariate calibration". Bruker Optik GmbH; 2006, 2rd edition.

[41] Peters B. "Prediction of pyrolysis of pistachio shells based on its components hemicellulose, cellulose and lignin". **Fuel Process. Technol**, vol. 92, 2011. Pp. 1993–1998.

[42] Chen D., Zhou J., Zhang Q. "Effects of heating rate on slow pyrolysis behavior, kinetic parameters and products properties of moso bamboo". **Bioresour. Technol**, vol. 169, 2014. Pp. 313–319.

[43] Sanchez-Silva L., LÒpez-González D., Villase J., Sánchez P., Valverde J.L. "Thermogravimetric–mass spectrometric analysis of lignocellulosic and marine biomass pyrolysis." **Bioresour. Technol**, vol. 109, 2012. Pp. 163–172.

[44] Kan T., Strezov V., Evans T.J. "Lignocellulosic biomass pyrolysis: A review of product properties and effects of pyrolysis parameters" **Renew Sust Energ Rev**, vol. 57, 2016. Pp. 1126–1140.

[45] Irfan M., Chen Q., Yue Y., Pang R., Lin Q., Zhao X., Chen H. "Co-production of biochar, bio-oil and syngas from halophyte grass (Achnatherum splendens L.) under three different pyrolysis temperatures". **Bioresour. Technol**, vol. 211, 2016. Pp. 457–463.

[46] Chen D., Li Y., Cen K., Luo M., Li H., Lu B. "Pyrolysis poly generation of poplar wood: Effect of heating rate and pyrolysis temperature." **Bioresour. Technol**, vol. 218, 2016. Pp. 780–788.

[47] Kim P., Weaver S., Labbé N. "Effect of sweeping gas flow rates on temperature-controlled multistage condensation of pyrolysis vapors in an auger intermediate pyrolysis system." **J. Anal. Appl. Pyrolysis**, vol. 118, 2016. Pp. 325–334.

[48] Williams P. "Near-Infrared Technology—Getting The Best Out Of Light Edition 5.0. A Short Course in the Practical Implementation of Near-Infrared Spectroscopy for the User" PDK Grain, Nanaimo, Canada, 2007.

[49] Zornoza R., Guerrero C., Mataix-Solera J., Scow K.M., Arcenegui V., Mataix-Beneyto J. "Near infrared spectroscopy for determination of various physical, chemical and biochemical properties in Mediterranean soils." **Soil Biol Biochem**, vol. 40(7), 2008. Pp. 1923–1930.

[50] El-Sayed S.A., Mostafa M.E. "Pyrolysis characteristic and kinetic parameters determination of biomass fuel powders by differential thermal gravimetric analysis (TGA/DTG)". **Energ Convers Manage**, vol. 85, 2014. Pp. 165-172.

[51] Baillères H., Davrieux F., Ham-Pichavant F. "Near infrared analysis as a tool for rapid screening of some major wood characteristics in a eucalyptus breeding program". **Annal Forest Sci**, vol. 59, 2002. Pp. 479–90.

[52] Yang H., Yan R., Chen H., Lee D.H., Zheng C. "Characteristics of hemicellulose, cellulose and lignin pyrolysis" **Fuel**, vol. 86, 2007. Pp. 1781–1788.

[53] Guan Y., Ma Y., Zhang K., Chen H., Xu G., Liu W., Yang Y. "Co-pyrolysis behaviors of energy grass and lignite" **Energ Convers Manage**, vol. 93, 2015. Pp. 132–140.

[54] Gaur S., Reed T.B. "Thermal data for natural and synthetic fuels, Pyrolysis of the components of biomass". Marcel Dekker, Inc. New York. Basel. Hong Kong, 1998. Pp. 83.

[55] Sills D.L., Gossett J.M. "Using FTIR to predict saccharification from enzymatic hydrolysis of alkali pretreated biomasses". **Biotechnol Bioeng**, vol. 109, 2012. Pp. 353–62.

[56] Jiang W., Han G., Via B.K., Tu M., Liu W., Fasina O. "Rapid assessment of coniferous biomass lignin carbohydrates with near-infrared spectroscopy" **Wood Sci Technol**, vol. 48, 2014. Pp. 109–122.

Chapter 4

Evaluation of lower heating value and elemental composition of bamboo using near infrared spectroscopy

4.1 Abstract

This study was to optimize models using near infrared spectroscopy for evaluation of lower heating value (LHV), carbon (C), hydrogen (H), nitrogen (N), sulfur (S) and oxygen content (O) of bamboo. Partial least squares regression was performed using 80 samples of bamboo where 64 samples was randomly assigned for calibration and 16 samples for validation. The result was that LHV and element composition did not depend on circumference size. The models showed the coefficient of determination of validation set and ratio of standard error of prediction to standard deviation of reference value of 0.934 and 3.96 for LHV, 0.803 and 2.31 for C; 0.856 and 2.65 for H; 0.973 and 6.6 for N; 0.785 and 2.19 for S and 0.522 and 1.46 for O, respectively. Models for LHV, N and H prediction provided the highest performance, which could be used for most application. The C and S models were fair and O model was poor. The result could be a guide for applying in bamboo trading as biomass, in design and operation control of energy conversion and in predicting flue gas flow rate, air requirement, and flue gas compositions in combustion, gasification or pyrolysis.

*This chapter constituted the journal article: Posom J and Sirisomboon P. "Evaluation of lower heating value and elemental composition of bamboo using near infrared Spectroscopy." **Energy**, vol. 121, 2017. Pp. 147-158.

4.2 Introduction

Bamboo's characteristic as a raw material for electricity production of biomass power plants in Thailand was studied by Sritong et al. [1]. They concluded that bamboo was appropriate for producing electricity with moisture contents (MC) of 14.30 % and 5.80%, ash (A) contents of 3.70% and 2.70%, volatile matter (VM) contents of 63.10% and 71.70%, fixed carbon (FC) contents of 18.90% and 19.80%, and higher heating values (HHVs) of 15.700 MJ kg^{-1} and 17.585 MJ kg^{-1} for Gimsung bamboo and Tong bamboo, respectively. The elemental composition of bamboo was also investigated by Scurlock et al. [2]. They reported approximately 52% for C, 5% for H, a range of 0.2–0.5% for N, 43.3% for cellulose, 24.6% for hemicellulose and 26.2% for lignin. Many researchers have been interested in the properties of bamboo as an energy resource such as biochar obtained from pyrolysis [3], bamboo pellets [4], pyrolysis characteristics [5], characteristics at different ages and bio-oil production [6], yield and feedstock characteristics of energy [7], pyrolysis behavior, product properties, and carbon and energy yields of bamboo pyrolysis [8].

Like wood, chemical properties of bamboo can be effected by crop location, plant species, collection method, harvesting age, and storage time [9]. Thus, energy content, element composition (C, H, N, O and S) and A could differ even if they were the same species. Additionally, energy content and elemental compositions of biomass are very important for analyzing the overall process of thermal conversion systems. LHV is the real energy content. Under actual operating conditions, LHV is better than HHV [10], however, HHV has been reported more often. For elemental compositions, S and N lead to oxide emissions and can be oxidized into SO_2, NO, and NO_2; released in the air; and become acid rain precursors and greenhouse gases [11]. High H leads to high ash content during combustion. They should be investigated.

In the combustion process, C and H had the effects of increasing calorific value and O decreasing calorific value [12]. In current trading, biomass is sold or bought by weight i.e., price per kg [13]. In the authors' opinion, this is incorrect due to biomass feedstock having variable energy characteristics i.e., heating value (HV) and element composition. In the future, it will be necessary to determine prices using chemical composition and HV such as using either the percent of C, H, O, N and S or heating

value. For example, with biomass that contains high C and H, that biomass will fetch a higher price. On other hand, if the biomass is high in N, O and S content, that biomass will sell for less.

There were also several reports on successfully using NIR spectroscopy with PLS regression to determine HHV of biomass [13,14,15,16,17]. However, no studies have been reported using NIR spectroscopy to evaluate the LHV of biomass. NIR spectroscopy of C of biomass was investigated by Gillespie et al. [15] and Fagan et al. [17]. They used NIR spectrometers in reflectance mode and the models were validated by cross validation, and provided R^2 of 0.78 and 0.88, respectively. They recommended that the models were fair and could be used for screening applications. Vis-NIR waveband of 400–1000 nm for C prediction of milled *Miscanthus* and two short rotation coppice willow varieties was investigated by Everard et al. [18], giving R^2 of 0.85. The use of NIR spectroscopy for determination of N in soil was investigated by Zhang et al. [19], who obtained fair performance of a PLS regression model, which provided R^2 of 0.634. In addition, the elemental content (C, H, N and S) from ultimate analysis of coal was estimated by NIR spectroscopy [20,21,22]. Chadwick et al. [23] reported that the prediction of C, H and O of biomass was not successful. Because there have been no reports on LHV determination using NIR spectroscopy and the prediction of C, H, N, O and S by the same method showing fair results.

4.3 Objective

The goal of this study was to evaluate LHV and element composition (C, H, N, O and S) of bamboo using a Fourier transform-NIR spectrometer in the wavenumber range of 12500–3600 cm^{-1} with diffuse reflection mode. PLS modelling was employed and validated by the test set method.

4.4 Materials and methods

4.4.1 Materials

The 80 bamboo samples used in this study were collected from the Uttaradit province, Thailand. Each sample was cut 10 cm above the ground. After harvest, it was chopped with a chopping machine (P5508, Patipong, Thailand), air-dried under the sun

until the moisture content was approximately 5%, and then ground through a sieve with a diameter of 3 mm (60201, QC, UK). After grinding, all samples were kept in sealed aluminum bags until experiments.

4.4.2 NIR measurement

The ground sample was stirred until homogeneous and poured into the sample cup 43 mm in diameter and 50 mm in height with the bottom made of quartz. The sample was scanned with the FT-NIR spectrometer (Bruker Optics, Ettlingen, Germany) in diffuse reflectance mode at room temperature of 25 ± 2 °C. The scanning was conducted with a spectral range of 12,500–3600 cm^{-1} and resolution of 8 cm^{-1} and each spectrum was obtained with an average of 64 scans. The spectral data were obtained by OPUS 7.0.129 software in log (1/R) unit and saved as OPUS files. In the measurement of diffuse reflection mode, it was assumed that the spectral data collected from equation of log Ṙ/R); where Ṙ was the reflectance of standard, that is reference material; and R was the diffuse reflectance radiation of the sample [34]. The reflectance of the reference material gives 100% reflection, meaning that Ṙ is equal to 1; and the sample was thick enough so that no light was emitted through the sample [24]. After scanning, the ground bamboo at the bottom of the cup was collected for determination of moisture content, ash content, HHV and elemental composition.

4.4.3 Reference methods

Each scanned sample was divided into three parts. The first part of the sample was used for determination of moisture and ash content using a thermogravimetric analyzer (TG 209 F3 Tarsus, Netzsch, Germany). A sample of 6 ± 0.5 mg was put into an AlO_3 crucible. The sample was heated from 30 to 700 °C at a heating rate of 10 °C/min in 20 ml/min N_2 flushed environment. When the temperature reached 700 °C, 20 ml/min O_2 was fed for 1 h for the combustion process. Moisture content and ash content were approximated by direct measurement of weight changes. The moisture and ash were obtained from TG profile by the difference from slope to slope [25]. The solid residue after complete combustion provided the ash content. The second part of the sample was used for determination of HHV where the ground bamboo was compressed into pellets (approximately 0.5 g) and subjected to a bomb calorimeter (C200, IKA,

Germany) in isoperibol mode. The HHV measurements were expressed on a wet weight basis (MJ/wet kg). The HHV was used to calculate the LHV as follows [26]:

$$LHW_{wb} = HHV_{wb} - 2.443M \quad (4.1)$$

where LHV_{wb} is the lower heating value (MJ/wet kg), HHV_{wb} is the higher heating value (MJ/wet kg), which is experimentally determined directly on wet samples with a known moisture content (M); M is the moisture content obtained from TG profile (expressed as a fraction on a wet weight basis), and 2.443 is the latent heat of the vaporization of water at 25 °C (MJ kg^{-1}). The third part of the sample was for determination of the elemental composition (C, H, N and S) and was determined using a CHNS analyzer (Vario EL CUBE, Elementar, Germany). O was calculated as follows:

$$O\% = 100\% - [C\% + H\% + N\% + S\% + A\%] \quad (4.2)$$

where A is the percentage of ash content, which was obtained from the TG chart. The elemental composition, moisture and ash content were measured in duplicate. After that, the repeatability of reference data and spectrum scanning were determined, which indicates the precision of laboratory and NIR spectrometer, respectively. Repeatability of reference data is the standard deviation of the difference between duplicates. Repeatability of spectrum data was determined using the absorbance value at a wavenumber of 5176 cm^{-1} (1932 nm) when the sample was re-scanned for 10 times and these values used to calculate the standard deviation of absorbance values in the same position. Repeatability data were also used to calculate the maximum coefficient of determination (R^2_{max}) using the formula:

$$R^2_{max} = \frac{SD_y^2 - Rep^2}{SD_y^2} \quad (4.3)$$

Where SD_y^2 and Rep^2 were the standard deviation of reference data and repeatability, respectively. The R^2_{max} was defined as the maximum of coefficient of determination when there was no error of spectral. R^2_{max} was dependent on standard deviation of reference data and repeatability, and it was high when standard deviation was wide and/or repeatability was low [27].

4.4.4 Spectrum pretreatment and chemometric analysis

The spectra pretreatment and chemometric analysis were conducted using the software program OPUS version 7.0.129, Germany. Spectra pretreatment methods were the constant offset elimination, straight line subtraction, vector normalization, min-max normalization, multiplicative scatter correction (MSC), first derivatives, second derivatives, first derivatives + straight line subtraction, first derivatives + vector normalization and first derivatives + MSC. Nicolaï et al.[28] recommended that the spectral pretreatment techniques were used to remove any irrelevant information. All 80 ground samples were randomly separated into a calibration set of 80% of samples and a validation set of 20%. The partial least squares regression (PLSR) was used for modelling. The PLSR algorithm could be described as follows [29]:

$$Y=aX+b \tag{4.4}$$

where Y is the response matrix of the samples, X is the predicted matrix of the samples, a is the matrix of regression coefficients obtained from PLSR, and b is the matrix of residual information.

4.4.5 Optimization of models

Optimization of models was carried out using PLS regression. There were three methods used i.e., General A, General B, and NIR mode. For example, if full wavenumber range was divided into three sub wavenumbers e.g., 1, 2, and 3; for General A mode: the modelling would start to remove each one out: 1 + 2 + 3 (full), 2 + 3 (1 was removed), 1 + 3 (2 was removed), 1 + 2 (3 was removed), 2 (1,3 were removed), and 1 (2 and 3 were removed), respectively; for General B: the optimization would start from individual sub wavenumber, then add new sub wavenumbers and some wavenumbers were repeated: 1, 2, 3, 1 + 2, 2 + 3, 2, 1, 1 + 2+3, 2 + 3, 1 + 3, and 1 + 2, respectively; and for NIR, the method was similar but not exactly the same as General B: 1, 2, 1 + 2, 3, 1 + 3, 2 + 3, 1 + 2 + 3, 1, and 2, respectively. If any combination gave the lowest root mean square error of estimation (RMSEE), that region was divided into two sub wavenumbers again. For example, if condition of 1 + 2 + 3 was the best result, it would be divided into two regions and examined again. Either full wavenumber or sub wavenumber ranges were used in combination for construction of the model with one of 11 spectrum pretreatment methods including non-pretreatment and 10 pretreatment methods (see 2.4.). Full wavenumber or sub

wavenumber ranges were crossed with 11 methods of spectrum pretreatment. The best model was selected by the lowest RMSEE. Then, the optimal sub wavenumber ranges and spectrum pretreatment method were selected.

The performance of the model for application could be considered. Commonly, many researchers have suggested the guidelines for the R^2 and RPD. Williams [24] recommended a guideline for R^2, i.e., if the model provided R^2 between 0.50 and 0.64, it could be used for rough screening; if between 0.66 and 0.81, it could be used with screening and some other "approximate" calibrations; if between 0.83 and 0.90, it could be used with caution for most applications; and if between 0.92 and 0.96, it could be used for most applications. Williams [24] also recommended for RPD that if the model provided RPD between 0.0 and 2.3, its use is not recommended, RPD between 2.4 and 3.0 could be used for very rough screening, RPD between 3.1 and 4.9 could be used for screening, RPD between 5.0 and 6.4 could be used for quality control, RPD between 6.5 and 8.0 could be used for process control; and RPD>8.1 could be used for any application. Zornoza et al. [30] also suggested about R^2 and RPD that the model provides excellent prediction if $R^2 > 0.90$ and RPD>3 and good prediction if $0.81 < R^2 < 0.90$ and $2.5 < RPD < 3$, and it permits only approximate prediction if $0.66 < R^2 < 0.80$ and $2.0 < RPD < 2.5$ and were poorly predicted if $R^2 < 0.66$ and $RPD < 2$. The RPD between 1.5 and 2 means that the model can discriminate low from high values of the response variable; a value between 2 and 2.5 indicates that coarse quantitative predictions are possible, and a value between 2.5 and 3 or above corresponds to good and excellent prediction accuracy [28].

4.5 Results and discussions

4.5.1 Measured values

Table 4.1 shows the statistical data regarding the LHV and elemental composition (in as-received basis) of bamboo obtained from bamboo trunks of different circumferences. It can be observed that there was no difference of average LHV and element composition even if the circumference sizes were different. In addition, every parameter had high standard deviation, which meant that circumference size did not influence LHV and the elemental composition. Table 4.2

shows the repeatability of the measured value and absorption data, which indicates the precision of the laboratory and NIR spectrometers, respectively, and the maximum coefficient of determination, which was the possible maximum coefficient of determination when there was no error from spectral collection. These results can be used to determine whether the models should be developed further. The number of samples, range, mean and standard deviation (SD) of LHV and elemental composition of ground bamboo of total samples, calibration set and validation set were presented in Table 4.3. The models would be considered robust if the reference value range of the calibration set is wider than the prediction set, due to the sample distribution within the calibration set being important for the model's reliability and performance. The LHV, C, H, N, S and O reference values were distributed around mean values of 17.68 MJ kg^{-1}, 46.270%, 6.232%, 0.382%, 0.059% and 43.231%, respectively, and standard deviations of 0.37 MJ kg-1, 0.956%, 0.095%, 0.126%, 0.015%, and 1.273%, respectively. For the bamboo, the C was the highest, and the S was the lowest.

Table 4.1 LHV, C, H, N, S and O of bamboo obtained from bamboo trunks with different circumferences of the culms

Culm range (cm)	N	LHV (MJ kg^{-1})	C (%)	H (%)	N (%)	S (%)	O (%)
16<L≤18	8	17.636±0.387a	45.948±0.8589a	6.2132±0.0706a	0.3262±0.0799bc	0.0677±0.0420a	43.3530±1.4844ab
18<L≤20	6	17.772±0.129a	46.5221±0.4831a	6.3011±0.0943a	0.2791±0.0595c	0.0528±0.0180a	43.1349±0.8154ab
20<L≤22	6	17.642±0.334a	46.451±0.7690a	6.2877±0.0524a	0.2966±0.0850bc	0.0588±0.0104a	42.8175±1.9144ab
22<L≤24	7	17.588±0.370a	46.0453±0.9793a	6.2068±0.1441a	0.4035±0.0828abc	0.0689±0.0147a	42.8911±1.5048ab
24<L≤26	6	17.628±0.134a	46.5462±0.6004a	6.2329±0.1330a	0.5325±0.1537a	0.0613±0.0125a	42.6595±1.0680b
26<L≤28	6	17.606±0.454a	46.1466±0.9160a	6.215±0.0525a	0.3808±0.1468bc	0.0735±0.0357a	43.6032±0.5586ab
28<L≤30	8	17.536a±0.567a	45.8007±1.2880a	6.2098±0.0615a	0.4150±0.1636abc	0.0661±0.0204a	43.7746±1.4172ab
30<L≤32	8	17.740±0.497a	46.4603±0.9893a	6.1957±0.0925a	0.3706±0.1658bc	0.0554±0.0231a	43.2417±1.3423ab
32<L≤34	7	17.701±0.464a	46.5084±1.5024a	6.2022±0.1157a	0.3328±0.0978bc	0.0533±0.0137a	42.8389±1.1061ab
34<L≤36	7	17.647±0.367a	46.6514±1.3805a	6.2237±0.1198a	0.4228±0.1257abc	0.0561±0.0095a	43.0780±1.5517ab
36<L≤38	5	17.888±0.225a	45.8643±0.1806a	6.2777±0.0801a	0.439±0.0579ab	0.0595±0.0069a	44.4515±0.7353a
38<L≤40	6	17.821±0.208a	46.3682±0.4525a	6.2534±0.0595a	0.4066±0.0583abc	0.0742±0.0194a	43.0442±0.8226ab

Different letters in the same column indicates the different means that are significantly at p>0.05 by the Duncan multiple range test. N is number of samples. L is circumference of the culm.

Table 4.2 Repeatability of the reference test and maximum R^2 for LHV, C, H, N, and S, and NIR scanning of ground bamboo

Parameter	Repeatability	R^2_{max}
LHV (MJ kg-1)	0.0674	0.967
Carbon content (%)	0.4368	0.792
Hydrogen content (%)	0.0538	0.676
Nitrogen content (%)	0.0447	0.874
Sulfur content (%)	0.0111	0.740
Oxygen content (%)	-	-
Absorption value at 5176 cm^{-1} (1932 nm) of sample number 28	0.0047	-

Table 4.3 Statistical data of LHV, C, H, N, S and O for ground bamboo used in model development

Parameters	Data set	N	Max	Min	Mean	Range	SD
LHV (MJ kg^{-1})	Total sample	80	18.25	16.34	17.68	1.91	0.370
	Calibration set	64	18.25	16.34	17.71	1.91	0.334
	Validation set	16	18.2	16.71	17.53	1.49	0.479
C (%)	Total sample	80	48.3735	43.15	46.27046	5.2235	0.9566
	Calibration set	64	48.3735	43.15	46.31577	5.2235	0.8781
	Validation set	16	47.9455	43.74	46.08925	4.2055	1.2397
H (%)	Total sample	79	6.4875	5.9255	6.231734	0.5620	0.0951
	Calibration set	63	6.4875	5.9255	6.229587	0.5620	0.0900
	Validation set	16	6.437	5.991	6.240188	0.4460	0.1160
N (%)	Total sample	79	0.755	0.18	0.381962	0.5750	0.1269
	Calibration set	63	0.755	0.18	0.37373	0.5750	0.1122
	Validation set	16	0.745	0.18	0.414375	0.5650	0.1742
S (%)	Total sample	78	0.105	0.0235	0.059833	0.0815	0.0157
	Calibration set	62	0.105	0.0235	0.059435	0.0815	0.0155
	Validation set	16	0.091	0.031	0.061375	0.0600	0.0169
O (%)	Calibration set	64	46.5305	40.594	43.23113	5.9365	1.2730
	Validation set	16	46.5305	40.594	43.16853	5.9365	1.1670

4.5.2 Spectral information

Figure 4.1 shows the NIR spectra of 80 samples covering the wavelength range of 12500–3600 cm^{-1} (x axis – wavenumber in cm^{-1}; y axis – absorbance value obtained from log(1/R)). The main bands were between 7151 and 6075 cm^{-1} (1398–1646 nm). The bands at 1395, 1415, 1417, 1440, and 1446 nm corresponded to the 2 × C-H stretching + C-H deformation [31], at 1410, 1420, 1440, 1450 1480, 1490, 1520, 1528, 1540, and 1580 nm corresponded to O-H stretching first overtone [31]. There were also the main bands at 5176 cm^{-1} (1932 nm), 4771 cm^{-1} (2096 nm), 4401 cm−1 (2272 nm) and 4019 cm^{-1} (2488 nm). The band at 1930 nm is O-H stretching + H-O-H bending combination of polysaccharides [32], 2100 nm is 2 × O-H deformation + 2 × C-O stretching of starch [31], 2500 nm is C-H stretching + C-C stretching of starch [31], and 2276 nm is O-H stretching + C-C stretching of starch [31]. The result of the absorption bands was similar to those reported by Yang et al. [33] in which there were many absorption bands of bamboo timber fractions occurring in the wavelength region of 1100–2500 nm, including prominent bands near 473, 1925, 2092, 2267, and 2328 nm. The wave band at 2267 nm is the overtone of O-H stretching and C-O stretching from lignin [33].

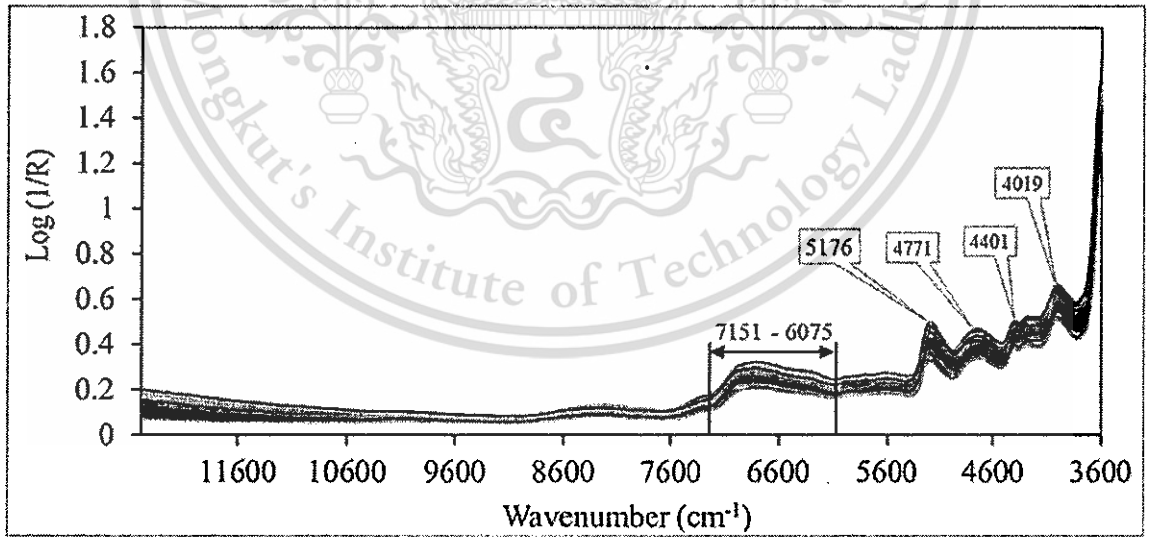

Figure 4.1 NIR spectra of 80 samples of ground bamboo

4.5.3 Predictions of LHV

Table 4.4 shows the results of optimum PLS models for LHV which was developed from multiplicative scattering correction of pretreated spectra in the

wavenumber ranges of 8373.9–7853.2 and 6827.2–5793.5 cm^{-1} and with a number of PLS latent variables of 3. The R_p^2, RMSEP, RPD and bias were 0.934, 0.119 MJ kg^{-1}, 3.96 and −0.0187 MJ kg^{-1}. R^2 of 0.934 meant that 93.4% of LHV variance could be explained by absorption variance, and 6.6% was the unexplained variance. The RPD value of more than 3 was acceptable. The obtained RMSEP indicated that the average uncertainty was 0.119 MJ kg-1 which could be expected for prediction of future samples. The bias of −0.0187 MJ kg^{-1} is the overall accuracy of the calibration model for the future applications. Zornoza et al. [30] indicated for R^2 and RPD that the model is excellent predicted if $R^2 > 0.90$ and RPD>3 and the RPD between 2.5 and 3 or above corresponded to good and excellent prediction accuracy [28]. Williams [24] recommended that R^2 between 0.92 and 0.96 could be used for most applications. The ratio between RMSEP and mean value of prediction set (0.119/17.53 MJ kg^{-1}) provided a small value of 0.678%. Therefore, the model was excellent for LHV prediction.

Table 4.4 Result of partial least squares regression models for determination of LHV, C, H, N, S and O of ground bamboo

Parameters	Wavenumber (cm^{-1})	Pretreatments	Calibration			Validation			
			Latent variables	R_c^2	RMSEE	R_p^2	RMSEP	RPD	Bias
LHV (MJ kg^{-1})	8373.9-7853.2 6827.2-5793.5	Multiplicative scattering correction	3	0.844	0.135	0.934	0.119	3.96	-0.0187
C (%)	12493.3-11602.3 10715.2-9824.2 8937-7155 6267.9-4485.9	Second derivative	4	0.890	0.301	0.803	0.532	2.31	-0.118
H (%)	9403.8-7498.3 5450.2-4597.7	Constant offset elimination	9	0.531	0.0667	0.856	0.0427	2.65	-0.00524
N (%)	7857-6823.3 5797.3-4246.7	Min-max normalization	8	0.860	0.045	0.973	0.0276	6.6	0.0103
S (%)	9403.8-7340.2 6827.2-5276.6 4763.6-4246.7	Multiplicative scattering correction	8	0.584	0.0107	0.785	0.0076 1	2.19	-0.00139
O (%)	8890.7-8370 6310.3-5793.5	Straight line substation	5	0.532	0.832	0.522	1.110	1.46	-0.158

R_c^2, R_p^2 is coefficient of determination of calibration set and validation set, respectively. RMSEE is root mean square error of estimation. RMSEP is root mean square error of prediction. RPD is standard error of prediction to standard deviation of reference value and Bias is average error of prediction.

The linear regression plot of measured values compared with the predicted value of calibration set and prediction set, regression coefficient plot and X-loading plot are shown in Figure 4.2a, b and c, respectively. Figure 4.2a also shows the target line with its slope equal to 1.00. For the regression coefficient and X-loading plot, if there was a high value at any wavenumber, it indicated that the vibration of a molecular bond at that wavenumber had the main influence on the model prediction. The dependent variable would change positively or negatively as the composition of bamboo related to the bond vibration was changed. This information is important for developing spectrometers for this specific application [9]. For the regression coefficient plot, the important absorbance bands were in the range of 6460 cm^{-1} (1548 nm) to 5793 cm^{-1} (1726 nm). The absorption at 1648–1659 nm corresponded to the bond vibration of $RCH=CH_2$ and $C=CH_2$, at 1678–1695 nm was the vibration of $RCH=CH_2$, HC=CH, and C=CH [31]. The high bands were found at 5994 cm^{-1} (1668), 6137 cm^{-1} (1629 nm), 6391 cm^{-1} (1565 nm), 6569 cm^{-1} (1522 nm). The wave band at 1664 nm related to C-H methyl and OH associated with ($R\text{-}OHCH_3$) alcohols, 1630 nm related to C-H vinyl and vinylidene C-H as ($CH_2=C(CH_3)\text{-}CH=CH_2$) [32]. For X-loading plots had a high band at 6823 cm^{-1} (1466 nm), 5805 cm^{-1} (1723 nm), 6025 cm^{-1} (1660 nm), 5955 cm^{-1} (1679 nm), 6137 cm^{-1} (1629 nm), 6368 cm^{-1} (1570 nm), 6002 cm^{-1} (1666 nm), 6137 cm^{-1} (1629 nm), and 6310 cm^{-1} (1585 nm). The vibration band of 1468 nm related to O-H (2v) (-C-OH) of tertiary alcohols [32], 1725 nm related to C-H stretching first overtone of CH_2 [31], 1660 nm related to C-H stretching first overtone of cis-RCH=CHR [31], 1678 nm related to C-H methyl, carbonyl adjacent as ($.C=OCH_3$) of ketones [32], 1630 nm related to C-H, vinyl and vinylidene (2-methyl-l, 3-butadiene), isoprene as ($CH_2=C(CH_3)\text{-}CH=CH_2$) of vinyl and vinylidene C-H as is isoprene [32], 1570 nm related to N-H stretching first overtone of CONH[31], 1584 nm related to structure of cellulose and hemicellulose [31], 1664 nm related to C-H methyl, OH associated as $ROHCH_3$ of alcohols [32]. Those wave bands corresponded mostly with hydrocarbon bands. As mentioned above, wavenumber ranges of 8373.9–7853.2

(1194–1273 nm) and 6827.2–5793.5 cm^{-1} (1465–1726 nm) were used to develop models, in which there was no band of water (760, 970, 1450, 1940 nm). This might be because LHV was calculated by subtracting the heat of vaporization of water in the biomass. In addition, the obvious bands of CH_2, CH_3, HC=CH influenced the LHV model. Those molecules were in the lignin structure. Demirbaş [34] noticed that lignin highly influenced HHV prediction and that HHV increased with increasing lignin content. This result was similar to Posom et al. [13]. In addition, the bands corresponded with the results of Xue et al. [9], which reported that the bond vibration of C-H stretch first overtone (1765 cm^{-1}), C-H stretch first overtone of CH_2 (1725 cm^{-1}), C-H stretch first overtone of CH_3 (1705 cm^{-1}), and O-H stretch first overtone (1540 cm^{-1}) had a strong influence on the lignin prediction of corn stover.

The linear regression plot (also called scatter plot) of measured value versus predicted value of calibration set and prediction set has been used for showing how accurate the developed model is. The regression coefficient plot and X-loading plot are the plots illustrating the model feature in which the effect of the chemical bond vibration in molecular level on the prediction of constituents could be determined.

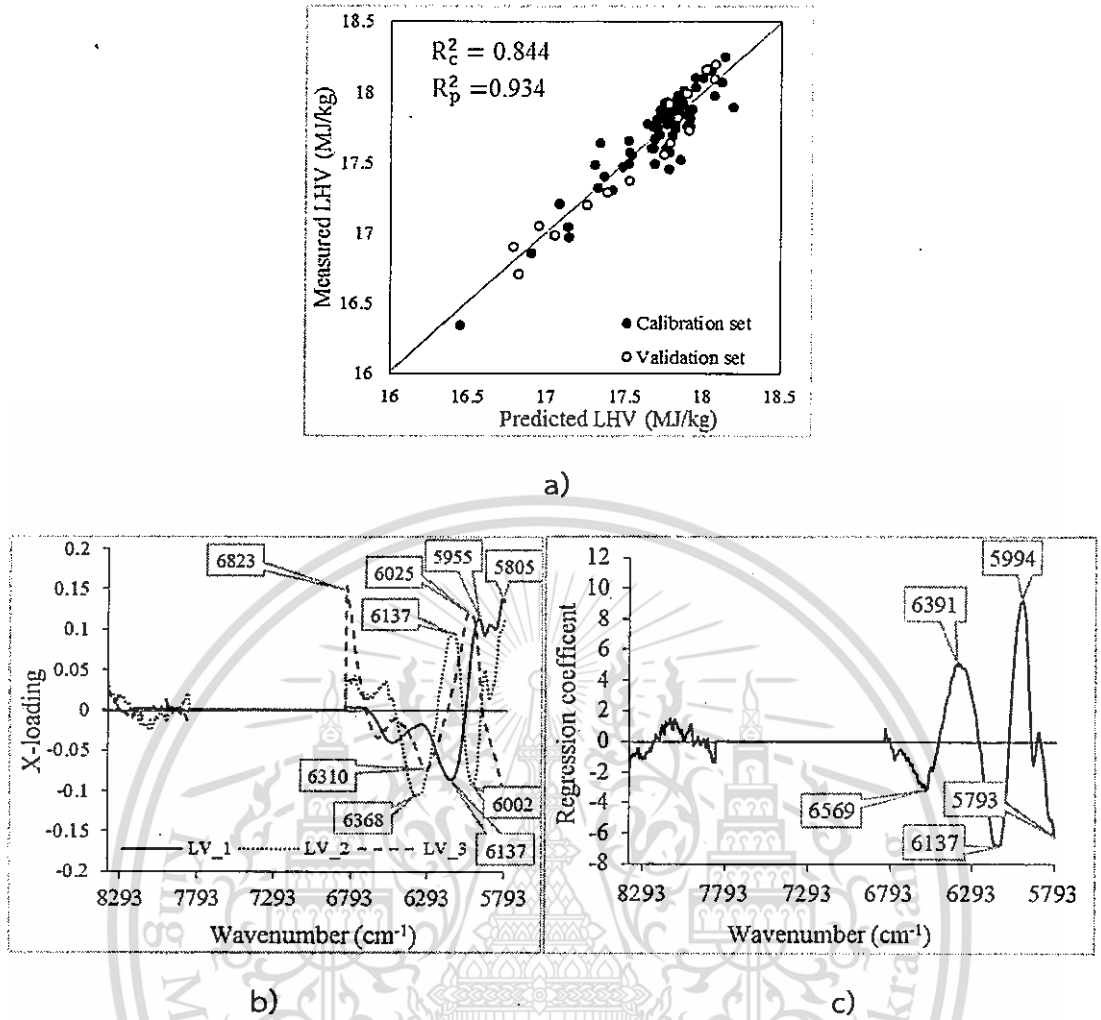

Figure 4.2 a) Linear regression plots of measured value of LHV versus predicted value of calibration set and prediction set, b) Regression coefficient plots and c) X-loading plots. R_c^2, R_p^2 is coefficient of determination of calibration set and validation set, respectively. LV is PLS latent variable.

4.5.4 Prediction models of element composition

Table 4.4 shows the results of partial least squares regression models for determination of LHV, C, H, N, S and O of ground bamboo. The best PLS model for C was optimized using the wavenumber ranges of 12493.3–11602.3, 10715.2–9824.2, 8937–7155, and 6267.9–4485.9 cm^{-1}, the number of latent variables of 4 and a spectral pretreatment method of second derivative. Xu et al. [35] indicated that the second derivative method was used to resolve spectral peak overlap. The model shows R_p^2, RMSEP, RPD and bias of 0.803, 0.532%, 2.31 and–0.118%, respectively. Linear regression plots of measured value versus predicted value of the calibration set and prediction set are displayed in Figure 4.3a, showing 80.3% of variation in the prediction set which

can be explained by the prediction models fitted with the calibration set. According to Williams [24] and Zornoza et al. [30], the C model could be used only for approximate predictions and screening and some other "approximate" calibrations. This result was compared to Gillespie et al. [15], Everard et al. [18] and Fagan et al. [17], who used NIR spectroscopy to evaluate C of biomass using cross validation and the models developed provided R^2 of 0.78 for wood, *Miscanthus* and herbaceous energy grasses pellets, 0.85 for milled *Miscanthus* and two short rotation coppice willow varieties, and 0.88 for *Miscanthus x giganteus* and short rotation coppice willow. They suggested that the accuracy of the models was fair and could be used in a screening application. Our result was rather similar to previous studies even though we used FT-NIR spectrometer for scanning and the model developed here was validated using test set method (calibration set of 64 samples and validation set of 16 samples). The regression coefficient and X-loading plots of C are shown in Figure 4.4a and Figure 4.5a, respectively. The high regression coefficient bands were observed approximately at 12331 cm^{-1} (810 nm) (808 nm corresponded to 2 × N-H stretching+2 × N-H deformation+2 × C-N stretching) [31], 5273 cm^{-1} (1896 nm) (1900 nm corresponded to O-H stretching + 2 × C-O stretching of starch) [31], and X-loading peaks were observed approximately at 5331 cm^{-1} (1876 nm), 5238 cm^{-1} (1909 nm) (1908 nm corresponded to OH stretching first overtone) [31], 5253 cm^{-1} (1903 nm) (1900 nm corresponded to O-H stretching + 2 × C-O stretching of starch) [31].

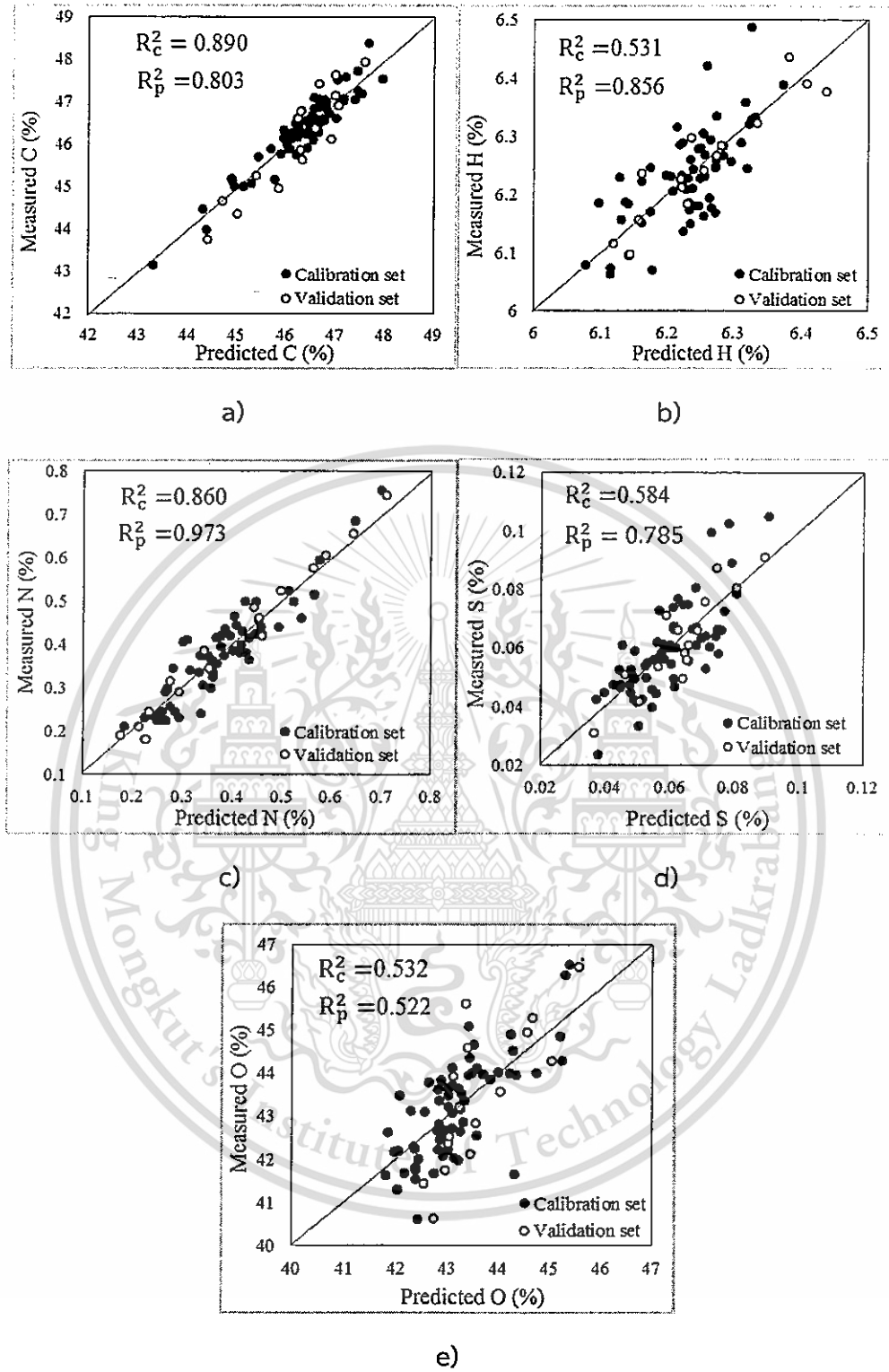

Figure 4.3 Linear regression plots of measured value versus predicted value of calibration set and prediction set; a) C, b) H, c) N, d) S, and e) O. R_c^2, R_p^2 is coefficient of determination of calibration set and validation set, respectively.

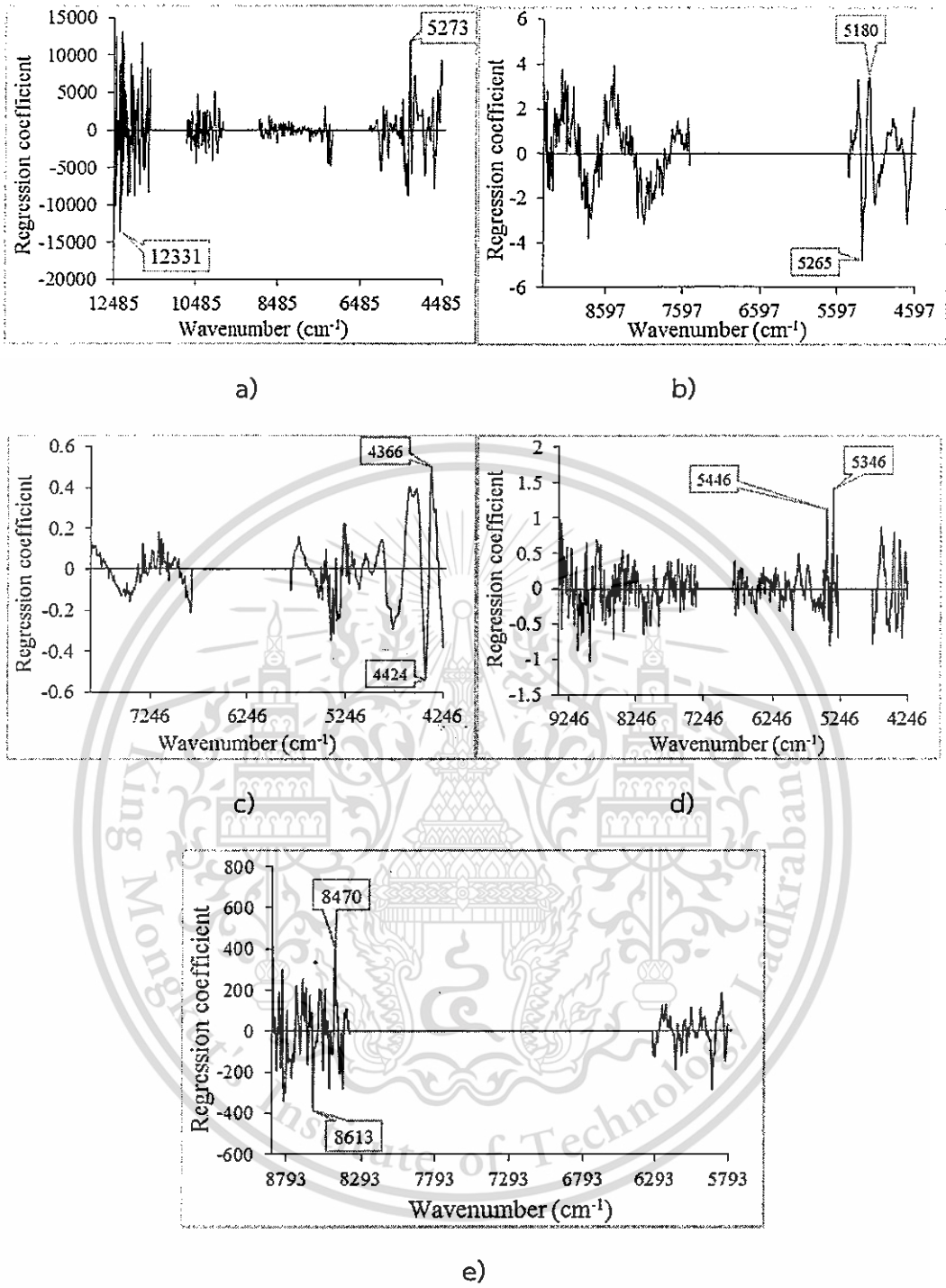

Figure 4.4 Regression coefficient of PLS prediction model for a) C, b) H, c) N, d) S and e) O

The best PLS model for H prediction was optimized using the wavenumber ranges of 9403.8–7498.3 and 5450.2–4597.7 cm^{-1}, with a latent variable number of 9, and spectral pretreatment method of constant offset elimination. Constant offset elimination and straight line substation were used to resolve spectra baseline drift [35]. The R_p^2, RMSEP, RPD and bias were 0.856, 0.0427%, 2.65 and –0.00524%, respectively.

Linear regression plots of measured value versus predicted value of calibration set and validation set are displayed in Figure 4.3b, and show explained variance of 85.6% meaning that unexplained variance was 14.4%. According to Williams [24] and Zornoza et al. [30], the H model was a good prediction model, which could be used with caution for most applications. Figure 4.4b shows the regression coefficient plot. The high peaks were observed at approximately 5265 cm^{-1} (1899 nm) (1900 nm corresponded to O-H stretching + 2 × C-O stretching of starch) [31], 5180 cm^{-1} (1930 nm) (1930 nm corresponded to O-H stretching and HOH bending combination of polysaccharides) [32]. X-loading plots are shown in Figure 4.5b, the high peaks were observed at approximately 5215 cm^{-1} (1918 nm), 5230 cm^{-1} (1912 nm) (1908 nm corresponded to O-H stretching first overtone), 4779 cm^{-1} (2093 nm) (2090 nm O-H combination) [32].

The optimum PLS models for N prediction were optimized using the wavenumber ranges of 7857–6823.3 and 5797.3–4246.7 cm^{-1}, the latent variable number of 8, and spectral pretreatment of min-max normalization. Min-max normalization was used to compensate for baseline shift and multiplicative effects [28]. The model provided R_p^2, RMSEP, RPD and bias of 0.973, 0.0276%, 6.6, and 0.0103%, respectively. Linear regression plots of measured value versus predicted value of calibration set and validation set are displayed in Figure 4.3c, proving that the model was robust. According to Williams [24] and Zornoza et al. [30], the N content model is an excellent prediction model and could be used with any application. The regression coefficient and X-loading plots are shown in Figure 4.4c and Figure 4.5c, respectively. For regression coefficient, the high peaks were observed at approximately 4424 cm^{-1} (2260 nm), 4366 cm^{-1} (2290 nm) (2294 nm N-H stretching + C=O stretching of amino acid) [32]. In X-loading plots, the important peaks were at 5107 cm^{-1} (1958 nm) (1960 nm N-H asym. stretching amide II) [32], 5180 cm^{-1} (1930 nm) (1930 nm O-H stretching and HOH bending combination of polysaccharides) [32], 6920 cm^{-1} (1445 nm) (1445 nm N-H primary aromatic amine) [32].

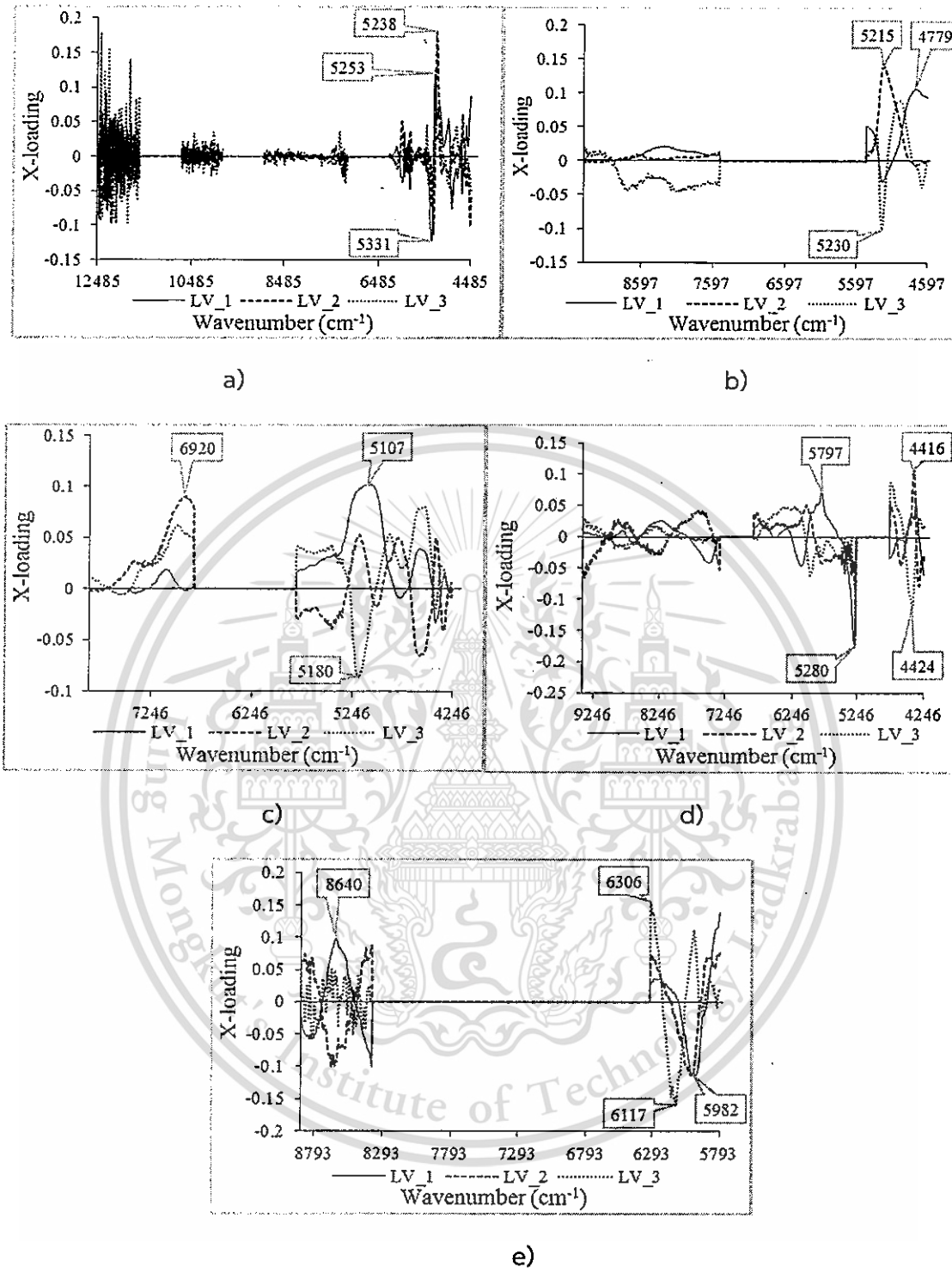

Figure 4.5 X-loading plots of PLS prediction models for a) carbon content, b) hydrogen content, c) nitrogen content, d) sulfur content and e) oxygen content

The PLS model for S prediction was optimized using the wavenumber ranges of 9403.8–7340.2, 6827.2–5276.6, and 4763.6–4246.7 cm^{-1}, a latent variable number of

8, spectral pretreatment method of multiplicative scattering correction. Nicolaï et al. [28] indicated that multiplicative scattering correction was used to compensate for multiplicative effects that were the physical effects. The model showed R_p^2, RMSEP, RPD and bias of 0.785, 0.00761%, 2.19, and −0.00139%, respectively. According to Williams [24] and Zornoza et al. [30], the S model only permitted approximate predictions which could be used for rough screening. Linear regression plots of measured value versus predicted value of calibration set and prediction set, regression coefficient and X-loading plots are shown in Figure 4.3d, Figure 4.4d and Figure 4.5d, respectively. For regression coefficient, the high peaks were observed at approximately 5346 cm^{-1} (1870 nm), 5446 cm^{-1} (1836 nm). The wavenumber of 5280 cm^{-1} (1894 nm) (1892 nm O-H bending bonding between water and exposed polyvinyl alcohol OH) [32], 4424 cm^{-1} (2260 nm), 4416 cm^{-1} (2265 nm), 5797 cm^{-1} (1725 nm) (1725 nm C-H stretching first overtone) [31] were the peaks of X-loading plots.

The best PLS model for O prediction was optimized using the wavenumber ranges of 8890.7–8370 and 6310.3–5793.5 cm^{-1}, the latent variable number of 5, and spectral pretreatment method of straight line substation. The model showed the R_p^2, RMSEP, RPD and bias of 0.522, 1.110%, 1.46, and −0.158%, respectively. According to Williams [24] and Zornoza et al. [30], the O model was poorly predicted and was not recommended for use. The regression plots of measured value versus predicted value of calibration set and prediction set, regression coefficient plot and X-loading plots are shown in Figure 4.3e, Figure 4.4e and Figure 4.5e, respectively. The important peaks were observed at approximately 8470 cm^{-1} (1180 nm), 8613 cm^{-1} (1161 nm) (1160 nm C=O (carbonyl > C=O)) [32] for regression coefficient and 6117 cm^{-1} (1635 nm) (C-H vinyl C-H, associated with (CH_2=CH-)) [32], 5982 cm^{-1} (1672 nm) (C-H aromatic C-H (aryl)) [32], 6306 cm^{-1} (1586 nm) (1583 nm O-H stretching band of alcohol or water O-H) [32] for X-loading plots.

4.5.5 Comparison of the results with other works

In general, there have been no reports on LHV prediction. There were only reports on HHV. The models in this study were not as accurate as the HHV predictions of straw [36], wood, *Miscanthus* and herbaceous energy grasses pellets [15], *Miscanthus x giganteus* and short rotation coppice willow [17], which demonstrated R^2

of 0.96, 0.94, and 0.99, respectively. The results of carbon models in this study had the same accuracy with wood, *Miscanthus* and herbaceous energy grasses [15], and *Miscanthus x giganteus* (R^2 of 0.78) and short rotation coppice willow (R^2 of 0.88) [17], where models were constructed using cross validation. The recommendations were fair and could be used for screening applications. In addition, the models were as accurate as straw models [36]. Their validation results gave R^2 of 0.97, 0.77 and 0.87 for C, H, and N, respectively. They concluded that prediction of C, H, N of straw samples using NIR spectroscopy gave satisfactory accuracy. These models were believed to be reliable for quantitative analysis. For O evaluation of biomass, there have been no reports of using NIR spectroscopy as an evaluation technique. Another method was investigated by Nhuchhen [37], where the predicted C, H, and O compositions of torrefied biomass were evaluated by proximate analysis, providing R^2 of 0.83, 0.70, and 0.84, respectively.

4.6 Conclusion

Models for prediction of LHV and the element composition of bamboo were developed using FT-NIR spectroscopy. The ground samples were scanned using the diffuse reflection mode. The most important finding of this study was the performance of the PLS models for evaluation of LHV and element composition by FT-NIR using test set validation. Moreover, the LHV model was not influenced by the band vibration of water. The models for prediction of LHV and N content were excellent and suitable for use in most applications. The C model could be used only for approximate prediction. The H model was a good predictive model and could be used with caution for most applications. The S model was only permitted for approximate predictions that could be used for rough screening. The O model was poor and was not recommended for use. These results could be a guide for future applications, such as for trading and operational control of energy conversion systems. The narrow statistical range of element composition might lead to fair performance. Therefore, the calibration model that was obtained from various biomass sources as a global model could provide better performance and more robustness due to a wider range of reference values.

4.7 References

[1] Sritong C, Kunavongkrit A, Piumsombun C. "Bamboo: An Innovative Alternative Raw Material for Biomass Power Plants." Int. **J of Innovation, Manage Technol**, vol. 3(6), 2012. Pp. 759-762.

[2] Scurlock J.M.O, Dayton D.C, Hames B. "Bamboo: an overlooked biomass resource?." **Biomass Bioenergy**, vol. 19, 2000. Pp. 229-244.

[3] Ye L, Zhang J, Zhao J, Luo Z, Tu S, Yin Y. "Properties of biochar obtained from pyrolysis of bamboo shoot shell." **J Anal Appl Pyrolysis**, vol.114, 2015. Pp. 172–178.

[4] Liu Z, Jiang Z, Cai Z, Fei B, Yu Y, Liu X. "The manufacturing process of bamboo pellets." Proceedings of the 55th International Convention of Society of Wood Sci Technol 2012 August 27-31, Beijing, CHINA. 1-14.

[5] Jiang Z, Liu Z, Fei B, Cai Z, Yu Y, Liu X. "The pyrolysis characteristics of moso bamboo." **J Anal Appl Pyrolysis**, vol.94, 2012. Pp. 48–52.

[6] Cheng L, Adhikari S, Wang Z, Ding Y. "Characterization of bamboo species at different ages and bio-oil production." **J Anal Appl Pyrolysis**, vol.116, 2015. Pp. 215–222.

[7] Darabant A, Haruthaithanasan M, Atkla W, Phudphong T, Thanavat E, Haruthaithanasan K. "Bamboo biomass yield and feedstock characteristics of energy plantations in Thailand." **Energy Procedia**, vol.59, 2014. Pp. 134 – 141.

[8] Chen D, Liu D, Zhang H, Chen Y, Li Q. "Bamboo pyrolysis using TG–FTIR and a lab-scale reactor: Analysis of pyrolysis behavior, product properties, and carbon and energy yields." **Fuel**, vol.148, 2015. Pp. 79–86.

[9] Xue J, Yang Z, Han L, Liu Y, Liu Y, Zhou CC. "On-line measurement of proximates and lignocellulose components of corn stover using NIRS." **Appl Energy**, vol.137, 2015. Pp. 18-25.

[10] Cooper C.D, Kim B, MacDonald J. "Estimating the Lower Heating Values of Hazardous and Solid Wastes. **J Air Waste Manage. Assoc**, vol.49, 1999.

[11] Basu P. "Biomass gasification and pyrolysis: practical design and theory." Academic press is an imprint of Elsevier, USA. Pp.23:2010.

[12] Runge TM., Zhang C, Mueller J, Wipperfurth P. "Economic and Environmental Impact of Biomass Types for Bioenergy Power Plants." Environmental and

economic research and development program. 2013. URL: https://www.focusonenergy.com/sites/default/files/research/1010RungeFinalReportx.pdf.

[13] Posom J, Shrestha A, Saechua W, Sirisomboon P. "Rapid non-destructive evaluation of moisture content and higher heating value of Leucaena leucocephala pellets using near infrared spectroscopy." **Energy**, vol. 107, 2016. Pp. 464–472.

[14] Posom J, Sirisomboon P. "Evaluation of the moisture content of Jatropha curcas kernels and the heating value of the oil extracted residue using near-infrared spectroscopy." **Biosystem Eng**, vol.130, 2015. Pp. 52-59.

[15] Gillespie G.D, Everard C.D, McDonnell K.P. "Prediction of biomass pellet quality indices using near infrared spectroscopy." **Energy**, vol.80, 2015. Pp. 582-588.

[16] Everard C.D, McDonnell K.P, Fagan C.C. "Prediction of biomass gross calorific values using visible and near infrared spectroscopy." **Biomass Bioenergy**, vol.45, 2012. Pp. 203-211.

[17] Fagan C.C, Everard C.D, McDonnell K. "Prediction of moisture, calorific value, ash and carbon content of two dedicated bioenergy crops using near-infrared spectroscopy." **Bioresour Technol**, vol.102, 2011. Pp. 5200–5206.

[18] Everard CD, Fagan CC, McDonnell K. "Visible-near infrared spectral sensing coupled with chemometric analysis as a method for on-line prediction of milled biomass composition pre-pelletising." **J Near Infrared Spectrosc**, vol.20, 2012. Pp.361-9.

[19] Zhang Y, Li M.Z, Zheng L.H, Zhao Y, Pei X. "Soil nitrogen content forecasting based on real-time NIR spectroscopy." **Comput Electron Agric**, vol.124, 2016. Pp. 29–36.

[20] Andŕes J.M, Bona M.T. "ASTM clustering for improving coal analysis by near-infrared spectroscopy." Talanta, vol.70, 2006. Pp.711–719.

[21] Bona M.T, Andŕes J.M. "Coal analysis by diffuse reflectance near-infrared spectroscopy: Hierarchical cluster and linear discriminant analysis." **Talanta**, vol.72, 2007. Pp. 1423–1431.

[22] Bona M.T, Andŕes J.M. "Reflection and transmission mid-infrared spectroscopy for rapid determination of coal properties by multivariate analysis." **Talanta**, vol.74, 2008. Pp. 998–1007.

[23] Chadwick D.T, McDonnell K.P, Brennan L.P, Fagan C.C, Everard C.D. "Evaluation of infrared techniques for the assessment of biomass and biofuel quality parameters and conversion technology processes: A review." **Renewable Sustainable Energy Rev**, vol.30, 2014. Pp. 672–681.

[24] Williams P. "Near-infrared technology-Getting the best out of light." Nanaimo, British Columbia, and Winnipeg, Manitoba, Canada: PDK Grain; 2007.

[25] García R, Pizarro C, Lavín AG, Bueno JL. "Biomass proximate analysis using thermogravimetry." **Bioresour Technol**, vol.139, 2013. Pp. 1–4.

[26] Komilis D, Kissas K, Symeonidis A. "Effect of organic matter and moisture on the calorific value of solid wastes: An update of the Tanner diagram." **Waste Manage**, vol.34, 2014. Pp. 249–255.

[27] Dardenne P. "Some considerations about NIR spectroscopy: Closing speech at NIR-2009." **NIR news**, vol.21, 2010. Pp. 8–14.

[28] Nicolaï B.M, Beullens K, Bobelyn E, Peirs A, Saeys W, Theron K.I, Lammertyn J. "Nondestructive measurement of fruit and vegetable quality by means of NIR spectroscopy: A review." **Postharvest Biol Tec**, vol.46, 2007. Pp.99–118.

[29] Xie C, Xu N, Shao Y, He Y. "Using FT-NIR spectroscopy technique to determine arginine content in fermented Cordyceps sinensis mycelium." **Spectrochim Acta, Part A**, vol.149, 2015. Pp. 971–977.

[30] Zornoza R, Guerrero C, Mataix-Solera J, Scow K.M, Arcenegui V, Mataix-Beneyto J. "Near infrared spectroscopy for determination of various physical, chemical and biochemical properties in Mediterranean soils." **Soil Biol Biochem**, vol.40(7): 2008. Pp. 1923–1930.

[31] Osborne BG, Fearn T. "Near infrared spectroscopy in food analysis." Theory of near infrared spectroscopy, USA, 133. New York: Longman Scientific & Technical; 1986. Pp. 36-40.

[32] Workman J, Weyer J.R.L. "Practical Guide to Interpretive Near-Infrared Spectroscopy." Taylor & Francis, Boca Raton, FL, p. 240–262;2007.

[33] Yang Z, Li K, Zhang M, Xin D, Zhang J. "Rapid determination of chemical composition and classification of bamboo fractions using visible–near infrared spectroscopy coupled with multivariate data analysis." **Biotechnol Biofuels**, 2016. Pp. 9-35.

[34] Demirbaş A. "Relationships between lignin contents and heating values of Biomass. **Energy Convers Manage**, vol.42, 2001. Pp. 183-188.

[35] Xu F, Zhou L, Zhang K, Yu J, Wang D. "Rapid determination of both structural polysaccharides and soluble sugars in sorghum biomass using near-infrared spectroscopy." **Bioenerg Res**, vol.8, 2015. Pp. 130–136.

[36] Huang C, Han L, Yang Z, Liu X. "Ultimate analysis and heating value prediction of straw by near infrared spectroscopy." Waste Manage 2009; ;, vol.29:1793–1797.

[37] Nhuchhen D.R. "Prediction of carbon, hydrogen, and oxygen compositions of raw and torrefied biomass using proximate analysis." **Fuel**, vol.180, 2016. Pp. 348–356.

Chapter 5

Near infrared spectroscopy as an alternative method to thermogravimetric analysis for evaluation of volatile matter and pyrolysis characteristics of bamboo wood chips

5.1 Abstract

The main objective of this study was to evaluate the pyrolysis characteristic (i.e. T_{peak}, T_{offset}, DTG_{peak}) and volatile matter (VM) of bamboo chips using near infrared spectroscopy as an alternative to thermogravimetric analysis. The bamboo samples (n=84) were obtained from different sizes of trunks. The models were optimized using partial least squares regression (PLRS) with 80% of samples for calibration set and 20% for validation set. The T_{peak}, T_{offset} and DTG_{peak} models provided R^2 of 0.891, 0.928, and 0.771; RMSEP of 3.59 °C, 3.21 °C, and 0.382%w/min; RPD of 3.21, 3.83, and 2.09; and bias of 1.2 °C, 0.749 °C, and -0.000581 %w/min, respectively. The VM gave in range of 68.68-61.02% on as-received and 75.60-68.96% on dry basis. The VM model on as-received provided R^2 of 0.874, RMSEP of 0.768%, RPD of 2.82, and bias of -0.0454%, while VM model on dry basis gave R^2 of 0.889, RMSEP of 0.665%, RPD of 3.00, and bias of 0.000433%. This indicated high possibility in applying NIR spectroscopy for prediction of pyrolysis characteristic and VM. This result will benefit for setting a price of biomass and could be used for planning and control in fast pyrolysis and gasification process.

* This chapter constituted the oral presentation article: Posom J, Sirisomboon P, Funke A, Heinrich J, Maier J and Griesheimer P. "Feasibility of evaluation of pyrolysis characteristic of bamboo chips using of near infrared spectroscopy." Asian NIR Symposium 2016 in Kagoshima, Japan, the Shiroyama hotel during 30 November to 3 December 2016.

Posom J, Sirisomboon P, Funke A, Heinrich J, Maier J and Griesheimer P. "Near infrared spectroscopy as an alternative method to thermogravimetric analysis for evaluation of volatile matter of bamboo wood chips." The 9th TSAE International conference: TSAE 2016, the Impact exhibition center, Bangkok, Thailand during 8-10 September 2016.

5.2 Introduction

Bamboo "*Dendrocalamus siriceus* cl. Phamon" which are planted everywhere in Thailand. It can be used as source of renewable energy. Pyrolysis characteristics included T_{peak}, T_{offset}, DTG_{peak} (Figure 5.2). Their parameters can be used to design and control pyrolysis system. T_{peak} is temperature as a highest degradation and presents the maximum of production rate. T_{offset} is the temperature of the end decomposition rate, it can be used to indicate which temperature should be stopped to heat. DTG_{peak} or (differential thermogravimetric) is the maximum of decomposition rate which can be used to manage feedstock. The previous study has only reported biomass composition [1,2] but there has no report on biomass degradation behavior determination using NIR spectroscopy. Meanwhile, VM of biomass is also considered to be an important parameter for evaluation of the amount of liquid fuel and gas fuel produced by fast pyrolysis and gasification. It is the specific characteristic of biomass feedstock to indicate whether it is suitable for fast pyrolysis process or gasification. In addition, VM can be also determined using thermogravimetric analysis (TGA). The results of the standard methods and TGA proximate analyses were in good agreement [3]. García et al. [4] determined proximate data of biomass using standard method and TGA, they found that the error criteria results were satisfactory with the average experimental error (AEE) under 6% for moisture content and VM, and close to 10% for fixed carbon. However, TGA are complicated that take a long time, destroyed sample and required special technician skills. In the future, VM in biomass can be used for setting a price of biomass instead of weight. Therefore, rapid method is needed.

5.3 Objective

The main objective of this study was to evaluate pyrolysis characteristic and VM of bamboo chips using near infrared spectroscopy as an alternative to thermogravimetric analysis. The interesting point for this work is that no previous work has been studied on bamboo chips. The model was developed from 84 samples of bamboo chips obtained from small to big size of circumferences.

5.4 Materials and methods

5.4.1 Sample

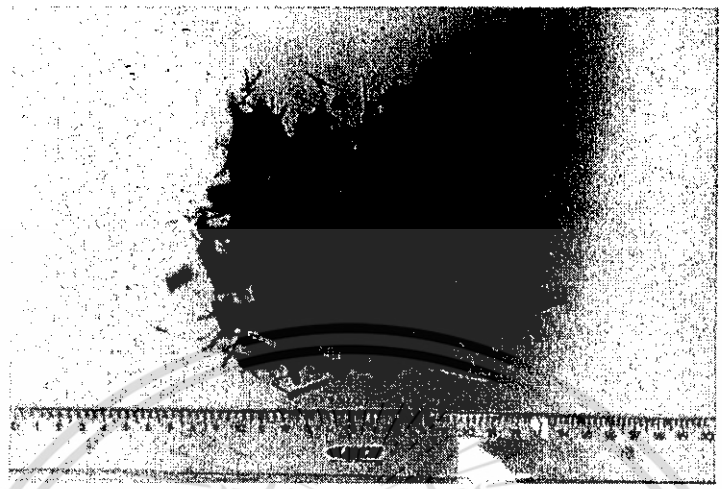

Figure 5.1 Bamboo chips

The total sample were 84 samples, obtained from Uttaradit province, Thailand. All samples were cut at 10 cm above the ground for 1 m length. Then were suddenly chopped by chopping machine (P5508, Patipong, Thailand) and dried under the sun until the moisture reached approximately 10%wb. Each sample was kept into aluminum bag at room temperature of 25±2 °C. Dried bamboo chips are shown in Figure 5.1.

5.4.2 NIR scanning

FT-NIR spectrometer (MPA, Bruker, Germany) in the wavenumber range of 12500 - 3600 cm^{-1} in diffuse reflectance mode at resolution of 16 cm^{-1} was used for scanning of bamboo chips at room temperature of 25±2 °C. The absorption was recorded in log1/R unit.

5.4.3 Moisture content of bamboo chips

After scanning, moisture content (MC) of each dried bamboo chips were measured according to standard method (ASTM E1756-08). About 5 g was seperated from scanned sample and was put in glass cans (18-cm diameter and 4 cm height) for measuring with a hot air oven (FDL 115, BINDER, Germany) at 105 °C for 24 h, The samples were re-heated at 6 h interval until the sample weights remained constant. Weighing was completed using a digital balance (METTLER AT261, Switzerland,

resolution of 0.0001 g). The moisture content (% wet basis) was calculated using Equation (1):

$$MC\ (\%wb) = \left[\frac{m_i - m_f}{m_i}\right] \times 100 \qquad (5.1)$$

where MC is moisture content in % wb, m is mass in g, and the subscripts i and f are initial and final, respectively. There were 3 replicates per sample.

5.4.4 pyrolysis characteristics and VM of milled bamboo

The remained bamboo chips were milled with a 6800-230 SPEX CertiPrep Freezer Mill (Methucen, SPEX CertiPrep Inc, USA). The milled samples were made balancing moisture humidity surrounding by kept in an opened cup and stored at room temperature for 2 days. After that, pyrolysis characteristic and VM were carried out with a thermogravimetric analyzer (STA 409, Netzsch Co., Ltd, Germany) using a flow rate of 15 ml min^{-1} of N_2, 55 ml min^{-1} of N_2 (protective gas), zero O_2 environment. Approximately 200 g of milled sample were heated range from 20-105°C with heating rate 5°C min^{-1}, and kept at 105°C for 30 min to determine moisture content, and then heated from 105-700°C with heating rate 10°C min^{-1}, and kept at 700°C for 1 hr to make completely pyrolysis. Each sample was subjected to the experiment 1 time, however there were 6 samples were randomly taken for duplicates to determine repeatability. After that, weight loss and temperature change and time were recorded (TG chart) as seen in Figure 5.2.

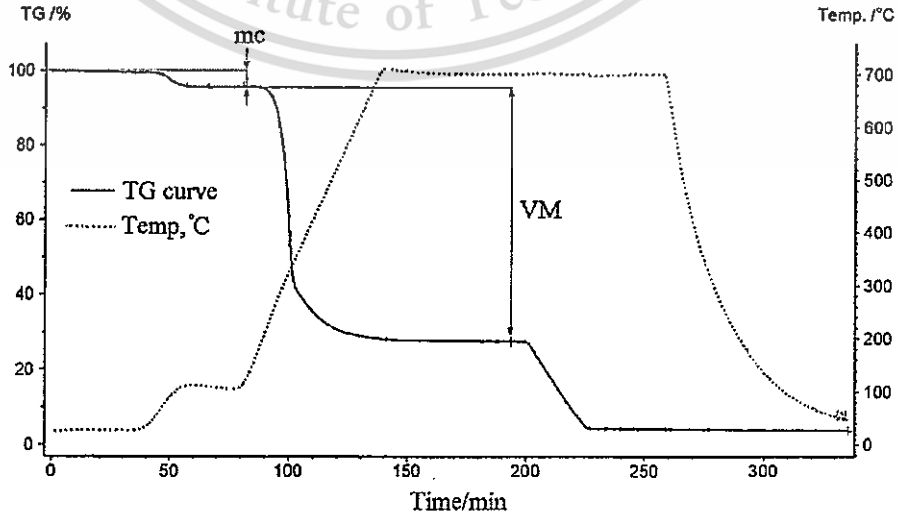

Figure 5.2 Thermogravimetric (TG) curve of bamboo

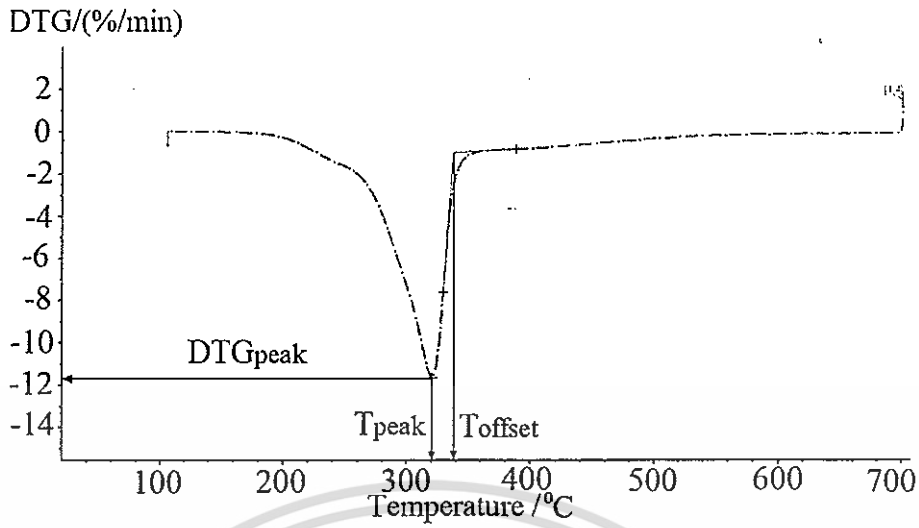

Figure 5.3 Pyrolysis characteristics of bamboo (DTG curve)

To determine the pyrolysis characteristic (T_{peak}, T_{offset}, DTG_{peak}), TG's chart was differentiated to be DTG's chart as seen in Figure 5.3. Moisture content (mc) and VM were obtained by direct measure of weight changes which their value was read on TG profile (Figure 5.2). VM on as-received can be calculated as:

$$VM_{as} = VM \times \frac{(100-MC)}{(100-mc)}, \quad (5.2)$$

while volatile matter on dry basis were calculated as:

$$VM_{dry} = VM \times \frac{100}{(100-mc)}, \quad (5.3)$$

where MC is moisture content obtained from dry oven (ASTM standard), mc and VM is moisture content and volatile matter obtained from TG profile.

After the reference data were obtained, the outliers were determined using Eq. (5.4).

$$\frac{(X_i-\overline{X})}{SD} \leq 3 \quad (5.4)$$

Where X_i, $\overline{X}$ and SD are the reference value of sample i, mean of reference values, and standard deviation of reference values, respectively. If the equation was not satisfied, the sample was the outlier and was removed.

5.4.4 Development and analysis of NIR models

NIR models were optimized using partial least squares regression by OPUS 7.0 (Bruker, Germany). Total data were divided into 80% of samples for calibration set and 20% for validation set by random sampling. Then the spectral were pre-treated using no pre-treatment, constant offset elimination, straight line subtraction, vector

normalization (SNV), min-max normalization, multiplicative scatter correction (MSC), first derivatives, second derivatives, first derivatives + straight line subtraction, first derivatives + SNV and first derivatives + MSC. After models were developed, the models were validated by validation set.

5.5 Results and discussions

5.5.1 Reference parameter

Repeatability (Rep), mean of the different of duplicate and R^2_{max} of pyrolysis characteristic and VM are shown in Table 5.1. Rep is the standard deviation between duplicate, it is the precision of laboratory. R^2_{max} of T_{peak} and T_{offset} were highest and lowest with DTG_{peak}. R^2_{max} is defined as the maximum of coefficient of determination when there was no spectra error. It is calculated as: $\frac{SD^2-Rep^2}{SD^2}$, where SD is standard deviation of reference data, Rep is repeatability of measured value. If the R^2_{max} is low, means that either range of measured value is narrow or there are more errors during duplication. It can be seen that pyrolysis characteristic and VM gave high R^2_{max}, were more than 0.950, then NIR model of those should be developed. The statistical data for pyrolysis characteristic and VM i.e. minimum (Min), maximum (Max), mean, range, standard deviation (SD) and number of sample for developed models are shown in Table 5.2.

Table 5.1 Repeatability, mean of the different of duplicate and R^2_{max} of pyrolysis characteristic and VM

Parameter	Mean of the different of duplicate	Repeatability	Maximum R^2 (R^2_{max})
T_{peak}	8.894	0.572	0.995
T_{offset}	9.791	0.633	0.995
DTG_{peak}	0.428	0.0875	0.958
VM on as-received	0.967	0.114	0.986
VM on dry basis	0.649	0.127	0.961

Table 5.2 Statistics of pyrolysis characteristics and VM of bamboo chips used in model development

Items	T_{peak}		T_{offset}		DTG_{peak}		VM (% mass on as-received)		VM (% mass on dry basis)	
	Cal	Val	Cal	Val	Cal	Val	Cal	Val	Cal	Val
Average	334.44	337.58	353.68	357.03	-11.20	-11.25	64.47	64.54	71.49	72.09
SD	10.13	11.23	11.13	12.35	0.65	0.824	1.59	2.24	1.52	2.06
Min	320.70	320.80	337.5	338.40	-13.01	-12.65	61.02	61.11	68.96	69.00
Max	357.20	356.4	377.8	377.50	-9.95	-9.99	68.68	68.25	75.60	75.39
Range	36.5	35.8	40.3	39.1	3.06	2.66	7.66	7.14	6.63	6.39
Number of samples	66	16	66	16	66	16	66	16	66	16

Cal is calibration set, Val is validation set.

Table 5.3 PLS calibration results for predicting pyrolysis characteristics and VM of bamboo chips

Parameters		T_{peak} °C	T_{offset} °C	DTG_{peak} (%/min)	VM (% mass on as-received)	VM (% mass on dry basis)
Wavelength region (cm^{-1})		6102-4242.9	7506-4597.7	11602.3-9820.3 8933.2-8038.3	8454.9- 7498.3 6102- 5770.3 4605.4- 4242.9	7506-5446.3
Pretreatments		Second derivative	First derivative	First derivative	Straight line subtraction	Vector normalization
F		8	6	3	8	9
Calibration	R^2	0.893	0.825	0.630	0.732	0.700
	RMSEE	3.54	4.88	0.404	0.875	0.897
Validation	R^2	0.891	0.928	0.771	0.874	0.889
	RMSEP	3.59	3.21	0.382	0.768	0.665
	Bias	1.2	0.749	-0.000581	-0.0454	0.000433
	RPD	3.21	3.83	2.09	2.82	3

F: The number of factors; R^2: the coefficient of determination; RMSEE: root mean square error of estimate, RMSEP: root mean square error of prediction; Bias: the average of differences between reference value and NIR value; RPD: the ratio of standard deviation of reference data in the validation set to SEP.

5.5.2 Spectra

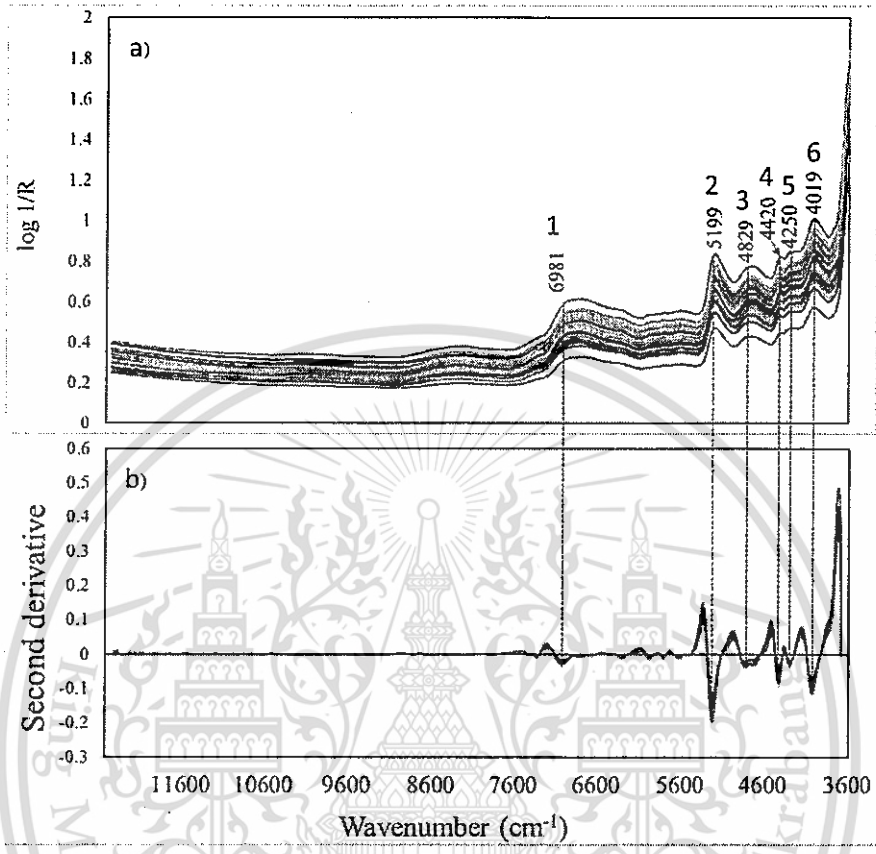

Figure 5.4 a) bamboo spectra, b) second derivative spectra

Table 5.4 Vibration bands of important peaks at any wavenumber appeared on raw spectra and its second derivative of bamboo chips

Point	Appeared wavenumber		Cited wavelength		
	cm^{-1}	nm	nm	Vibration band[a]	Structure
1	6981	1432	1431[8]	-	cellulose
2	5199	1923	1916[6]	OH str + OH def	water
3	4829	2071	2080[6]	OH str + CH def	Cellulose
4	4420	2262	2266[7]	OH, CO combination	Cellulose
5	4250	2353	2352[8]	CH def. second overtone	Cellulose
6	4019	2488	2488[8]	CH str + CC str	starch

[a] *def* deformation, *str* stretching

The NIR spectra of bamboo chips and its second derivative were presented in Figure 5.4a and 5.4b, respectively. The raw spectra had overlapped peaks. To solve the complexity of overlapped peaks and baseline shift were done by second derivative. As seen in Figure 5.4b, the obvious peaks were appeared and were shown the vibration bands in Table 5.4. The obvious peaks were water, cellulose, lignin and starch band. The major components of the plant cell wall are hemicellulose, cellulose, and lignin [9]. Cellulose is a linear polysaccharide polymer. It is the primary component of biological cell walls. Starch also is a major source of energy for plant cells.

5.5.3 Prediction of T_{peak}

The result of PLS models are shown in Table 5.3. For T_{peak}, the PLS model was performed with wavenumber in the range of 6102-4242.9 cm^{-1}; second derivative; and PLS factor number of 8. The R^2, RMSEP, bias and RPD were 0.891, 3.59°C, 1.2°C and 3.21, respectively. Scatter plots of measured and predicted value of calibration and validation set of T_{peak} illustrated in Figure 5.7a. Zornoza et al. [10] and Fagan et al. [11] suggested that R^2 and RPD has excellent predictions if R^2>0.90 and RPD>3. Williams [12] recommended a guideline that the model could be used with caution for most application if provide with R^2 between 0.83-0.90. Bias (1.2°C) was small compared to the mean of reference value (337.58°C). The ration of bias to its mean value was (1.2/337.58°C) 0.355%.

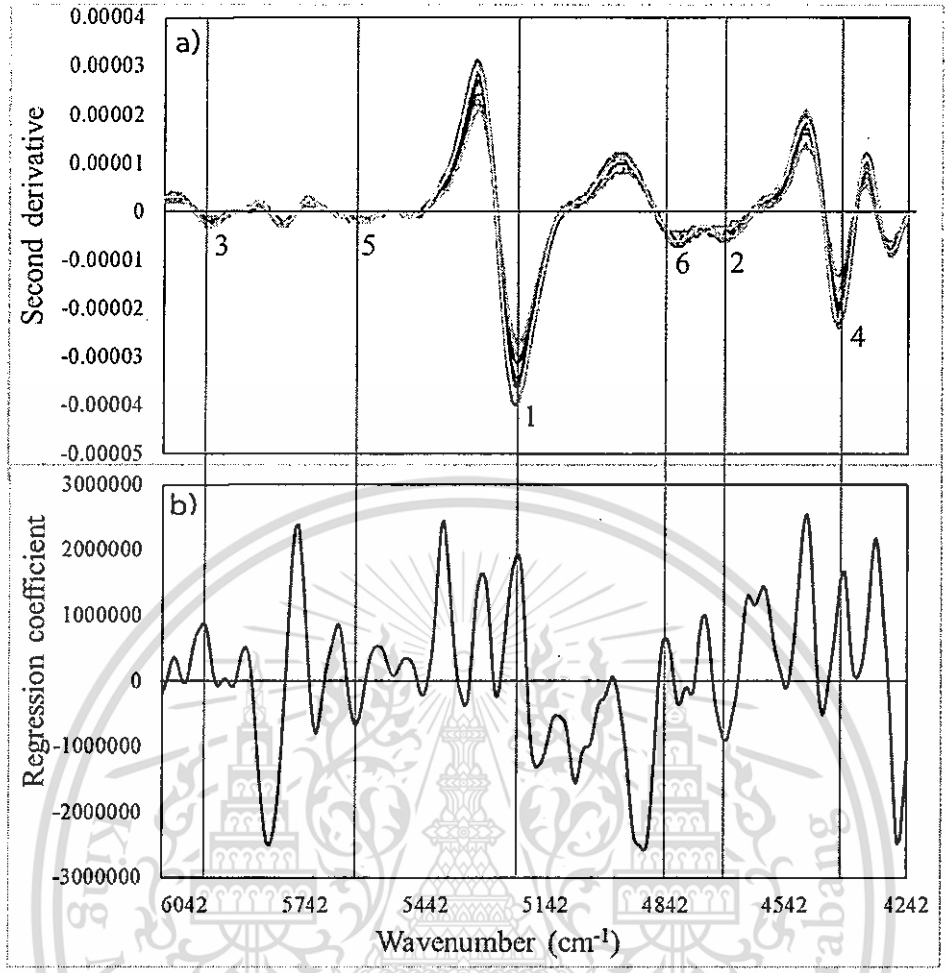

Figure 5.5 a) Second derivative spectra, b) PLS regression coefficient of T_{peak}

Figure 5.5 illustrates the second derivative spectra (a) and its corresponding peaks in regression coefficient plot (b) of the optimum model for predicting the T_{peak} of bamboo chips. The vibration bands appeared in second derivative spectra and PLS regression coefficient reported in Table 5.5. There were bands of water (peak 1) and cellulose (peak 4 and 5) appeared on the second derivative plots.

Table 5.5 Vibration bands of important peaks at any wavenumber appeared on second-derivative spectra and regression coefficient plot of bamboo chips for T_{peak} model

Peak	Appeared wavenumber		Cited wavelength (nm)	Vibration band[a]	Structure
	cm^{-1}	nm			
1	5214	1918	1916 [13]	OH str + OH def	Water
2	4698	2128	-	-	-
3	6001	1666	-	-	-
4	4397	2274	2273 [8]	-	Cellulose
5	5616	1780	1780[8]	C- H stretching first overtone	Cellulose
6	4836	2068	-	-	-

[a] *def* deformation, *str* stretching

5.5.4 Prediction of T_{offset}

The result of PLS models are shown in Table 5.3. For T_{offset}, the PLS model was performed with wavenumber in the range of 7506-4597.7 cm^{-1}; first derivative; and PLS factor number of 6. The R^2, RMSEP, bias and RPD were 0.928, 3.21°C, 0.749°C and 3.83, respectively. Scatter plots of measured and predicted value of calibration and validation set of T_{peak} illustrated in Figure 5.7b. R^2 and RPD is excellent predictions if R^2>0.90 and RPD>3 [10,11] and the model could be used with most application if provide with R^2 between 0.92-0.96 [12]. The bias (0.749°C) was small compared to the mean of reference value (357.03°C). The ratio of bias to its mean value was (0.749/357.03°C) 0.209%.

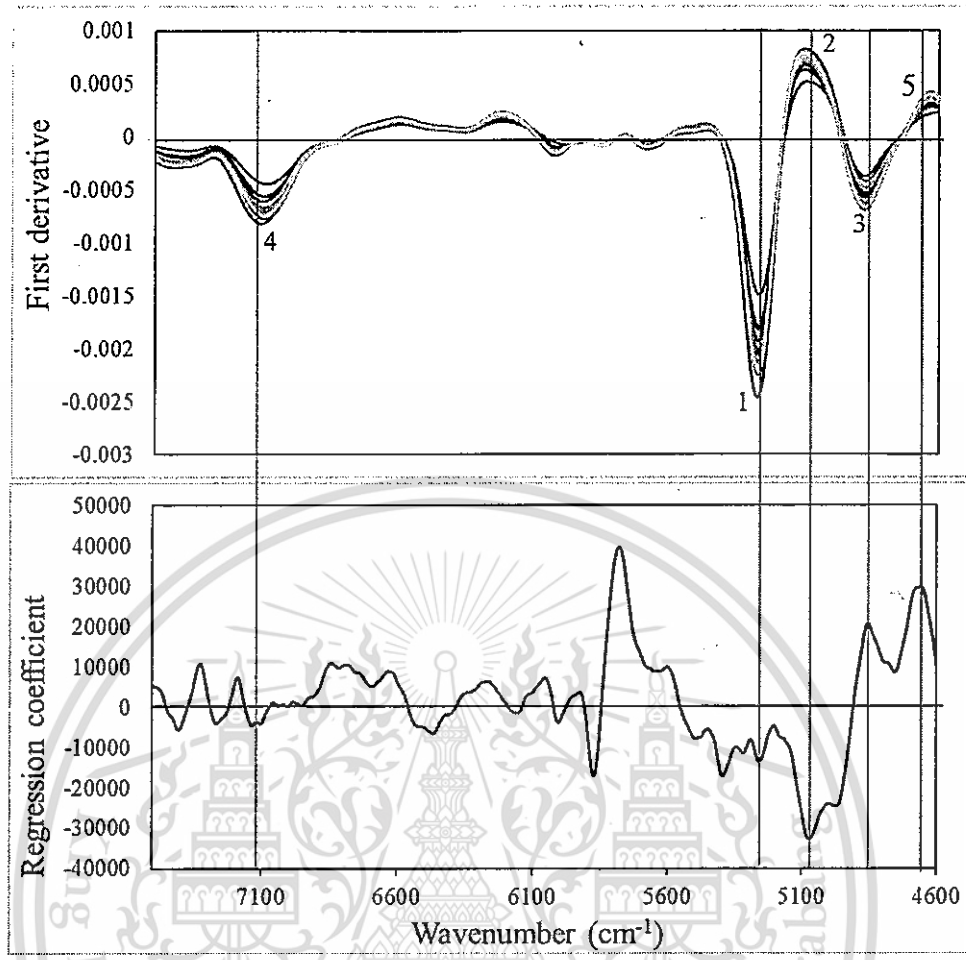

Figure 5.6 a) First derivative spectra, b) PLS regression coefficient of T_{offset}

Table 5.6 Vibration bands of some peaks at any wavenumber appeared on first derivative spectra of bamboo chips and regression coefficient plot for T_{offset} model

Peak	Appeared wavenumber		Cited wavelength (nm)	Vibration band[a]	Structure
	cm^{-1}	nm			
1	5261	1900	1900[8]	OH str + 2×CO str	starch
2	5060	1976	-	-	-
3	4852	2061	-	-	-
4	7128	1402	-	-	-
5	4668	2142	2134[14]	-	lignin

[a] *def* deformation, *str* stretching

Figure 5.6 demonstrates the first derivative spectra and its corresponding in regression coefficient plot of the optimum model for predicting the T_{offset} of bamboo chips. The vibration bands appeared in first derivative spectra and PLS regression coefficient reported in Table 5.6. There were bands of starch and lignin appeared on the plot at peak 1 and 5, respectively.

5.5.5 Prediction of DTG_{peak}

Scatter plots of the measured DTG_{peak} value obtained by the reference laboratory technique (Y axis) and the predicted value by NIR spectroscopy (X axis) of calibration and validation set are shown in Figure 5.7c. The most effective model for the prediction of DTG_{peak} were developed using a wavenumber range between 11602.3-9820.3 cm^{-1} (862-1018 nm) and 8933.2-8038.3 cm^{-1} (1119-1244 nm), spectrum preprocessing of first derivative and PLS factor number of 3. The R^2, RMSEP, RPD and bias of validation model were 0.771, 0.382%/min, 2.09 and -0.000581%/min. This model is not recommended [10,12]. The low RPD was due to either narrow measured value or high standard error of prediction. As seen in Table 5.1 and 5.2, the range of calibration set was narrow and repeatability was high, which led to poor performance. This low R^2 means that only 77.1 % of the variance in absorbance values can be accounted for by variance in DTG_{peak}, meanwhile, 22.9% was unexplained variance.

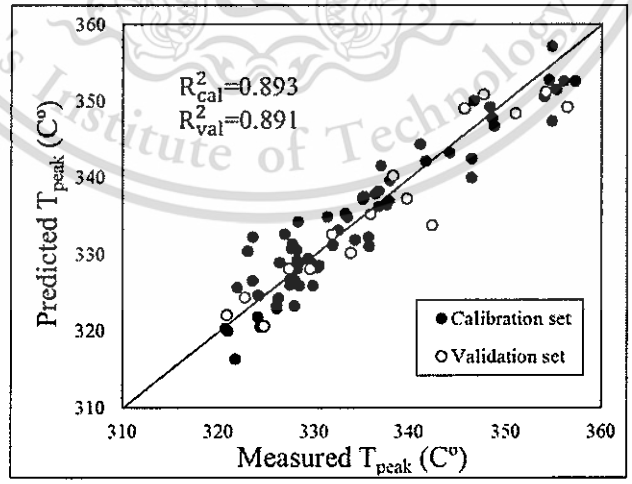

a)

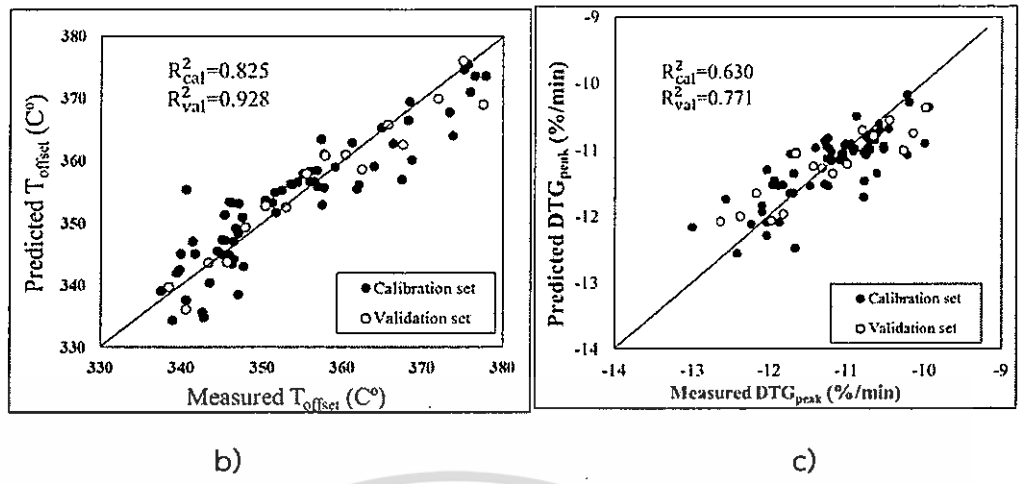

b) c)

Figure 5.7 Scatter plots of measured and predicted value of calibration and validation set of a) T_{peak}, b) T_{offset} and c) DTG_{peak}

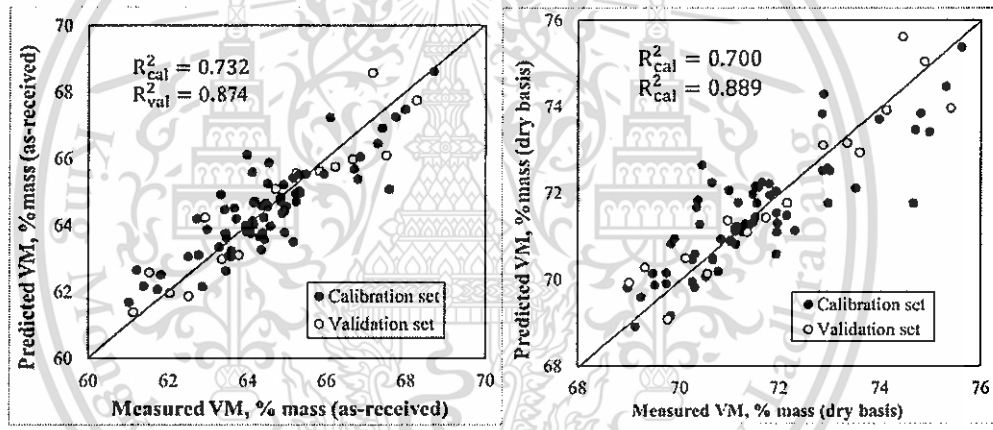

a) b)

Figure 5.8 Scatter plots of measured and predicted value of calibration and validation set of a) VM on as-received and b) VM on dry basis

5.5.6 Prediction of VM on as-received

The result of PLS models are shown in Table 5.3. For VM on as-received, the PLS model was performed with wavenumber in the range of 8454.9- 7498.3, 6102-5770.3 and 4605.4- 4242.9 cm^{-1}; pre-processing of straight line subtraction; and PLS factor number of 8. The R^2, RMSEP, bias and RPD were 0.874, 0.768%, -0.0454% and 2.83, respectively. Scatter plots of measured and predicted value of calibration and validation set of VM on as-received illustrated in Figure 5.8a. Good predictions If $0.81<R^2<0.9$ and $2.5< RPD<3$ is if $0R^2>0.81$ and $RPD>3$ [10][11], usable with caution for

most application [12]. The bias (-0.0454%) was small compared to the mean of reference value (64.45%). The ration of bias to its mean value was (-0.0454/64.45%) 0.070%.

Figure 5.9 shows the straight line subtraction spectra (a) and its corresponding in regression coefficient plot (b) of the optimum model for predicting the VM on as-revived of bamboo chips. The important peaks appeared in straight line subtraction spectra and PLS regression coefficient plots were reported in Table 5.7. There were bands of hemicellulose, cellulose, glucose and lignin appeared on the plot at peak 1; 2 and 4; 3; and 5, respectively.

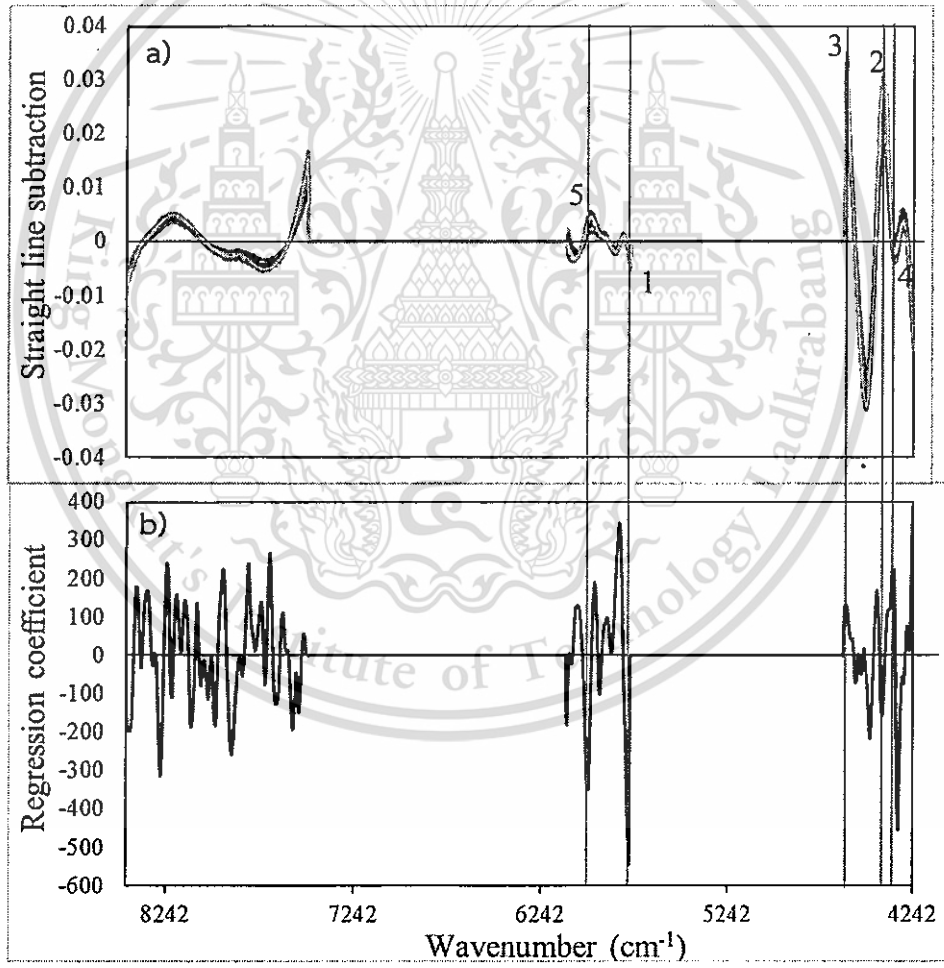

Figure 5.9 a) Straight line substraction spectra, b) PLS regression coefficient of VM on as-received

Table 5.7 Vibration bands of important peaks at any wavenumber appeared on straight line substraction spectra and regression coefficient plot of bamboo chips for VM on as-received model

Peak	Appeared wavenumber		Cited wavelength (nm)	Vibration band[a]	Structure
	cm^{-1}	nm			
1	5700	1754	1750[15]	-	hemicellulose
2	4404	2271	2273[8]	-	cellulose
3	4605	2172	-	-	-
4	4350	2299	2291[16]	CO + OH	cellulose
5	5986	1671	1672[17]	-	lignin

[a] *def* deformation, *str* stretching

5.5.7 Prediction of VM on dry basis

The result of PLS models are shown in Table 5.3. For VM on dry basis, the PLS model was performed with wavenumber in the range of 7506-5446.3 cm^{-1}; pre-processing of vector normalization; and PLS factor number of 9. The R^2, RMSEP, bias and RPD were 0.889, 0.665%, 0.000433% and 3, respectively. Scatter plots of measured and predicted value of calibration and validation set of VM on dry basis illustrated in Figure 5.8b. Good predictions If $0.81<R^2<0.9$ and $2.5<$ RPD<3 is if $0R^2>0.81$ and RPD>3 [10,11], usable with caution for most application [12]. The bias (0.000433%) was small compared to the mean of reference value (72.09%). The ration of bias to its mean value was (0.000433/72.09%) 0.6×10^{-3}%.

Figure 5.10 shows the vector normalization spectra (a) and its corresponding in regression coefficient plot (b) of the optimum model for predicting the VM on dry basis of bamboo chips. The important peaks appered in vector normalization spectra and PLS regression coefficient were reported in Table 5.8. There were bands of hemicellulose, cellulose and lignin appeared on the pretreated spectral and regression coefficient plot. It could be seen that the lignocellulosic substance was related to VM. The PLS model of VM also depended on molecular vibration of hemicellulose, cellulose, and lignin.

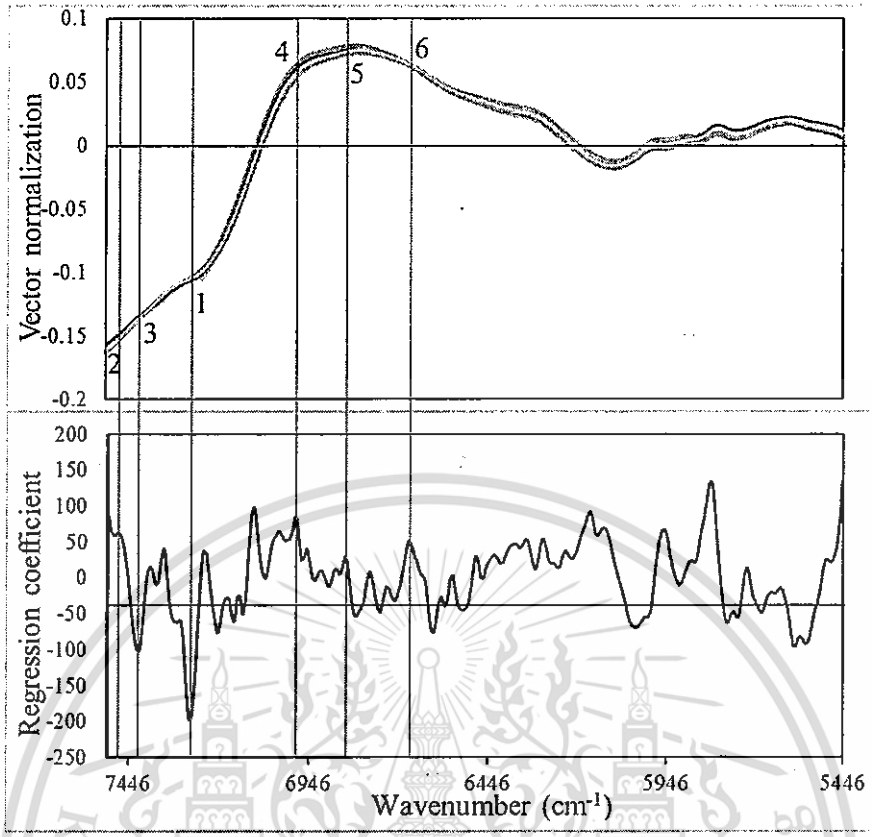

Figure 5.10 a) Vector normalization spectra, b) PLS regression coefficient of VM on dry basis

Table 5.8 Vibration bands of important peaks at any wavenumber appeared on vector normalization spectra and regression coefficient plot of bamboo chips for VM on dry basis model

Peak	Apperaed wavenumber		Cited wavelength (nm)	Vibration band[a]	Structure
	cm^{-1}	nm			
1	7274	1375	1370[18]	CH str+CH def	hemicellulose
2	7475	1338	1335[15]	-	cellulose, lignin, hemicellulose
3	7413	1349	-	-	-
4	6981	1432	1431[8]	-	cellulose
5	6842	1462	1465[15]	-	lignin
6	6657	1502	1500[15]	-	lignin

[a] *def* deformation, *str* stretching

5.6 Conclusion

In summary, PLS calibration models established by near infrared spectroscopy (NIRS) were found to suitable for rapid and non-destructive quantification of bamboo properties i.e. T_{peak}, T_{offset}, and VM. The model for T_{offset} was excellent and could be used with most applications. The T_{peak}, VM on as-received and VM on dry basis model was good and could be used with caution for most applications. Meanwhile, DTG_{peak} was not recommended. The $R^2_{max} > R^2$ for all parameter, meant that there were the errors from error of spectra due to the particle size which influence on the optical path length. The peak of the plant cell wall included cellulose and lignin occurred on second derivative spectra. The water and cellulose band effected to predicted T_{peak}, starch and lignin had effected to predictd T_{offset}. The vibration band of cellulose, hemicellulose and lignin influnced on VM models.

5.7 Reference

[1] Yang Z., Li K., Zhang M., Xin D., Zhang J., "Rapid determination of chemical composition and classification of bamboo fractions using visible–near infrared spectroscopy coupled with multivariate data analysis". **Biotechnol Biofuels**, vol. 9, 2016. Pp. 35.

[2] Xue J., Yang Z., Han L., Liu Y., Liu Y., Zhou C. "On-line measurement of proximates and lignocellulose components of corn stover using NIRS". **Applied Energy**, vol. 137, 2015. Pp. 18–25.

[3] Karatepe, N., Kűçűkbayrak, S. "Proximate analysis of some Turkish lignites by thermogravimetry." **Thermochimical Acta**, vol. 213, 1993. Pp. 147-150.

[4] García, R., Pizarro, C., Lavín, A.G., Bueno, J.L. "Biomass proximate analysis using thermogravimetry." **Bioresource Technology**, vol. 139, 2013. Pp. 1–4.

[5] Shenk JS, Workman JJ, Westerhaus MO. "Application of NIR spectroscopy to agricultural products." In: Burns DA, Ciurzack EW (eds), Handbook of near infrared analysis. Marcel Dekker, New york, 2001. Pp. 383-431.

[6] Workman, J., Weyer, J.R.L. 2007. "Practical Guide to Interpretive Near-Infrared Spectroscopy". Taylor & Francis, Boca Raton, FL, Pp. 240–262.

[7] Baillères H, Davrieux F, Ham-Pichavant F. "Near infrared analysis as a tool for rapid screening of some major wood characteristics in a eucalyptus breeding program." **Annal Forest Sci**, vol. 59, 2002. Pp. 479-490.

[8] Osborne B.G., Fearn T. "Near Infrared Spectroscopy in Food Analysis." Longman Science & Technical, London, 1986.

[9] Xu F., Yu J., Tesso T., Dowell F., Wang D. "Qualitative and quantitative analysis of lignocellulosic biomass using infrared techniques: A mini-review." **Applied energy**, vol. 104, 2013. Pp. 801-809.

[10] Zornoza R., Guerrero C., Mataix-Solera J., Scow K.M, Arcenegui V., Mataix-Beneyto J. "Near infrared spectroscopy for determination of various physical, chemical and biochemical properties in Mediterranean soils." **Soil Biol Biochem**, vol. 40(7), 2008. Pp. 1923–1930.

[11] Fagan CC, Everard CD, McDonnell K. "Prediction of moisture, calorific value, ash and carbon content of two dedicated bioenergy crops using near-infrared spectroscopy." **Bioresour Technol**, vol. 102, 2011. Pp. 5200–5206.

[12] Williams P. "Near-infrared technology-Getting the best out of light." Nanaimo, British Columbia, and Winnipeg, Manitoba, Canada: PDK Grain, 2007.

[13] Workman Jr J., Weyer L. "Practical Guide to Interpretive Near-Infrared Spectroscopy." Taylor & Francis, Boca Raton, FL, 2007. Pp. 240–262.

[14] Shenk JS, Workman JJ, Westerhaus MO. "Application of NIR spectroscopy to agricultural products." In: Burns DA, Ciurzack EW (eds), Handbook of near infrared analysis. Marcel Dekker, New York, 2001. Pp 383-431.

[15] Sills DL, Gossett JM. "Using FTIR to predict saccharification from enzymatic hydroysis of alkali preteated biomasses." **Biotechnol Bioeng**, vol. 109, 2012. Pp. 353-62.

[16] Mitchell AJ, Schimleck LR. "NIR spectroscopy of woods from Eucalyptus." **Appita J**, vol. 49(1), 1996. Pp. 23-26.

[17] Fujimoto T, Yamamoto H, Tsuchikawa S. "Estimation of wood stiffness and strength properties of hybrid larch by near-infrared spectroscopy." **Appl Spectrosc**, vol. 61(8), 2007. Pp. 882-888.

[18] Schwanninger M, Rodrigues JC, Fackler K. "A review of band assignments in near infrared spectra of wood and wood components." **J Near infrared Spectrosc**, vol, 19, 2001. Pp. 287-308.

Summary

Energy characteristics of biomass including MC, HHV, LHV, VM, FC, A, C, H, N, O, S, T_{onset}, T_{sh}, T_{peak}, T_{offset}, and DTG_{peak} were investigated. According to hypothesis, it was summarised that the energy characteristics of biomass were not parameters and absorbers which could be directly predicted by NIR radiance. They can be predicted using the correlated information between NIR radiance and their organic compound. As the results of pre-treated spectra, regression coefficients, and X-loading plots, the obvious peaks showed relation between vibration band of lignocellulosic and water. This was obviously showed their effects to energy characteristics.

The first experiment (chapter 1), the effect of MC on HHV of *Leucaena* was investigated. It was found a good relationship between MC and HHV with linear regression equations as HHV = -159MC + 18,780: HHV is the higher heating value (J g^{-1}) and MC is the moisture content (%wb) with a coefficient of determination (R^2) of 0.962. The HHV of pellets was decreased with increasing of its moisture content. In commercial, the MC and HHV are stated as quality assurance of products, their values must be determined before the pellets were traded. Moreover, the HHV could also be determined by MC content. This method was not only convenient and easy to use, but also offered cost-saving per sample because of cheaper cost of determination of MC using standard method. According to implementing of NIR, MC model was excellent for using in any application, and the HHV model could also be used for quality assurance.

From previous experiment, it was shown the fact that MC quite affects to HHV. Chapter 2, 3, 4 and 5 aimed to study the effects of the culm circumference size of bamboo on energy properties including the HHV, LHV, VM, FC, A, C, H, N, O, S, T_{onset}, T_{sh}, T_{peak}, T_{offset}, and DTG_{peak} when the initial MC of raw material was approximately of 5 %wb. The experiment was assumed that the parameters were varied with the culm. The objective was whether NIR spectroscopy could be estimated bamboo properties when MC was constant. The assumption was that different culm circumference size led to difference between element composition and chemical properties. The results were found that the statistical data of the HHV, LHV, VM, FC, A, C, H, N, O, S, T_{onset}, T_{sh}, T_{peak}, T_{offset}, and DTG_{peak} values did not vary with the culm circumference. Their values showed

a high standard deviation meaning the culm size did not influence the reference value. The PLS model development for the evaluation of the HHV, VM and FC of ground bamboo were feasible for screening. However, it was not possible to develop a largely useful predictive method for A, because the ash was not NIR absorber. The models developed for T_{sh} and T_{offset} may be used as a nondestructive technique with caution for most applications, and the model developed for T_{peak} can be used for most applications. On the other hand, the model of DTG_{peak} may be used for screening. However, the predictive model for T_{onset} was not usable due to high RMSEP and low R^2 value. The models for prediction of LHV and N content were excellent and suitable for using in most applications. The C model could be used only for approximate prediction. The H model was a good predictive model and could be used with caution for most applications. The S model was only permitted for approximate predictions that could be only used for rough screening. The O model was poor and was not recommended for using.

Prediction of MC and HHV, the vibration band of water and lignin depended on their models, because water was high sensitivity with NIR radiance and HHV had high relationship to MC. For prediction of LHV, was found that band of lignin quite affected to model development, and had no peak of water because LHV was calculated without MC. Generally, VM obtains by evaporation of lignocellulosic, then model VM and FC appeared the peaks of hemicellulose, lignin and cellulose. The A (ash) model was not recommended because its composition was not absorber and range of reference data was narrow. Generally, the A content relates to HHV in order to improve the A model, it must be optimized using many type of biomass samples. Pyrolysis is the thermal decomposition of biomass occurring in the absence of oxygen. T_{peak} stated the maximum decomposition of biomass which relates to VM, VM and lignocellulosic. Therefor, it could be seen the band of lignocellulosic appeared on the PLS regression coefficient. DTG_{peak} provided poor prediction because the reference data was not different. For predicting elemental composition, C and N models gave a good prediction. S and H models showed fair prediction. O model gave poor prediction because the reference data had high repeatability value, this meant that the sample was non-homogeneous

and the error of reference value was high. The author recommended that to evaluate energy properties of biomass, vibration band of lignocellulosic should be selected for developing the PLS models.

Appendix

Published papers

International Published papers:

1. Jetsada Posom, Panmanas Sirisomboon, Evaluation of lower heating value and elemental composition of bamboo using near infrared Spectroscopy. Energy, vol. 121, Pp. 147-158, 2017.

2. Jetsada Posom, Wanphut Saechua, Panmanas Sirisomboon. "Evaluation of pyrolysis characteristics of milled bamboo using near-infrared spectroscopy." Renewable energy, vol. 103, Pp. 653-665, 2016.

3. Jetsada Posom, Amrit Shrestha, Wanphut Saechua, Panmanas Sirisomboon. "Rapid non-destructive evaluation of moisture content and higher heating value of *Leucaena leucocephala* pellets using near infrared spectroscopy." Energy, vol. 107(15), Pp. 464-472, 2016.

4. Jetsada Posom, Panmanas Sirisomboon. "Evaluation of the higher heating value, volatile matter, fixed carbon and ash content of ground bamboo using near infrared spectroscopy." J Near Infrared Spectroscopy, vol. xx, Pp. xxx-xxx, 2017. (second revision and re-submitted on 17/05/2017).

Oral presentation:

1. Jetsada Posom, Panmanas Sirisomboon, Axel Funke, Jessica Heinrich, Jessica Maier and Pia Griesheimer. Feasibility of evaluation of pyrolysis characteristic of bamboo chips using of near infrared spectroscopy. Asian NIR Symposium 2016 in Kagoshima, Japan, the Shiroyama hotel during 30 November to 3 December 2016.

2. Jetsada Posom, Panmanas Sirisomboon, Axel Funke, Jessica Heinrich, Jessica Maier, Pia Griesheimer. Near infrared spectroscopy as an alternative method to thermogravimetric analysis for evaluation of volatile matter of bamboo wood chips. The 9th TSAE International conference: TSAE 2016, the Impact exhibition center, Bangkok, Thailand during 8-10 September 2016.

Author biography

Name: Mr. Jetsada Posom

Nationality: Thai

Date of Birth: 1987, December 10

Marital Status: Single

Address: 90 M.5, B. Nareang, T. Nong Khong, O. Namphong, J. Khonkaen, 40140

Tel. 061-773-9618 E-mail: jetsadaposom@gmail.com, jetsada-posom@hotmail.com

Educational Background:

D.Eng. (Agricultural Engineering) in King Mongkut's Institute of Technology Ladkrabang, Thailand. (between 2014-2016).

Research title: 'Fast analysis of energy characteristics of biomass using near-infrared spectroscopy'.

M.Eng. (Agricultural Engineering) from King Mongkut's Institute of Technology Ladkrabang, Thailand. (2011-2013), (GPA 4:00, Master thesis examination result was outstanding).

Research title: 'Development of the technique for measuring of thermal properties, moisture content, oil content and heating value of biomass by nondestructive method using near infrared spectroscopy: case study of *Jatropha curcas* kernels'.

B.Eng. (Tool & material Engineering) from King Mongkut's University of Technology Thonburi, Thailand. (2007-2010), (GPA 3.32, second class honours, ranked 3 in a class of 38 students).

Research title: 'Improvement of forging die collar part'.

Training attended:

- Training course in multiplicative analysis of Technical Chemistry, Nagoya University, Japan. 28th October – 27th December 2016.
- Training course in fast pyrolysis at Institute of Technical Chemistry, Karlsruhe Institute of Technology, Campus North, Germany. 15th January – 15th July 2016.

Scholarships:

- **Royal Golden Jubilee scholarship (RGJ)** from the Thailand Research Fund (TRF) to study the Doctor of Engineering Program in Agricultural Engineering at King Mongkut's Institute of Technology Ladkrabang, Thailand. (PHD/0070/2557).
- **TRF Master Research Grants (2013):** TRF-MAG scholarship for studying Master Engineering at King Mongkut's Institute of Technology Ladkrabang, Thailand.
- **Industrial and research projects for undergraduate students (IRPUS)** scholarship to study Bachelor Engineering in 2009, King Mongkut's University of Technology Thonburi, Thailand.

Oral presentation:

Doctor of Engineering degree program:

- Jetsada Posom, Panmanas Sirisomboon, Axel Funke, Jessica Heinrich, Jessica Maier and Pia Griesheimer. Feasibility of evaluation of pyrolysis characteristic of bamboo chips using of near infrared spectroscopy. Asian NIR Symposium 2016 in Kagoshima, Japan, the Shiroyama hotel during 30 November to 3 December 2016.
- Jetsada Posom, Panmanas Sirisomboon, Axel Funke, Jessica Heinrich, Jessica Maier, Pia Griesheimer. Near infrared spectroscopy as an alternative method to thermogravimetric analysis for evaluation of volatile matter of bamboo wood chips. The 9th TSAE International conference: TSAE 2016, the Impact exhibition center, Bangkok, Thailand during 8-10 September 2016.

Master of Engineering degree program:

- Jetsada Posom and Panmanas Sirisomboon. Development of the technique for measuring of oil content and thermal properties of biomass by non-destructive method using near infrared spectroscopy: case study of *Jatropha curcas* as kernels. RRI-MAG Congress I, the Twin Tower, Bangkok, Thailand during April 3-5, 2014.

International Published papers:

Doctor of Engineering degree program:

- Jetsada Posom, Panmanas Sirisomboon, Evaluation of lower heating value and elemental composition of bamboo using near infrared Spectroscopy. Energy, 121, (2017), 147-158.

- Jetsada Posom, Wanphut Saechua, Panmanas Sirisomboon. Evaluation of pyrolysis characteristics of milled bamboo using near-infrared spectroscopy. Renewable energy, 103 (2016), 653-665.
- Jetsada Posom, Amrit Shrestha, Wanphut Saechua, Panmanas Sirisomboon. Rapid non-destructive evaluation of moisture content and higher heating value of *Leucaena leucocephala* pellets using near infrared spectroscopy. Energy, 107(15), 464-472, 2016.
- Jetsada Posom, Panmanas Sirisomboon Evaluation of the higher heating value, volatile matter, fixed carbon and ash content of ground bamboo using near infrared spectroscopy. J Near Infrared Spectroscopy, xxx,xx,xxx-xxx. (Second revised).

Master of Engineering degree program:

- Jetsada Posom, Panmanas Sirisomboon, Evaluation of the moisture content of *Jatropha curcas* kernels and the heating value of the oilextracted residue using near-infrared spectroscopy, Biosystems Engineering, 130, 52-59, 2015. (Impact factor (2015: 1.997).
- Jetsada Posom, Panmanas Sirisomboon, Evaluation of the thermal properties of *Jatropha curcas* L. kernels using near-infrared spectroscopy, Biosystems Engineering, 125, 45-53, 2014. (Impact factor (2015: 1.997).
- Panmanas Sirisomboon, Jetsada Posom, Thermal properties of *Jatropha curcas* L. kernels. Biosystems Engineering, 113(4), 402-409, 2012.

Work experiences:

- Yanmar SP, Thailand. (1st October 2012-30th September 2015), R & D Engineering department. The main major was the designing and testing of Combine harvester, Power tiller, Rice transplanted and Tractor.
- Thai Honda Manufacturing, Thailand. (1st March 2011-30th September 2012), Quality Engineering department. The main major was performance and material testing.
- Work at Mitsubishi Heavy Duty Air-Conditioners, Thailand. (1st June 2010-28th February 2011), Pipe & Heat exchanger Engineer department.

Research interesting:

Near Infrared spectroscopy for agricultural product, implement in farm (combine harvester, rotary, power tiller, and plough), Renewable energy (biomass).

Reference Persons:

Assoc. Prof. Dr. Panmanas Sirisomboon

Curriculum of Agricultural Engineering,

Department of Mechanical Engineering, Faculty of Engineering,

King Mongkut's Institute of Technology Ladkrabang,

Bangkok 10520, Thailand, Tel: +66 2 739-2412, +66 2 3298000 ext. 5120, 5008

E-mail: panmanas@hotmail.com and kspanman@kmitl.ac.th